PhD Program in Energy and Process Control

SINGLE-STEP BIOGAS CONVERSION TO BIO-HYDROGEN: SORPTION ENHANCED CATALYTIC REFORMING

Doctoral Thesis

Alma Capa Tamargo

2023

Universidad de Oviedo

Programa de Doctorado en Energía y Control de Procesos

PRODUCCIÓN DE BIO-HIDRÓGENO A PARTIR DE BIOGÁS EN UNA SOLA ETAPA : REFORMADO CATALÍTICO CON CAPTURA INTEGRADA DE CO_2

Tesis Doctoral

Alma Capa Tamargo

2023

SUMMARY OF THE PhD THESIS CONTENTS

1.- Title of the Thesis	
Spanish/Other languages: Producción de bio-hidrógeno a partir de biogás en una sola etapa: Reformado catalítico con captura integrada de CO_2	English: Single-step biogas conversion to bio-hydrogen: Sorption-enhanced catalytic reforming.

2.- Author	
First name: Alma	ID/Passport/I
PhD Programme: Energía y Control de procesos	
Body responsible: Centro Internacional de Postgrado	

SUMMARY (in Spanish)

Esta tesis se centra en el estudio de la producción de hidrógeno renovable de alta pureza a partir de biogás utilizando una novedosa tecnología de reformado catalítico con captura integrada de CO_2 (*Sorption Enhanced Steam Reforming*, SESR). Se utilizaron dolomía ártica comercial como sorbente de CO_2, y un catalizador de tipo hidrotalcita con composición 1%Pd/20%Ni-20%Co para la producción de H_2 a través del proceso SESR de biogás.

Así, se evaluó experimentalmente el efecto de la composición del biogás y se concluyó que se puede obtener H_2 de alta pureza (98,4% en volumen) y alto rendimiento (91%) mediante el reformado mejorado con captura integrada de CO_2 de biogás (CH_4+CO_2) sobre un catalizador de Pd/Ni-Co y utilizando dolomía ártica como sorbente de CO_2.

También se estudió el efecto de la concentración de H_2S (150, 350, 500 y 1000 ppm) en el biogás (60 CH_4/40 CO_2 vol./vol.%) sobre el rendimiento del proceso SESR. No se detectó desactivación del catalizador debido a envenenamiento por H_2S durante cinco ciclos de reformado mejorado con captura de CO_2 de biogás a 600 ºC para concentraciones de H_2S de 150 y 350 ppm. Sin embargo, para 1000 ppm de H_2S, se encontró una ligera disminución en el rendimiento de H_2 (entre 4,5% y 10,8%) y en la pureza del H_2 (entre 2% y 3% en volumen).

Además del trabajo experimental, en esta tesis también se aborda el diseño del proceso SESR para optimizar su eficiencia, así como un análisis tecno-económico. Se diseñaron diferentes diagramas de flujo del proceso con el software AspenPlus y se realizó el análisis económico del más prometedor utilizando biogás como materia prima. También se utilizó gas natural con fines comparativos. En el caso del biogás, el valor más bajo del coste normalizado del hidrógeno (*levelised cost of hydrogen*, LCOH) se obtuvo cuando el calor se aportaba al calcinador mediante combustión indirecta de aire en un quemador externo (2,8 €/kg H_2 incluido el almacenamiento de CO_2). En el caso del gas natural el coste LCOH para un escenario similar fue sólo ligeramente inferior (2,6 €/kg H_2, incluido el almacenamiento de CO_2), lo que indica que el biogás podría ser un potencial sustituto del gas natural, al ser renovable y económicamente competitivo.

Finalmente, se estudia la integración del proceso de reformado mejorado con captura integrada de CO_2 de biogás con el proceso mejorado de síntesis de Dimetil Éter con adsorción de H_2O (*Sorption Enhanced Dimethyl Ether (DME) Synthesis*, SEDMES). Para ello se ha evaluado la producción de bio-DME a partir de biogás integrando eficientemente los procesos SESR y SEDMES, logrando una eficiencia de gas frío (*Cold Gas Efficiency*, CGE) final del 74%.

SUMMARY (in English)

This thesis focuses on the study of the production of renewable high-purity hydrogen from biogas using a novel catalytic reforming technology. This process is known as Sorption Enhanced Steam Reforming (SESR) . In this framework, commercial Arctic dolomite and a 1%Pd/20%Ni-20%Co hydrotalcite-like material were used as CO_2 sorbent and catalyst, respectively, for the production of H_2 through biogas SESR.

The effect of biogas composition (with respect to CH_4 content) on H_2 production from biogas SESR was evaluated experimentally. It was concluded that high-purity (98.4 vol.%) and high-yield (91%) H_2 can be obtained by SESR of biogas (CH_4+CO_2) over a Pd/Ni-Co catalyst and using Arctic dolomite as a carbon dioxide sorbent.

The effect of the H_2S concentration (150, 350, 500, and 1000 ppm) in the biogas (60 CH_4/40 CO_2 vol./vol.%) on the performance of the SESR process was also studied. No catalyst deactivation due to H_2S poisoning was detected during cyclic SESR of biogas at 600 ºC for H_2S concentrations of 150 and 350 ppm (five cycles). However, for 1000 ppm H_2S, a slight decrease in H_2 yield (between 4.5% and 10.8% points) and H_2 purity (between 2% and 3% points) was found.

In addition to the experimental proof of concept of the biogas SESR process, this work also addresses the SESR process design to optimise its efficiency and a techno-economic analysis. Different process flowsheets were designed in AspenPlus software and the economic analysis of the most promising one was carried out using biogas as feedstock. Natural gas was also used for comparison purposes. In the case of biogas, the lowest value of the levelised cost of hydrogen (LCOH) was obtained when the heat was provided to the calciner by indirect air combustion in an external burner (2.8 €/kg H_2 including CO_2 storage). In the case of natural gas using an indirectly heated calciner, the LCOH was only slightly lower (2.6 €/kg H_2 including CO_2 storage), indicating that biogas could be a potential substitute for natural gas, being renewable and economically competitive.

Finally, the integration of the biogas SESR process with the Sorption Enhanced Dimethyl Ether (DME) Synthesis (SEDMES) process is studied. This work evaluated the production of bio-DME from biogas by efficiently integrating the SESR and SEDMES processes, achieving a final Cold Gas Efficiency (CGE) of 74%.

DIRECTOR OF THE DEPARTMENT FOR_____/
PRESIDENT OF THE ACADEMIC COMMISSION OF THE PhD PROGRAMME IN _____

A mis padres.

ACKNOWLEDGMENTS

A mis directoras, las Doctoras Covadonga Pevida y M. Victoria Gil por darme la oportunidad de realizar esta tesis y por la confianza puesta en mí durante estos cuatro años. Gracias por todo vuestro asesoramiento y por todo el aprendizaje durante esta etapa.

Al Ministerio de Ciencia, Innovación y Universidades por la concesión de la ayuda predoctoral FPI cofinanciada por el fondo social europeo.

Al Consejo Superior de Investigaciones Científicas (CSIC) por autorizar la realización de este trabajo en el Instituto de Ciencia y Tecnología del Carbono (INCAR). A mis compañeros y amigos del INCAR por los cafés y comidas que daban la vida en días complicados gracias a las risas.

Al Doctor Jorge Parrondo Gayo de la Universidad de Oviedo por ser tutor de esta tesis y ayudarme en las gestiones pertinentes. Gracias también a la Doctora Leonor Castrillón Peláez, de la Universidad de Oviedo, por tenerme siempre presente.

To Dr. Peter Clough, from Cranfield University. Thank you for giving me the opportunity to join your team. To Dr. Yongliang Yan, from Newcastle University, thank you for your unconditional support. To my friends in The UK, thank you for all the trips to London and the beers every Friday in Bedford.

To Dr. Jurriaan Boon, from the TNO, and to STIP. Thank you for the opportunity that has just begun. See you soon, new colleagues! To the Vennewaard family, I have no words, thank you.

A la Doctora Victoria Masaguer por confiar en mí durante mi primera experiencia laboral. Gracias por ser inspiración no solo en lo profesional, sino también en lo personal. Gracias a *By-products team*, donde empecé mi andadura y mi pasión por este mundo. A Álvaro, por todo lo aprendido contigo de este mundillo y por estar siempre.

A todos mis amigos por ser luz fuera del trabajo. *And last but not least*, a mi familia y a Sergio. Sin vosotros esto no habría sido posible. Gracias, por el apoyo y la comprensión en los momentos más difíciles y por estar siempre a mi lado.

TABLE OF CONTENTS

List of figures ---------- *VII*

List of tables ---------- *XV*

Abstract ---------- *XIX*

Resumen ---------- *XXI*

Thesis Structure ---------- *XXIII*

1. INTRODUCTION ---------- *3*

1.1. ENERGY AND CLIMATE CHANGE ---------- **3**

1.2. PILLARS OF DECARBONISATION ADDRESSED IN THIS THESIS ---------- **6**

1.2.1. Carbon Capture Utilisation and Storage (CCUS) ---------- 6

1.2.2. Bioenergy and biogas ---------- 9

1.2.3. Hydrogen and hydrogen-based fuels ---------- 10

1.3. THESIS OBJECTIVES ---------- **13**

2. REVIEW OF RELEVANT LITERATURE ---------- *17*

2.1. GENERAL OVERVIEW OF SESR ---------- **17**

2.1.1. Thermodynamics of SESR ---------- 19

2.1.2. The catalyst and the sorbent in SESR ---------- 21

2.1.2.1. The sorbent ---------- 21

2.1.2.2. Catalyst for SESR ---------- 25

2.1.3. How to operate a SESR process: fixed and fluidised beds ---- 29

2.1.4. Challenges in further scaling-up SESR technology ---------- 32

2.2. EFFECT OF BIOGAS COMPOSITION ON H_2 PRODUCTION BY SESR: STATE OF THE ART ---------- 33

2.3. EFFECT OF H_2S ON H_2 PRODUCTION BY SESR OF BIOGAS: STATE OF THE ART ---------- 34

2.4. PROCESS SIMULATIONS OF HIGH-PURITY HYDROGEN PRODUCTION BY SESR OF BIOGAS: STATE OF THE ART ---------- 36

2.5. TECHNO-ECONOMIC ANALYSIS OF H_2 PRODUCTION BY SESR OF BIOGAS: STATE OF THE ART ---------- 38

2.6. PRODUCTION OF DIMETHYL ETHER (DME) AS HYDROGEN CARRIER: STATE OF THE ART ---------- 39

3. EXPERIMENTAL AND SIMULATION METHODOLOGIES ----- 45

3.1. EXPERIMENTAL METHODOLOGY ---------- 45

3.1.1. Experimental set-up: fluidised and fixed bed reactors -------- 45

3.1.2. Breakthrough curve of a SESR experiment ---------- 48

3.1.3. Materials: catalyst and sorbent ---------- 49

3.1.4. Characterisation techniques ---------- 52

3.1.5. Experimental key performance indicators ---------- 55

3.2. PROCESS SIMULATIONS OF H_2 PRODUCTION BY SESR OF BIOGAS ---------- 57

3.2.1. Model development and process configurations ---------- 57

3.2.1.1. Theoretical background ---------- 57

3.2.1.2. Process configurations ---------- 61

3.2.1.3. Model development ---------- 64

3.2.2. Key performance indicators for the SESR process performance ---------- 66

3.3. TECHNO-ECONOMIC ANALYSIS METHODOLOGY ---------- 67

3.3.1. Methodology for the techno-economic analysis ----------67

3.3.2. Key performance indicators for the techno-economic analysis ----------70

3.4. PRODUCTION OF BIO-DME FROM BIOGAS AS HYDROGEN CARRIER ---------- 72

3.4.1. Modelling methodology for bio-DME production----------72

3.4.2. Key performance indicators for the bio-DME production evaluation ----------74

4. RESULTS ----------79

4.1. EFFECT OF BIOGAS COMPOSITION ON H_2 PRODUCTION BY SORPTION ENHANCED STEAM REFORMING (SESR) ---------- 79

4.1.1. Set I of experiments: Effect of biogas composition considering CH_4 as the only reactant gas ----------81

4.1.2. Set II of experiments: Effect of biogas composition considering CH_4 and CO_2 as reactant gases ----------86

4.1.3. Conclusions on the effect of the biogas composition on SESR ----------89

4.2. EFFECT OF H_2S ON H_2 PRODUCTION BY SORPTION ENHANCED STEAM REFORMING (SESR) OF BIOGAS---------- 90

4.2.1. Effect of the biogas H_2S content on SESR cyclic operation ---92

4.2.1.1. Catalyst activity and process performance in the presence of H_2S ----------92

4.2.1.2. Sorbent CO_2 capture capacity in the presence of H_2S -------93

4.2.1.3. Sulphur distribution in spent catalyst and sorbent after SESR cycles ----------94

4.2.2. Characterisation of the spent catalyst and sorbent after cyclic SESR operation ---------- 97

4.2.2.1. SEM analysis of spent catalyst and sorbent ---------- 97

4.2.2.2. XRD analysis of spent catalyst and sorbent ---------- 101

4.2.2.3. N_2 adsorption analysis of spent sorbent ---------- 103

4.2.2.1. XPS analysis of spent catalyst and sorbent ---------- 104

4.2.3. Discussion comparing catalyst deactivation during SESR and conventional SR ---------- 111

4.2.4. Conclusions on the effect of H_2S on biogas SESR ---------- 113

4.3. PROCESS SIMULATIONS OF H_2 PRODUCTION BY SORPTION ENHANCED STEAM REFORMING (SESR) OF BIOGAS ---------- 115

4.3.1. Effect of biogas composition ---------- 117

4.3.2. Effect of SESR temperature ---------- 121

4.3.3. Effect of SESR pressure ---------- 125

4.3.4. Effect of S/CH_4 ratio ---------- 130

4.3.5. Discussion on SESR designs to optimise H_2 purity and captured CO_2 ---------- 133

4.3.6. Conclusions on process simulation of H_2 production by SESR of biogas ---------- 137

4.4. TECHNO-ECONOMIC ANALYSIS OF H_2 PRODUCTION BY SORPTION ENHANCED STEAM REFORMING (SESR) OF BIOGAS -------- 138

4.4.1. Technical performance of the SESR process of biogas and natural gas ---------- 138

4.4.2. Economic analysis of biogas and natural gas SESR ---------- 142

4.4.2.1. Estimation of CAPEX and OPEX ---------- 142

4.4.2.2. Estimation of the levelised cost of hydrogen – LCOH ----- 146

4.4.3. Conclusions on the techno-economic analysis of biogas SESR ---------- 148

4.5. PRODUCTION OF BIO-DME AS HYDROGEN CARRIER: PROCESS SIMULATION OF THE INTEGRATION OF BIOGAS SESR AND SEDMES ---------- 149

4.5.1. Simulation of the integration of biogas SESR and SEDMES to efficiently produce low-carbon bio-DME ---------- 149

4.5.2. Conclusions on the integration of biogas SESR and SEDMES for the production of bio-DME ---------- 158

5. CONCLUSIONS ---------- 161

Conclusiones ---------- 163

REFERENCES ---------- 165

Annexes ---------- 193

Annex I: Techno-economic analysis ---------- 195

Flowsheet diagram used in the techno-economic analysis -------- 195

Assumptions for the techno-economic analysis ---------- 196

Annex II: Publications ---------- 199

Paper I ---------- 199

Paper I – Supplementary information ---------- 208

Paper II ---------- 217

Paper II – Supplementary information ---------- 234

Paper III ---------- 241

Annex III: Other Scientific contributions ---------- 259

Paper IV---------- 259

Communications to scientific congresses ---------- 260

LIST OF FIGURES

Figure 1.1: The keeling curve. CO_2 concentration at Mauna Loa Observatory [5]. 3

Figure 1.2: Distribution of the global greenhouse gas emissions by sector [7]. 4

Figure 1.3: Emissions reduction by mitigation measure in the NZE, 2020-2050 [10]. 5

Figure 1.4: Ways CCUS technologies contribute to the clean energy transition (graph adapted from [11]). 6

Figure 1.5: Classification of CO_2 capture technologies (figure adapted from [16]). 8

Figure 1.6: Hydrogen demand by sector in the announced pledges and Net Zero Emissions scenarios, 2020-2050 [28]. 11

Figure 2.1: Simplified schematic of a SESR reactor (Figure adapted from [41]). 19

Figure 2.2: Equilibrium calculations to estimate the H_2 content as a function of temperature during a reforming process with and without a CO_2 acceptor [43]. 20

Figure 2.3: Thermodynamic study on the effect of the temperature and CO_2 partial pressure at equilibrium on the conversion of $CaCO_3$ to CaO in air [45]. 21

Figure 2.4: CO_2 uptake capacity of limestone-derived CaO through two reaction regimes [4]. 22

Figure 2.5: Conversion profiles of CaO typically observed for different pore size distributions [50]. 23

Figure 2.6: Typical weight change vs. time for a repeated number of calcination/carbonation cycles [52]. 23

Figure 2.7: Scheme of the textural transformation of CaO upon cycling. The $CaCO_3$ phase is represented in dark grey, while CaO in light grey [51]. 24

Figure 2.8: Schematic representation of the structure of a hydrotalcite [73]. 28

Figure 2.9: Schematic example of SESMR over a bifunctional catalyst sorbent (a) [83]; and example of a core-shell structured bifunctional material (b) [84]. 29

Figure 2.10: Example of a battery of fixed bed reactors as a configuration for SESR [89]. 30

Figure 2.11: Schematic diagram of SESR performed with circulating fluidised beds [90]. 31

Figure 2.12: Scheme of the 1.5 MWth pilot system under commissioning at Cranfield University [91]. 32

Figure 2.13: Overview of the main DME production routes [145]. 40

Figure 3.1: Experimental setup (a) and its schematic flow diagram (b). 46

Figure 3.2: Details of the experimental device: interior of the hot box (a), water pump (b) and condenser (c). 47

Figure 3.3: Example of a typical breakthrough curve of a SESR experiment [43]. 48

Figure 3.4: Sieved sorbent (a) and catalyst (b). 49

Figure 3.5: Setup used for the catalyst synthesis (a) and filtering (b), and the final precipitate obtained (c). 51

Figure 3.6: Simplified flow diagrams of the three base configurations proposed for the biogas SESR process. In Case 1 (SESR+REG_H2), a fraction of the produced H_2 is used as fuel for the sorbent regeneration (a). In Case 2 (SESR+REG_BG), biogas is utilised as fuel for the sorbent regeneration (b). Finally, in Case 3 (SESR+REG_BG+PSA), biogas is used as fuel for the sorbent regeneration and a PSA unit is included (c). 63

Figure 3.7: Indirect (a) and direct (b) heating of the calciner as energy integration strategies used for the evaluation of the economic performance of the different case studies. 69

Figure 3.8: Simplified diagram of bio-DME production, as hydrogen carrier, from biogas. 72

Figure 4.1: Effect of methane content in biogas on the H_2 (a), CH_4 (b), CO (c) and CO_2 (d) concentrations during SESR and SR at 600 and 650 ^oC. Reaction conditions: steam/CH_4=6 mol/mol, $GHSV_{CH4}$ = 1969 mL_{CH4} g_{cat}^{-1} h^{-1}, sorbent/catalyst ratio=20 g/g, Pd/Ni-Co HT catalyst and dolomite sorbent. 83

Figure 4.2: Effect of methane content in biogas on the H_2 yield (a), H_2 selectivity (b) and CH_4 conversion (c) during SESR and SR at 600 and 650 ^oC. Conditions: steam/CH_4=6 mol/mol, $GHSVCH_4$ = 1969 mL_{CH4} g_{cat}^{-1} h^{-1}, sorbent/catalyst ratio=20 g/g, Pd/Ni-Co HT catalyst and dolomite sorbent. 85

Figure 4.3: Effect of methane content in biogas on the H_2 (a), CH_4 (b), CO (c) and CO_2 (d) concentrations during SESR and SR at 600 and 650 ^oC. Conditions: steam/C = 3 mol/mol, GHSVbiogas = 3937 mL biogas g_{cat}^{-1} h^{-1}, sorbent/catalyst ratio = 20 g/g, Pd/Ni-Co HT catalyst and dolomite sorbent. 88

Figure 4.4: H_2 yield (a), H_2 purity (b), CH_4 conversion (c) and CH_4 concentration (d) during five cycles of SESR for all H_2S concentrations. Operating conditions: Biogas=60/40 CH_4/CO_2 vol.%; T=600 ^oC; S/CH_4=6 mol/mol; GHSV=1803 mL_{CH4} g_{cat}^{-1} h^{-1}; sorbent/catalyst ratio=20 g/g; Pd/Ni-Co HT catalyst and dolomite sorbent. 93

Figure 4.5: CO_2 captured by the sorbent during five SESR cycles for all H_2S concentrations. Operating conditions: Biogas=60/40 CH_4/CO_2 vol.%; Treforming=600 ^oC; S/CH_4=6 mol/mol; GHSV=1803 mL_{CH4} g_{cat}^{-1} h^{-1}; sorbent /catalyst ratio=20 g/g; Tregeneration=800 ^oC; Pd/Ni-Co HT catalyst and dolomite sorbent. 94

Figure 4.6: Total S distribution (wt.%) between sorbent, catalyst and gas after five cycles of the SESR process for biogas H_2S concentrations of 150 (a), 350 (b), 500 (c), and 1000 ppm (d). Operating conditions: Biogas=60/40 CH_4/CO_2 vol.%; T=600 ^oC; S/CH_4=6 mol/mol; GHSV=1803 mL_{CH4} g_{cat}^{-1} h^{-1}; sorbent/catalyst ratio=20 g/g; Pd/Ni-Co HT catalyst and dolomite sorbent. 96

Figure 4.7: SEM images of the fresh and spent Pd/Ni-Co HT catalyst after one and five cycles of the SESR process for different biogas H_2S concentrations:

(a) fresh sorbent; (b) 350 ppm H_2S, 1 cycle; (c) 150 ppm H_2S, 5 cycles; (d) 350 ppm H_2S, 5 cycles; (e) 500 ppm H_2S, 5 cycles; and (f) 1000 ppm H_2S, 5 cycles. Operating conditions: Biogas=60/40 CH_4/CO_2 vol.%; T=600 ^oC; S/CH_4=6 mol/mol; GHSV=1803 $mL_{CH4}\ g_{cat}^{-1}\ h^{-1}$; sorbent/catalyst ratio=20 g/g; Pd/Ni-Co HT catalyst and dolomite sorbent.....98

Figure 4.8: EDX elemental mapping of Ni, Co, Pd and S in the spent Pd/Ni-Co HT catalyst after five cycles of the SESR process for different biogas H_2S concentrations: (a) 150 ppm; (b) 350 ppm; (c) 500 ppm; and (d) 1000 ppm. Operating conditions: Biogas=60/40 CH_4/CO_2 vol.%; T=600 ^oC; S/CH_4=6 mol/mol; GHSV=1803 $mL_{CH4}\ g_{cat}^{-1}\ h^{-1}$; sorbent/catalyst ratio=20 g/g; Pd/Ni-Co HT catalyst and dolomite sorbent.....99

Figure 4.9: SEM images of the fresh and spent dolomite sorbent after one and five cycles of the SESR process for different biogas H_2S concentrations: (a) fresh sorbent; (b) 350 ppm H_2S, 1 cycle; (c) 150 ppm H_2S, 5 cycles; (d) 350 ppm H_2S, 5 cycles; (e) 500 ppm H_2S, 5 cycles; and (f) 1000 ppm H_2S, 5 cycles. Operating conditions: Biogas=60/40 CH_4/CO_2 vol.%; T=600 ^oC; S/CH_4=6 mol/mol; GHSV=1803 $mL_{CH4}\ g_{cat}^{-1}\ h^{-1}$; sorbent/catalyst ratio=20 g/g; Pd/Ni-Co HT catalyst and dolomite sorbent.....100

Figure 4.10: XRD patterns of the fresh and spent Pd/Ni-Co HT catalyst after five cycles of the SESR process for biogas H_2S concentrations of 150, 350, 500, and 1000 ppm. Operating conditions: Biogas=60/40 CH_4/CO_2 vol.%; T=600 ^oC; S/CH_4=6 mol/mol; GHSV=1803 $mL_{CH4}\ g_{cat}^{-1}\ h^{-1}$; sorbent/catalyst ratio=20 g/g; Pd/Ni-Co HT catalyst and dolomite sorbent. 101

Figure 4.11: XRD patterns of the fresh and spent dolomite sorbent after five cycles of the SESR process for biogas H_2S concentrations of 150, 350, 500, and 1000 ppm. Operating conditions: Biogas=60/40 CH_4/CO_2 vol.%; T=600 ^oC; S/CH_4=6 mol/mol; GHSV=1803 $mL_{CH4}\ g_{cat}^{-1}\ h^{-1}$; sorbent/catalyst ratio=20 g/g; Pd/Ni-Co HT catalyst and dolomite sorbent. 103

Figure 4.12: XPS surface spectra for S 2p of the fresh (a) and spent Pd/Ni-Co HT catalyst after five cycles of the SESR process for biogas H_2S concentrations of 150 (b), 350 (c), 500 (d), and 1000 ppm (e). Operating conditions: Biogas=60/40 CH_4/CO_2 vol.%; T=600 ^oC; S/CH_4=6 mol/mol; GHSV=1969 $mL_{CH4}\ g_{cat}^{-1}\ h^{-1}$; sorbent/catalyst ratio=20 g/g; Pd/Ni-Co HT catalyst and dolomite sorbent. 106

Figure 4.13: XPS surface spectra for Ni 2p of the spent Pd/Ni-Co HT catalyst after five cycles of the SESR process for biogas H_2S concentrations of 150 (a), 350 (b), 500 (c), and 1000 ppm (d). Operating conditions: Biogas=60/40 CH_4/CO_2 vol.%; T=600 C; S/CH_4=6 mol/mol; GHSV=1969 $mL_{CH4}g_{cat}^{-1}h^{-1}$; sorbent/catalyst ratio=20 g/g; Pd/Ni-Co HT catalyst and dolomite sorbent. 107

Figure 4.14: XPS surface spectra for Co 2p of the spent Pd/Ni-Co HT catalyst after five cycles of the SESR process for biogas H_2S concentrations of 150 (a), 350 (b), 500 (c), and 1000 ppm (d). Operating conditions: Biogas=60/40 CH_4/CO_2 vol.%; T=600 ^oC; S/CH_4=6 mol/mol; GHSV=1969 $mL_{CH4}\, g_{cat}^{-1}\, h^{-1}$; sorbent/catalyst ratio=20 g/g; Pd/Ni-Co HT catalyst and dolomite sorbent. 108

Figure 4.15: XPS surface spectra for S 2p of the spent dolomite sorbent after five cycles of the SESR process for biogas H_2S concentrations of 150 (a), 350 (b), 500 (c), and 1000 ppm (d). Operating conditions: Biogas=60/40 CH_4/CO_2 vol.%; T=600 ^oC; S/CH_4=6 mol/mol; GHSV=1803 $mL_{CH4}\, g_{cat}^{-1}\, h^{-1}$; sorbent/catalyst ratio=20 g/g; Pd/Ni-Co HT catalyst and dolomite sorbent. 111

Figure 4.16: Effect of biogas composition on H_2 purity, H_2 yield, and CH_4 conversion (a-c) and on cold gas efficiency (CGE), net efficiency (NE, using both air, Net Eff. A, and oxy-combustion, Net Eff-B, in REG) and fuel consumption for sorbent regeneration (d-f) for the different process configurations studied: (a and d) use of a fraction of the produced hydrogen as fuel for sorbent regeneration (SESR+REG_H_2); (b and e) use of biogas as fuel for sorbent regeneration (SESR+REG_BG); and (c and f) addition of a PSA unit and use of biogas and off-gas (PSA-OG) for sorbent regeneration (SESR+REG_BG+PSA). SESR conditions: S/CH_4 = 5.5, T = 600 ^oC, P = 10 bar, and 50% sorbent excess. 119

Figure 4.17: Comparison of the CGE with (red line) and without (blue line) waste heat recovery (WHR) from the CO_2 stream for the Case 3 (SESR+REG_BG+PSA)..... 121

Figure 4.18: Effect of SESR temperature on H_2 purity, H_2 yield, and CH_4 conversion (a-c) and on cold gas efficiency (CGE), net efficiency (NE, using both air, Net Eff. A, and oxy-combustion, Net Eff-B, in REG), and fuel

consumption for sorbent regeneration (d-f) for the different process configurations studied: (a and d) use of a fraction of the produced hydrogen as fuel for sorbent regeneration (SESR+REG_H_2); (b and e) use of biogas as fuel for sorbent regeneration (SESR+REG_BG); and (c and f) addition of a PSA unit and use of biogas and off-gas (PSA-OG) for sorbent regeneration (SESR+REG_BG+PSA). SESR conditions: S/CH_4 = 5.5, P = 10 bar, biogas = 60/40 vol.% CH_4/CO_2, and 50% sorbent excess. 124

Figure 4.19: Effect of SESR pressure on H_2 purity, H_2 yield, and CH_4 conversion (a-c) and on cold gas efficiency (CGE), net efficiency (NE, using both air, Net Eff. A, and oxy-combustion, Net Eff-B, in REG), and fuel consumption for sorbent regeneration (d-f) for the different configurations: (a and d) use of a fraction of the produced hydrogen as fuel for sorbent regeneration (SESR+REG_H_2); (b and e) use of biogas as fuel (SESR+REG_BG); and (c and f) addition of a PSA unit and use of biogas and off-gas (PSA-OG) for sorbent regeneration (SESR+REG_BG+PSA). SESR conditions: S/CH_4 = 5.5, T = 600 ^oC, biogas = 60/40 vol.% CH_4/CO_2, and 50% sorbent excess. 127

Figure 4.20: Effect of S/CH_4 on H_2 purity, H_2 yield, and CH_4 conversion (a-c) and on cold gas efficiency (CGE), net efficiency (NE, using both air, Net Eff. A, and oxy-combustion, Net Eff-B, in REG), and fuel consumption for sorbent regeneration (d-f) for the different process configurations studied: (a and d) use of a fraction of the produced hydrogen as fuel for sorbent regeneration (SESR+REG_H2); (b and e) use of biogas as fuel for sorbent regeneration (SESR+REG_BG); and (c and f) addition of a PSA unit and use of biogas and off-gas (PSA-OG) for sorbent regeneration (SESR+REG_BG+PSA). SESR conditions: 600 ^oC, P = 10 bar, biogas = 60/40 vol.% CH_4/CO_2, and 50% sorbent excess. 131

Figure 4.21: Comparison of the proposed biogas SESR + PSA (orange column) with different literature biogas reforming processes without CCS (grey columns; conventional SR [196], SR+SOFC [197], ATR: autothermal reforming [196,198], DR: dry reforming [199], membrane reformer [140]) and with CCS or PSA/VPSA (green columns; SESR [136], SR+CL: chemical looping [160], SR+Iron looping/Ca looping/MDEA scrubbing [200], SR+ VPS/PSA [160,201]). 136

Figure 4.22: Breakdown of CAPEX (a) and variable OPEX (b) for the SESR of biogas (BIOG) and natural gas (NG). 145

Figure 4.23: Splitting of the different costs of LCOH for the SESR of biogas (BIOG) and natural gas (NG) with CO_2 storage (a) and without CO_2 storage (b). 147

Figure 4.24: AspenPlus diagram of the basic bio-DME production plant from biogas coupling biogas SESR and SEDMES.....153

Figure 4.25: AspenPlus diagram of the heat integration between biogas SESR and SEDMES.....154

Figure 4.26: AspenPlus diagram of the second synergy; the recycling of SEDMES by-products to the external burner of SESR unit. 155

Figure 4.27: AspenPlus diagram of the last strategy included; the recycling of the steam from SEDMES to SESR.....156

Figure 4.28: Carbon balance of the different strategies studied for the integration of biogas SESR and SEDMES for bio-DME production. 158

LIST OF TABLES

Table 2.1: Main reaction steps of the steam methane reforming process [57]. 26

Table 3.1: Composition of the cationic and anionic solutions for the synthesis of the 20%Ni-20%Co HT catalyst precursor. 51

Table 3.2: Case studies evaluated for the energy integration of the SESR process of biogas. 62

Table 4.1: Composition of the biogas mixtures studied. 80

Table 4.2: Experimental conditions used in two sets of experiments to study the effect of biogas composition on the SESR process. 81

Table 4.3: Total sulphur content of the spent Pd/Ni-Co HT catalyst and dolomite sorbent after five cycles of SESR of biogas containing different concentrations of H_2S (normalized by the feeding time). 95

Table 4.4: XRD characterisation of the fresh and spent dolomite sorbent after five cycles of SESR of biogas containing different concentrations of H_2S. . 103

Table 4.5: Physical characterisation by means of N_2 adsorption of the fresh and spent dolomite sorbent after five cycles of SESR of biogas containing different concentrations of H_2S. 104

Table 4.6: Design assumption made to develop the base case flowsheet in Aspen Plus 116

Table 4.7: Range in which the different process variables are analysed. .. 116

Table 4.8: Effect of biogas composition on the heat recovered from SESR (heat losses considered). SESR conditions: S/CH_4 = 5.5, T = 600 ^oC, P = 10 bar, and 50% sorbent excess. 120

Table 4.9: Excess of heat not used that is remaining in the CO_2 stream as a function of the biogas composition. SESR conditions: S/CH_4 = 5.5, T = 600 ^oC, P = 10 bar, and 50% sorbent excess. 121

Table 4.10: Effect of SESR temperature on the composition of the solids circulating between SESR and REG. SESR conditions: S/CH_4 = 5.5, P = 10 bar, biogas = 60/40 vol.% CH_4/CO_2, and 50% sorbent excess. 125

Table 4.11: Effect of SESR temperature on the heat recovered from SESR (heat losses considered). SESR conditions: S/CH_4 = 5.5, P = 10 bar, biogas = 60/40 vol.% CH_4/CO_2, and 50% sorbent excess. 125

Table 4.12: Effect of SESR pressure on the composition of the solids circulating between SESR and REG. SESR conditions: S/CH_4 = 5.5, T = 600 ^oC, biogas = 60/40 vol.% CH_4/CO_2, and 50% sorbent excess. 129

Table 4.13: Effect of SESR pressure on the heat recovered from SESR (heat losses considered). SESR conditions: S/CH_4 = 5.5, T = 600 ^oC, biogas = 60/40 vol.% CH_4/CO_2, and 50% sorbent excess. 129

Table 4.14: Effect of S/CH_4 on the composition of the solids circulating between SESR and REG. SESR conditions: 600 ^oC, P = 10 bar, biogas = 60/40 vol.% CH_4/CO_2, and 50% sorbent excess. 132

Table 4.15: Effect of S/CH_4 ratio on the heat recovered from SESR (heat losses considered). SESR conditions: 600 ^oC, P = 10 bar, biogas = 60/40 vol.% CH_4/CO_2, and 50% sorbent excess. 133

Table 4.16: Optimal operating conditions with maximum H_2 purity for the biogas SESR configurations evaluated. SESR conditions: biogas = 60/40 vol.% CH_4/CO_2, and 50% sorbent excess. 135

Table 4.17: Operating conditions used in the simulations for the techno-economic analysis. 139

Table 4.18: Biogas and natural gas compositions used for the techno-economic analysis. 139

Table 4.19: Simulation results obtained for the three case studies proposed for the techno-economic analysis. 140

Table 4.20: Results for the main KPIs obtained for the three case studies proposed for the techno-economic analysis. 142

Table 4.21: Results of CO_2 capture and emissions obtained for the three case studies proposed for the techno-economic analysis. 142

Table 4.22: Main assumptions for the economic analysis. 143

Table 4.23: Total CAPEX and OPEX obtained for the SESR of biogas and natural gas. 144

Table 4.24: Thermodynamic assumptions of the biogas SESR unit..... 149

Table 4.25: Assumption of the three blocks that conform the SEDMES unit. 150

Table 4.26: Sensitivity analysis of the percentage of water removal in the SEDMES unit and outlet gas composition..... 151

Table 4.27: Specifications for the first distillation column of the DME purification train. 151

Table 4.28: Specifications for the second distillation column of the DME purification train. 151

Table 4.29: Results of the three synergies in terms of efficiencies and global yield of bio-DME production from the integration of biogas SESR and SEDMES. 157

Table I.1: Extra economic assumptions. 196

Table I.2: Complete results sets for the estimation of the CAPEX and OPEX of biogas and natural gas SESR. 196

ABSTRACT

In recent years, the importance of hydrogen as a future clean and renewable energy source has become more prominent as climate change and global warming have attracted increasing attention worldwide. However, most of the hydrogen produced comes from fossil resources, either through steam reforming (SR) of methane/natural gas and oil/naphtha or coal gasification, both without CO_2 capture. Therefore, advanced technologies have been developed to implement CO_2 capture into the process and to replace fossil resources by renewables.

This thesis focuses on the study of the production of renewable high-purity hydrogen from biogas using a novel catalytic reforming technology. This process is known as Sorption Enhanced Steam Reforming (SESR) since it combines the reforming reaction for H_2 production with in situ CO_2 separation. Thus, CO_2 capture is applied while improving the purity and yield of the H_2 produced due to Le Chatelier's principle.

In this framework, commercial Arctic dolomite and a 1%Pd/20%Ni-20%Co hydrotalcite-like material were used as CO_2 sorbent and catalyst, respectively, for the production of H_2 through biogas SESR.

The effect of biogas composition (with respect to CH_4 content) on H_2 production from biogas SESR was evaluated experimentally. The H_2 yield, H_2 selectivity, CH_4 conversion, H_2 purity, and CH_4, CO, and CO_2 concentrations in the effluent gas were analysed for different CH_4 and CO_2 compositions (vol.%) of the biogas. The results were compared with the biogas steam reforming (SR) process without CO_2 capture. High-purity (98.4 vol.%) and high-yield (91%) H_2 can be obtained by SESR of biogas (CH_4+CO_2) over a Pd/Ni-Co catalyst and using Arctic dolomite as a carbon dioxide sorbent.

The effect of the H_2S concentration (150, 350, 500, and 1000 ppm) in the biogas (60 CH_4/40 CO_2 vol./vol.%) on the performance of the SESR process was also studied. No catalyst deactivation due to H_2S poisoning was detected during cyclic SESR of biogas at 600 ^oC for H_2S concentrations of 150 and 350 ppm (five cycles). However, for 1000 ppm H_2S, a slight decrease in H_2 yield (between 4.5% and 10.8% points) and H_2 purity (between 2% and 3% points) was found.

In addition to the experimental proof of concept of the biogas SESR process, this work also addresses the SESR process design to optimise its efficiency and a techno-economic analysis. Different process flowsheets were designed in AspenPlus software and the economic analysis of the most promising one was carried out using biogas as feedstock. Natural gas was also used for comparison purposes. In the case of biogas, the lowest value of the levelised cost of hydrogen (LCOH) was obtained when the heat was provided to the calciner by indirect air combustion in an external burner (2.8 €/kg H_2 including CO_2 storage). In the case of natural gas using an indirectly heated calciner, the LCOH was only slightly lower (2.6 €/kg H_2 including CO_2 storage), indicating that biogas could be a potential substitute for natural gas, being renewable and economically competitive.

Finally, the integration of the biogas SESR process with the Sorption Enhanced Dimethyl Ether (DME) Synthesis (SEDMES) process is studied. SEDMES is a novel process for synthesizing DME in which water is removed in situ with a solid adsorbent, following the same concept based on Le Chatelier's principle as the SESR process. This work evaluated the production of bio-DME from biogas by efficiently integrating the SESR and SEDMES processes, achieving a final Cold Gas Efficiency (CGE) of 74%.

RESUMEN

En los últimos años, el hidrogeno ha cobrado importancia como futura fuente de energía limpia y renovable a medida que el cambio climático y el calentamiento global han atraído una atención cada vez mayor en todo el mundo. Sin embargo, en la actualidad, la mayor parte del hidrógeno proviene de recursos fósiles, ya sea mediante reformado con vapor de metano/gas natural y petróleo/nafta o gasificación de carbón, ambos sin captura de CO_2. Por lo tanto, se han desarrollado tecnologías avanzadas para implementar la captura de CO_2 en el proceso y sustituir los recursos fósiles por fuentes renovables.

Esta tesis se centra en el estudio de la producción de hidrógeno renovable de alta pureza a partir de biogás utilizando una novedosa tecnología de reformado catalítico con captura integrada de CO_2 (*Sorption Enhanced Steam Reforming*, SESR) En este proceso se aplica la captura de CO_2 con el objetivo de desplazar el equilibrio hacia la producción de hidrógeno debido al principio de Le Chatelier. Así, se consigue un mayor rendimiento y pureza del hidrógeno.

En esta tesis, se utilizaron dolomía ártica comercial como sorbente de CO_2, y un catalizador de tipo hidrotalcita con composición 1%Pd/20%Ni-20%Co para la producción de H_2 a través del proceso SESR de biogás.

Así, se evaluó experimentalmente el efecto de la composición del biogás (con respecto al contenido de CH_4) en la producción de H_2. Además, se analizaron el rendimiento de H_2, la selectividad de H_2, la conversión de CH_4, la pureza de H_2 y las concentraciones de CH_4, CO y CO_2 en el producto para diferentes composiciones de CH_4 y CO_2 (% en volumen) en el biogás. Los resultados se compararon con el proceso convencional de reformado con vapor de biogás sin captura de CO_2. Se puede obtener H_2 de alta pureza (98,4% en volumen) y alto rendimiento (91%) mediante el reformado mejorado con captura integrada de CO_2 de biogás (CH_4+CO_2) sobre un catalizador de Pd/Ni-Co y utilizando dolomía ártica como sorbente de CO_2.

También se estudió el efecto de la concentración de H_2S (150, 350, 500 y 1000 ppm) en el biogás (60 CH_4/40 CO_2 vol./vol.%) sobre el rendimiento del proceso SESR. No se detectó desactivación del catalizador debido a

envenenamiento por H_2S durante cinco ciclos de reformado mejorado con captura de CO_2 de biogás a 600 ^oC para concentraciones de H_2S de 150 y 350 ppm. Sin embargo, para 1000 ppm de H_2S, se encontró una ligera disminución en el rendimiento de H_2 (entre 4,5% y 10,8%) y en la pureza del H_2 (entre 2% y 3% en volumen).

Además del trabajo experimental de reformado mejorado con captura integrada de CO_2 de biogás, en esta tesis también se aborda el diseño del proceso SESR para optimizar su eficiencia, así como un análisis tecno-económico. Se diseñaron diferentes diagramas de flujo del proceso con el software AspenPlus y se realizó el análisis económico del más prometedor utilizando biogás como materia prima. También se utilizó gas natural con fines comparativos. En el caso del biogás, el valor más bajo del coste normalizado del hidrógeno (*levelised cost of hydrogen*, LCOH) se obtuvo cuando el calor se aportaba al calcinador mediante combustión indirecta de aire en un quemador externo (2,8 €/kg H_2 incluido el almacenamiento de CO_2). En el caso del gas natural el coste LCOH para un escenario similar fue sólo ligeramente inferior (2,6 €/kg H_2, incluido el almacenamiento de CO_2), lo que indica que el biogás podría ser un potencial sustituto del gas natural, al ser renovable y económicamente competitivo.

Finalmente, se estudia la integración del proceso de reformado mejorado con captura integrada de CO_2 de biogás con el proceso mejorado de síntesis de Dimetil Éter con adsorción de H_2O (*Sorption Enhanced Dimethyl Ether (DME) Synthesis*, SEDMES). SEDMES es un proceso novedoso para sintetizar DME en el que el agua se elimina in situ con un adsorbente sólido, siguiendo el mismo concepto basado en el principio de Le Chatelier que el proceso de reformado mejorado. En esta tesis se evalúa la producción de bio-DME a partir de biogás integrando eficientemente los procesos SESR y SEDMES, logrando una eficiencia de gas frío (*Cold Gas Efficiency*, CGE) final del 74%.

THESIS STRUCTURE

This thesis dissertation is organized into five chapters. The first two chapters are dedicated to explaining the framework of the thesis. Then, the methodologies and results are discussed in Chapters 3 and 4, and the conclusions are collected in Chapter 5. Fig. I shows an outline of the structure of the thesis dissertation.

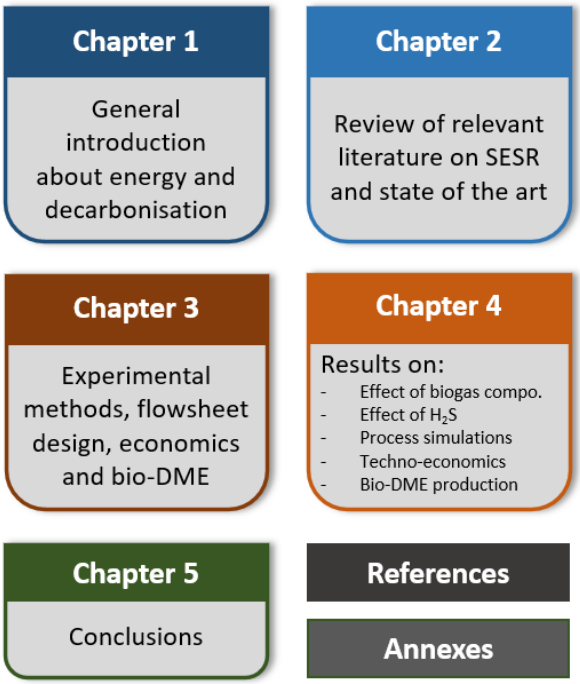

Fig. I: Outline of the structure of the thesis dissertation.

In **Chapter 1**, a general introduction to the energy context and the pillars of decarbonisation are depicted. This chapter also includes the objectives of the thesis. **Chapter 2** addresses a review of the literature on SESR and a description of the state of the art of the topics covered in the subsequent chapters.

In **Chapter 3**, the experimental and modelling methodologies are included. The experimental methodology is applicable to the study of the effect of the biogas composition (i.e., CH_4/CO_2 ratio) and to the study of the

effect of the biogas H_2S content. Moreover, the modelling methodology focuses on the flowsheet design of the process applied to both the techno-economic analysis and the production of bio-DME by integrating the biogas SESR and SEMDES technologies.

In **Chapter 4**, the results of the different works are collected and discussed. The first three sections correspond to the three articles that make up the compendium of publications of this thesis, as follows:

- Effect of biogas composition on H_2 production by SESR of biogas.
- Effect of H_2S on H_2 production by SESR of biogas.
- Process simulations of H_2 production by SESR of biogas.

The fourth section, related to the simulation of the SESR process, shows the research carried out in collaboration with Cranfield University (UK) during a short stay as a visiting researcher. The fifth section shows the results and discussion of the techno-economic analysis of biogas SESR, carried out in collaboration with Cranfield and Newcastle Universities (UK). The last section describes the work performed in collaboration with TNO (The Netherlands) on the topic of the production of bio-DME as an H_2 carrier by coupling the biogas SESR and SEDMES processes.

Finally, **Chapter 5** presents a summary of the main conclusions of this thesis.

Chapter 1

INTRODUCTION

1.1. ENERGY AND CLIMATE CHANGE

As a modern society, we are facing two massive challenges related to sustainability: climate change and global warming. Climate change is driven by the dominance of fossil fuels in the energy sector, the associated greenhouse gas emissions, and increasing demand for energy [1].

As established by the Kyoto Protocol [2], the gases responsible for the greenhouse effect that contribute the most to the global warming are the so-called greenhouse gases (GHGs): carbon dioxide (CO_2), methane (CH_4), nitrous oxide (N_2O), hydrofluorocarbons (HFCs), perfluorocarbons (PFCs) and sulphur hexafluoride (SF_6). A recent analysis by the *World Meteorological Organization* (WMO) showed the global surface average mole fractions of CO_2 (413.2 ± 0.2 ppm), CH_4 (1889 ± 2 ppb) and N_2O (333.2 ± 0.1 ppb), which constitute, respectively, 149%, 262% and 123% of pre-industrial (before 1750) mole fraction levels [3].

Among them, CO_2 and CH_4 have gained special relevance due to their effect. CO_2 is the most important anthropogenic GHG in the atmosphere. Its release and accumulation have led to an increase in atmospheric CO_2 levels over the years, well above pre-industrial levels. This is considered the main factor that contributes to global warming through the greenhouse effect [3,4]. The concentration of CO_2 in the atmosphere has been collected at the Mauna Loa Observatory in Hawaii since 1958, and is represented by the Keeling curve shown in Figure 1.1, where it can be clearly seen that we are now above 400 ppm and increasing.

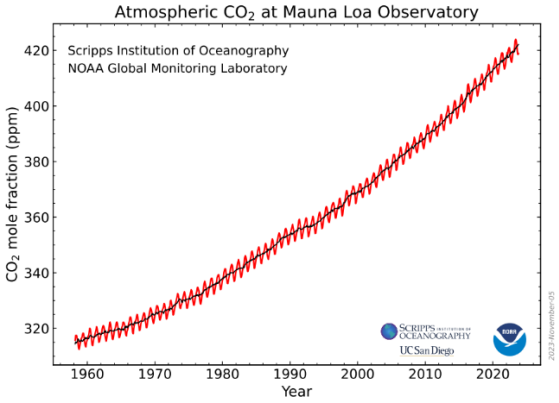

Figure 1.1: The keeling curve. CO_2 concentration at Mauna Loa Observatory [5].

Since CO_2 is the gas that contributes the most to global warming, the measurement of GHG emissions is based on the concept of CO_2 equivalents, globally recognised for discussing any result associated with GHG emissions. Thus, one ton of CO_2eq is the universal unit of measurement for the global warming potential (GWP) of GHGs, where GWP is defined as the factor that describes the impact of the radiation force (degree of damage to the atmosphere) of one unit of a given GHG per unit of CO_2 [6].

To drive action against climate change, we need to reduce greenhouse gas emissions on a global scale. It is then crucial to address the distribution of emissions by sector. The *Climate Watch* and the *World Resource Institute* have recently published a chart showing the breakdown of global greenhouse gas emissions per sector (Figure 1.2).

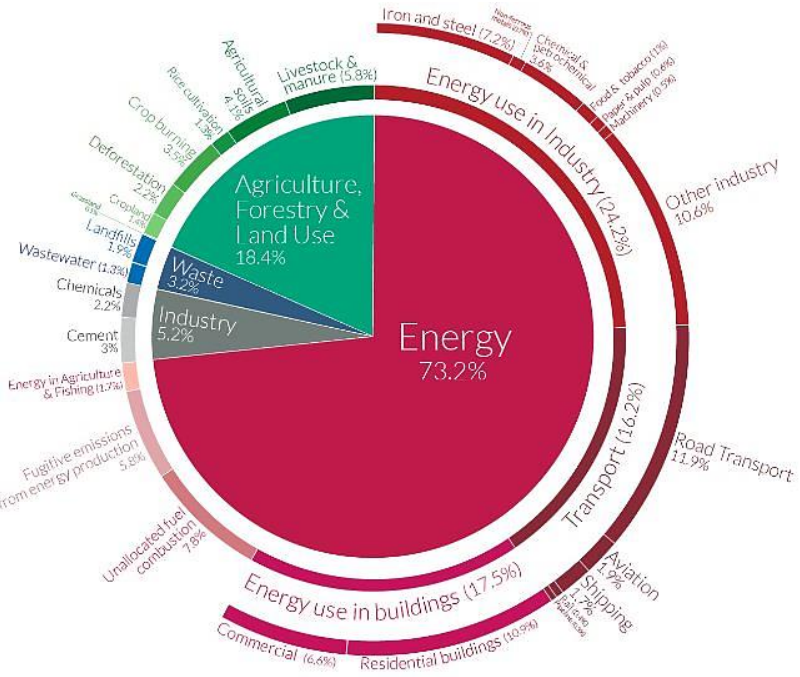

Figure 1.2: Distribution of the global greenhouse gas emissions by sector [7].

As can be seen in Figure 1.2, almost three quarters of the emissions (73.20%) come from the energy sector, highlighting the need for action in this sector in order to mitigate climate change and GHG emissions.

As a consequence of this problem, today's society is facing and implementing an energy transition and a net zero emissions (NZE) strategy with the aim of keeping global warming at no more than 1.5 °C, as claimed in the Paris Agreement [8]. To achieve this, the *European Climate Law* [9] says that the emissions must be reduced by at least 55% by 2030 compared to 1990 levels in light of the goal of climate-neutrality by 2050.

As the *International Energy Agency* (IEA) recently stated, achieving rapid reductions in CO_2 emissions in the coming years to achieve NZE requires a broad range of policy and technology deployment [10]. The driving force for changing the current energy system to achieve these ambitious goals is the decarbonisation of the global energy system through the so-called energy transition. The main pillars of decarbonisation are shown in Figure 1.3: energy efficiency, behavioural changes, electrification, renewable energy, hydrogen and hydrogen-based fuels, bioenergy, and Carbon Capture, Utilization and Storage (CCUS).

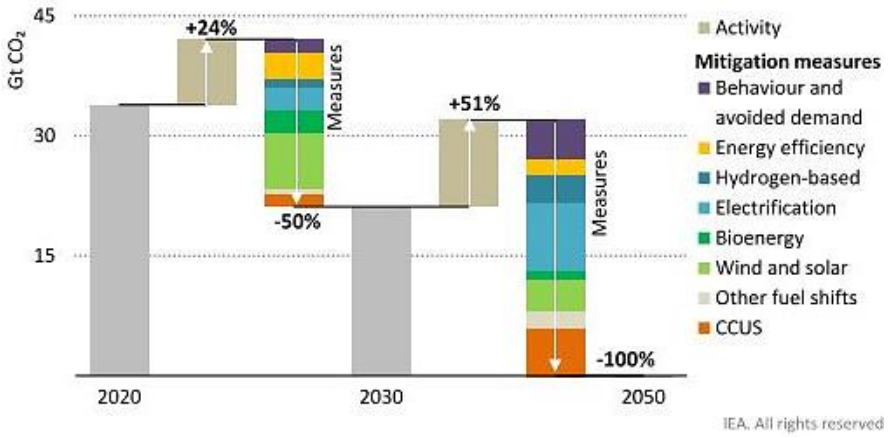

Figure 1.3: Emissions reduction by mitigation measure in the NZE, 2020-2050 [10].

Some of these pillars have been addressed in this work, providing a holistic approach to this thesis under the topic *Single-step biogas conversion to bio-hydrogen: sorption enhanced catalytic reforming*.

1.2. PILLARS OF DECARBONISATION ADDRESSED IN THIS THESIS

In this section, the main pillars of decarbonisation related to the topic of this thesis will be discussed in more detail.

1.2.1. Carbon Capture Utilisation and Storage (CCUS)

As mentioned above, one of the pillars of decarbonisation is Carbon Capture, Utilization and Storage (CCUS) from stationary point sources. This is the only group of technologies that contribute to directly reducing emissions in key sectors and removing CO_2 to balance emissions that cannot be avoided. As explained in the *Energy Technology Perspectives* report by the International Energy Agency (IEA) [11], achieving net zero will be impossible without CCUS, as shown in Figure 1.4.

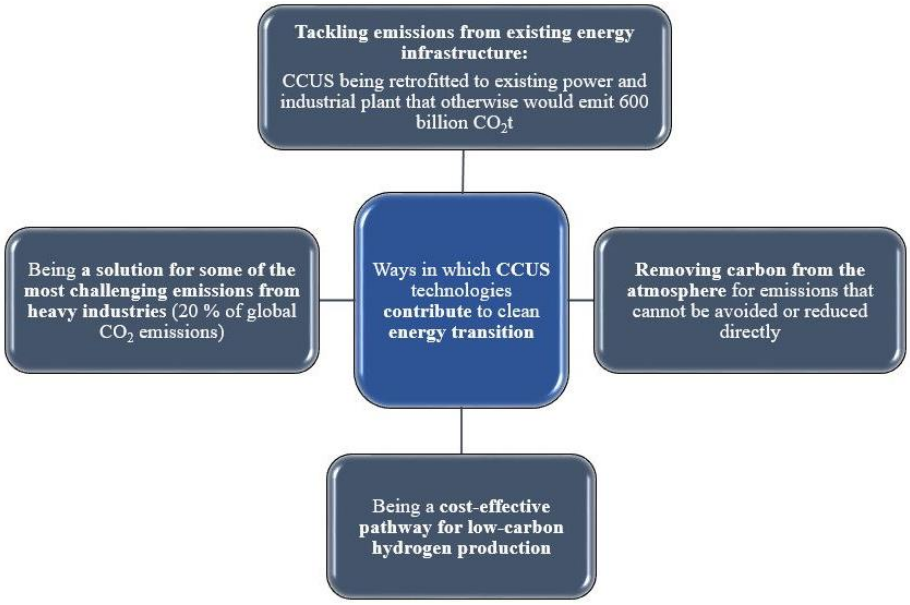

Figure 1.4: Ways CCUS technologies contribute to the clean energy transition (graph adapted from [11]).

This thesis focuses on a cost-efficient pathway for low-carbon hydrogen production: Sorption Enhanced Steam Reforming (SESR) of biogas.

The first step in the CCUS strategy is to capture the CO_2. This step contributes to 70-80% of the total cost of the CCUS technology chain [12]. Depending on the plant configuration, the partial pressure of carbon dioxide

and the pressure of the gas stream, three different approaches are proposed to capture carbon dioxide [13]: post-combustion, pre-combustion and oxy-combustion (see Figure 1.5):

- Post-combustion → CO_2 is captured from flue gases before emission to the atmosphere in the temperature range of 120-180 ^{o}C [12]. The biggest challenge is the low volumetric concentration of CO_2 in the flue gas (3-20%) and the high flow that is almost at atmospheric pressure. In most cases, CO_2 removal is carried out by gas scrubbing with solvents (i.e., amines), but dry adsorption technologies and membranes can also be used for post-combustion CO_2 capture [14].

- Pre-combustion → This route is used to decarbonise the fuel before or even during combustion. The fuel is transformed into a mixture of H_2 and CO_2 or syngas. The recovered rich H_2 stream can be used as fuel or raw material for chemical production, among other uses [15]. The pre-combustion approach is mainly used in integrated gasification combined cycle (IGCC) plants, fertilizer or hydrogen production plants [13].

- Oxy-combustion → Fuels are burnt in an O_2/CO_2 mixture to avoid dilution of flue gases with N_2 from the air. The use of pure oxygen requires an Air Separation Unit (ASU). It is estimated that the ASU represents ~85% of the total energy requirement in this approach. Thus, the consumption of O_2 makes this technology more expensive and involves an energy penalty of around 7-11% [12]. In oxy-combustion, the CO_2 concentration in the final gas increases, since it is not diluted with N_2, helping the separation of CO_2 [15]. The exhaust gases mainly consist of CO_2 and water vapour, and high-purity CO_2 can be easily separated [14].

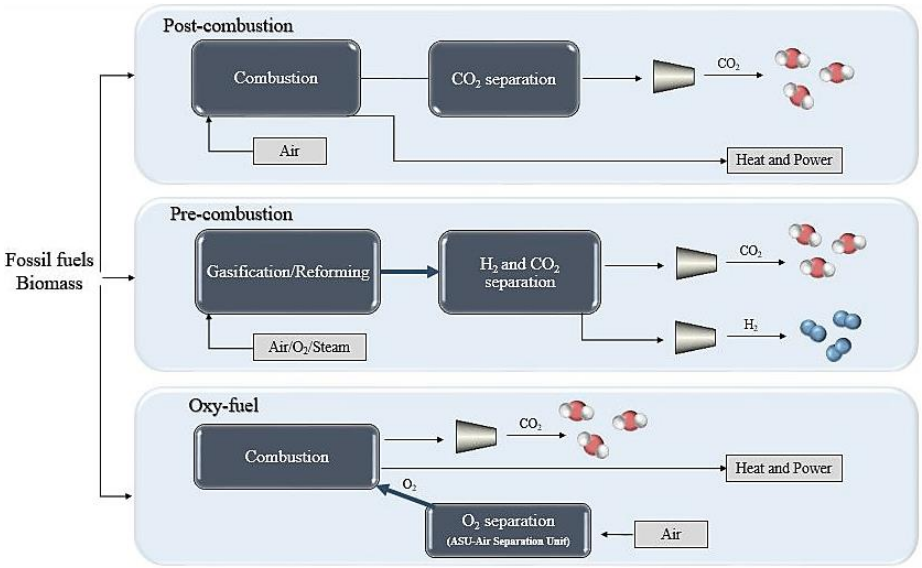

Figure 1.5: Classification of CO_2 capture technologies (figure adapted from [16]).

Once CO_2 is captured, it can be either used or stored. Carbon dioxide storage involves injecting the captured CO_2 into a deep underground geological reservoir of porous rock properly structured to prevent the CO_2 from escaping to the atmosphere [11]. CO_2 is permanently trapped through several mechanisms, such as structural trapping by the seal, trapping by solubility in pore space water, residual trapping in individual or groups of pores, and mineral trapping by reacting with reservoir rocks to form carbonate minerals. Mineral carbonation and geological storage are examples of CO_2 storage options [11,17].

In the SESR process investigated in this thesis, a pure CO_2 stream can be produced by regeneration of the spent CO_2 sorbent. This stream could be suitable for storage or susceptible to utilization depending on the quality requirements.

CO_2 utilisation is a benefit when compared to storage, as it involves the reuse of CO_2 to convert it into a resource [18]. Future prospects for reducing CO_2 emissions include the development of new strategies to recycle CO_2, e.g., into energy carriers and chemical intermediates [19].

Conversion to chemicals and fuels, mineral carbonation, enhanced oil recovery, biological conversion, and direct utilisation are the main categories

of CO_2 utilisation [18]. In the context of the present thesis, chemical conversion has been explored. Carbon dioxide can be converted to fuels such as methane, methanol, and syngas [18]. Recently, the CO_2 conversion to dimethyl ether (DME) has received increasing attention because DME can be used as an intermediate product to synthesise several value-added products, in addition to being an alternative fuel itself [19]. In the present thesis, the utilisation of CO_2 captured by the SESR process in the sorption enhanced DME production process, SEDMES, was evaluated.

1.2.2. Bioenergy and biogas

Another pillar of the decarbonisation related to the topic of this thesis is bioenergy, since the research conducted focuses on the use of biogas for H_2 production through the SESR process.

Biomass can be considered an alternative to fossil fuels, as it is a carbon neutral energy source. The total biomass potential estimated by various studies ranges from 200 to 700 EJ/year. It currently provides approximately 10% of the world's energy supply [20] and it has been claimed that biomass could meet energy demand by more than 25% by 2050 [21]. By combining bioenergy (BE) with CCS, the so-called BECCS concept emerges, which includes the transformation of biomass into power, heat, steam, hydrogen or other gaseous or liquid fuels, combined with technologies that can capture the CO_2 emitted in biomass conversion [22].

In a BECCS system, CO_2 is removed from the atmosphere through biomass growth during photosynthesis and then released again when the biomass is burnt or used by thermochemical processes (i.e., reforming) for fuel or energy production [20,23]. Because BECCS simultaneously provides energy and reduces atmospheric CO_2 concentration, it is considered one of the most promising Negative Emissions Technologies (NETs) and many climate scientists now include it in *Integrated Assessment Models* (IAMs) in modelling pathways to meet 1.5-2 ^{o}C emissions trajectories. BECCS net emissions will be negative when the amount of CO_2 stored is greater than that emitted during biomass production, transport, conversion, and utilisation [24].

The link of this thesis with bioenergy is based on the use of biogas. Biogas is a renewable resource produced by the anaerobic digestion process

of the biodegradable residual biomass from various origins, such as animal waste, sewage sludge from wastewater treatment plants, and municipal waste from landfills.

Since biogas is produced commercially in large quantities and the availability of CO_2 and CH_4 is relatively inexpensive, the conversion of biogas into higher-value products by catalytic reforming methods (dry reforming, steam reforming, and partial oxidative reforming) to produce syngas/hydrogen is becoming attractive [25]. Among all higher-value products, hydrogen is considered a critical player in future energy scenarios, although most hydrogen currently comes from non-renewable resources, mainly natural gas [26]. Therefore, the actual environmental benefit of hydrogen requires its production from renewable sources, such as biomass.

1.2.3. Hydrogen and hydrogen-based fuels

Hydrogen is the lightest of the known elements, the most abundant gas in the universe and has the highest energy content per weight unit among conventional fuels (the energy content of H_2 is about three times that of gasoline, ranging from 120 to 142 MJ/kg). It is an important chemical used in various fields, such as clean energy for engines and fuel cells, petroleum refining, the chemical industry (such as methanol and ammonia production), and fertilizer manufacture [1,21,27].

In recent years, the importance of hydrogen as a future source of clean and renewable energy has become more relevant as environmental issues such as climate change and global warming have caused worldwide concern [1]. For example, in 2020, about 90 Mt of H_2 were used and about 80% were produced from fossil fuels (all the rest came from waste gases). Therefore, most of the H_2 produced is considered unabated. The H_2 demand comes mainly from refining and industrial uses, as explained in the International Energy Agency's *Global Hydrogen Review 2021* [28]. Industry is reported to account for more than 50 Mt H_2 mainly for feedstock. Chemical production accounts for a demand of about 45 Mt H_2, of which about three-quarters is for ammonia production and one-quarter for methanol production. The remaining 5 Mt H_2 are consumed in the direct reduction of iron (DRI) process for steelmaking.

Hydrogen demand will also increase in the Net Zero Emissions scenario. As can be seen in Figure 1.6, the path to net-zero emissions in 2050 requires substantially increases use of hydrogen in existing applications, such as the chemical industry, and significant use of hydrogen and hydrogen-based fuels for new uses in heavy industry, heavy road transport, shipping, and aviation. In the Net Zero Emissions scenario, hydrogen demand increases almost six-fold to 530 Mt H_2 in 2050, with half of this demand coming from industry and transport. As reflected by the *International Energy Agency*, synthetic fuels (synfuels) made from hydrogen and CO_2 captured from biomass applications, such as bioenergy-fired power or biofuel production, will also be used in energy applications in this scenario and are therefore important for achieving the sustainability and emissions targets foreseen for 2050.

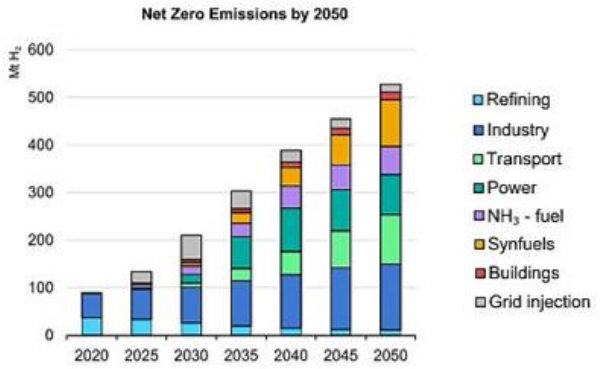

Figure 1.6: Hydrogen demand by sector in the announced pledges and Net Zero Emissions scenarios, 2020-2050 [28].

The main routes to produced H_2 include water splitting, and thermochemical and biological conversion [21]. Today, 96% of H_2 is produced from fossil resources, in particular from natural gas, oil and oil derivatives, and coal, but these processes are costly and environmentally unfriendly. There are other ways to produce sustainable H_2, such as the valorisation of bioresources (i.e., biogas) through thermochemical conversion [27,29]. Biogas is produced by microorganisms under anaerobic conditions as a result of the natural degradation of organic matter. The potential of this bioresource is enormous. In fact, the EU is the world leader in electricity production from biogas, with more than 10 GW installed and 17400 biogas plants [30].

In this thesis, the production of hydrogen from biogas will be investigated using the SESR process. In addition, as mentioned above, the efficiency of the production of sustainable DME will also be evaluated by integrating the production process with the biogas SESR process. DME is a fuel that can be an excellent substitute for diesel in ignition engines. Due to its chemical structure, with 35 wt% oxygen and no carbon-carbon bonds, the combustion of this compound reduces the amount of pollutants such as hydrocarbons, carbon monoxide, NO_x, and soot and particulates in the exhaust gases [31,32]. DME production will be studied in this thesis by an emerging technology, the sorption enhanced DME synthesis (SEDMES) [33].

1.3. THESIS OBJECTIVES

This thesis is framed in the context of the energy transition for a more sustainable society. The main objective is to produce high-purity, low-carbon hydrogen from biogas, regardless of the composition of the biogas, through an emerging process known as Sorption Enhanced Steam Reforming (SESR).

To pursue this general objective, the following specific objectives were defined and addressed:

- **First specific objective** → To study the effect of the biogas composition (CH_4 and CO_2 concentrations) on the performance of the SESR process.

The influence of CH_4 and CO_2 concentrations (vol.%) in the biogas on the process performance was evaluated experimentally, together with a thermodynamic analysis of the process by simulation, to achieve this objective. The process parameters studied include H_2 yield, H_2 selectivity, CH_4 conversion, H_2 purity, and CH_4, CO and CO_2 concentrations in the effluent gas. In addition, the experimental results of the biogas SESR were compared with the biogas steam reforming (SR) process without in situ CO_2 capture.

- **Second specific objective** → To study the effect of biogas H_2S content on the hydrogen production by the SESR process.

Cyclic SESR experiments were conducted with biogas streams of a set CH_4/CO_2 composition (60/40 vol.%) and different concentrations of H_2S: 150, 350, 500, and 1000 ppm. Experiments were also carried out in the absence of H_2S for comparison purposes. To figure out the fate of sulphur during the SESR process, both the spent catalyst and sorbent were characterised by X-ray diffraction (XRD), Inductively Coupled Plasma Optical Emissions Spectrometry (ICP-OES), Scanning Electron Microscopy – Energy Dispersive X-ray spectroscopy (SEM-EDX), N_2 adsorption to determine the specific surface area (BET), and X-ray photoelectron spectroscopy (XPS).

- **Third specific objective** → To estimate the energy efficiency of the biogas SESR process by simulation of the hydrogen production under different process configurations.

To achieve this objective, three process configurations were simulated: 1) SESR with a H_2-fired calciner for sorbent regeneration, 2) SESR with a biogas-fired calciner for sorbent regeneration, and 3) SESR with a biogas-fired calciner for sorbent regeneration and a pressure swing adsorption (PSA) unit for H_2 purification. The process was analysed under air (for all the configurations) and oxy-fuel combustion (when using biogas as fuel in the calciner). A sensitivity analysis based on the effect of biogas composition, SESR temperature, SESR pressure, and S/CH_4 ratio, alongside a techno-economic analysis of H_2 production by biogas SESR were performed. CAPEX, OPEX, and levelised cost of hydrogen (LCOH) were estimated. Besides, the production of H_2 using biogas and natural gas as feedstock to the SESR process was compared according to the economic performance.

Finally, a study on the efficiency of bio-DME production (as hydrogen carrier) from biogas was carried out by simulation integrating the biogas SESR and SEDMES processes according to their existing synergies.

Chapter 2

REVIEW OF RELEVANT LITERATURE

This chapter provides a technical overview of the state of the art of the biogas SESR process.

2.1. GENERAL OVERVIEW OF SESR

Hydrogen is a versatile feedstock and an attractive energy carrier, positioned as one of the main pillars for the imminent energy transition towards climate change mitigation [34]. However, most of hydrogen produced comes from fossil resources, either by steam reforming (SR) of methane/natural gas and oil/naphtha, or from coal gasification without CO_2 capture [29].

The conventional SR process usually operates at high temperatures (700-1000 ºC) and pressures (15-40 bar). In this process, the endothermic reforming reaction takes place in high-alloy reformer tubes where the catalyst is placed, which in most cases is Ni-based. The reformer operates using typical steam to carbon (S/C) ratios of 2 to 6, and external gas burners heat the reformer tubes [21,35]. The process is endothermic and produces low yield and purity H_2, resulting in the need for several high and low-temperature water-gas shift (WGS) reactors, as well as a hydrogen purification unit.

To improve the efficiency of conventional SR by reducing the total energy consumption, different advanced technologies have been studied, such us sorption enhanced steam methane reforming (SE-SMR), oxidative SMR (O-SMR), chemical looping, photocatalytic SRM, thermo-photo hybrid SRM, solid oxide fuel cell (SOFC), plasma SRM, or electro-catalytic SRM [36]. In this thesis, the sorption enhanced steam reforming (SESR) process is studied.

Rostrup-Nielsen reported that the concept of sorption enhanced was first described in 1865 [37]. In 1933, Roger Williams published a patent for a process in which hydrogen is produced by reacting steam and methane in the presence of a mixture of catalyst and lime [38]. A few years later, Goring and Retallick published another patent based on a process carried out in a fluidised bed for the production of H_2 using a reforming catalyst and a CO_2 acceptor [39].

Sorption enhanced steam reforming (SESR) has become a novel intensification process of conventional SR technology [40]. This process combines the reforming reaction for hydrogen production with the in situ CO_2 separation in a single step. During the steam reforming (SR) of methane, the steam reforming reaction (Eq. 2.1) coexists with the water-gas shift (WGS) reaction (Eq. 2.2).

$$CH_4 + H_2O \leftrightarrow CO + 3H_2 \qquad \Delta H_r^0 = +206 \text{ kJ mol}^{-1} \qquad \text{Eq. 2.1}$$

$$CO + H_2O \leftrightarrow CO_2 + H_2 \qquad \Delta H_r^0 = -41 \text{ kJ mol}^{-1} \qquad \text{Eq. 2.2}$$

For carbon dioxide separation, natural CaO based materials are widely used in high-temperature CO_2 adsorption due to their high CO_2 capture capacity, fast CO_2 carbonation/calcination kinetics, low cost, and wide availability. Therefore, CaO sorbents are typically used in SESR processes, despite their lower reactivity after multiple carbonation/calcination cycles.

CO_2 reacts with CaO and is converted into a solid calcium carbonate through the carbonation reaction (Eq. 2.3). The overall sorption enhanced steam reforming (SESR) reaction of methane is shown in Eq. 2.4:

$$CaO_{(s)} + CO_2 \leftrightarrow CaCO_{3(s)} \qquad \Delta H_r^0 = -178 \text{ kJ mol}^{-1} \qquad \text{Eq. 2.3}$$

$$CH_4 + 2H_2O + CaO_{(s)} \rightarrow 4H_2 + CaCO_{3(s)} \qquad \Delta H_r^0 = -13 \text{ kJ mol}^{-1} \qquad \text{Eq. 2.4}$$

During SESR, as CO_2 is removed in situ from the gas phase by the sorbent (Eq. 2.3), the thermodynamic equilibrium of the methane steam reforming (Eq. 2.1) and water-gas shift (Eq. 2.2) reactions shifts towards the products side according to the Le Chatelier's principle, which enhances the production of hydrogen in one single reactor. Shifting the equilibrium towards H_2 production results in an increase in H_2 yield and also in H_2 purity and reactant conversion [41]. Furthermore, it allows the use of lower reaction temperatures (typically 550-650 °C) than in conventional SR processes while achieving high H_2 purities.

A simplified schematic of the SESR concept is shown in Figure 2.1, where it can be seen that the SESR reactor consists of an active bed containing the catalyst and sorbent materials. Therefore, the conversion reactions and in situ CO_2 sorption simultaneously occur [41].

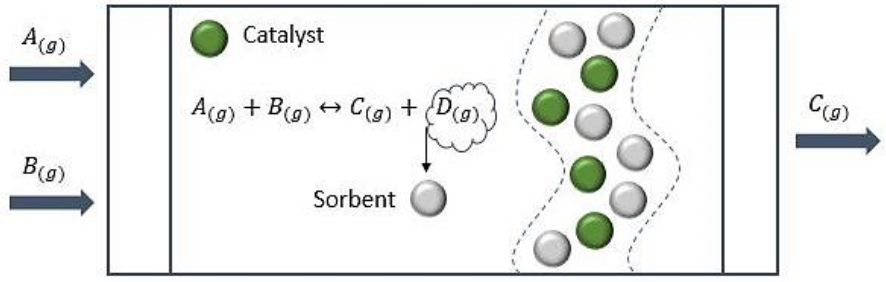

Figure 2.1: Simplified schematic of a SESR reactor (Figure adapted from [41]).

2.1.1. Thermodynamics of SESR

The benefits of adding CaO to conventional SR can be understood from a thermodynamic point of view [42]. B. Balasubramanian et al. [43] compared the equilibrium molar percentage of hydrogen in the product gas for conventional SR and SESR as a function of temperature at 15 atm and a steam to methane ratio of 4 (see Figure 2.2). It can be observed that in conventional SR the H_2 content increases with temperature and a maximum H_2 content of 76% is reached at 850 ^oC. The endothermic reforming process is the driving force for this increase in H_2 concentration.

In the case of SESR, when CaO is present in the system, two equilibrium lines can be seen based on the formation of $Ca(OH)_2$. The bottom line indicates the formation of $CaCO_3$ and calcium hydroxide ($Ca(OH)_2$) during the reforming step. Under the conditions selected in Figure 2.2, $Ca(OH)_2$ begins to decompose at approximately 600 ^oC and the two lines converge at a slightly higher temperature. At 650 ^oC, the H_2 concentration reaches a maximum value of around 96%, much higher than that obtained in conventional SR. It is due to the equilibrium shift caused by the in situ CO_2 removal. It implies that during SESR at lower temperatures, most of the CO and CO_2 can be converted, while the main impurity that remains unreacted will be CH_4. At higher temperatures, more CH_4 is converted, causing carbon oxides to become the major impurities.

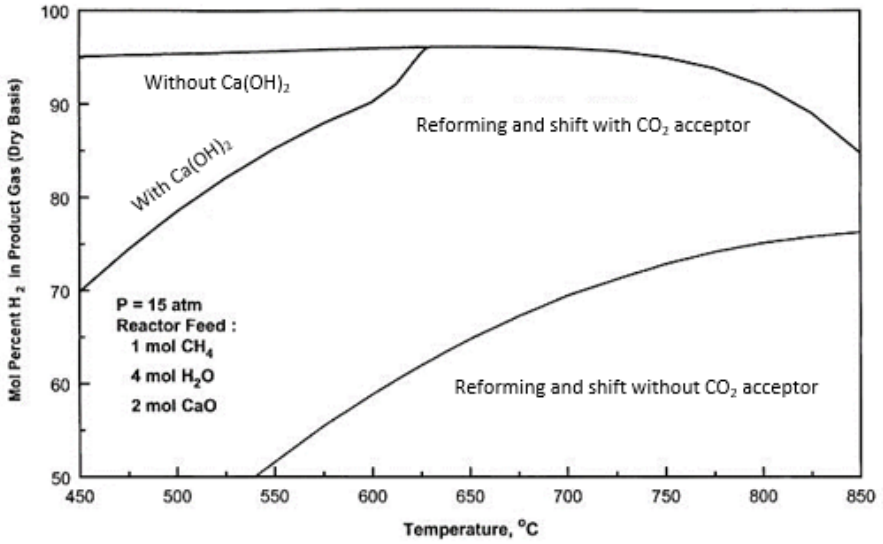

Figure 2.2: Equilibrium calculations to estimate the H_2 content as a function of temperature during a reforming process with and without a CO_2 acceptor [43].

In a commercial reforming process, the sorbent must be used in many carbonation-regeneration cycles [43]. With the presence of CaO, CO_2 sorption occurs by carbonation (Eq. 2.3), while regeneration occurs through calcination (reverse of Eq. 2.3) by raising the temperature beyond the equilibrium of the carbonation reaction depending on the CO_2 partial pressure ($p_{CO2,eq}$) in the surrounding gas [40]. The equilibrium partial pressure of CO_2 as a function of temperature in an air atmosphere is shown in Figure 2.3, reported by A. Ortiz et al. [44]. This diagram may be useful to select the experimental regeneration temperature under this atmosphere.

Although the decomposition of $CaCO_3$ in a CO_2-free atmosphere can be thermodynamically favoured over a wide range of temperatures, a temperature of at least 800 °C is recommended to ensure adequate decomposition kinetics [44].

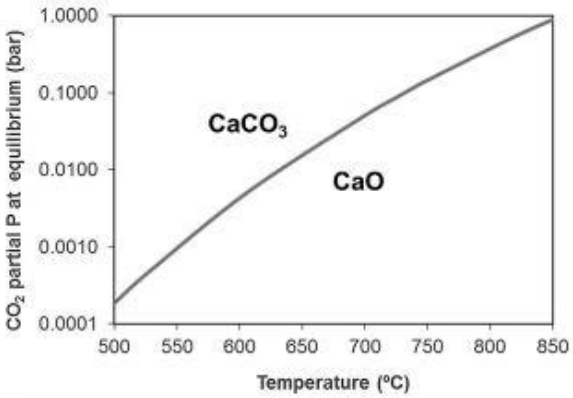

Figure 2.3: Thermodynamic study on the effect of the temperature and CO_2 partial pressure at equilibrium on the conversion of $CaCO_3$ to CaO in air [45].

2.1.2. The catalyst and the sorbent in SESR

2.1.2.1. The sorbent

CaO-based materials are widely used for high-temperature CO_2 capture due to their low cost, effectively CO_2 removal, and suitable kinetics. Research works on CO_2 sorbents based on solid oxides usually focus on the behaviour of the material over several cycles, analysing sintering, sorption capacity or mechanical stability to avoid deactivation of the sorbent throughout subsequent CO_2 sorption-desorption cycles [46–50].

The reversible gas-solid carbonation reaction of CaO with CO_2 occurs through two different stages as can be seen in Figure 2.4, the fast regime and the slow regime. As explained by Andy N. Antzaras [4], during the initial stage, known as the kinetically controlled regime, the rate-controlling step for carbonation is the rapid surface reaction between CO_2 and CaO that occurs at the interface of the product layer and the unreacted CaO core. As $CaCO_3$ formation progresses, the overall CO_2 capture process is mainly influenced by the diffusion of CO_2 through the $CaCO_3$ product layer.

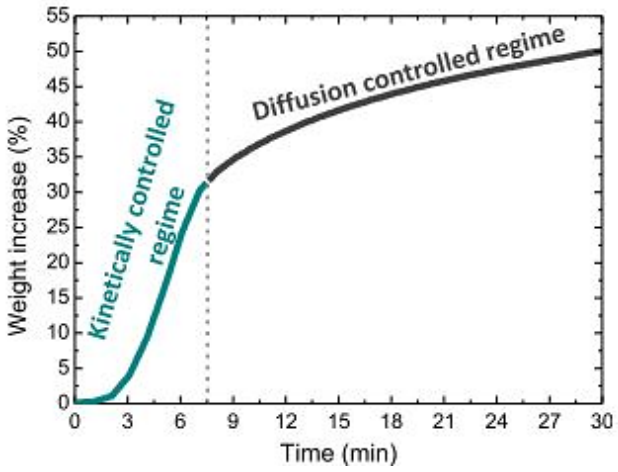

Figure 2.4: CO_2 uptake capacity of limestone-derived CaO through two reaction regimes [4].

Therefore, the second slow stage is known as the diffusion controlled regime, where, as the product layer thickens, the availability of CO_2 to react with the CaO active sites becomes limited. The conversion profile of CaO can be different depending of the pore network structure of the sorbent particle [50] (see Figure 2.5). Of all the cases, the one most frequently observed with natural sorbents is the case in which diffusional resistance and blockage of narrow pores occurs (Figure 2.5d).

On the other hand, a typical deactivation profile during a long number of carbonation/calcination cycles for limestone is shown in Figure 2.6. The deterioration effect on the cyclic stability of these sorbents is caused by the high temperatures used during regeneration. This effect has been attributed in the literature to the low Tammann temperature of the formed $CaCO_3$ and consequently to the intense agglomeration of the regenerated CaO particles [4]. A tentative mechanism of textural transformations that may take place during carbonation/calcination cycles is shown in Figure 2.7 [51].

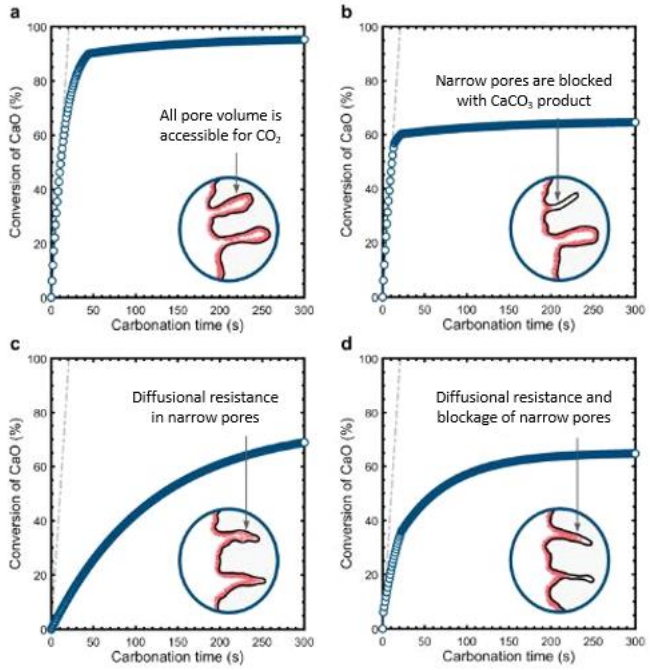

Figure 2.5: Conversion profiles of CaO typically observed for different pore size distributions [50].

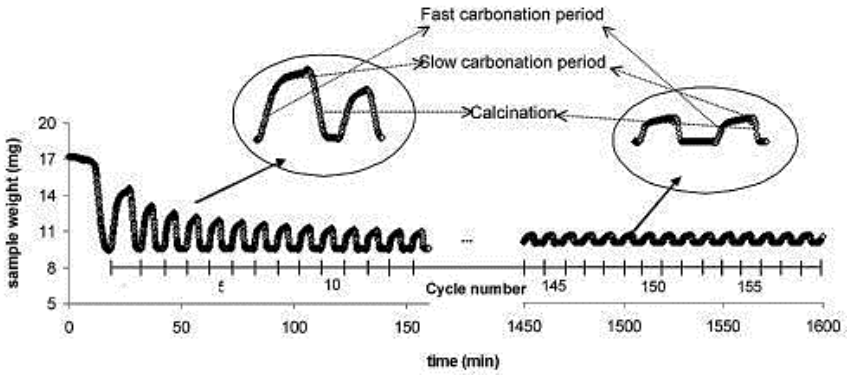

Figure 2.6: Typical weight change vs. time for a repeated number of calcination/carbonation cycles [52].

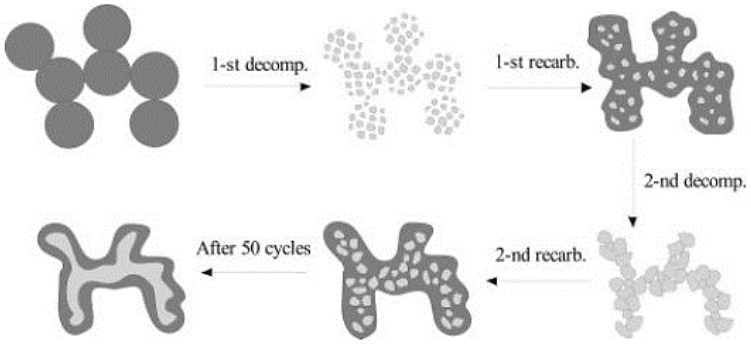

Figure 2.7: Scheme of the textural transformation of CaO upon cycling. The $CaCO_3$ phase is represented in dark grey, while CaO in light grey [51].

Figure 2.7 illustrates that when freshly calcined sorbent undergoes recarbonation, it tends to be incomplete because the particles shrink during the first decomposition. In subsequent cycles, the newly formed CaO grains tend to grow and agglomerate and the connections between neighbouring CaO grains gradually thicken. This process results in the formation of an interconnected network of CaO particles. In this way, only the outer layer of the CaO network is recarbonated.

Among natural CaO-based sorbents, the low cost and wide availability of natural limestone ($CaCO_3$) explain its industrial competitiveness and its use in processes involving long carbonation/calcination cycles. However, natural dolomite ($MgCa(CO_3)_2$) has been proposed as an alternative sorbent to limestone [53]. When dolomite is used for SESR, MgO is inert to CO_2 sorption at typical process temperatures (450-750 ^oC) since carbonation of MgO is not thermodynamically favourable [53,54]. However, dolomite has been reported to exhibit enhanced multicycle capture capacity performance [55]. It appears that the ultimate mechanism governing the thermal decomposition of dolomite is still not well understood, as the Tamman temperature, which indicates the onset of MgO sintering (T_t around 1276 ^oC), is only slightly above the Tamman temperature of CaO (T_t around 1170 ^oC) both above the regeneration temperatures commonly used in carbonation/calcination cycles [53]. Nevertheless, it has been shown that CaO incorporated into a MgO matrix can react with CO_2 with competitive cyclic stability among CaO-based acceptors [54]. Therefore, dolomite has been suggested as one of the most suitable sorbents for large-scale sorption

enhanced processes and an advantageous alternative to limestone [53,56]. Thus, in the present thesis, dolomite has been used as a CO_2 sorbent to study the SESR process of biogas.

2.1.2.2. Catalyst for SESR

As reported by S. Wang et al. [57], since both SMR and SESMR are catalytic-based processes, the commonly used catalysts for SMR can be taken as a reference to choose the catalyst for SESR. In a typical SMR process, the reforming reaction occurs first (Eq. 2.1) and then the produced CO reacts with steam by the WGS reaction (Eq. 2.2).

The main reaction steps of the SMR process are collected in Table 2.1, where * represents a surface site. This reactions steps can be summarised as follows [57,58]:

- Reaction step number 1 represents how methane dissociates to adsorb on the metal surface. This step is key in the overall SR reaction and is generally interpreted as the rate-determining step for SMR on several metal surfaces.

- Reaction step number 2 corresponds to the dissociative adsorption of vapour on two free sites. This step is faster than the dissociation of CH_4, since the dissociation of a water molecule is easier compared to methane.

- Reaction steps 3 to 6 represent the dehydrogenation of CH_x.

- The last steps, reaction steps 7 to 9, correspond to the desorption of CO and H_2. It is generally agreed that the activation of the first C-H bond of the CH_4 decomposition step (reaction step 1) is the rate-determining step of SMR. However, at lower temperatures (< 500 ^oC), the CO formation (step 7) becomes dominant.

Table 2.1: Main reaction steps of the steam methane reforming process [57].

Reaction step	No.
$CH_{4(g)} + 2^* \leftrightarrow CH_3^* + H^*$	1
$H_2O_{(g)} + 2^* \leftrightarrow OH^* + H^*$	2
$OH^* + 1^* \leftrightarrow O^* + H^*$	3
$CH_3^* + 1^* \leftrightarrow CH_2^* + H^*$	4
$CH_2^* + 1^* \leftrightarrow CH^* + H^*$	5
$CH^* + 1^* \leftrightarrow C^* + H^*$	6
$C^* + O^* \leftrightarrow CO^* + 1^*$	7
$2H^* \leftrightarrow H_{2(g)} + 2^*$	8
$CO^* \leftrightarrow CO_{(g)} + 1^*$	9

Both SMR and WGS reactions benefit from the presence of specific catalysts. In the SMR process, both noble and non-noble metals have shown good catalytic properties. However, owing to the high cost of noble metals, Ni-based catalysts are the preferred choice industrially since they are comparatively cheaper and show a catalytic activity similar to Ir or Pt [59]. In addition, the energy barrier for C-H bond activation over the Ni surface is relatively low, and at the same time, the adsorption of C*, H*, and O* is not so strong that the species cannot react off the surface with ease [57].

One of the main limitations of Ni-based catalysts is the formation or deposition of carbon on the catalyst surface which can lead to deactivation of the material [60]. Therefore, in addition to Ni, some other transition metals, such as Co, Cu and Fe, have been used as catalysts for reforming processes, since a possible way to improve the anti-coking property of catalysts is to introduce a second metallic component to form a bimetallic system [57,60]. Thus, bimetallic Ni-Co catalysts derived from hydrotalcite-like material have been synthesised and tested in the SESR process of different biomass-derived compounds [54,61–69] showing promising results with respect to H_2 yield, selectivity and purity [70].

On the other hand, hydrotalcite-derived supports belong to a large class of anionic and basic clays, also known as layered double hydroxides [71]. Upon high-temperature calcination, HTs form mixed metal oxides exhibit important properties, such as large surface area, basic character, high homogeneity, thermally stable dispersion of metal ion components, and synergetic effects between the elements [72].

Due to these properties, HT-like compounds are widely used as catalysts, catalysts supports, ion exchangers, molecular sieves, and sorbents, and generally rank among the catalytic systems that produce the highest methane conversions over a wide range of temperatures [72,73]. In addition, these materials have also shown better resistance to coke formation and sintering than those shown by commercial catalysts supported on alumina [74].

Hydrotalcites are composed of positively charged brucite-like ($Mg(OH)_2$)) layers with trivalent cations substituting for divalent cations at the centres of the octahedral sites of a hydroxide sheet whose vertex contains hydroxides ions, and each –OH group is shared by three octahedral cations and points to the interlayer regions [71]. Hydrotalcites are represented by the formula shown in Eq. 2.5, where M^{2+} and M^{3+} are metal cations, A is an anion, x is the charge of the anion, n>m, and y is the number of interlayer water molecules [74].

$$[M_n^{2+}M_m^{3+}(OH)_{2(n+m)}]^{m+}A_{m/x}^{x-} \times yH_2O \qquad \text{Eq. 2.5}$$

Hydrotalcites can be easily synthesised by the co-precipitation method, generally at slightly elevated temperatures and at constant pH [72]. This material retains a memory effect that allows the reconstruction of its structure [75]. When heated, hydrotalcites dehydrate and lose their characteristic structure (at approximately 473 K the interlayer water leaves and at 723 K the layered hydroxides dehydrate), but the dehydrated material retains the memory of the layered structure [74]. A schematic representation of the typical structure of a hydrotalcite is shown in Figure 2.8.

On the other hand, with regard to the addition of another metal to form a bimetallic catalyst, although Co is less prone to coke formation compared to Ni, the interaction between Co and the metal oxide support is strong, leading to the formation of cobalt oxides with limited reducibility [57]. Due to that, the effect of adding small amounts of noble metals to the catalyst has been investigated using the wet impregnation method.

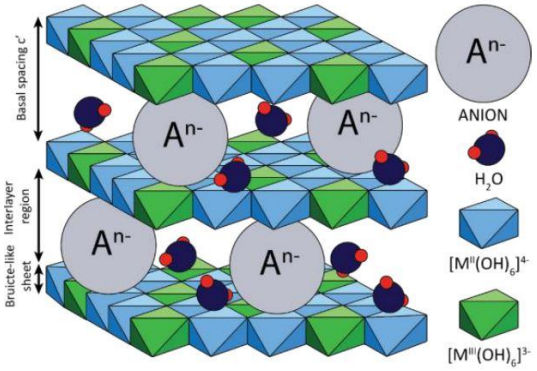

Figure 2.8: Schematic representation of the structure of a hydrotalcite [73].

By adding a small amount of noble metal (known as promoter), the reducibility of transition metal-based catalysts can be improved due to the hydrogen spill over effect [57]. The hydrogen spill over effect is an interfacial phenomenon in which active H atoms generated by the dissociation of H_2 in one phase (metal surface) migrate to other phases (support surface) and participate in the catalytic reaction of an adsorbed substance on that site [76].

According to a previous work of the group [63], the addition of small amounts of Pd to the Ni-Co HT-derived catalyst promotes the reduction of Ni-Co oxides to metallic Ni-Co during the reforming step of the SESR process, which could avoid the need for a reduction step after the sorbent regeneration stage of the process. Jacobs et al. [77] reported the addition of noble metal promoters to catalysts of Co over alumina facilitates catalyst reducibility because the promoter would first reduce and then catalyse the reduction of Co oxide, thereby shifting the reduction temperature to lower values. The authors suggested that a fraction of the promoter atoms would be positioned at the edge of the Co clusters, where reduction can affect the promoter first. The adsorbed H_2 would first dissociate on the previously reduced noble metal atoms and be converted to active hydrogen atoms, which could migrate to the neighbouring Co oxide clusters, facilitating its reduction.

In the case of the Pd/Ni-Co HT-derived catalyst, hydrogen spill over from the reduced Pd metal would facilitate the reduction of the metal oxides and significantly increase the reducibility of the Pd-promoted catalyst. In this

thesis, a Pd/Ni-Co HT-like material was used as a catalyst to experimentally investigate the SESR process of biogas.

Currently, the development of hybrid sorbent-catalyst materials for the SESR process is an important research topic. The main advantage of hybrid materials is that the distance between the catalytic and adsorption sites could be reduced, improving the reaction kinetics. However, the chemical stability of hybrid materials remains a concern and is more challenging than for segregated particle systems [78–82]. Two examples of bifunctional materials are shown in Figure 2.9a and 2.9b.

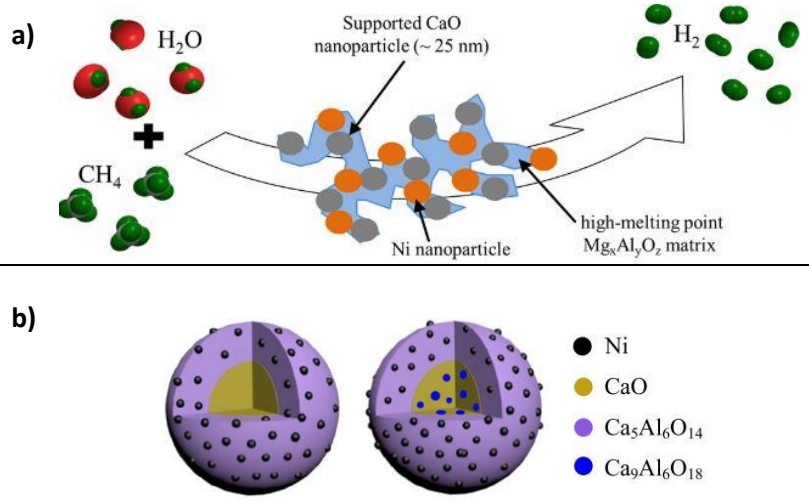

Figure 2.9: Schematic example of SESMR over a bifunctional catalyst sorbent (a) [83]; and example of a core-shell structured bifunctional material (b) [84].

2.1.3. How to operate a SESR process: fixed and fluidised beds

Two main types of reactors can be used for the SESR process: fixed or packed bed reactors and fluidised bed reactors. In general, fluidised bed reactors can provide uniform temperature distribution throughout the bed and typically allow for a more straightforward supply of heat from an external source than fixed bed reactors [85].

Bubbling fluidised beds (BFB) and circulating fluidised beds (CFB) are two different fluidised bed reactor designs that can be used for SESR. The use of two interconnected units allows the SESR process to be operated in

continuous mode [86]. However, efforts to scale up the SESR process are now focused on the CFB mode with continuous sorbent regeneration [87].

On the other hand, in packed bed reactors, a cyclic operation can be carried out including SESR and sorbent regeneration stages. Under reforming conditions, once the sorbent is fully saturated with CO_2, the feed stream (feedstock + steam) is shut down and the bed is heated to regenerate the sorbent in the selected regeneration atmosphere. Fixed bed reactors have been proposed as a viable alternative to fluidised beds because they can be operated more easily at high pressures, there is no need for the gas/solid separation step and operational problems caused by attrition and elutriation of the solid material are negligible [88].

An example of a fixed bed configuration for high pressure SESR, where a battery of reactors is working in parallel, is shown in Figure 2.10 [41]. In this case, the main steps involve are: reaction (reforming + CO_2 capture) at high pressure, depressurization (also known as blowdown) after sorbent saturation, regeneration of the sorbent at low pressure and, finally, H_2 product purge and pressurization to ensure high purity of the product in the next cycle.

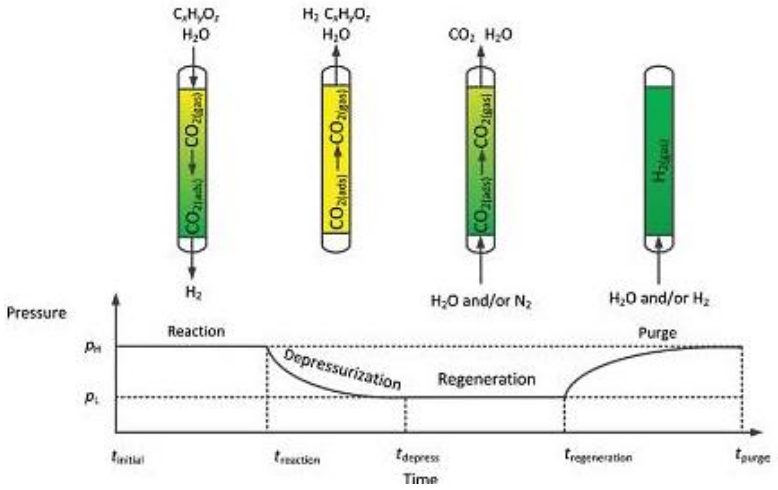

Figure 2.10: Example of a battery of fixed bed reactors as a configuration for SESR [89].

On the other hand, Figure 2.11 shows an example of a fluidised bed configuration. In the CFB reactors, a system of two fluidisation columns (reactor and regenerator) operates simultaneously. The solid phase

consisting of the catalyst and sorbent particles circulates between the reactor and the sorbent regenerator unit [41]. In this system, the regenerator is usually a fluidised bed operating in the bubbling regime, while the reformer can either be a bubbling bed or a riser reactor operating in the fast fluidisation regime [87]. In fact, CFB reactors are commonly used in pilot plant configurations for the combustion of solid fuels and for various chemical processes involving solid catalysts, due to the efficient gas-solid contact, improved heat transfer and reaction rates, as well as continuous operation [90].

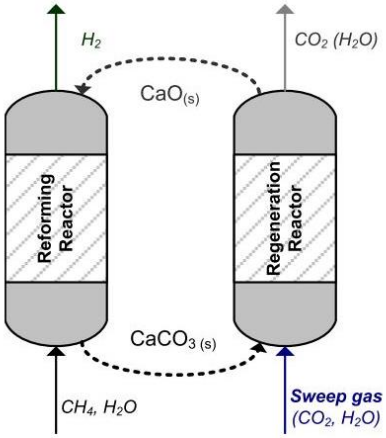

Figure 2.11: Schematic diagram of SESR performed with circulating fluidised beds [90].

The SESR of methane is currently at the Technology Readiness Level (TRL) of approximately 4. A new 1.5 MWth pilot plant is in commissioning phase at Cranfield University in the context of the HyPER project (Bulk Hydrogen Production by Sorbent Enhanced Steam Reforming) with the aim of achieving TRL 6. This pilot plant is based on a system comprising two interconnected reactors: a bubbling fluidised bed reactor for the reformer and a entrained flow reactor for the calciner (see Figure 2.12).

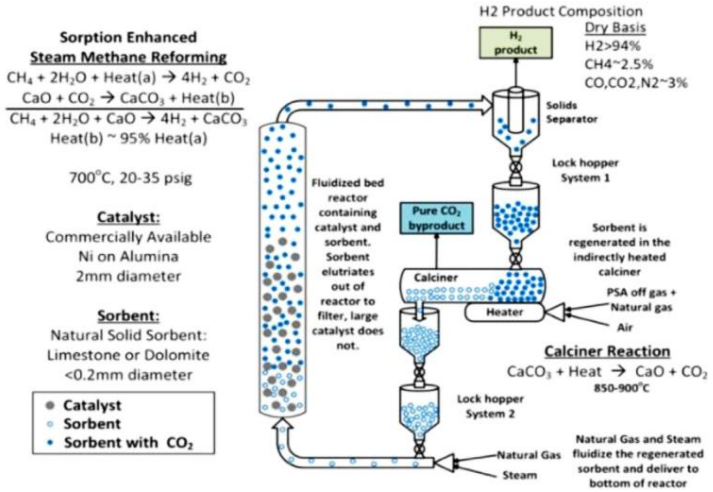

Figure 2.12: Scheme of the 1.5 MWth pilot system under commissioning at Cranfield University [91].

2.1.4. Challenges in further scaling-up SESR technology

The sorption enhanced concept has been investigated for several years, and, recently, several review articles has been published in the literature on this topic [41,42,59,92]. Accordingly, the main challenges for the deployment of the SESR technology that are highlighted are as follows:

- Development of efficient, stable and cheap catalysts to improve conversion efficiency that, ideally, are sulphur resistant.

- Development of suitable CO_2 sorbents with adequate sorption rate, high sorption capacity, as well as mechanical, chemical and thermal stability. Therefore, research currently focuses on improving multicycle durability, either by altering process conditions or synthesising new sorbents with intrinsically better durability.

- Optimisation of the energy efficiency of the process, taking into account the high energy demand during sorbent regeneration. Robust heat and energy recovery systems are required to improve energy integration throughout the overall process.

- Optimisation of the process configuration through techno-economic analysis to optimise total cost of production.

2.2. EFFECT OF BIOGAS COMPOSITION ON H_2 PRODUCTION BY SESR: STATE OF THE ART

Recent research studies have focused on the SESR process of different biomass materials to generate renewable hydrogen such as ethanol [93], glycerol [94,95] or bio-oil from biomass fast pyrolysis [45,63,64,66,67].

However, the SESR of biogas is a topic scarcely studied in the literature. Assabumrungrat et.al [96] performed a thermodynamic analysis of the combined sorption enhanced steam reforming and partial oxidation of biogas (50/50 CH_4/CO_2 vol.%), studying the effects of the steam/CH_4, CaO/CH_4, and O_2/CH_4 ratios on the equilibrium hydrogen production. Saebea et al. [97] carried out a thermodynamic analysis of the SESR of biogas (60/40 CH_4/CO_2 vol.%) to study the effects of the temperature and steam/CH_4 ratio on the equilibrium hydrogen production. Both works concluded that the use of a CO_2 sorbent clearly enhances the production of hydrogen compared to the conventional steam reforming of biogas based on the predicted equilibrium results. Liu et al. [98] reported the simulation of a biogas steam reforming process for hydrogen production using nano-sized CaO sorbents, showing their advantages compared to conventional steam reforming and micro-sized CaO sorbents. On the other hand, an experimental study of the SESR of biogas (60/40 CH_4/CO_2 vol.%) was performed with the objective of comparing the activity of different catalysts based on Ni and CaO under a selected operating condition [99,100].

Moreover, Phromprasit et al. [101] studied different bed arrangements of catalyst and sorbent for the biogas SESR in a fixed bed reactor, demonstrating that the best results are obtained when the catalyst is physically mixed with the sorbent. Finally, preliminary batch tests under a fixed condition have been performed on a sorption enhanced reforming dual fluidised bed reactor system using upgraded biogas, obtaining a hydrogen concentration of 94 vol.% [102].

A main characteristic of the biogas is that it may contain variable concentrations of CH_4 and CO_2 as a function of its origin. For instance, biogas from sewage sludge digesters usually contains 55-75% of CH_4, 20-40% of CO_2 and <1% of nitrogen, whereas the composition of biogas from organic waste digesters is usually 45-75% of CH_4, 25-55% of CO_2 and <1% of nitrogen. On

the other hand, in landfills, CH_4 content often varies from 35% to 55%, CO_2 from 15% to 40% and nitrogen from 5% to 25% [103,104].

However, the works in the literature on the SESR of biogas have usually used a representative biogas composition (mainly 60/40 CH_4/CO_2 vol.%). Therefore, in this thesis a comprehensive study on the effect of the biogas composition on the SESR process has been carried out, evaluating the influence of CH_4 and CO_2 concentrations (vol.%) in biogas on the process performance.

The methodology applied in this work is explained in section 3.1, while the results on the effect of biogas composition on the SESR performance are presented in section 4.1.

2.3. EFFECT OF H_2S ON H_2 PRODUCTION BY SESR OF BIOGAS: STATE OF THE ART

As mentioned above, biogas mainly contains 35-70% of CH_4 and 30-65% of CO_2, with other minor components, such as N_2, O_2, H_2, H_2S, H_2O, CO, NH_3, and siloxanes. Purification or cleaning technologies (physical and chemical absorption, adsorption, biological desulphurization or membrane separation) are commonly applied to control the level of impurities in biogas and remove harmful and toxic compounds such as H_2S, N_2, O_2, CO, and NH_3, which can affect the end-users, grid transmission, machineries or storage facilities. However, one of the main challenges in the use of biogas, and a common poisoning problem, is the presence of H_2S, as it can deactivate the catalytic activity of Ni, which is the most commonly used metal in reforming catalysts. The composition of biogas depends on the biogas source [103,104] and variable H_2S concentrations can be found: 0-10000 ppm from sewage sludge digesters, 10-2000 ppm from organic waste digesters, and 0-100 ppm from landfills [25].

Ni has been found more sensitive to sulphur poisoning than other metals [105], and nickel-based catalysts are particularly susceptible to deactivation by sulphur compounds. The accepted mechanism of sulphur poisoning on Ni catalysts is the chemisorption of sulphur on the Ni surface, i.e., catalyst is deactivated through sulfidation of the active Ni particles and

formation of Ni–S species that do not take part in the reforming reactions, as shown in Eq. 2.6 [106].

$$Ni + H_2S \leftrightarrow Ni–S + H_2 \quad \text{Eq. 2.6}$$

Other metals, such as Ag, Cu, Fe, Co, Mo, Ru, Pt, can also react with sulphur compounds [107]. Although cobalt metal has a slightly lower affinity for sulphur as compared to nickel [108,109] it could also chemisorbs sulphur by Eq. 2.7.

$$Co + H_2S \leftrightarrow Co–S + H_2 \quad \text{Eq. 2.7}$$

However, it has been reported that the addition of Co to a Ni catalyst delays the catalyst deactivation in the presence of H_2S by altering sulphur chemisorption kinetics [109]. On the other hand, Ni is more sensitive to sulphur deactivation than noble metals [107], and catalyst deactivation by sulphur poisoning of Pd is not expected to occur under the studied reforming conditions, since the p_{H2S}/p_{H2} ratio during the SESR experiments is below the value needed for the reaction between Pd and H_2S as estimated by Iyoha et al. [110].

The effect of the biogas H_2S content on the reforming process has been extensively studied under conventional SR [111–113], dry reforming [114–116] and also for biogas tri-reforming, which combines dry and steam reforming with exothermic oxidation [117,118]; however, the deactivation of the catalyst by sulphur poisoning in conventional reforming processes has been restricted to low H_2S concentrations (< 250 ppm). On the other hand, the use of calcined limestone/dolomite for sulphur capture (H_2S) has also been previously studied in gasification processes [119–121]. However, the effect of biogas H_2S on hydrogen production through the cyclic SESR process has hardly been studied. The SESR process is a more complex system than conventional steam reforming due to the presence of a CaO-based CO_2 sorbent. For example, under the reducing conditions during the reforming step, CaO could react with H_2S to form calcium sulfide by Eq. 2.8 [122,123].

$$CaO + H_2S \leftrightarrow CaS + H_2O \quad \Delta H_r^0 = -59 \text{ kJ mol}^{-1} \quad \text{Eq. 2.8}$$

Although there have been recent efforts focused on the development of sulphur-resistant catalysts (i.e., the addition of rare-earth, alkaline, alkaline-

earth or noble metals, or the use of inherently resilient material frameworks such as alloys, perovskites and core-shell structures [124,125]), the presence of H_2S is still a challenge in reforming systems and a significant barrier for their commercial implementation. A desulphurization unit can reduce the H_2S content in biogas, but removing trace amounts of H_2S is often an economically unattractive option, especially in small-scale applications [111]. Furthermore, sulphur-containing compounds remaining after desulphurization can still reach the catalyst, blocking the active sites [114,126]. Therefore, it has been highlighted that some resistance to sulphur poisoning in reforming processes is crucial to ensure proper operation under industrial conditions [124].

Thus, this work addresses the effect of the biogas H_2S concentration on the H_2 production by an advanced reforming process, such as catalytic SESR, which involves using a CaO-based sorbent material to produce high-purity hydrogen.

The methodology applied in this work is explained in section 3.1, while the results are presented in section 4.2.

2.4. PROCESS SIMULATIONS OF HIGH-PURITY HYDROGEN PRODUCTION BY SESR OF BIOGAS: STATE OF THE ART

One of the main challenges of the SESR process is the heat required for sorbent regeneration. In fact, the optimisation of the energy demand in the process and the development and implementation of robust heat and energy recovery systems have been recently highlighted as key existing challenges for viable H_2 production by sorption enhanced processes [59]. As mentioned above, the SR reaction of methane is highly endothermic, but the WGS and the carbonation reactions are exothermic. Thus, the heat generated by the carbonation and WGS reactions balances the heat demand for reforming, and so the reactor where the SESR step occurs is thermally neutral or slightly exothermic (Eq. 2.4). However, the subsequent sorbent regeneration step by the calcination reaction (reverse of Eq. 2.3) is highly endothermic, so the overall process requires energy.

Theoretically, the SESR of biogas is more exothermic than the SESR of pure methane since CO_2 in the biogas is also removed from the gas phase by

the carbonation reaction [127] and provides additional heat into the system. In fact, this could be an advantage regarding the energy demand of the process. However, to study the effect of the addition of CO_2 in the feeding, an energy analysis by simulation of the SESR process of biogas is needed to understand the thermodynamic limitations of the system under different process configurations and optimise the energy efficiency.

Some works have performed simulation studies of the SESR process showing its advantages over SR regarding exergy efficiency. Tian et al. [128] reported the exergetic evaluation of the hydrogen production comparing SESR and conventional SR of acetic acid, finding a better performance (98.67% H_2 purity at 450-600 ^oC) and a 5% higher exergy efficiency in the SESR system. Tzanetis et al. [129] also compared the SESR with conventional SR of methane, finding an increase of 17.3% in the H_2 purity and 3.2% in the exergy efficiency.

In order to optimise the energy efficiency of SESR processes, some works have proposed the coupling of SESMR with chemical looping combustion (CLC) for hydrogen production from methane. Alam et al. [130] proposed an efficient process for high purity hydrogen production by integrating SESMR with CLC obtaining an energy efficiency of 70.3%. Yan et al. [131] reported energy efficiency values of 72% for a process integrating SESMR with CLC and 74% for SESMR with oxy-fuel combustion integration. However, the CO_2 capture was higher when coupling CLC or oxy-fuel combustion to the SESMR process using air in the calcination reactor. Other authors have compared SESR and sorption enhanced chemical looping reforming (SECLR) of methane for hydrogen production, reporting higher values of H_2 yield and purity in the case of SESMR, but lower energy requirements and higher CO_2 capture in the case of SECLR [132,133]. On the other hand, an autothermal sorbent regeneration process using combined combustion, methane reforming, and a hydrogen-selective membrane in the regenerator has been simulated by Ebneyamini et al. [134].

Despite the possible improvements in energy efficiency by SESR integration with CLC or selective membranes, those processes require additional devices, such as membrane reactors or separate reactors for re-oxidation of the oxygen carrier, which unavoidably increase the equipment costs and provide less efficient heat integration [132]. A techno-economic evaluation of the overall process should therefore be considered. In the case

of the SESR of biogas for high purity hydrogen production, little work has been done on the topic, and studies addressing thermodynamic analysis and process simulations are very limited in the literature. Barelli et al. [135,136] performed a thermodynamic study of hydrogen production with CO_2 capture of different gas mixtures, such as syngas and biogas, reaching adiabatic reforming for methane contents in the feed gas of 55-65% and obtaining hydrogen purity higher than 99% and energy efficiency of 72%. However, the simulation of the SESR process using biogas is still needed to understand the energy utilisation under different process configurations, taking advantage of the additional heat that CO_2 in the biogas may provide to the system.

Therefore, in this work, different process layouts for renewable hydrogen production from biogas SESR, targeting the recovery of the heat released in the reformer while maximising CO_2 capture, have been proposed. The process has been designed to achieve energy-self-sufficient operation, avoiding external utilities.

The modelling methodology applied in this work is explained in section 3.2, while the results obtained are presented in section 4.3.

2.5. TECHNO-ECONOMIC ANALYSIS OF H_2 PRODUCTION BY SESR OF BIOGAS: STATE OF THE ART

Economic assessment is an essential tool to understand the potential of the SESR process to be implemented on a large scale. Some studies on the economic analysis of sorption enhanced steam reforming have been reported in the literature. Thus, the techno-economic performance of SE-SMR in a network of fixed bed reactors and its integration with a solid oxide fuel cell for power generation was studied by Diglio et. al. [137]. The authors reported a levelised cost of hydrogen (LCOH) of 1.6 €/kg for SE-SMR without CO_2 capture and 2.4 €/kg when CO_2 capture is included. On the other hand, Yan et al. [138] reported the economic performance of current and emerging technologies for low-carbon hydrogen production (e.g., SMR with chemical looping, autothermal reforming with CCS, chemical looping reforming or gas switching reforming), finding LCOH values in the range of £1.42-2.84/kg H_2. These authors also evaluated six SE-SMR configurations integrated with an indirect natural gas or biomass-fired calciner, oxy-fuel combustion and

chemical looping combustion for large scale production of blue and carbon-negative H_2, resulting in LCOH values in the range of £1.90-2.80/kg H_2.

An emerging trend for the production of more sustainable hydrogen, is electrified steam methane reforming (e-SMR) with renewable electricity. However, this technology has the drawback of a higher cost of H_2 production of 3.49$/kg H_2, as reported by Do et al. [139].

For the specific case of biogas as a feedstock, some techno-economic studies have recently been reported. Di Marcoberardino et al. [140] studied the potential of a biogas membrane reformer for decentralised H_2 production, estimating a hydrogen production cost of 4€/kg H_2. A fixed bed chemical looping system coupled to a 3MW_{th} biogas digester was studied to produce fuel-cell-grade hydrogen, reporting hydrogen production costs (including feedstock costs) of 4.6-6.2€/kg H_2 [141]. On the other hand, Dumbrava et al. [142] studied different thermochemical looping cycles, including their techno-economic analysis. These authors reported that calcium looping has a cost of 37€/MWh including a decarbonisation unit compared to 33€/MWh in the case of steam reforming without CCS and 42€/MWh in the case of an iron looping process.

The works reported in the literature mainly focus on chemical looping or conventional steam reforming. Although some efforts have been made to evaluate the techno-economic analysis of sorption enhanced steam reforming coupled to a biomass-fired calciner, the specific case of biogas use has not been explored. Therefore, a techno-economic analysis of the process was performed in this thesis. The methodology applied is shown in section 3.3, while the results are discussed in section 4.4.

2.6. PRODUCTION OF DIMETHYL ETHER (DME) AS HYDROGEN CARRIER: STATE OF THE ART

Dimethyl ether (DME) appears to have a large potential impact on society compared to other liquid organic hydrogen carriers (LOHCs), especially if inserted into technological chains of CO_2 sequestration and utilization [143]. DME is a non-toxic, ultra-low emissions fuel that can be easily handled similarly than conventional LPG. Thus, it can serve as an

alternative fuel in compression ignition engines, replacing diesel and significantly improving combustion emissions [144].

DME can be produced by different routes: indirect production, direct production, and the novel sorption enhanced route, which is called Sorption Enhanced DME Synthesis (SEDMES) [145]. An overview of these routes is shown in Figure 2.13.

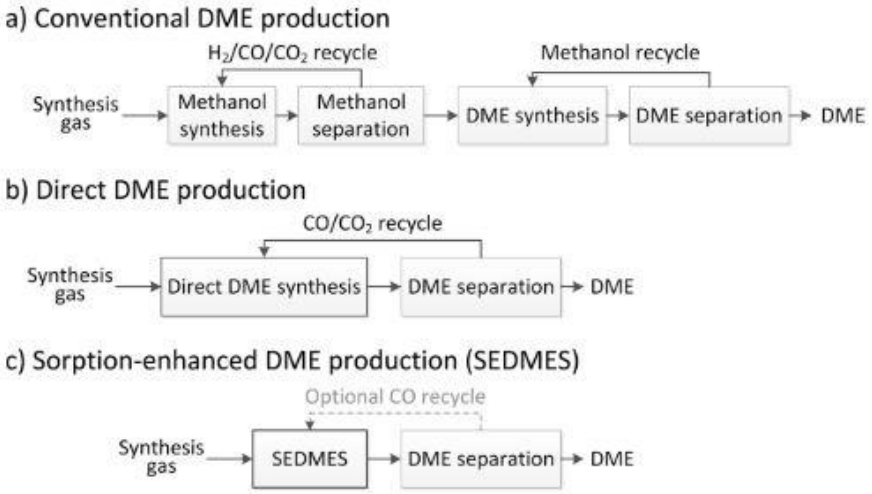

Figure 2.13: Overview of the main DME production routes [145].

Indirect DME production is a two-step process. First, intermediate methanol is synthesised from syngas, followed by the dehydration of methanol to DME in a separate reactor. However, the synthesis of methanol (Eq. 2.9 and Eq. 2.10) and the subsequent dehydration (Eq. 2.12) reactions are both thermodynamically constraint, resulting in limited yield, extensive separations and large recycles. Therefore, in recent years, a lot of effort has been devoted to research on direct DME production in a single-step process (Eq. 2.13). In this regard, SEDMES is a novel process for the production of DME from synthesis gas (Eq. 2.14), in which water is removed in situ through the use of a solid sorbent. The concept is based on Le Chatelier's principle, as in the SESR process. The complete set of reactions is as follows (Eq. 2.9-Eq. 2.14):

Methanol synthesis

$CO_2 + 3H_2 \leftrightarrow CH_3OH + H_2O$ $\Delta H_r^0 = -49$ kJ mol^{-1} Eq. 2.9

$CO + 2H_2 \leftrightarrow CH_3OH$ $\Delta H_r^0 = -90$ kJ mol^{-1} Eq. 2.10

Water gas shift

$CO + H_2O \leftrightarrow CO_2 + H_2$ $\Delta H_r^0 = -41$ kJ mol^{-1} Eq. 2.11

Methanol dehydration

$2\ CH_3OH \leftrightarrow CH_3OCH_3 + H_2O$ $\Delta H_r^0 = -24$ kJ mol^{-1} Eq. 2.12

Direct DME synthesis (from CO)

$3CO + 3H_2 \leftrightarrow CH_3OCH_3 + CO_2$ $\Delta H_r^0 = -245$ kJ mol^{-1} Eq. 2.13

Sorption Enhanced direct DME synthesis (from CO_2)

$2CO_2 + 6H_2 \leftrightarrow CH_3OCH_3 + 3H_2O$ $\Delta H_r^0 = -122$ kJ mol^{-1} Eq. 2.14

DME production using SEDMES technology has been recently demonstrated for the first time with a multi-column test rig at TNO (Petten, the Netherlands) [146]. Multi-column experiments showed continuous production of DME with high CO_2 conversion in a single step with 95% carbon yield. To ensure sustainability, the H_2 supplied must be renewable. When a PEM electrolyser is used for H_2 production, the main factors that contribute to the cost are indeed related to the electrolyser [147]. Therefore, other routes have recently been proposed, such as the direct synthesis of DME from landfill gas [32,148].

In this thesis, the production of bio-DME, as a hydrogen carrier, from biogas has been studied. The H_2 produced during the SESR process of biogas has been used, along with part of the CO_2 produced. The main objective of this work was to integrate efficiently the biogas SESR and the SEDMES processes by exploiting different synergies found between both. The methodology applied for this work is explained in section 3.4, while the results are discussed in section 4.5.

Chapter 3

EXPERIMENTAL AND SIMULATION METHODOLOGIES

This chapter explains the experimental devices and materials, as well as the modelling methodologies, used to obtain the results of this thesis.

3.1. EXPERIMENTAL METHODOLOGY

Here, the experimental methodology used to study the effect of the biogas composition in terms of CH_4 content and the effect of H_2S content on biogas SESR are described.

3.1.1. Experimental set-up: fluidised and fixed bed reactors

The experiments were performed in fluidised or fixed bed reactors (conveniently specified in the results chapter), which have similar characteristics. Therefore, a general overview is given here as a reference for guidance.

Both reactors are Microactivity type systems manufactured by PID Eng&Tech that are coupled to a gas analyser (MicroGC) to track the gas composition at the outlet of the device. The operation is fully automated. The experimental setup and its schematic flow diagram are shown in Figure 3.1a and 3.1b, respectively.

The gases are supplied by means of Bronkhorst® mass flow controllers and mixed to enter the reactor. To prevent backflow of the products through the lines, the controllers are protected with check valves fitted with Kalretz elastomer (elastomeric Teflon) seals.

To produce steam, distilled water is supplied to the system using a positive displacement HPLC pump (HPLC 307-5S Gilson®) capable of operating in the range 0.010 – 5 $mL \cdot min^{-1}$ and pressures up to 600 bar. Steam is subsequently produced inside the system by means of a coil. The steam and feed gases pass to the hot box system to preheat the gas mixture up to 200 ^oC and prevent any possible condensation in the system. Once the gases are preheated and the liquids evaporated, all the streams are merged and pass through a 6-port valve that allows the feed stream to go to the reactor for reaction or to the outlet by-passing the reactor.

a)

b)

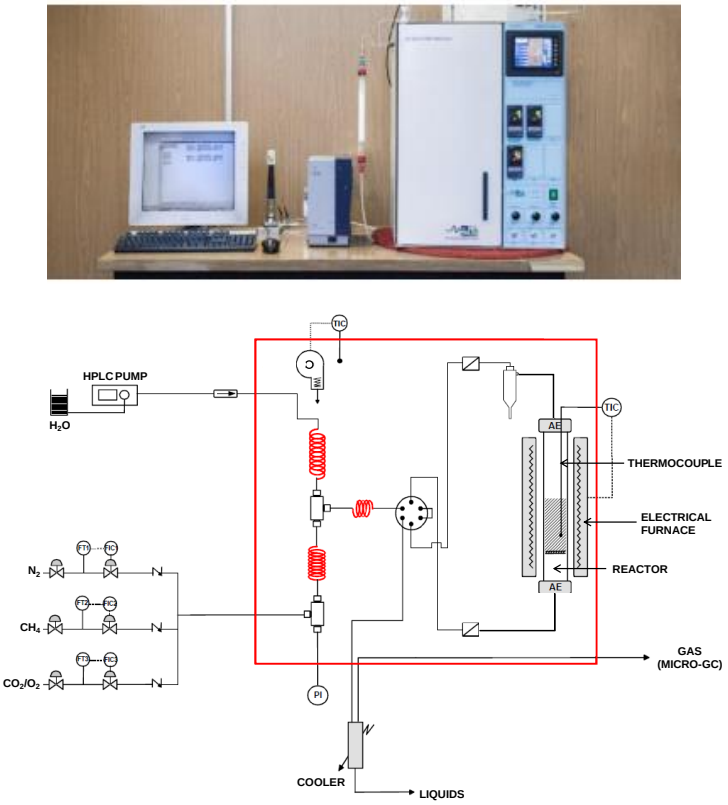

Figure 3.1: Experimental setup (a) and its schematic flow diagram (b).

The experimental setup consists of a stainless steel reactor with an inner diameter of 21.5 mm that is located inside a tubular electric furnace. To perform experiments, a bed formed by sorbent and catalyst in the selected ratio (previously physically mixed) is placed inside the reactor. The reaction temperature is controlled by a K-type thermocouple inserted into the catalyst/sorbent bed connected to a temperature controller and a data recorder. To carry out experiments under pressure, the device has a pressure control system consisting of a servo positioned micrometric regulating valve that provides a continuous and constant flow of gases at the outlet at the defined pressure. Finally, to collect solid particles that may have been elutriated from the bed, the fixed bed device has a ceramic filter, while the fluidised bed system has a cyclone and a ceramic filter.

Figure 3.2 shows the interior of the hot box (Figure 3.2a), water pump (Figure 3.2b) and condenser (Figure 3.2c) of the fluidised bed reactor device. The entire system is controlled by a software that allows the user to perform experiment control and data acquisition.

Once the gases leave the reactor, they pass through a condenser, to separate the condensable gases (i.e., steam or tars) from the non-condensable ones. The composition of the dried gas is analysed using an on-line dual-channel Varian® CP-4900 MicroGC, equipped with molecular sieve Molsieve 5 Å and PPQ columns and a thermal conductivity detector (TCD). Helium is used as the carrier gas in the MicroGC. The main species detected are H_2, CH_4, CO, and CO_2. The gas composition is calculated on nitrogen-free and dry bases. Through a nitrogen balance, the flow rates of the products are also calculated.

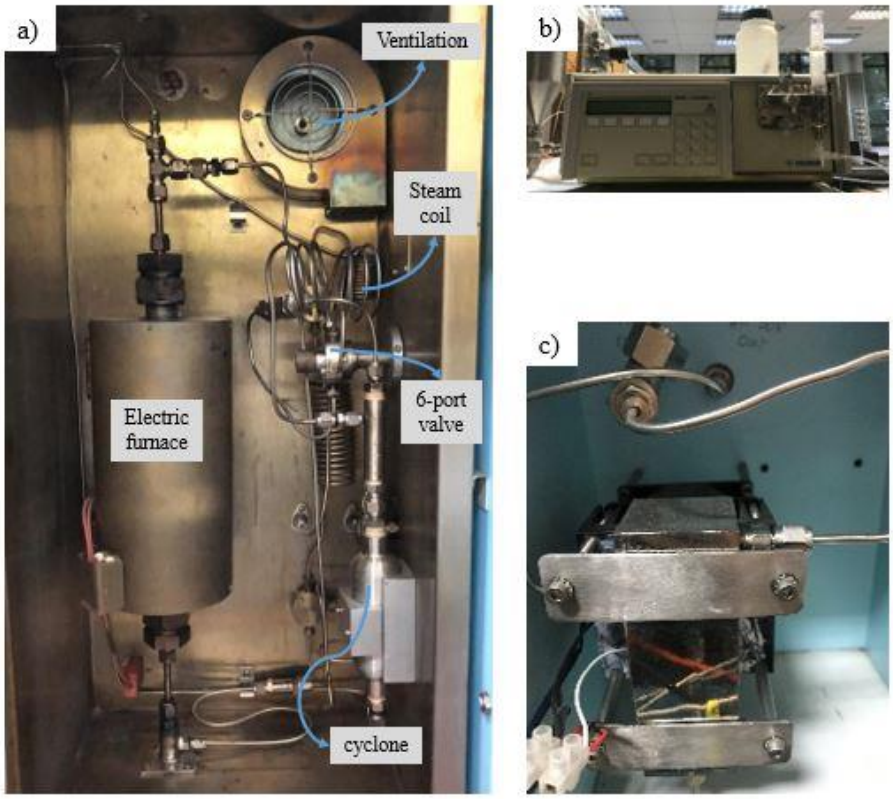

Figure 3.2: Details of the experimental device: interior of the hot box (a), water pump (b) and condenser (c).

3.1.2. Breakthrough curve of a SESR experiment

The typical breakthrough curve of a SESR experiment is shown in Figure 3.3. The main stages of the breakthrough curve are as follows [40]:

- Pre-breakthrough. CaO is fully available and the CO_2 capture reaction (Eq. 2.3) occurs simultaneously with SMR (Eq. 2.1) and WGS (Eq. 2.2) reactions. Due to in situ CO_2 sorption, the reaction equilibrium shifts towards H_2 production. Therefore, the H_2 concentration increases above the equilibrium values of the conventional SMR process.

- Breakthrough. As the sorbent reaches its saturation point, the sorption rate progressively decreases, leading to a transition stage towards the conventional SMR process. This is experimentally indicated by an increase in the CO_2 concentration in the outlet gas due to the loss of CO_2 capture capacity of the sorbent.

- Post-breakthrough. When the CO_2 capture capacity of the sorbent is negligible, conventional SMR and WGS are assumed to occur.

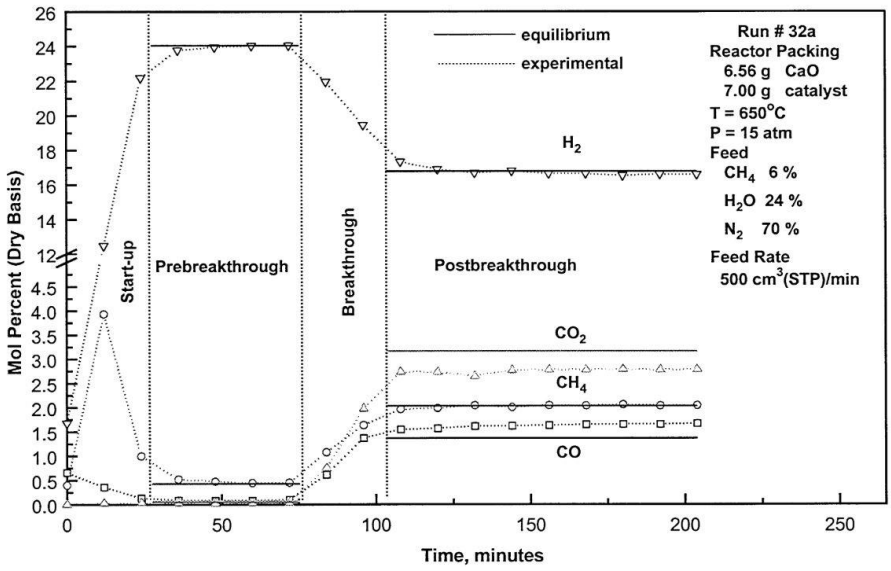

Figure 3.3: Example of a typical breakthrough curve of a SESR experiment [43].

3.1.3. Materials: catalyst and sorbent

The SESR process is characterised by the use of a reforming catalyst and a CO_2 sorbent. In this thesis, the catalyst was synthesised in the laboratory while a commercial material was used as CO_2 sorbent. Both materials were sieved to have the same particle size (250 – 500 µm) and physically mixed to form the reactor bed. The sieved sorbent and catalyst are shown in Figure 3.4a and 3.4b, respectively.

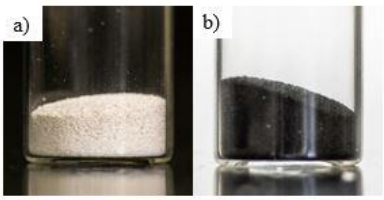

Figure 3.4: Sieved sorbent (a) and catalyst (b).

The CO_2 sorbent has two main functions in the SESR process, i.e., to capture CO_2 from the gaseous phase, and to shift the equilibrium of the reactions according to Le Chatelier's principle. CO_2 is a reactant in the biogas SESR chemical system, so removing it shifts the reaction equilibrium towards the products side. Therefore, the H_2 production increases due to in situ CO_2 capture. In all the experiments, commercial Arctic dolomite supplied by Franefoss Miljøkalk As, Norway, has been used as solid sorbent material.

The purity of the Arctic dolomite, as determined by X-ray fluorescence, is approximately 98.5 wt.% $CaMg(CO_3)_2$, with no detectable sulphur content. Arctic dolomite was specifically selected to avoid sulphur poisoning of the reforming catalyst. The estimated initial maximum CO_2 capture capacity of dolomite was 0.46 g CO_2/g sorbent. Before use, it was calcined in an air flow of 200 mL min^{-1} at 800 ^oC for 4 h and stored in a desiccator.

A 1%Pd/20%Ni-20%Co hydrotalcite-like material (Pd/Ni-Co HT) catalyst was synthesised in the laboratory by the incipient wetness impregnation method using the experimental setup shown in Figure 3.5a. It consists of a 17 cm diameter spherical reactor flask with about 2 L of capacity. The reactor is immersed in a glycerine bath as a heating medium. The reactor lid has several connections to allocate a thermometer that helps control the reactor temperature, a water-cooled coil to prevent evaporation that favours the

reflux of vapours, and a Teflon stirrer to achieve efficient mixing of reactants. The catalyst synthesis procedure of the catalyst is based on the previous experience of the group [62,63].

A 20%Ni-20%Co hydrotalcite-like material (Ni-Co HT) was used as a precursor. It was previously synthesised by co-precipitation of $Ni(NO_3)_2{\cdot}6H_2O$, $Co(NO_3)_2{\cdot}6H_2O$, $Mg(NO_3)_2{\cdot}6H_2O$, and $Al(NO_3)_3{\cdot}9H_2O$. A stoichiometric ratio of cations was chosen to yield a 40 wt.% metal load of Ni and Co, resulting in a nominal composition of 20%Ni-20%Co. Therefore, the synthesis is as follows:

- Firstly, 400 mL of the cationic solution is prepared. This solution contains the metal precursors that will be present in the catalyst (Ni, Co, Mg and Al) in the form of nitrates. The amount of each salt added to the solution is shown in Table 3.1.

- Secondly, 400 mL of the anionic solution is prepared to provide the OH^- groups using sodium hydroxide and carbonate in the amounts indicated in Table 3.1.

- Both solutions are then mixed. The cationic mixture is kept inside the reactor under constant stirring while the anionic mixture is added at a flow rate of 2.0 mL min^{-1} using a peristaltic pump.

- The pH of the mixture is adjusted using a 0.8 M solution of HNO_3 to reach a pH value close to 8.

- The mixture is stirred at 80 ^oC during 16 h maintaining the refrigeration system to avoid losses by evaporation. Subsequently, a grey precipitate is obtained.

During the second step of the synthesis, the precipitate obtained is filtered, washed, dried overnight, and calcined at 600 ^oC for 6 h.

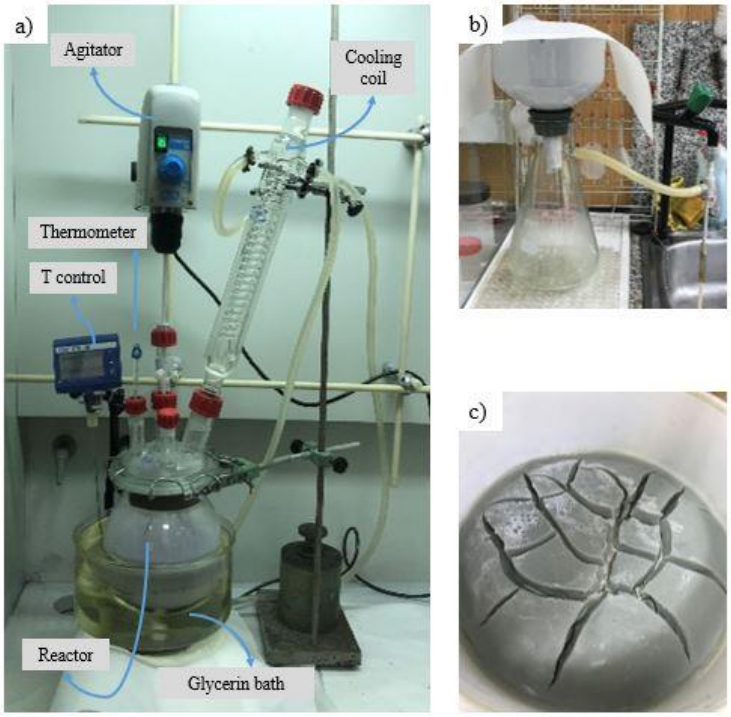

Figure 3.5: Setup used for the catalyst synthesis (a) and filtering (b), and the final precipitate obtained (c).

Table 3.1: Composition of the cationic and anionic solutions for the synthesis of the 20%Ni-20%Co HT catalyst precursor.

Component	Amount (g)
Cationic solution	
$Ni(NO_3)_2 \cdot 6H_2O$	14.61
$Co(NO_3)_2 \cdot 6H_2O$	14.57
$Mg(NO_3)_2 \cdot 6H_2O$	31.97
$Al(NO_3)_3 \cdot 9H_2O$	28.14
Anionic solution	
NaOH	24.00
Na_2CO_3	5.96

Finally, the catalyst was impregnated with Pd. Ni-Co catalysts used in continuous cyclic operation, as in SESR, undergo reversible deactivation due to the loss of active sites during the sorbent regeneration step with oxidising gases that oxidise Ni and Co. Due to the oxidation of the catalyst metals, a reduction step is necessary between cycles [65]. With the use of Pd, it has been shown that this step can be avoided [63].

As mentioned in the literature, Pd is known to be less sensitive to oxidative treatment at high temperatures. The presence of Pd would promote the rapid production of H_2, which would reduce the Ni and Co oxides in the catalyst and, consequently, the reforming reaction would start [149]. The Ni-Co HT precursor was impregnated with a Pd solution to yield a 1 wt.% load of Pd. The Pd solution was prepared by dissolving $PdCl_2$ into two equivalents of HCl and diluting them in ethanol to the concentration necessary to be able to uniformly impregnate the catalyst. The sample was then dried for 14 h at 100 ^oC and calcined in an air flow at 500 ^oC for 1 h in a muffle oven using a heating rate of 5 $^oC\ min^{-1}$. The calcined catalyst was pelletised, grounded and sieved to obtain a particle size of 250-500 µm. It was then reduced at 670 ^oC (heating rate of 2 $^oC\ min^{-1}$) for 10 h in a mixed flow of H_2 (50 NmL min^{-1}) and N_2 (50 NmL min^{-1}).

3.1.4. Characterisation techniques

The different materials have been characterised to discuss and understand the results obtained during the experiments. The characterisation techniques used to analyse the sorbent and catalyst were as follows:

- **X-ray diffraction (XRD)**

XRD was used to determine the crystal phase composition of the catalyst and sorbent. The XRD analysis is performed on a Bruker AXS Difraktometer d8, 230V 50Hz and 6.5 KVA. The samples were subjected to X-rays and the intense peaks of reflected radiation produced by the crystals of the material at certain wavelengths and incident angles (Bragg's law) were recorded. The size of the crystals was also determined using the Scherrer equation (Eq. 3.1).

$$\tau = \frac{K\lambda}{B\cos\theta} \qquad \text{Eq. 3.1}$$

where:

- τ is the mean size of the ordered (crystalline) domains, which can be less than or equal to the grain size;
- *K* is a dimensionless shape factor, with a value close to 1. The shape factor varies with the actual shape of the crystals between 0.62 and 2.08. In all calculations in this thesis, the value 0.89 has been used, which corresponds to the value for the integral width of spherical crystals with cubic symmetry;
- λ is the X-ray wavelength;
- *B* is the width of the diffraction peak, in radians, at a height halfway between the background and the peak maximum (FWHM=Full Width at Half Maximum) after subtracting the instrumental line broadening, as shown in Eq. 3.2. In this equation, B is the corrected half-width of the observed half-width: Bm is that of the (111) reflection in the sample and Bs is that of the (111) reflection in a standard sample;
- and θ is the diffraction angle (Bragg angle).

$$B = \sqrt{Bm^2 - Bs^2} \qquad \text{Eq. 3.2}$$

It should be noted that the crystal size is different from the particle size, since a particle may consist of several crystals. The crystal size usually coincides with the grain size, but there are exceptions. XRD, with data interpreted on the basis of the Scherrer equation, provides a quick and simple method to determine volume-averaged particles size [105].

- **X-ray fluorescence (XRF)**

XRF was used to determine the elemental chemical composition of the sorbent. This technique is based on the measurement of the wavelength or energy of X-ray emitted by a sample that has previously been excited by a characteristic radiation due to the ionization of their atoms. This analysis was performed on a SRS 3000 Bruker XRF spectrometer. First, 0.5 g of the sample was calcined at 1000 ^{o}C for 30 min and then melted with 9.0 g of lithium tetraborate/lithium metaborate 66:34 (Equilab EQF-TML 66:34) at 1100 ^{o}C for 8 min in a fusion machine (EQUILAB F1) to destroy its particulate and mineralogical composition. The resulting material is subjected to glass bead casting, which are then introduced in the XRF spectrometer. The X-ray

fluorescence intensities of the required elements are measured in the bead and the chemical composition of the ashes is analysed in relation to previously determined graphs or calibration equations, applying corrections for inter-elemental effects. Calibration equations and inter-elemental corrections are based on beads made from certified reference materials.

- **Inductively Coupled Plasma Optical Emissions Spectrometry (ICP-OES)**

ICP-OES was used to determine total sulphur content in the spent catalyst and sorbent materials after biogas SESR in the presence of H_2S using a Agilent 5110 SVDV ICP-OES analyser. Before analysis, the samples were digested in a microwave oven. For the digestion, 0.5 g of dolomite or 0.25 g of catalyst were added to a mixture of 5 mL of nitric acid (63%), 2mL of hydrochloric acid (37%), 2 mL of hydrogen peroxide (30%), and 3mL of deionized water. The reactants were reacted at room temperature for 30 min and then the digestion was performed in a closed glass at 190^{o}C for 30 min, increasing the temperature with a gradual increase over 10 minutes. Afterwards, the analysis was carried out using yttrium as internal standard.

- **Scanning Electron Microscopy – Energy Dispersive X-ray spectroscopy (SEM-EDX)**

SEM analysis provides two-dimensional images of the surface of a material by shining a beam of electrons onto the sample, ionizing the atoms, which will emit secondary electrons. These secondary electrons are collected by the detector, while the vacancies generated are replaced by electrons from an external orbital.

SEM analysis was performed in a Quanta FEG 650 scanning electron microscope coupled to an energy-dispersive X-ray (EDX) detector for detailed elemental mapping. SEM analysis was used for the characterisation of the catalyst and sorbent, as well as for the study of the spent catalyst and sorbent materials after biogas SESR in the presence of H_2S.

- **Specific surface area – BET**

The specific surface area is determined by the Brunauer-Emmet-Teller (BET) equation. This estimation is based on the indirect determination of the number of moles of adsorbate that complete a monolayer on its free surface.

BET was determined for the study of the sorbent material after biogas SESR in the presence of H_2S. Samples were characterised by physical adsorption of N_2 at −196 ^oC using a Micromeritics ASAP 2420 V2.09 analyser. Samples were outgassed overnight under vacuum at 120 ^oC before adsorption measurement. The specific surface area (S_{BET}) was calculated using the Brunauer-Emmett-Teller (BET) equation in the relative pressure interval of 0.01 to 0.1 [150]. The total pore volume (Vp) was also estimated using the amount of nitrogen adsorbed at a relative pressure of 0.99.

- **X-ray photoelectron spectroscopy (XPS)**

XPS analysis allows the identification of the oxidation state of the elements present on the surface of a sample. The fundamental principle behind this technique is the photoelectric effect.

In this thesis, XPS was used to determine the chemical states of the surface Ni, Co, and S species present in the fresh and spent catalysts after biogas SESR in the presence of H_2S. The analysis was performed using a SPECS instrument under a pressure of 10^{-7} Pa and a non-monochromatic Al Kα X-ray source (14 kV at 175 W). XPS data were analysed using CasaXPS software. The binding energy (BE) values were referred to the BE of environmental carbon C 1s at 285 eV.

3.1.5. Experimental key performance indicators

To perform the SESR experiments with biogas, the reactor was heated to the desired temperature under N_2 atmosphere (100 $NmL \cdot min^{-1}$). Once the bed reached the reaction temperature, biogas, steam, and N_2 were introduced into the reactor through the catalyst/sorbent bed. Nitrogen is used as internal standard. Liquid water was first evaporated in an evaporator and then mixed with the gas stream in the preheating zone of the hot box, as explained above.

The S/C molar ratio of the inlet stream is calculated as the ratio between the molar flow rate of steam and the molar flow rate of the carbonaceous species that are reactive under reforming conditions, such as CH_4. On the other hand, the Gas Hourly Space Velocity (GHSV) is defined as the ratio of the reactant volumetric flow rate to the mass of catalyst, according to Eq. 3.3.

$$\text{GHSV (mL } CH_4\text{/biogas } g_{cat}^{-1} h^{-1}) = \frac{\text{Vol. flow rate of inlet } CH_4\text{/biogas (mL } CH_4\text{/biogas } h^{-1})}{\text{Mass of catalyst (g)}} \quad \text{Eq. 3.3}$$

To evaluate the performance of the biogas SESR experiments the key performance indicators (KPIs) studied were: CH_4 conversion (Eq. 3.4), H_2 purity (Eq. 3.5), CH_4, CO, and CO_2 concentrations (Eq. 3.6), H_2 yield (Eq. 3.7), and H_2 selectivity (Eq. 3.8).

$$CH_4 \text{ conversion (\%)} = 100 \cdot ((F_{CH4,in} - F_{CH4,out})/F_{CH4,in}) \quad \text{Eq. 3.4}$$

$$H_2 \text{ purity (vol.\%)} = 100 \cdot (y_{H2}/\Sigma_i y_i) \quad \text{Eq. 3.5}$$

$$CH_4/CO/CO_2 \text{ (vol.\%)} = 100 \cdot (y_{CH4/CO/CO2}/\Sigma_i y_i) \quad \text{Eq. 3.6}$$

$$H_2 \text{ yield (\%)} = 100 \cdot (F_{H2,out}/4 \cdot F_{CH4,in}) \quad \text{Eq. 3.7}$$

$$H_2 \text{ selectivity (\%)} = 100 \cdot [2 \cdot y_{H2}/(2 \cdot y_{H2} + 4 \cdot y_{CH4})] \quad \text{Eq. 3.8}$$

where $F_{CH4,in}$ and $F_{CH4,out}$ are the molar flow rate of methane fed in and that at the outlet of the reactor, respectively; $F_{H2,in}$ and $F_{H2,out}$ are the molar flow rate of hydrogen fed in and that in the product gas, respectively. Finally, y_i is the molar flow rate of each species i produced. H_2 yield represents the percentage of H_2 produced during the experiment with respect to the maximum H_2 production according to the SESR reaction stoichiometry (Eq. 2.4). The component distribution was calculated based on the nitrogen-free and dry composition of the gas effluent. The flow rates of the species generated during the experiment were calculated running a nitrogen balance since the amount of nitrogen fed in and evolved is known.

3.2. PROCESS SIMULATIONS OF H_2 PRODUCTION BY SESR OF BIOGAS

This section describes the methodology used to carry out the simulation of H_2 production from biogas by the SESR process.

3.2.1. Model development and process configurations

The biogas SESR was simulated in the Aspen Plus V11 software (AspenTech). An equilibrium model was developed assuming steady-state conditions. An autothermal SESR process of biogas that includes a first stage of steam reforming coupled to in situ CO_2 capture and a second stage of sorbent regeneration is considered. The model incorporates a heat exchanger network (HEN) to recover as much heat as possible from the process streams.

3.2.1.1. Theoretical background

The chemical equilibrium of the reforming and regeneration reactors is calculated by minimisation of the Gibbs free energy of the system. This non-stoichiometric approach offers greater flexibility when tackling complex problems where the reaction pathways are unclear [151]. Therefore, the reformer, where reforming with in situ CO_2 capture occurs, and the calciner, where sorbent regeneration takes place, were simulated using *RGibbs* blocks. The *RGibbs* unit is used to perform thermodynamic equilibrium calculations with phase isolation and without specifying the chemistry of the reaction. It calculates the chemical equilibria of the different components involved in the different phases.

The Gibbs free energy is a thermodynamic function of state that represents the energy change experienced by a system at constant pressure, as shown in Eq. 3.9, where ΔH is the enthalpy change, ΔS is the entropy change, and T is the temperature of the system.

$$\Delta G = \Delta H - T \cdot \Delta S \qquad \text{Eq. 3.9}$$

This equation establishes the spontaneity of chemical reactions. A chemical reaction is considered spontaneous when it has a $\Delta G < 0$. Conversely, when $\Delta G > 0$ the opposite reaction would be spontaneous. The system will be at equilibrium when $\Delta G = 0$. Therefore, it is possible to

calculate the equilibrium of the system by minimising the Gibbs free energy with the *RGibbs* unit in Aspen Plus.

For an isobaric and isothermal system, the general Gibbs free energy equation can be written as in Eq. 3.10, where NF is the total number of phases in the system, NC is the number of components, n_i^k is the number of moles of component i in phase k, and g^k is the Gibbs free energy of each phase.

$$G = \sum_{K=1}^{NF} n^k g^k = \sum_{k=1}^{NF} (\sum_{i=1}^{NC} n_i^k) g^k \qquad \text{Eq. 3.10}$$

The simulation also considers two fixed constraints that refer to the principle of mass conservation for each phase and component present in the different elements, as reflected in Eq. 3.11 and Eq. 3.12:

$$\sum_{k=1}^{NF} n_i^k = n_i, \text{for each component } i \qquad \text{Eq. 3.11}$$

$$\sum_{i=1}^{N} n_i \alpha_{im} = b_m, \text{for each element } m \qquad \text{Eq. 3.12}$$

where:

- n_i = total number of moles of component i,
- α_{im} = number of atoms of the element m in each molecule of component i,
- b_m = total number of atoms m in the system.

The Gibbs free energy can be reformulated as a function of the chemical potential of a reference state, μ_i^0, and the fugacity of each component in each phase, $\hat{f}_i^k$, resulting in the Eq. 3.13:

$$G = \sum_{i=1}^{NC} \sum_{k=1}^{NF} n_i^k (\mu_i^0 + RT\ln \frac{\hat{f}_i^k}{\hat{f}_i^0}) \qquad \text{Eq. 3.13}$$

In the present work, the Peng-Robinson equation of state was used to calculate the thermodynamic properties of each component and the binary interaction coefficients. The Peng-Robinson equation of state is shown in Eq. 3.14, where P is the gas pressure, T is the temperature, R is the gas constant (8.31451 $J \cdot mol^{-1} \cdot K^{-1}$), and V_m is the molar volume. The parameters a and b of the Peng-Robinson equation can be calculated by Eq. 3.14 to Eq. 3.20.

$$P = \frac{RT}{V_m - b} - \frac{a}{V_m(V_m + b) + b(V_m - b)} \quad \text{Eq. 3.14}$$

$$a = \sum_i \sum_j x_i x_j (a_i a_j)^{0.5} (1 - K_{ij}) \quad \text{Eq. 3.15}$$

$$k_{ij} = k_{ij}^{(1)} + k_{ij}^{(2)} T + \frac{k_{ij}^{(3)}}{T}, \text{ siendo } k_{ij} = k_{ji} \quad \text{Eq. 3.16}$$

$$a_i = f(T, T_{ci}, P_{ci}, w_i) \quad \text{Eq. 3.17}$$

$$a_j = f(T, T_{cj}, P_{cj}, w_j) \quad \text{Eq. 3.18}$$

$$b = \sum_i x_i b_i \quad \text{Eq. 3.19}$$

$$b_i = f(T_{ci}, P_{ci}) \quad \text{Eq. 3.20}$$

The process design also includes a HEN to perform heat integration between the hot and cold streams of the process to optimise the process heating and cooling utilities with the objective of avoiding the use of external utilities for steam production and heating the reactants to reaction temperature in the reformer and calciner as much as possible. The heat exchangers were modelled using the Aspen Plus MHeatX unit in counter-current mode, generally recognised as the most efficient heat transfer method. This unit is used to represent heat transfer between multiple hot and cold streams flowing through the heat exchanger, where heat is transferred from the hot stream to the cold stream.

In counter-current mode, the two streams enter from opposite sides of the heat exchanger. The steady-state energy balance solved during the simulation is shown in Eq. 3.21, where $\dot{m}$ is the mass flow rate, $\hat{H}$ is the enthalpy per unit of mass of each stream, and the subscripts H and C

represent the hot and cold streams, respectively. In this balance, heat losses to the surroundings are neglected, as performed in the simulation.

$$Q = \dot{m}_C(\hat{H}_{C,out} - \hat{H}_{C,in}) = \dot{m}_H(\hat{H}_{H,in} - \hat{H}_{H,out}) \quad \text{Eq. 3.21}$$

Since enthalpy is a function of pressure (P) and temperature (T), Eq. 3.21 can be rewritten as a differential change in enthalpy, as shown in Eq. 3.22. Assuming that the rate of change of enthalpy with pressure at constant temperature is negligible, the equation can be approximated as shown in Eq. 3.23. Here, C_P is the specific heat of the fluid in the stream at a constant pressure. If small variations in the specific heat between the streams are neglected, then the equation can be finally expressed as Eq. 3.24.

$$d\hat{H} = (\frac{\partial \hat{H}}{\partial T})_P \, dT + (\frac{\partial \hat{H}}{\partial P})_T \, dP \quad \text{Eq. 3.22}$$

$$d\hat{H} = (\frac{\partial \hat{H}}{\partial T})_P \, dT = C_P \, dT \quad \text{Eq. 3.23}$$

$$Q = \dot{m}_C \, C_{P,C}(T_{C,out} - T_{C,in}) = \dot{m}_H \, C_{P,H}(T_{H,in} - T_{H,out}) \quad \text{Eq. 3.24}$$

Aspen Energy Analyser, an energy management software from AspenTech, was used to estimate the cost of the HEN.

The rate equation for a heat exchange is shown in Eq. 3.25, where the temperature difference (ΔT) is the driving force for heat transfer. In this equation, U is an overall average heat transfer coefficient, A is the contact area of the heat exchanger, and ΔT_{lm} is the logarithmic mean temperature difference for the heat exchanger. ΔT_{lm} can be calculated by Eq. 3.26, where ΔT_1 is the temperature difference at the hot end of the heat exchanger, while ΔT_2 is the temperature difference at the cold end.

$$Q = UA \cdot \Delta T_{lm} \quad \text{Eq. 3.25}$$

$$\Delta T_{lm} = (\frac{\Delta T_1 - \Delta T_2}{\ln \frac{\Delta T_1}{\Delta T_2}}) \quad \text{Eq. 3.26}$$

3.2.1.2. Process configurations

A thermodynamic approach to process modelling has been used to demonstrate the thermodynamic feasibility of the SESR process and provide the optimal process operating conditions and configurations that maximise energy efficiency when using biogas as feedstock.

The SESR process was simulated as an autothermal process, including sorbent regeneration for a cyclic operation and using a HEN to recover waste heat from the process and also waste heat from SESR reactor. With the additional objective of reducing CO_2 emissions, sorbent regeneration under oxy-combustion was also investigated.

Three process configurations were designed and five case studies were compared to estimate the potential energy efficiency of the biogas SESR process. A detailed parametric analysis was performed to study the effect of the biogas composition, reforming temperature, pressure, and steam to methane (S/CH_4) ratio on the process performance. The KPIs evaluated were H_2 purity, H_2 yield, CH_4 conversion, cold gas efficiency (CGE), net efficiency (NE), fuel consumption during sorbent regeneration, and captured CO_2. Simplified diagrams of the three process configurations studied are shown in Figure 3.6. The description of each case study is summarised in Table 3.2.

In the first configuration (Figure 3.6a), the use of a fraction of the produced H_2 as a renewable fuel to supply energy for sorbent regeneration through calcination is studied (SESR+REG_H_2), whereas in the second process configuration (Figure 3.6b) biogas is used for this purpose (SESR+REG_BG). In Case 1, SESR+REG_H_2, the recycled H_2 contains mainly hydrogen, unreacted CH_4, and trace quantities of CO and CO_2. The amount of hydrogen recycled to the REG reactor is calculated with a design specification to fulfil the energy requirement of the unit and to avoid incomplete oxidation products in the effluent gas.

Table 3.2: Case studies evaluated for the energy integration of the SESR process of biogas.

Process configuration	Sorbent regeneration atmosphere	Sorbent regeneration fuel	H_2 purification
Case 1: SESR+REG_H2	Air	H_2	-
Case 2: SESR+REG_BG	Air	Biogas	-
	Oxy-fuel	Biogas	-
Case 3: SESR+REG_BG+PSA	Air	Biogas + PSA off-gas	PSA
	Oxy-fuel	Biogas + PSA off-gas	PSA

In Case 2, SESR+REG_BG, the amount of fuel (i.e., biogas) and oxidising agent required in the calciner are similarly calculated using the design specifications.

Moreover, in the third configuration, represented by Case 3 (Figure 3.6c), the dry hydrogen product (H2RICH) is further purified using a Pressure Swing Adsorption (PSA) unit (SESR+REG_BG+PSA) to increase the hydrogen product purity up to levels that allow its use in applications as fuel cells. A compressor is placed before the PSA unit to maintain the inlet stream at a pressure higher than 25 bar, which is the typical operating pressure for PSA [131]. In this work, a fixed backup pressure of 30 bar was established. The off-gas from the PSA unit (PSA-OG) contains mainly H_2 and CH_4 and trace amounts of CO and CO_2, and it is sent to the calciner to reduce the amount of additional biogas required as fuel. The separation efficiency of the PSA unit is set at 95% [131].

In all the cases, a compressor with 83% isentropic efficiency and 98% mechanical efficiency [131] is placed to match the operating pressure of the reactor (which varies in the different simulations). Similarly, a water pump with the same efficiencies matches the pressure of the water stream used to produce the steam. Furthermore, the flow of oxidant agent used in the REG unit is controlled to meet a 5% excess of oxygen [131]. In the calciner, not only direct combustion using air was analysed but also oxy-fuel combustion (30% O_2 and 70% CO_2 mole fraction gas supplied to REG reactor) was studied to evaluate the reduction in CO_2 emissions.

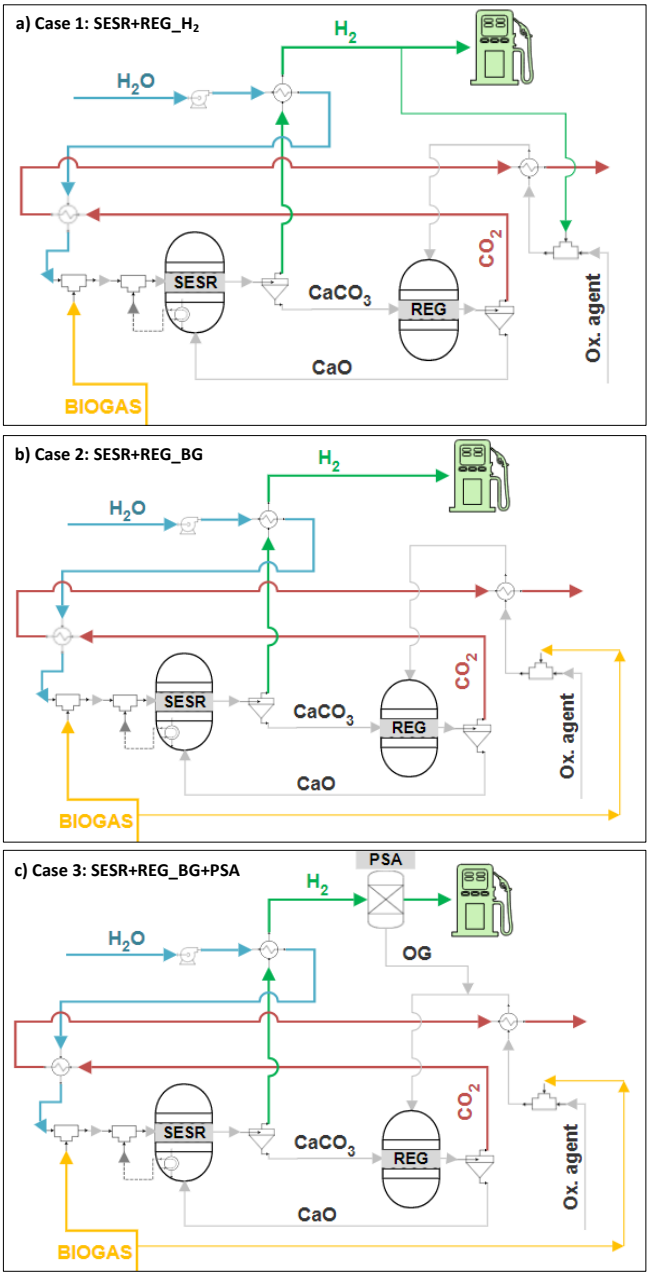

Figure 3.6: Simplified flow diagrams of the three base configurations proposed for the biogas SESR process. In Case 1 (SESR+REG_H2), a fraction of the produced H_2 is used as fuel for the sorbent regeneration (a). In Case 2 (SESR+REG_BG), biogas is utilised as fuel for the sorbent regeneration (b). Finally, in Case 3 (SESR+REG_BG+PSA), biogas is used as fuel for the sorbent regeneration and a PSA unit is included (c).

It resulted in five scenarios: Cases 2 and 3 with direct air and oxy-fuel combustion and Case 1 with direct air combustion in the calciner. Due to the challenges associated with hydrogen in oxy-combustion (high temperatures and overheating, flame instability, flame blowout) derived from its broader flammability range, much higher adiabatic flame temperature, and higher flame propagation rate, the oxy-fuel scenarios have been restricted to biogas used as fuel. The Aspen Plus flowsheet diagrams are included in the *Annexes*, *Paper II – Supplementary information.*

3.2.1.3. Model development

The base flowsheet of the process mainly consists of two reactors: a reformer (SESR) and a calciner (REG). In the SESR reactor, biogas is the feedstock, and H_2 is rich in the product due to coexistence of the SR (Eq. 2.1), WGS (Eq. 2.2), and carbonation for CO_2 capture (Eq. 2.3) reactions. Due to CO_2 removal, the equilibrium of SR and WGS reactions shifts toward a higher H_2 production according to Le Chatelier's principle.

Furthermore, owing to the extra content of CO_2 in biogas, the carbonation reaction turns pivotal in the overall duty of the SESR unit, which could be highly exothermic when biogas is used as feedstock [152]. Therefore, the model developed in this work includes the extra heat recovery from the SESR unit to achieve an autothermal operation, assuming in the flowsheet design a 10% of heat loss during the heat transfer [131]. This value agrees with the thermal efficiency of reverse flow reactors, which is a reactor type suggested to be sustainable for exothermic reactions [153]. From a practical point of view, to recover the heat released from the SESR reactor, a fluidised bed heat exchanger, consisting of a fluidised bed with heat exchange tubes immersed in it, could be used [35,154]. Likewise, heat pipes have been suggested for indirect heating of the calciner in the chemical looping technology [155–157] and also recently for SESMR [131].

On the other hand, the spent sorbent, forming $CaCO_3$, is separated from the H_2 rich gas stream and sent to the REG reactor, where the sorbent is regenerated to CaO to ensure process operation in a cyclic fashion. The spent sorbent is calcined, which is an endothermic reaction (reverse of Eq. 2.3) favoured at high temperatures and low pressures (i.e., > 800^{o}C and ~ 1bar) [158]. Therefore, the calciner requires a high amount of heat to regenerate the sorbent. The desired temperature for the decomposition of $CaCO_3$ to CaO

can be reached supplying heat by either burning a fuel in the calciner or indirect heating [48,159]. This work focused on direct combustion of renewable fuels to cover the duty required in the REG reactor: hydrogen and biogas.

Moreover, two combustion atmospheres were under study: air and oxy-fuel combustion. In the case of biogas, it matches the composition of the biogas feeding the SESR reactor for each particular simulation. The extra fuel feeding REG corresponds to the minimum amount necessary to fulfil the duty of this unit. Hence, combustion proceeds without incomplete oxidation products (i.e., CO, H_2, or elemental C) leaving the REG reactor [160], which is controlled by using different design specifications. The regeneration temperature is set at 850 ^{o}C unless otherwise specified, ensuring that the regeneration of CaO is performed at 1 bar since low pressures are favourable for the calcination reaction.

An average carbonation conversion of 50% was assumed for the CaO-based sorbent, according to the results of cyclic SESR experiments shown in the literature [78,161]. This value was used to estimate the molar Ca/C ratio in the reformer, as recently reported elsewhere [131]. Therefore, a molar Ca/C ratio of 1.5 is selected, where C refers to the carbon contained in both CH_4 and CO_2 in the biogas fed to the SESR unit. All the calcium accounted for the Ca/C molar ratio comes from the CaO, initially added in excess, circulating between SESR and REG.

The reformer (SESR) and calciner (REG) were simulated using RGibbs blocks, as suggested in the literature [131,160]. The species considered were H_2, CH_4, CO, CO_2, H_2O, O_2, N_2, CaO, $Ca(OH)_2$, and $CaCO_3$. C_2H_4, C_2H_6, and C (solid carbon graphite to account for the possible formation of coke deposits) were also included in the product pool, but their concentrations at equilibrium were negligible under the studied conditions.

Furthermore, a HEN was designed to recover the maximum heat from the process streams with a minimum number of heat exchangers. It aims not only to preheat the reactants but also to produce the steam needed for reforming and circumventing the energy penalty of its production. In the HEN, water is preheated using the maximum heat extracted from the hydrogen stream from the SESR reactor while avoiding condensation by specifying 5 ^{o}C of superheat at the outlet of the hot stream. Since this heat is

not enough, the evaporation continues using the CO_2 stream from the REG reactor. Thus, another heat exchanger is used to complete the steam production when needed and to preheat the reactants using the heat released from the SESR reactor (assuming 10% of heat losses).

The energy that remains in the CO_2 stream is used to preheat the inlet streams of the REG reactor. Finally, the exhausted hydrogen-rich gas is cooled to 25 ^{o}C to condense and separate most of the water in a separation unit. The dry H_2 stream is then ready for downstream processing (i.e., purification, compression, etc.) according to the application.

3.2.2. Key performance indicators for the SESR process performance

The thermodynamic performance of the process was evaluated in terms of H_2 purity, H_2 yield and CH_4 conversion (experimental KPIs explained in section 3.1.5), together with other specific KPIs, such as Cold Gas Efficiency (CGE), Net Efficiency (NE), fuel consumption for sorbent regeneration, and CO_2 captured.

CGE is calculated as the ratio between the chemical energy of the produced H_2 stream to the sum of the feed thermal input (chemical energy of the CH_4 feed consumed in the SESR reactor and the additional CH_4 required to meet the heat requirements of the sorbent regeneration). CGE is calculated by Eq. 3.27, where $F_{CH_4,additional}$ is the molar flow rate of methane contained in the additional biogas fed in the calciner to meet the duty requirement of the REG unit. LHV_{H_2} and LHV_{CH_4} are the low heating values of hydrogen (242 MJ/kmol) and methane (800 MJ/kmol), respectively.

NE is calculated by Eq. 3.28, where the electric utility requirement of the auxiliaries (P_e) is added to the CGE equation with a thermal-to-electric conversion efficiency (η_{elect}) of 50%. For scenarios where oxy-combustion is used to supply heat to the calciner, the energy penalty of producing oxygen with an Air Separation Unit (ASU) must be considered. Thus, the auxiliary power consumption of the ASU is assumed to be 160 kWh/t oxygen [131].

The fuel required for combustion in REG can be part of the hydrogen produced in the process or part of the biogas used as feedstock. When hydrogen is used, the amount recycled to the calciner as fuel is calculated

using Eq. 3.29, while in the case of biogas, the fuel consumption is calculated using Eq. 3.30.

Finally, the captured CO_2 is calculated by Eq. 3.31, where $F_{CO2,\ captured}$ is the molar flow of CO_2 in the outlet CO_2 stream.

$$CGE\ (\%)=\left(\frac{F_{H_2,out}\cdot LHV_{H_2}}{(F_{CH_4,in}+F_{CH_4,additional})\cdot LHV_{CH_4}}\right)\cdot 100 \qquad \text{Eq. 3.27}$$

$$NE\ (\%)=\left(\frac{F_{H_2,out}\cdot LHV_{H_2}}{(F_{CH_4,in}+F_{CH_4,additional})\cdot LHV_{CH_4}+\frac{P_e}{\eta_{elect}}}\right)\cdot 100 \qquad \text{Eq. 3.28}$$

$$Fuel_{H_2\ recycled}\ (\%)=\left(\frac{F_{H_2\ recycled\ to\ REG}}{F_{H_2\ recycled\ to\ REG}+F_{H_{2out}}}\right)\cdot 100 \qquad \text{Eq. 3.29}$$

$$Fuel_{BIOGAS}\ (\%)=\left(\frac{F_{BIOGAS\ fed\ to\ SESR}}{(F_{BIOGAS\ fed\ to\ SESR}+F_{BIOGAS\ fed\ to\ REG}}\right)\cdot 100 \qquad \text{Eq. 3.30}$$

$$Capt.\ CO_2\ (\%)=\left(\frac{F_{CO_2,captured}}{F_{CH_4,in}+F_{CH_4,add.}+F_{CO_2,in}+F_{CO_2,add.}}\right)\cdot 100 \qquad \text{Eq. 3.31}$$

3.3. TECHNO-ECONOMIC ANALYSIS METHODOLOGY

This section describes the methodology used to carry out the techno-economic analysis of the SESR process for H_2 production from biogas.

3.3.1. Methodology for the techno-economic analysis

The simulation of the biogas SESR process studied in section 3.2 evaluated the thermodynamic performance in five case studies applying direct heating to the calciner. However, the techno-economic analysis addressed both direct and indirect heating of the calciner. Indirect heating can offer more flexibility to the calciner, reducing CO_2 emissions. To heat the calciner indirectly, one can supply energy from an external combustor via a fluidised bed heat exchanger [35,154] or include heat pipes [155–157]. The CO_2 recovered from the calciner can then be stored or used independently of the combustion atmosphere in the external burner.

The combustion gases leaving the burner can be considered zero carbon emissions if biogas is used as fuel. Indirect heating of the calciner is especially relevant when air combustion is carried out instead of oxy-combustion since the dilution of the CO_2 stream leaving the calciner with N_2 from the air is avoided allowing the option of having a sequestration-ready stream of CO_2.

Therefore, the techno-economic analysis was performed using two different energy integration strategies in the calciner, i.e., direct and indirect heating, alongside fuels of opposite origins: fossil fuels, such as natural gas, and bio-based fuels, such as biogas. Thus, the case studies for the techno-economic analysis were as follows:

1. **Case 1_BIOG_IndAIR.** Biogas SESR with calciner indirectly heated by air combustion in an external combustor. With this approach, the CO_2 from the calciner would be ready for storage or use, and could potentially mean negative carbon emissions. On the other hand, the flue gas from the external combustor could be considered zero carbon emissions, since a renewable fuel is used.
2. **Case 2_BIOG_DirOXY.** Biogas SESR with calciner directly heated by using in situ oxy-combustion in the calciner. In this case, no external burner is used and all the carbon leaving the calciner can potentially be considered as negative emissions.
3. **Case 3_NG_IndAIR.** Natural gas SESR with calciner indirectly heated by air combustion in an external combustor. In this configuration, the CO_2 stream leaving the calciner can be directly stored or used and the flue gas will be a source of carbon emissions. This case was studied for comparison purposes.

In summary, two scenarios with indirect heating of the calciner were considered (Cases 1 and 3), while one scenario (Case 2) involved direct heating of the calciner with in situ oxy-combustion. A simplified diagram of both strategies is shown in Figure 3.7. In all the cases, a PSA unit was the final stage and the exhaust gases were recycled to the calciner or to the external burner.

For the simulation of the direct heating scenario, Case 2_BIOG_DirOXY, the methodology explained above in section 3.2.1 was used. Thus, the reformer (SESR) and the calciner (REG) were simulated using RGibbs blocks

and a HEN was designed to recover as much heat as possible from the process streams.

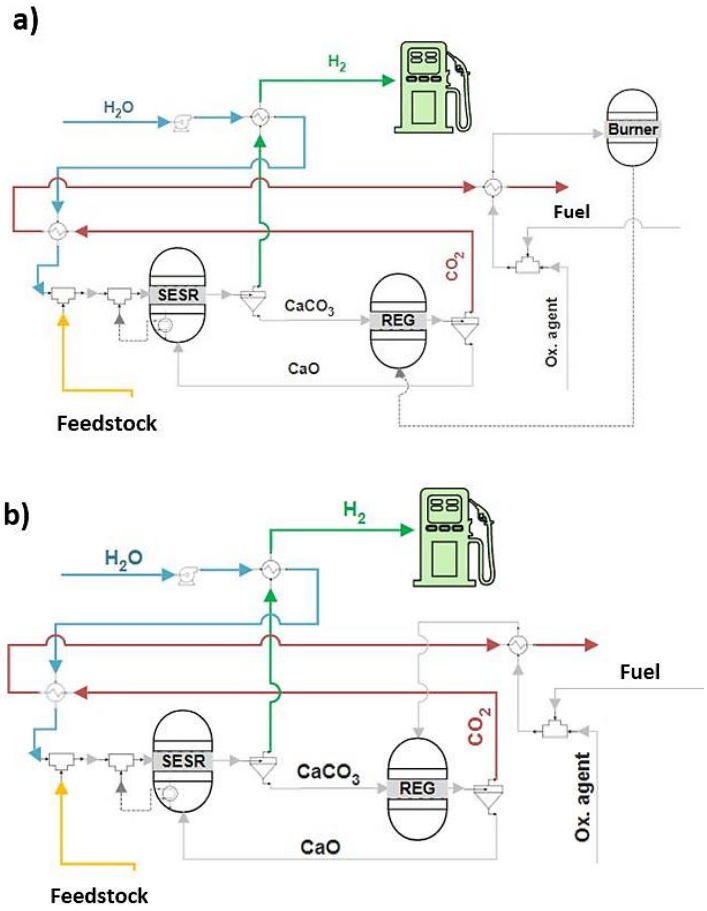

Figure 3.7: Indirect (a) and direct (b) heating of the calciner as energy integration strategies used for the evaluation of the economic performance of the different case studies.

On the other hand, for the simulation of the indirect heating configurations, Case 1_BIOG_IndAIR and Case 3_NG_IndAIR, a similar methodology was used, but an external burner was added to burn biogas or natural gas and transfer heat from this reactor to the calciner.

The external burner is also simulated using RGibbs blocks. To ensure an adequate heat transfer between reactors, the burner's temperature is kept above the calciner. Typically, the calciner temperature would be around 900 ^{o}C and, therefore, the external burner should operate at about 950-1000 ^{o}C.

Furthermore, based on recent pilot tests of a 300 KW_{th} indirectly heated calciner, a 10% heat loss from the external burner to the calciner was assumed [157].

In addition, the HEN is modified in cases of indirect heating to also recover as much heat as possible from the process streams. The flue gas leaving the burner is used to support steam production and preheat the oxidising agent and fuel entering the burner. This stream is not available in direct heating scenarios. The heat from the CO_2 stream leaving the calciner is used to complete the heating of the burner reactants. The detailed Aspen Plus flowsheet for the case of biogas SESR with indirectly heated calciner is shown in the *Annexes*, Annex I: Techno-economic analysis, Fig. II.

3.3.2. Key performance indicators for the techno-economic analysis

To compare the economic analysis of the different scenarios explained above, a detailed cost analysis was performed. To calculate the capital and operating costs, the chemical plant cost estimation methodology developed by Sinnott et al. [162] was used.

The capital cost comprises the direct capital cost of key equipment (i.e., reformer, calciner, PSA, compressors) together with the indirect capital cost. The direct capital cost estimate is based on the relevant units described in the literature sources, which are adjusted to a common baseline year (2021). This estimation is performed using the chemical engineering plant cost index factors and the scaling exponents for the equipment, as shown in Eq. 3.32, where C_A is the cost of the new scaled equipment, C_B is the cost of the base equipment, CI_A and CI_B are the annual cost index factor of the chemical engineering plant in year A and B, respectively, S_A is the capacity of the new equipment, S_B is the capacity of the base equipment, and *x* is the scaling exponent for the equipment, which is taken as 0.6 according to the six-tenths rule, as reported in the literature [138].

$$C_A = \left(\frac{CI_A}{CI_B}\right) \cdot C_B \cdot \left(\frac{S_A}{S_B}\right)^x \qquad \text{Eq. 3.32}$$

As mentioned above, the SESR of natural gas was included in the techno-economic analysis for comparison purposes. Therefore, the KPIs explained in

section 3.2.2 were also used to compare the SESR process performance of biogas and natural gas. Along with the technical performance, the economic evaluation was carried out. The KPI to evaluate the economics of the process was the levelised cost of hydrogen (LCOH), calculated using Eq. 3.33 [138].

$$LCOH = \frac{(TOC \times FCF + FOM)}{(CF \times 8760)} + (FC \times HR) + VOM \qquad \text{Eq. 3.33}$$

where:

- TOC: total overnight capital cost.
- FOM: fixed operating and maintenance costs.
- VOM: variable operating and maintenance costs.
- FC: fuel costs.
- CF: capacity factor.
- HR: plant net heat rate.
- FCF: fixed charge factor, which is defined in Eq. 3.34:

$$FCF = \frac{r \cdot (1+r)^t}{(1+r)^t - 1} \qquad \text{Eq. 3.34}$$

In Eq. 3.34, *t* is the economic lifetime of the plant relative to its base year, and *r* is the discount rate. As recently reported in the economic evaluation of the SE-SMR process, a plant lifetime of 30 years and a discount rate of 12% were used in the present work [138].

The cost estimation in terms of LCOH relies on the methodology proposed by the Global CCS Institute, used in previous works in the literature for the economic evaluation of hydrogen production by reforming [137,163–165], gasification [166] or chemical looping [167] processes. According to the Global CCS Institute [168], the term *levelised cost* was first defined for electricity as the *levelised cost of electricity* (LCOE), and represents all costs required to build and operate a power plant over its economic life, normalised over the total net electricity generated. Thus, the levelised cost value basis resides on technical inputs (i.e., process modelling) alongside economic and financial inputs necessary to establish an economic assessment.

3.4. PRODUCTION OF BIO-DME FROM BIOGAS AS HYDROGEN CARRIER

This section describes the methodology used to study the production of bio-DME by reusing the captured CO_2 and renewable hydrogen from the SESR process.

3.4.1. Modelling methodology for bio-DME production

The bio-DME plant was simulated using Aspen Plus V11 software. A biogas SESR plant with 40 MW of H_2 production capacity was coupled with the SEDMES process. Biogas SESR is carried out in *Unit 1* and SEDMES in *Unit 2*. The process diagram is shown in Figure 3.8.

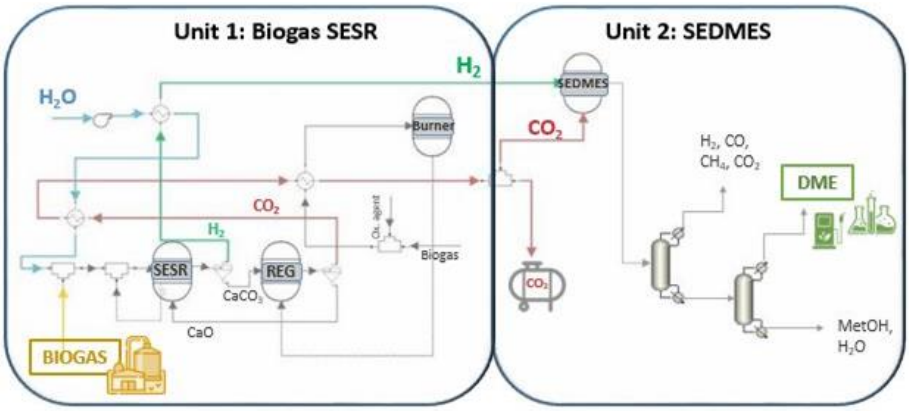

Figure 3.8: Simplified diagram of bio-DME production, as hydrogen carrier, from biogas.

Unit 1, biogas SESR, represents the model developed earlier (see sections 3.2 and 3.3). Therefore, the reformer (SESR) and calciner (REG) were simulated using RGibbs blocks and a heat exchanger network (HEN) was designed to use the available heat to preheat the inlet streams and produce steam. The efficiency of Unit 1 is improved by recovering the extra heat available in the exothermic reformer. For this study, the energy required for sorbent regeneration is provided by indirect heating from an external burner in which biogas is burned in an air atmosphere.

In *Unit 2,* DME is produced using the renewable hydrogen and pure CO_2 produced in *Unit 1*. Hydrogen and CO_2 are first compressed and cooled, as

the SEDMES unit operates at high pressure (50 bar) and low temperature (250 ^{o}C). The two gases are then mixed.

The H_2-rich gas produced in SESR fully supplies the SEDMES process. However, only a part of the CO_2 from SESR is used since the value of the M-module (calculated using Eq. 3.35) must be equal to 2. M-module is the reference value for the ratio of H_2 and CO_2 in the feedstock. As indicated in the literature [145], a target value of 2 is used for the SEDMES process.

$$\text{M-module} = \frac{F_{H2\ \text{reformer gas}} - F_{CO2\ \text{reformer gas}}}{F_{CO\ \text{reformer gas}} + F_{CO2\ \text{reformer gas}}} \qquad \text{Eq. 3.35}$$

The SEDMES unit is modelled using 3 blocks:

- (i) Stoichiometric reactor → A stoichiometric reactor in which an almost complete conversion of CO_2 and CO to DME is assumed. Thus, the maximum amount of H_2O production is estimated.

- (ii) Water removal → A separator block simulates water adsorption. The amount of water to be removed is a design parameter. A sensitivity analysis determined this parameter to obtain similar results to the experiments [146].

- (iii) RGibbs block → At the end, a RGibbs block is included to estimate the equilibrium composition of the mixture. In this block, CH_4, C_2H_4, C_2H_6 and C are considered inert, so they are neither formed nor consumed.

Finally, a distillation train is added in order to purify the DME to the desired specifications (DME purity > 99.5%). For this purpose, the output stream from the last block of the SEDMES unit is sent to a first distillation column where light components (i.e., H_2, CO, etc.), and especially CO_2 are separated from the DME/MetOH mixture. The heavy components from the first distillation column are sent to a second column to separate the MetOH from the DME and reach a purity >99.5% to meet the requirements of ISO 16861:2015.

3.4.2. Key performance indicators for the bio-DME production evaluation

Different KPIs have been defined to quantify the performance of the SEDMES process, as well as the overall performance of the integrated system composed of biogas SESR and SEDMES units.

The Cold Gas Efficiency (CGE) and the Net Efficiency (NE) evaluate the efficiency of the system. Both parameters have been redefined for the specific case of bio-DME production as shown in Eq. 3.36 and Eq. 3.37.

$$CGE\ (\%)=\left(\frac{F_{DME,\,out}\cdot LHV_{DME}}{(F_{CH_4,in}+F_{CH_4,additional})\cdot LHV_{CH_4}}\right)\cdot 100 \qquad \text{Eq. 3.36}$$

$$NE\ (\%)=\left(\frac{F_{DME,\,out}\cdot LHV_{DME}}{(F_{CH_4,in}+F_{CH_4,additional})\cdot LHV_{CH_4}+\frac{P_e}{\eta_{elect}}}\right)\cdot 100 \qquad \text{Eq. 3.37}$$

In addition, the overall process yield is calculated to evaluate the conversion efficiency of biogas to DME. The Global Massive Yield (GMY) is calculated using Eq. 3.38 [32].

$$GMY\ (\%)=\left(\frac{\text{Mass of purified DME [kg/h]}}{\text{Mass of biogas}_{\text{ feedstock fuel}}\text{ [kg/h]}}\right)\cdot 100 \qquad \text{Eq. 3.38}$$

The purity of DME is evaluated using Eq. 3.39, where $F_{DME,out}$ is the molar flow of DME, and F_{total} is the total molar flow of the stream at the head of the second distillation column.

$$\text{DME purity}\ (\%) = 100\cdot(F_{DME,out}/F_{total}) \qquad \text{Eq. 3.39}$$

Finally, a carbon balance determines the distribution of carbon in the different streams. Utilised C is determined using Eq. 3.40 and represents the captured carbon that ends as DME. Sequestered C is determined by Eq. 3.41 and refers to carbon that will end up as stored CO_2 since it is not used for DME synthesis due to the M-module = 2 limitation. On the other hand, wasted C is determined by Eq. 3.42, which is the carbon that ends up in the flue gas or in the different by-products and is therefore not used.

$$\text{Utilised C (\%)} = 100 \cdot (F_{C,\ DME} / F_{total\ C,in}) \quad \text{Eq. 3.40}$$

$$\text{Sequestered C (\%)} = 100 \cdot (F_{C,\ storage} / F_{total\ C,in}) \quad \text{Eq. 3.41}$$

$$\text{Wasted C (\%)} = 100 \cdot (F_{C,\ flue\ gas/by\text{-}products} / F_{total\ C,in}) \quad \text{Eq. 3.42}$$

Chapter 4

RESULTS

4.1. EFFECT OF BIOGAS COMPOSITION ON H_2 PRODUCTION BY SORPTION ENHANCED STEAM REFORMING (SESR)

This study is included in *Publication I* of the thesis. A summary of the results of this work is presented in this section, while the complete document is shown in *Annex II: Publications*.

Globally, raw biogas is composed of CH_4 and CO_2, with minor concentrations of H_2S, N_2, CO, NH_3, etc. Heat and steam production are the traditional biogas utilisation methods. Combined heat and power (CHP) generation has attracted increasing attention over the past decades, although the high CO_2 content of biogas decreases the heating value and flame stability of the gas mixture and prevents the use of biogas as a common energy source [103]. However, during SESR, produced CO_2 is removed in situ from the gas phase by the sorbent by the exothermic carbonation reaction. If the amount of CO_2 contained in the biogas is also removed, it will provide additional heat to the system, which can reduce global energy.

However, biogas contains variable concentrations of CH_4 and CO_2 depending on its origin. Biogas from sewage sludge digesters usually contains 55-75% of CH_4, 20-40% of CO_2 and <1% of nitrogen, whereas the composition of biogas from organic waste digesters is usually 45-75% of CH_4, 25-55% of CO_2 and <1% of nitrogen. On the other hand, in landfills, CH_4 content often varies from 35% to 55%, CO_2 from 15% to 40% and nitrogen from 5% to 25% [103,104]. The works in the literature on biogas SESR usually use a representative biogas composition (i.e., 60/40 CH_4/CO_2 vol.%). Therefore, the objective of this work was to study the effect of the biogas composition on the SESR process.

With this aim, the influence of CH_4 and CO_2 concentrations (vol.%) in biogas on the process performance was assessed. The process parameters under study included H_2 yield, H_2 selectivity, CH_4 conversion, H_2 purity, and CH_4, CO and CO_2 concentrations in the effluent gas. The experimental results from biogas SESR were compared with the conventional biogas steam reforming (SR) process. For this purpose, the SESR process proceeded until the calcined dolomite became saturated (pre-breakthrough) and lost its capacity for CO_2 removal. Afterwards, CO_2 capture by the sorbent was negligible (post-breakthrough) and the conventional catalytic SR was

assumed to occur and allowed to reach a steady state to compare the results with the SESR process.

Experiments were conducted using simulated biogas (CH_4 and CO_2 mixtures) at atmospheric pressure and isothermally, at temperatures of 600 and 650 ^oC. For comparison purposes, SESR experiments were also carried out using 100% CH_4. This work was carried out in a fluidised bed reactor. The biogas compositions studied are shown in Table 4.1.

A thermodynamic analysis of the process was also performed using Aspen Plus V10 software (Aspentech) to determine the theoretical feasibility of the process at the selected conditions and to compare the equilibrium values obtained with the experimental results. The RGibbs reactor and the Peng-Robinson property method were used for the equilibrium calculations. The main species produced were H_2, CH_4, CO, CO_2, H_2O, CaO and $CaCO_3$. C_2H_4, C_2H_6 and C (graphite as solid carbon) were also included in the products pool, but their concentrations in the equilibrium stream were null or not high enough to be considered relevant products [54]. The product mole fractions were calculated on a dry basis.

Table 4.1: Composition of the biogas mixtures studied.

Biogas mixture	CH_4 (vol.%)	CO_2 (vol.%)	CH_4/CO_2 molar ratio
50/50	50	50	1.00
60/40	60	40	1.50
70/30	70	30	2.33
80/20	80	20	4.00
90/10	90	10	9.00
95/5	95	5	19.00

Two sets of biogas SESR experiments were performed:

- (I) → the CH_4 flow in the feed gas was maintained constant, i.e., constant steam/CH_4 molar ratio of 6 and $GHSV_{CH4}$ value of 1969 mL CH_4 g_{cat}^{-1} h^{-1} were used.

- (II) → the biogas flow in the feed gas was maintained constant, i.e., constant steam/C molar ratio of 3 and $GHSV_{biogas}$ value of 3937 mL biogas g_{cat}^{-1} h^{-1} were used.

Table 4.2 shows the range of experimental conditions used in the experiments.

Table 4.2: Experimental conditions used in two sets of experiments to study the effect of biogas composition on the SESR process.

Parameter	**Set I – Constant CH_4 flow**	**Set II - Constant biogas (CH_4+CO_2) flow**
CH_4 in feed gas (vol.%)	50-100	50-100
Temperature	600 ^oC, 650 ^oC	600 ^oC, 650 ^oC
Steam/CH_4, H_2O/CH_4 molar ratio	6.0	3.2-6.0
Steam/C, $H_2O/(CH_4+CO_2)$ molar ratio	3.0-5.7	3.0
$GHSV_{CH4}$ (mL CH_4 g_{cat}^{-1} h^{-1})	1969	1969-3740
$GHSV_{biogas}$ (mL biogas g_{cat}^{-1} h^{-1})	2072-3937	3937

4.1.1. Set I of experiments: Effect of biogas composition considering CH_4 as the only reactant gas

During these experiments, the CH_4 flow in the feed gas was maintained constant, i.e., a constant steam/CH_4 molar ratio of 6 and a $GHSV_{CH4}$ value of 1969 mL CH_4 g_{cat}^{-1} h^{-1} were used. In this way, only CH_4 is considered as reactant gas in the process, and so the steam to carbon molar ratio and the space velocity regarding methane are kept constant. Figure 4.1 shows the experimental concentrations of gases produced and the corresponding equilibrium values obtained from thermodynamic analysis.

For the SESR process, H_2 (Figure 4.1a), CH_4 (Figure 4.1b), CO (Figure 4.1c) and CO_2 (Figure 4.1d) concentrations have an approximately constant value for all the biogas compositions studied (50-95 vol.% of CH_4). These values are similar to those obtained from the SESR of pure methane (100 vol.% CH_4 in the plots), indicating that the sorbent removes from the gas phase all the extra CO_2 added with the biogas by the carbonation reaction.

On the other hand, the experimental values for the gas concentrations are quite close to those of the equilibrium under all the conditions. The experimental results of the biogas SESR also indicate that there is no visible effect of the CO_2 contained in the biogas on the SESR performance compared to pure methane. CO_2 is effectively removed from the gas phase by reaction with the sorbent under the studied conditions. This provides great flexibility to the SESR process when it comes to the use of biogas with different compositions derived from a wide range of sources.

For the SR process, H_2 concentration (Figure 4.1a) increases with the increase in the CH_4 content of biogas. CH_4 concentration (Figure 4.1b) does not significantly vary, while CO and CO_2 concentrations (Figure 4.1c and 4.1d, respectively) decrease as the CH_4 content in biogas increases. The higher CO_2 concentration obtained with lower methane content in biogas is due to the higher amount of CO_2 added with the biogas, which is not removed by any sorbent under SR conditions. The increase in H_2 concentration with the CH_4 content in biogas is in accordance with the lower concentration of CO_2 for the highest CH_4 contents in biogas, together with the lower CO concentration obtained.

These results suggest that higher CO_2 concentrations in the gas phase supplied by the biogas prevent the WGS reaction from occurring to a higher extent (or the equilibrium between CO and CO_2 could tend to favour the reverse WGS), resulting in higher CO contents, and in turn lower H_2 concentrations. Therefore, higher CH_4 partial pressures in the feed favour the steam methane reforming process.

It has been highlighted in the literature that the presence of CO_2 in biogas is advantageous for the SR process when the desired product is syngas (H_2+CO), which is used to produce higher-value products such as synthetic liquid fuels or other chemicals. However, when the desired product is hydrogen, CO needs to be converted to CO_2 by the WGS reaction and CO_2 in biogas adds no benefit [169], in accordance with the results obtained in this work. For hydrogen production, the lower the CO_2 content in biogas, the more efficient the CH_4 conversion, which facilitates obtaining high-purity H_2 by SR of biogas [170]. It can be seen that H_2 and CO_2 concentrations closely follow the equilibrium pattern, while slightly higher experimental values of CH_4 and lower values of CO are obtained compared to equilibrium (Figure 4.1).

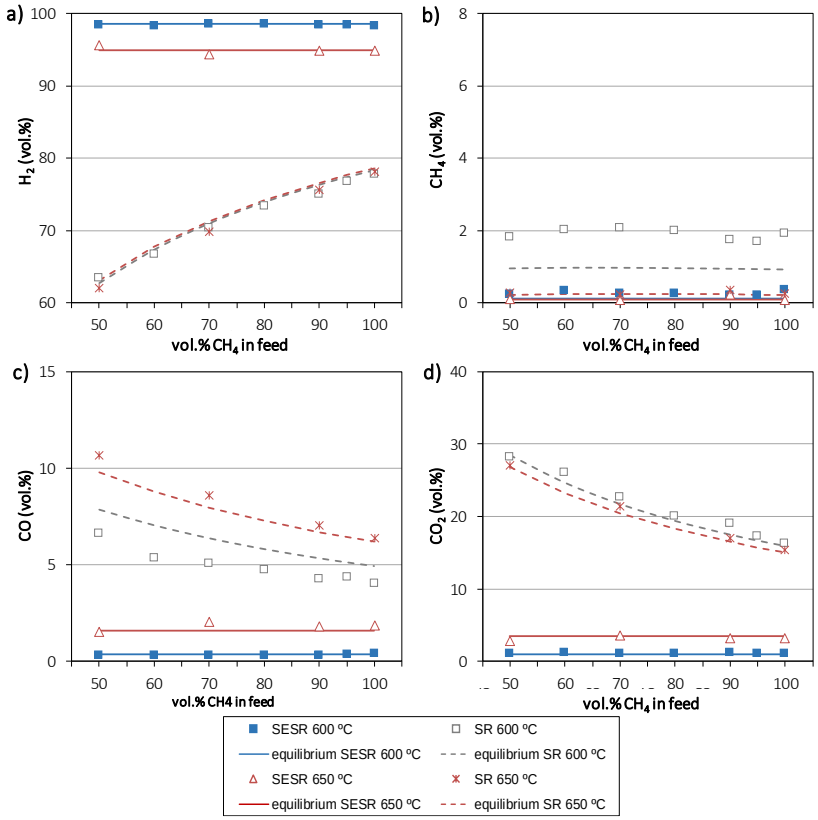

Figure 4.1: Effect of methane content in biogas on the H_2 (a), CH_4 (b), CO (c) and CO_2 (d) concentrations during SESR and SR at 600 and 650 ºC. Reaction conditions: steam/CH_4=6 mol/mol, $GHSV_{CH4}$ = 1969 $mL_{CH4}\ g_{cat}^{-1}\ h^{-1}$, sorbent/catalyst ratio=20 g/g, Pd/Ni-Co HT catalyst and dolomite sorbent.

Figure 4.2 shows the H_2 yield (Figure 4.2a), H_2 selectivity (Figure 4.2b) and CH_4 conversion (Figure 4.2c) as a function of methane content in biogas. For SESR, their values are similar, independent of the biogas composition, and very close to the equilibrium in the case of the H_2 selectivity and CH_4 conversion. However, H_2 yield values are below those predicted by the thermodynamic equilibrium under all the conditions studied. For SR, a slight increase in the H_2 yield, H_2 selectivity, and CH_4 conversion is detected as the methane content in biogas increases, and their values are below those of the equilibrium calculations.

During biogas steam reforming, given that CO_2 is supplied to the process with the feed, a combination of steam reforming of methane and dry methane reforming (Eq. 4.1) could be considered to occur:

$$CH_4 + CO_2 \leftrightarrow 2CO + 2H_2 \qquad \Delta H_r^0 = +247 \text{ kJ mol}^{-1} \qquad \text{Eq. 4.1}$$

However, dry methane reforming is a highly endothermic reaction that occurs at high temperatures (>700 ^oC) and plays a minor role when enough H_2O is available [45,46].

In addition, the water-gas shift reaction is typically faster than dry methane reforming in the presence of reforming catalysts [112]. According to the results, the absence of dry methane reforming is evidenced because CH_4 conversion is not significantly enhanced during the SR of biogas compared to pure methane under the conditions studied. Moreover, no excess amount of CO in relation to the amount of CH_4 converted was detected, which could have derived from CO_2 reforming by Eq. 4.1 according to Ahmed et al. [169].

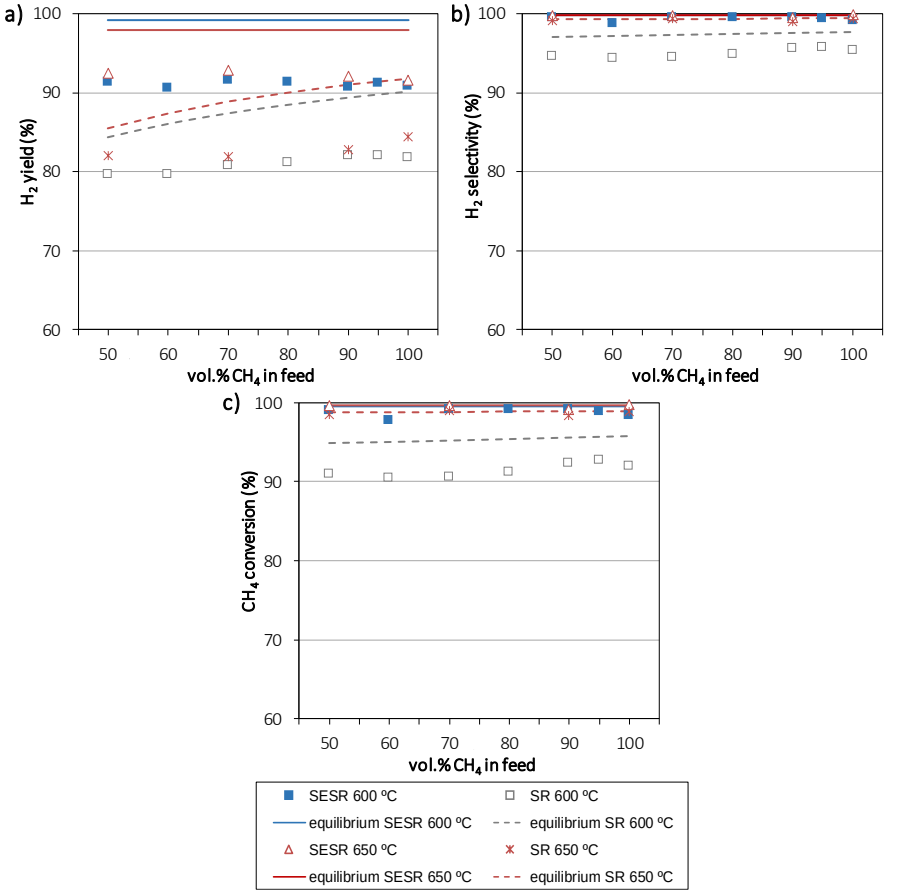

Figure 4.2: Effect of methane content in biogas on the H_2 yield (a), H_2 selectivity (b) and CH_4 conversion (c) during SESR and SR at 600 and 650 ºC. Conditions: steam/CH_4=6 mol/mol, $GHSVCH_4$ = 1969 mL_{CH4} g_{cat}^{-1} h^{-1}, sorbent/catalyst ratio=20 g/g, Pd/Ni-Co HT catalyst and dolomite sorbent.

Regarding the effect of the temperature, the results follow similar trends for both temperatures, 600 and 650 ºC, in accordance with the equilibrium predictions. For the SESR process:

- H_2 concentration is higher under lower temperatures (Figure 4.1a).
- CO concentration is lower at lower temperatures (Figure 4.1c) due to the favoured exothermic WGS reaction.
- CO_2 concentration is lower at lower temperatures (Figure 4.1d) due to the favoured exothermic carbonation reaction.

- CH_4 concentration is lower at higher temperatures (Figure 4.1b) due to the methanation reaction being thermodynamically unfavourable at high temperatures when the steam methane reforming reaction is favoured.

These results support the higher H_2 concentration at lower temperatures and are in agreement with the literature [48,49]. On the other hand, for the SR process:

- H_2 concentration is quite similar for both temperatures studied (Figure 4.1a).
- CO concentration is higher at higher temperatures (Figure 4.1c) due to the WGS reaction being unfavourable, which leads to a slightly lower CO_2 concentration at higher temperatures (Figure 4.1d).
- CH_4 concentration is markedly lower at higher temperatures (Figure 4.1b) since the methanation reaction is unfavourable, and the steam methane reforming reaction is favoured at high temperatures.

4.1.2. Set II of experiments: Effect of biogas composition considering CH_4 and CO_2 as reactant gases

The second set of experiments was also performed at 600 and 650 ^oC. In this case, the biogas flow in the feed gas was maintained constant, i.e., a constant steam/C molar ratio of 3.0 and a $GHSV_{biogas}$ value of 3937 mL_{biogas} g_{cat}^{-1} h^{-1} were used. In this way, both CH_4 and CO_2 are considered as possible reactant gases in the process and so the steam to carbon molar ratio and the space velocity regarding biogas are kept constant. For this set, the steam/CH_4 molar ratio changed from 3.2 to 6.0, while the $GHSV_{CH4}$ changed from 1969 to 3740 mL CH_4 g_{cat}^{-1} h^{-1}, as shown in Table 4.2. Figure 4.3 shows the concentrations of gases obtained from these experiments together with the equilibrium values obtained from the thermodynamic analysis. For the SESR process:

- H_2 concentration (Figure 4.3a) slightly decreases as methane content in biogas increases.
- CH_4 (Figure 4.3b) and CO (Figure 4.3c) concentrations slightly increase with methane content in biogas.

- CO_2 concentration (Figure 4.3d) does not change significantly under the studied conditions.

When a constant CH_4 flow in the feed gas was used (Figure 4.1 and Figure 4.2), no effect of biogas composition on the SESR performance was observed (since CO_2 is removed from the gas phase by the carbonation reaction). For the experiments with constant biogas flow (Figure 4.3), as methane content in biogas increases, the steam/CH_4 molar ratio decreases and, correspondingly, the space velocity related to methane increases (Table 4.2). The lower steam content reduces both the steam methane reforming and WGS reactions, accounting for the higher CH_4 and CO contents and the lower H_2 obtained for methane-enriched biogas compositions. In addition, lower H_2 production and fuel conversion might be expected at high space velocities due to shorter contact times of gas and solid phases, i.e., with lower methane contents in biogas.

On the other hand, for the results of the SR process, the trends for each gas are as follows:

- H_2 and CH_4 concentrations (Figure 4.3a and Figure 4.3b, respectively) increase with methane content in biogas.
- CO concentration (Figure 4.3c) slightly increases as methane content in biogas increases until 80 vol.%, and then slightly decreases with a further increase in methane content of biogas.
- CO_2 concentration (Figure 4.3d) decreases as methane content in biogas increases.

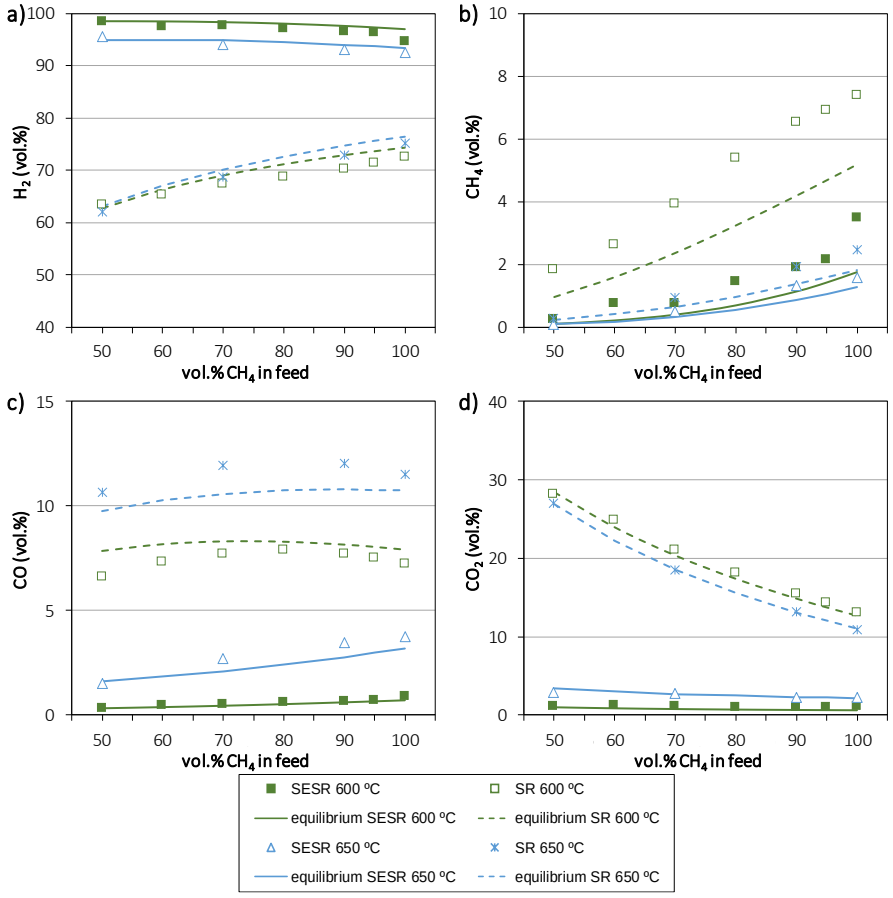

Figure 4.3: Effect of methane content in biogas on the H_2 (a), CH_4 (b), CO (c) and CO_2 (d) concentrations during SESR and SR at 600 and 650 ºC. Conditions: steam/C = 3 mol/mol, GHSVbiogas = 3937 mL biogas g_{cat}^{-1} h^{-1}, sorbent/catalyst ratio = 20 g/g, Pd/Ni-Co HT catalyst and dolomite sorbent.

Comparing the performance of conventional SR in both sets of experiments, it can be seen that with constant biogas flow in the feed (Figure 4.3), the CO_2 concentration decreases when CH_4 content in biogas increases due to the lower amount of CO_2 in the biogas, together with the lower steam/C molar ratios that could reduce the steam methane reforming and WGS reactions. An increase in the H_2 concentration with methane content in biogas is also detected, which is in accordance with the lower concentration of CO_2 that is added with biogas at these conditions, as well as with the decrease in the steam/CH_4 molar ratio and the increase in the space velocity.

The effect of the temperature on the process performance for the experiments with a constant biogas flow (Figure 4.3) agrees with the equilibrium predictions and follows the same tendency as the experiments with constant CH_4 flow (Figure 4.1 and Figure 4.2).

For the experiments with constant biogas flow, the absence of dry methane reforming (Eq. 4.1) is confirmed by the absence of excess CO derived from CO_2 reforming concerning the converted CH_4 [169]. It can be ascribed to the temperature used in these experiments (600-650 ^oC) does not promote the endothermic dry methane reforming reaction. On the other hand, the presence of steam favours the steam methane reforming and WGS reactions at the expense of the dry methane reforming reaction. Therefore, these results confirm that the CO_2 supplied with the biogas is effectively removed from the gas phase by the sorbent during the SESR of biogas, and it does not influence the sorption enhanced reforming process compared to pure methane since it does not act as a reactant in the process.

4.1.3. Conclusions on the effect of the biogas composition on SESR

The conclusions of the study on the effect of biogas composition on H_2 production by SESR are as follows:

- The production of renewable H_2 by the sorption enhanced steam reforming of biogas has been demonstrated both thermodynamic and experimentally.

- High H_2 purity (98.4 vol.%) and yield (91%) have been obtained by SESR of biogas containing 50-95 vol.% of CH_4 (balance CO_2) on a Pd/Ni-Co catalyst and using Arctic dolomite as carbon dioxide sorbent.

- During the SESR of biogas with different compositions (from 50 to 95 vol.% of CH_4), all CO_2 supplied with the biogas is effectively removed from the gas phase by the sorbent and does not affect the performance of the SESR process. Thus, a constant H_2 production is achieved regardless of the biogas composition. However, higher CH_4 partial pressures in the biogas favour the steam methane reforming reaction, giving higher H_2 concentrations, during steam

reforming of biogas without sorbent, which makes the process highly dependent on the biogas composition.

Overall, the results of this study demonstrate that the sorption enhanced steam reforming of biogas is a promising process for producing sustainable hydrogen from renewable energy sources.

4.2. EFFECT OF H_2S ON H_2 PRODUCTION BY SORPTION ENHANCED STEAM REFORMING (SESR) OF BIOGAS

This study is included in *Publication II* of the thesis. This section presents a summary of the results of this work, while the complete document is shown in *Annex II: Publications*.

One of the major challenges in the use of biogas in conventional reforming processes is the presence of H_2S, since it may deactivate the reforming catalyst. Variable H_2S concentrations can be found in the composition of biogas [103,104]: 0-10000 ppm from sewage sludge digesters, 10-2000 ppm from organic waste digesters, and 0-100 ppm from landfills [25]. Nickel-based catalysts are particularly susceptible to deactivation by sulphur compounds. The accepted mechanism of sulphur poisoning is the chemisorption of sulphur on the Ni surface, i.e., the catalyst deactivates through sulfidation of the active Ni particles and formation of Ni–S species that do not take part in the reforming reactions, as shown in Eq. 4.2 [106].

$$Ni + H_2S \leftrightarrow Ni–S + H_2 \qquad \text{Eq. 4.2}$$

Addressing the effect of biogas H_2S on hydrogen production by the cyclic SESR process, a complex system where different steps under varying gaseous atmospheres are needed due to the presence of a CaO-based CO_2 sorbent is challenging and scarcely studied. CaO could, for example, react with H_2S to form calcium sulphide by Eq. 4.3 [122,123] under the reducing conditions during the reforming step.

$$CaO + H_2S \leftrightarrow CaS + H_2O \qquad \text{Eq. 4.3}$$

Although there have been recent efforts focused on the development of sulphur-resistant catalysts (addition of rare-earth, alkaline-earth or noble metals, or use of resilient materials such as alloys, perovskites, and core-shell structures [124,125]), the presence of H_2S is still a challenge in reforming systems and a significant barrier for their commercial implementation. The content of H_2S in biogas can be reduced by employing a desulphurisation unit; however, the removal of trace amounts of H_2S is often an economically unattractive option, especially in small-scale applications [111], and sulphur-containing compounds remaining after desulphurisation can still reach the catalyst blocking the active sites [114,126]. Therefore, some resistance to sulphur poisoning in reforming processes is crucial to ensure proper operation at the industrial scale [124].

In this frame, the effect of the H_2S concentration in biogas on the H_2 production by catalytic SESR, which involves a CaO-based sorbent material, has been studied in this thesis. This work was performed in a fixed bed reactor using the Pd/Ni-Co HT-like catalyst and Arctic dolomite as CO_2 sorbent. The catalyst deactivation during cyclic SESR experiments feeding biogas ($60CH_4/40CO_2$ vol.%) with different concentrations of H_2S, as well as the interaction of sulphur with the CO_2 sorbent, were analysed.

The reactor was loaded with a 10.5 g mixture of calcined dolomite and catalyst at a ratio of 20 $g_{sorbent}/g_{catalyst}$. H_2S was introduced into the reactor from a cylinder containing H_2S (200 ppm) diluted in N_2. Different concentrations of H_2S in the biogas were studied (150, 350, 500, and 1000 ppm), alongside the absence of H_2S for comparison purposes. The experiments were performed at 600 ^oC and atmospheric pressure, under a steam/CH_4 molar ratio (S/CH_4) of 6 (i.e., three times higher than the stoichiometric value) and a gas hourly space velocity (GHSV) of 1803 mL_{CH4} g_{cat}^{-1} h^{-1}.

During a typical experiment, the SESR reaction occurs until the calcined dolomite becomes saturated (pre-breakthrough) and loses its capacity for CO_2 removal. Afterwards, CO_2 capture by the sorbent is negligible (post-breakthrough) and the conventional catalytic steam reforming process is assumed to occur. The SESR of biogas containing H_2S was evaluated during the pre-breakthrough stage. After the reforming stage, the bed was subjected to a regeneration step before the next SESR cycle at 800 ^oC in airflow (200 NmL min^{-1}) until the CO_2 levels dropped to less than 0.1 vol.%. A

reduction step at 670 °C, was then performed after regeneration. The experiments were carried out during five consecutive SESR cycles for all H_2S concentrations.

4.2.1. Effect of the biogas H_2S content on SESR cyclic operation

To study the catalyst activity during cyclic SESR of biogas containing H_2S, five carbonation/calcination cycles were performed for different H_2S concentrations in the inlet biogas.

4.2.1.1. Catalyst activity and process performance in the presence of H_2S

Figure 4.4 shows the H_2 yield, H_2 concentration, CH_4 conversion, and CH_4 concentration during five cycles of SESR for all H_2S concentrations. In the experiments without H_2S and with 150 ppm H_2S, all variables remain constant during all cycles, indicating no detectable deactivation of the catalyst. However, for higher H_2S concentrations, a decrease in H_2 production is detected during the last cycles. In the case of a H_2S concentration of 350 ppm of H_2S, a slight decrease in H_2 production is detected in cycle 5, which is explained by a slightly lower value of the CH_4 conversion (Figure 4.4c) and a higher value of the CH_4 concentration (Figure 4.4d). For H_2S concentrations of 500 and 1000 ppm of H_2S, the decrease in H_2 production (Figure 4.4a and Figure 4.4b) is more evident during cycles 4 and 5, and higher CH_4 concentrations are produced as a result of lower CH_4 conversion.

After cycle 4, the H_2 yield decreased slightly (~3%) for biogas H_2S concentrations of 500 and 1000 ppm, with a very low decrease in H_2 purity (~1 vol.%). However, after cycle 5, the H_2 yield decreased by 10.8 and 4.5% points for biogas H_2S concentrations of 500 and 1000 ppm, respectively (while H_2 purity decreased by only 3 and 2 vol.%, respectively).

The results for the SESR process evaluated in the present study show signs of poisoning on the catalyst for the highest biogas H_2S concentrations studied, but it is far from a complete deactivation.

From a practical point of view, after five SESR cycles, it was found that 150 ppm of H_2S in the biogas could be a sufficiently low H_2S concentration that does not decrease the process performance. As suggested in the

literature [171], to obtain a suitably low H_2S concentration, the biogas could be diluted with steam or cleaned to reduce the H_2S content.

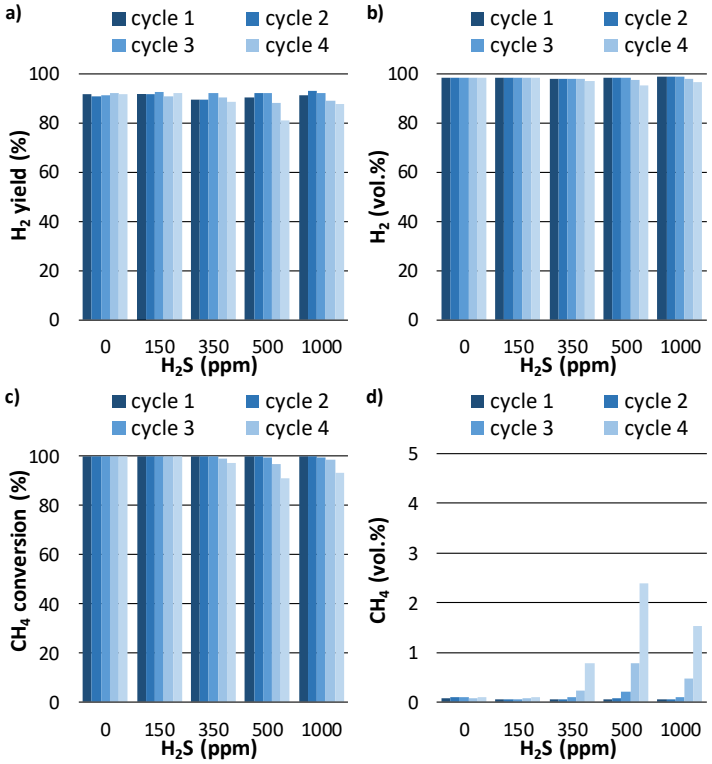

Figure 4.4: H_2 yield (a), H_2 purity (b), CH_4 conversion (c) and CH_4 concentration (d) during five cycles of SESR for all H_2S concentrations. Operating conditions: Biogas=60/40 CH_4/CO_2 vol.%; T=600 ^oC; S/CH_4=6 mol/mol; GHSV=1803 $mL_{CH4}\ g_{cat}^{-1}\ h^{-1}$; sorbent/catalyst ratio=20 g/g; Pd/Ni-Co HT catalyst and dolomite sorbent.

4.2.1.2. Sorbent CO_2 capture capacity in the presence of H_2S

To evaluate how the presence of H_2S in the biogas influences the in situ CO_2 sorption by the dolomite sorbent, the CO_2 capture capacity of the sorbent during cyclic SESR of biogas containing different concentrations of H_2S was studied. CO_2 captured by the sorbent was estimated from the CO_2 released during the sorbent regeneration step. Figure 4.5 shows the CO_2 captured by the sorbent during five carbonation/calcination cycles for all H_2S concentrations studied. As expected, CO_2 captured by the sorbent decreases with the number of cycles for all biogas H_2S concentrations due to a loss in the sorbent capacity.

Regarding the H_2S effect, the results show that the CO_2 captured during the first SESR cycle is similar for all biogas H_2S contents. This value is close to the theoretical estimated maximum CO_2 capture capacity of 0.46 g CO_2/g sorbent. However, a clear effect of the H_2S concentration on the CO_2 sorption performance of the sorbent is detected after longer cyclic operation. For cycles 2 to 5, a decrease in the CO_2 captured is detected as the H_2S concentration in the inlet biogas increases. The loss rate in CO_2 sorption capacity increases with the biogas H_2S concentration from 150 to 500 ppm, but similar values of CO_2 captured along cycles are found for 500 and 1000 ppm of H_2S.

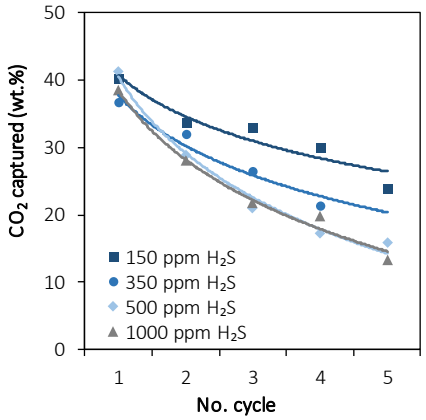

Figure 4.5: CO_2 captured by the sorbent during five SESR cycles for all H_2S concentrations. Operating conditions: Biogas=60/40 CH_4/CO_2 vol.%; Treforming=600 ºC; S/CH_4=6 mol/mol; GHSV=1803 $mL_{CH4}\ g_{cat}^{-1}\ h^{-1}$; sorbent /catalyst ratio=20 g/g; Tregeneration=800 ºC; Pd/Ni-Co HT catalyst and dolomite sorbent.

4.2.1.3. Sulphur distribution in spent catalyst and sorbent after SESR cycles

To determine the total sulphur content, ICP-OES analysis was performed on the spent catalyst and sorbent. The analysis was carried out just after the end of five SESR cycles (including the calcination and reduction steps after cycle 5). The S concentration in the spent catalyst and sorbent materials is shown in Table 4.3. In the case of the catalyst, an increase in S concentration is found as the biogas H_2S concentration increases from 150 to 500 ppm. However, no further increase is seen with the increase in biogas H_2S concentration up to 1000 ppm. This indicates that the poisoning effect of the

H_2S on the catalyst does not proportionally increase when the biogas H_2S concentration increases from 500 to 1000 ppm, since the accumulated sulphur is slightly lower, which could explain the higher values of hydrogen production for the 1000 ppm H_2S experiment (Figure 4.4).

On the other hand, the S concentration in the sorbent increases with the biogas H_2S concentration from 150 to 1000 ppm. It should be highlighted that an exponential increase in the sorbent S content is detected when the biogas H_2S concentration increases up to 1000 ppm.

Table 4.3: Total sulphur content of the spent Pd/Ni-Co HT catalyst and dolomite sorbent after five cycles of SESR of biogas containing different concentrations of H_2S (normalized by the feeding time).

Biogas H_2S concentration (ppm)	Total S (ppm)	
	Catalyst	Sorbent
150	1209	37
350	3132	76
500	4141	122
1000	3728	552

Operating conditions: Biogas=60/40 CH_4/CO_2 vol.%; T=600 ^oC; S/CH_4=6 mol/mol; GHSV=1803 mL_{CH4} $gcat^{-1}$ h^{-1}; sorbent/catalyst ratio=20 g/g; Pd/Ni-Co HT catalyst and dolomite sorbent.

The distribution of sulphur between the sorbent, catalyst and evolved gas relative to the H_2S introduced into the process was estimated from the total S contents in the sorbent and catalyst materials. The S content in the gas phase was calculated by difference.

Figure 4.6 shows the total S distribution between sorbent, catalyst and gas after the 5 SESR cycles. The S distribution between the different products of the process was similar for the H_2S concentrations of 150 (Figure 4.6a), 350 (Figure 4.6b) and 500 ppm (Figure 4.6c). Almost half of the sulphur introduced (43-48%) was found in the catalyst and 32-37% in the sorbent. Therefore, 19-20% of the sulphur is assumed to be released with the gas.

However, for a biogas H_2S concentration of 1000 ppm (Figure 4.6d), 77.5% of the sulphur introduced was found in the sorbent, while a much lower percentage, 19.7%, was detected in the catalyst. Therefore, only a 2.8% would be released with the outlet gas. This suggests that the reaction of sulphur with the sorbent is more favourable at higher H_2S contents. This distribution of sulphur in the spent catalyst and sorbent could explain the

lower catalyst poisoning effect than expected with 1000 ppm H_2S, since the higher biogas H_2S concentrations would decrease the reaction of sulphur with the catalyst at the expense of the sorbent. Moreover, from the results obtained for 1000 ppm of H_2S, we can deduce that it is more difficult to remove H_2S from the gas phase when its initial concentration is lower.

On the other hand, these results show that CO_2 and H_2S can be captured simultaneously during SESR under the studied conditions. Previous experiments on sorption enhanced gasification at 640-775 ^oC have also reported the simultaneous removal of CO_2 and H_2S by CaO [121,172,173]. It has been found that sulphur in the syngas was around 15% of the total sulphur introduced into the gasification reactor, while 65-85% was found as CaS in the sorbent particles (no catalyst was used in those experiments) [173]. In the present work, we have found that a high proportion of sulphur remained in the solid catalyst and sorbent materials after the cyclic SESR process of biogas containing H_2S.

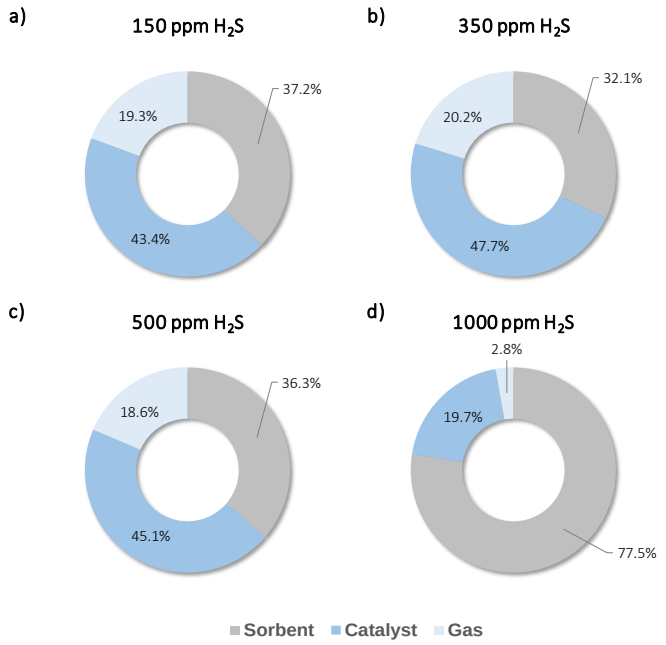

Figure 4.6: Total S distribution (wt.%) between sorbent, catalyst and gas after five cycles of the SESR process for biogas H_2S concentrations of 150 (a), 350 (b), 500 (c), and 1000 ppm (d). Operating conditions: Biogas=60/40 CH_4/CO_2 vol.%; T=600 ^oC; S/CH_4=6 mol/mol; GHSV=1803 $mL_{CH4}\ g_{cat}^{-1}\ h^{-1}$; sorbent/catalyst ratio=20 g/g; Pd/Ni-Co HT catalyst and dolomite sorbent.

4.2.2. Characterisation of the spent catalyst and sorbent after cyclic SESR operation

4.2.2.1. SEM analysis of spent catalyst and sorbent

SEM analysis of the spent Pd/Ni-Co HT catalyst was performed after five SESR cycles for all H_2S concentrations of the biogas. For comparison purposes, the spent catalyst was analysed after the first cycle in the case of the experiment with 350 ppm of H_2S. Figure 4.7 shows the SEM images of the fresh sorbent (Figure 4.7a), spent sorbent after 1 cycle (Figure 4.7b) and spent sorbent after 5 cycles (Figure 4.7c-f) of the SESR process for different H_2S concentrations in the biogas.

No visible differences are detected between fresh and spent catalyst after one cycle. However, a clear decrease in particle size is detected in all spent catalyst samples after 5 SESR cycles. Furthermore, no appreciable differences are observed in the spent catalyst for the different biogas H_2S concentrations after five cycles. On the other hand, no apparent agglomeration of the catalyst particles by sintering is observed after five cycles.

In addition, Figure 4.8 shows the EDX elemental mapping of Ni, Co, Pd, and S in the spent Pd/Ni-Co HT catalyst after five cycles of the SESR process with biogas containing between 150 and 1000 ppm of H_2S. Elemental mapping by SEM-EDX shows the presence of sulphur in the spent catalyst for all H_2S concentrations, indicating the conversion of H_2S on the catalyst surface during the SESR process. It can be seen that sulphur has a distribution in the catalyst similar to that of Ni, Co and Pd, suggesting interaction between sulphur and one (or more) metals in the catalyst. Under the experimental conditions studied, nickel/cobalt sulphides could be formed. From a qualitative point of view, EDX mapping shows that the amount of sulphur in the spent catalyst for the experiments with 150 ppm of H_2S is visibly lower than that for the experiments with higher H_2S biogas concentration.

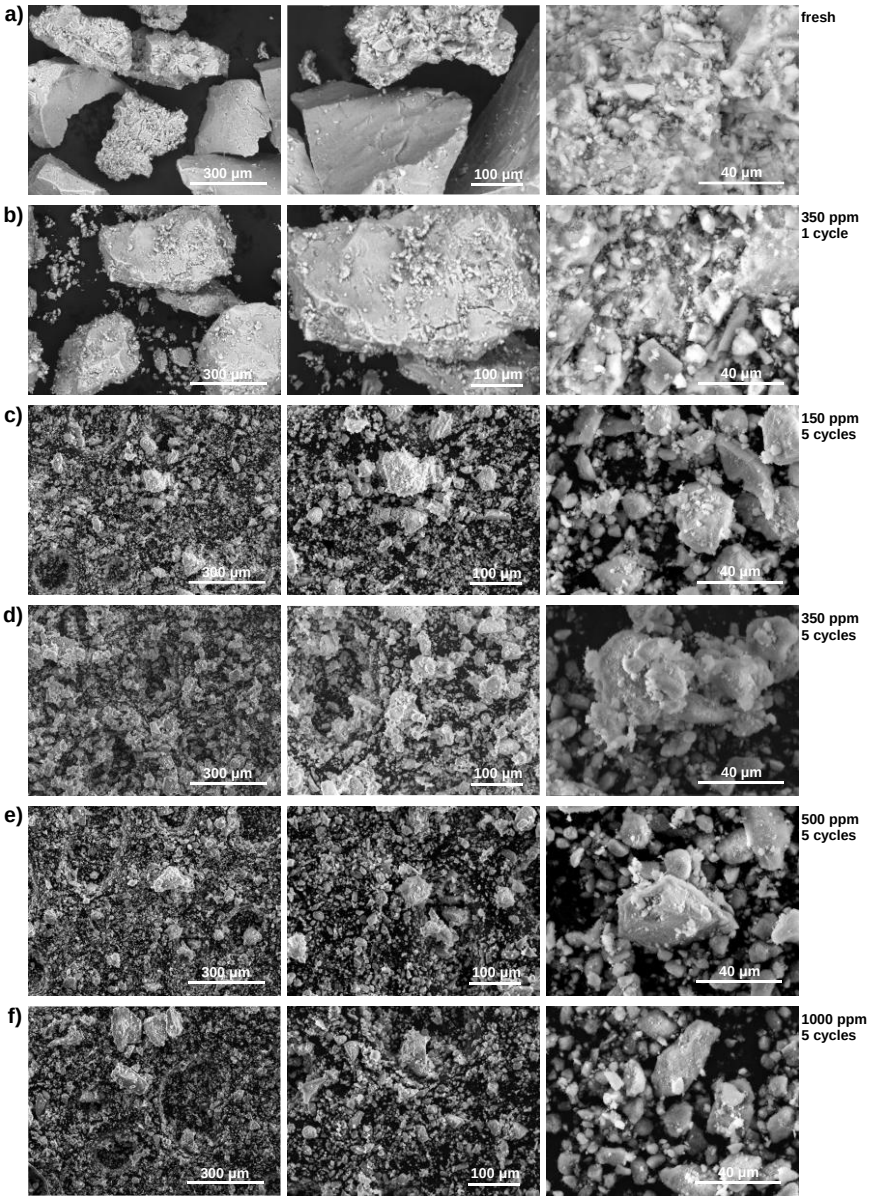

Figure 4.7: SEM images of the fresh and spent Pd/Ni-Co HT catalyst after one and five cycles of the SESR process for different biogas H_2S concentrations: (a) fresh sorbent; (b) 350 ppm H_2S, 1 cycle; (c) 150 ppm H_2S, 5 cycles; (d) 350 ppm H_2S, 5 cycles; (e) 500 ppm H_2S, 5 cycles; and (f) 1000 ppm H_2S, 5 cycles. Operating conditions: Biogas=60/40 CH_4/CO_2 vol.%; T=600 ^oC; S/CH_4=6 mol/mol; GHSV=1803 $mL_{CH4}\ g_{cat}^{-1}\ h^{-1}$; sorbent/catalyst ratio=20 g/g; Pd/Ni-Co HT catalyst and dolomite sorbent.

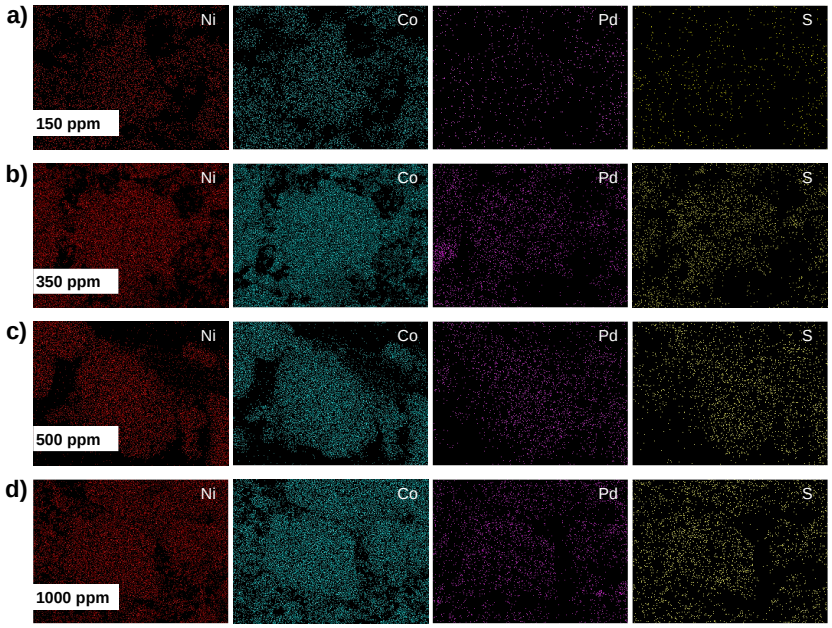

Figure 4.8: EDX elemental mapping of Ni, Co, Pd and S in the spent Pd/Ni-Co HT catalyst after five cycles of the SESR process for different biogas H_2S concentrations: (a) 150 ppm; (b) 350 ppm; (c) 500 ppm; and (d) 1000 ppm. Operating conditions: Biogas=60/40 CH_4/CO_2 vol.%; T=600 ^oC; S/CH_4=6 mol/mol; GHSV=1803 $mL_{CH4}\ g_{cat}^{-1}\ h^{-1}$; sorbent/catalyst ratio=20 g/g; Pd/Ni-Co HT catalyst and dolomite sorbent.

On the other hand, Figure 4.9 shows the SEM analysis of the spent sorbent after five SESR cycles. For comparison purposes, the spent sorbent after the first SESR cycle was analysed for the experiment with 350 ppm of H_2S. EDX elemental mapping of S was also performed on the spent sorbent, but no sulphur was detected at any of the operating conditions, at its concentration was below the detection limit of the SEM analyser. Figure 4.9 shows the SEM images of the fresh sorbent (Figure 4.9a), spent sorbent after 1 cycle (Figure 4.9b), and spent sorbent after 5 cycles (Figure 4.9c-f). Comparing the images of the fresh and spent sorbent, a growth of the CaO grains is detected in the sorbent after five SESR cycles. This effect is less marked in the spent sorbent after one cycle. However, no appreciable differences are observed in the spent sorbent after 5 cycles for the different biogas H_2S concentrations. On the other hand, some agglomeration and fusion of the CaO grains as a result of sintering can be detected in the spent sorbent after five cycles.

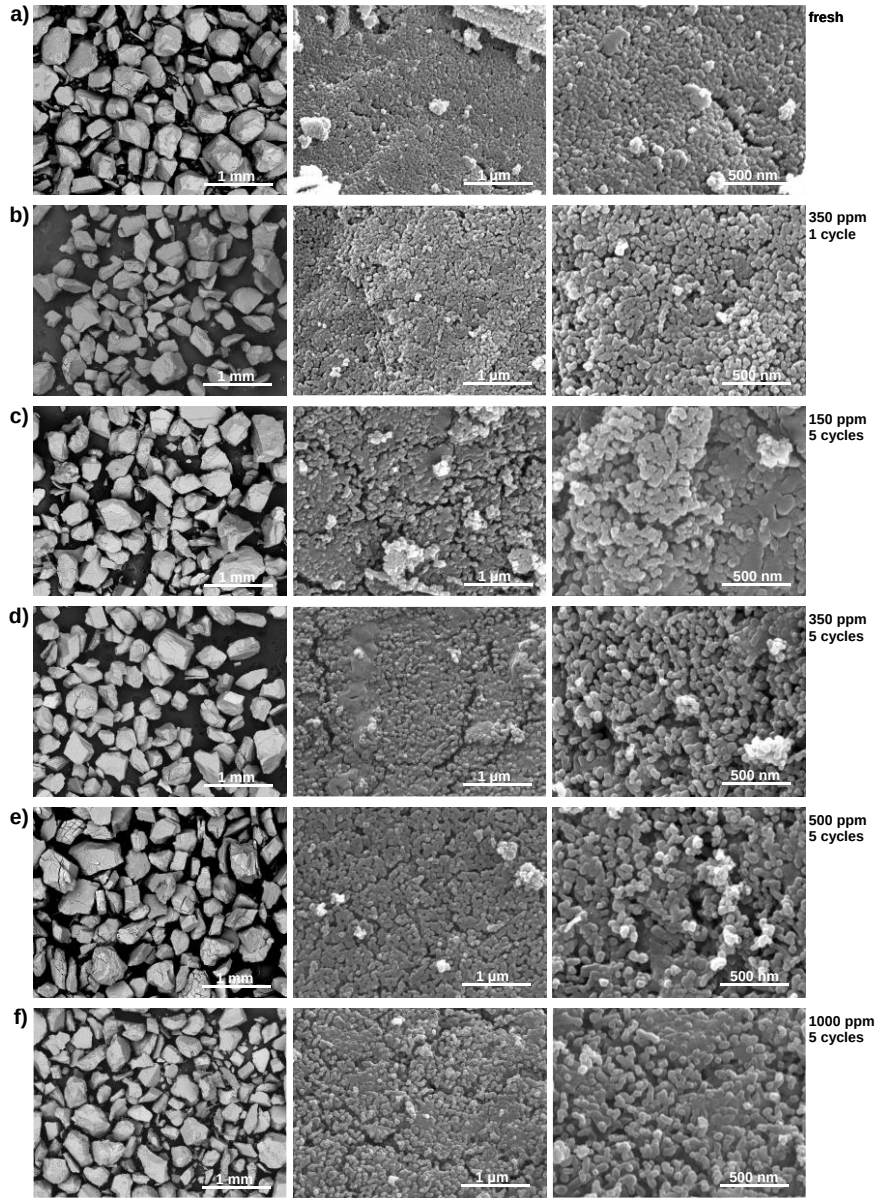

Figure 4.9: SEM images of the fresh and spent dolomite sorbent after one and five cycles of the SESR process for different biogas H_2S concentrations: (a) fresh sorbent; (b) 350 ppm H_2S, 1 cycle; (c) 150 ppm H_2S, 5 cycles; (d) 350 ppm H_2S, 5 cycles; (e) 500 ppm H_2S, 5 cycles; and (f) 1000 ppm H_2S, 5 cycles. Operating conditions: Biogas=60/40 CH_4/CO_2 vol.%; T=600 ^oC; S/CH_4=6 mol/mol; GHSV=1803 $mL_{CH4}\ g_{cat}^{-1}\ h^{-1}$; sorbent/catalyst ratio=20 g/g; Pd/Ni-Co HT catalyst and dolomite sorbent.

4.2.2.2. XRD analysis of spent catalyst and sorbent

XRD analysis was performed to identify the crystalline phase composition of fresh and spent catalyst and sorbent. Figure 4.10 shows the XRD spectra of the fresh and spent catalyst after 5 cycles of the SESR process for different H_2S concentrations in the biogas. Compared to the fresh catalyst, the intensity of Ni and Co diffraction peaks (2θ = 44.5°, 51.8°, and 76.3°, JCPD 87-0712) increased after cyclic SESR operation, suggesting the growth of Ni/Co crystallite size. XRD spectra show no clear evidence of the formation of nickel/cobalt sulphide or sulphate phases, possibly due to these compounds being poorly crystalline or their content being below the XRD detection limit.

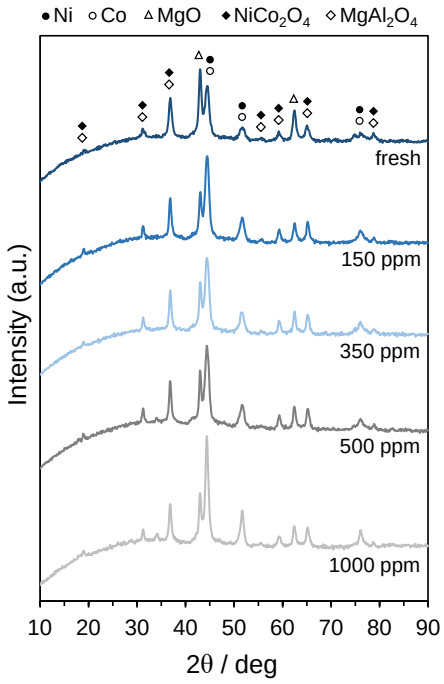

Figure 4.10: XRD patterns of the fresh and spent Pd/Ni-Co HT catalyst after five cycles of the SESR process for biogas H_2S concentrations of 150, 350, 500, and 1000 ppm. Operating conditions: Biogas=60/40 CH_4/CO_2 vol.%; T=600 °C; S/CH_4=6 mol/mol; GHSV=1803 $mL_{CH4}\ g_{cat}^{-1}\ h^{-1}$; sorbent/catalyst ratio=20 g/g; Pd/Ni-Co HT catalyst and dolomite sorbent.

It has been shown that hydrogen sulphide chemisorption on a nickel catalyst is reversible, while sulphur coverage is a function of ratio p_{H2S}/p_{H2}. A

saturation layer has been observed in the temperature range of 550-645 °C at p_{H2S}/p_{H2} ratios above 2–5e10^{-6}, whereas bulk nickel sulphide (Ni_3S_2) formation (Eq. 4.4) was estimated at ratios above 10^{-3} [106].

$$3Ni + 2H_2S \leftrightarrow Ni_3S_2 + 2H_2 \qquad \text{Eq. 4.4}$$

Bulk sulphide formation would not be favourable during the reforming step in SESR, as it requires significantly high H_2S partial pressures, and surface adsorbed sulphur is expected under the operating conditions used [174]. Even if formed, the nickel sulphide peaks would be difficult to identify due to the overlap in the diffraction patterns of the metal oxide compounds (i.e., MgO periclase and $MgAl_2O_4$ spinel phases) [109].

On the other hand, Figure 4.11 shows the XRD spectra of the fresh and spent sorbent after five cycles of the SESR process for different biogas H_2S concentrations. The XRD spectra indicates the presence of mainly CaO and MgO phases in the fresh and spent sorbent samples, although the presence of $Ca(OH)_2$ is also detected. It has been reported that when regenerated samples come into contact with air, CaO can absorb moisture and is transformed into $Ca(OH)_2$ [175]. However, the XRD spectra do not show the presence of S-containing phases, which may be because these compounds in the sorbent are amorphous or of very low crystallinity, or because their amounts are below the detection limit of the XRD analyser.

The average crystal sizes have been estimated from the XRD peaks using the Scherrer equation, and their values are shown in Table 4.4. These results show a slight increase in the CaO crystals after SESR cyclic operation compared to fresh sorbent. In addition, the average crystal size of CaO increases (from 36.4 for 150 ppm to 39.6 nm for 1000 ppm) as the biogas H_2S concentration increases. An effect of the H_2S concentration on the MgO crystal size is not detected. The growth in the CaO crystal size can be explained by the sorbent sintering, which also agrees with the results of SEM analysis, where a growth of the CaO grains in the sorbent was observed after five SESR cycles (Figure 4.9). According to the XRD results, this effect would be higher as biogas H_2S concentration increases, which could explain the decrease in the CO_2 capture capacity with the H_2S content in biogas.

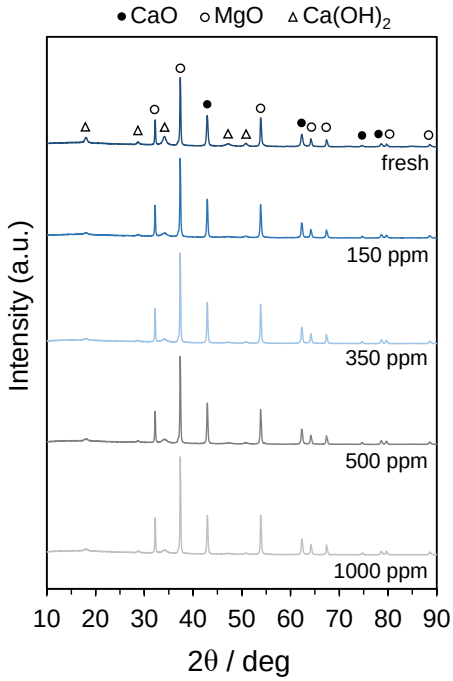

Figure 4.11: XRD patterns of the fresh and spent dolomite sorbent after five cycles of the SESR process for biogas H_2S concentrations of 150, 350, 500, and 1000 ppm. Operating conditions: Biogas=60/40 CH_4/CO_2 vol.%; T=600 °C; S/CH_4=6 mol/mol; GHSV=1803 $mL_{CH4}\ g_{cat}^{-1}\ h^{-1}$; sorbent/catalyst ratio=20 g/g; Pd/Ni-Co HT catalyst and dolomite sorbent.

Table 4.4: XRD characterisation of the fresh and spent dolomite sorbent after five cycles of SESR of biogas containing different concentrations of H_2S.

	Dolomite sorbent sample				
	fresh	150 ppm H_2S	350 ppm H_2S	500 ppm H_2S	1000 ppm H_2S
Crystallite size CaO (nm)	35.2	36.4	37.9	38.1	39.6
Crystallite size MgO (nm)	22.7	28.3	28.9	28.5	29.1

4.2.2.3. N_2 adsorption analysis of spent sorbent

Table 4.5 shows the results of the surface area analysis by N_2 adsorption at −196 °C after 5 cycles of the SESR process for different biogas H_2S concentrations. The BET surface area of the fresh sorbent was 23.9 $m^2\ g^{-1}$, and its value was reduced to ~11 $m^2\ g^{-1}$ after 5 cycles of biogas SESR. Likewise,

the total pore volume was reduced from 0.27 $cm^3\ g^{-1}$ up to ~0.10 $cm^3\ g^{-1}$ after cycling. A reduction of the surface area and pore volume has been previously reported in cyclic experiments of bio-oil SESR [63] and sorption enhanced water gas shift (SEWGS) [65]. The surface area and pore volume of CaO-based materials decrease with the number of CO_2 capture cycles due to the sintering during their regeneration at high temperature [176]. However, no differences in the BET surface area and total pore volume were detected for different biogas H_2S concentrations.

Table 4.5: Physical characterisation by means of N_2 adsorption of the fresh and spent dolomite sorbent after five cycles of SESR of biogas containing different concentrations of H_2S.

	Dolomite sorbent sample				
	fresh	150 ppm H_2S	350 ppm H_2S	500 ppm H_2S	1000 ppm H_2S
N_2 adsorption at −196 °C					
BET surface area, S_{BET} ($m^2\ g^{-1}$)	22.9	10.8	10.7	10.9	11.2
Total pore volume, V_p ($cm^3\ g^{-1}$)	0.27	0.12	0.10	0.09	0.10

Operating conditions: Biogas=60/40 CH_4/CO_2 vol.%; T=600 °C; S/CH_4=6 mol/mol; GHSV=1803 $mL_{CH4}\ gcat^{-1}\ h^{-1}$; sorbent/catalyst ratio=20 g/g; Pd/Ni-Co HT catalyst and dolomite sorbent.

The decrease in CO_2 capture capacity of the sorbent shown in Figure 4.5 can be explained by deactivation due to the decrease in surface area and pore volume by CaO sintering. The oxidation reactions are highly exothermic, while the reduction is endothermic. High O_2 concentration in oxidation may cause sintering of sorbent due to the strong exothermic reaction, which can explain the loss of CO_2 capture capacity in cyclic operation. However, reduction should not cause sintering of the sorbent [175].

4.2.2.1. XPS analysis of spent catalyst and sorbent

XPS analysis was performed to determine the chemical states of the surface Ni, Co, and S species present in the fresh and spent catalyst after five cycles of the SESR process. Figure 4.12 shows the S 2p XPS spectra of the fresh (Figure 4.12a) and spent catalyst after five cycles of the SESR process for biogas containing different concentrations of H_2S (Figure 4.12b-e). No sulphur peak was found in the XPS spectra of the fresh catalyst. However, sulphur was detected for all H_2S concentrations in the spent catalyst. We can see two peaks corresponding to S $2p_{3/2}$ and S $2p_{1/2}$ at around 162.1 and 163.4

eV, respectively, which could suggest the presence of sulphur as the S^{2-} ion [171,177]. Moreover, two other peaks corresponding to S $2p_{3/2}$ and S $2p_{1/2}$ are also observed around 168.9 and 170.1 eV, respectively, indicating the presence of sulphur with a higher oxidation state. This could be attributed to sulphur oxides, such as SO_4^{2-} species [177], suggesting the oxidation of hydrogen sulphide or adsorbed sulphur during the calcination step of the SESR process in air atmosphere [178].

Figure 4.13 shows the Ni 2p XPS spectra of the spent catalyst after five cycles of the SESR process for biogas containing different concentrations of H_2S. We can see two peaks corresponding to Ni $2p_{3/2}$ and Ni $2p_{1/2}$ around 854.6 and 871.1 eV, respectively. In addition, two other peaks corresponding to Ni $2p_{3/2}$ and Ni $2p_{1/2}$ are seen around 856.3 and 873.6 eV, respectively. Moreover, two shake-up satellite peaks (around 861.8 and 879.1 eV) are detected. These peaks can indicate the presence of nickel as Ni^{2+}, meaning that one or more nickel-oxygen species can be present [179]. Binding energy of metallic Ni 2p is around 852.0 eV, values around 854.0 eV are characteristic of Ni^{2+} species in NiO, while binding energy around ~857.5±0.4 can indicate the presence of Ni^{2+} species present in the $NiAl_2O_4$ phase [72,180,181]. On the other hand, binding energies around 856.3 ± 1 eV have been associated with Ni^{2+} species in $NiSO_4$ [109,182].This peak was attributed in the literature [109] to surface nickel sulphide (or sulphur chemisorbed on Ni surface) that has been converted to sulphates when exposed to air. These results would be consistent with those shown by the S 2p XPS spectra.

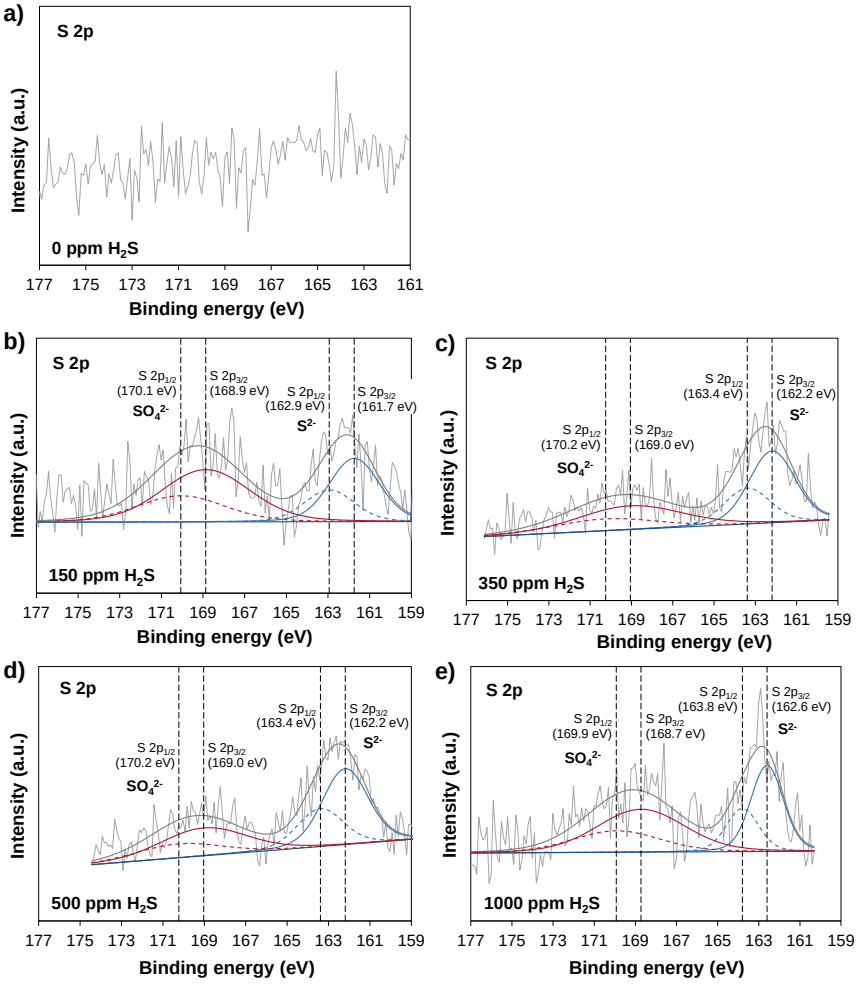

Figure 4.12: XPS surface spectra for S 2p of the fresh (a) and spent Pd/Ni-Co HT catalyst after five cycles of the SESR process for biogas H_2S concentrations of 150 (b), 350 (c), 500 (d), and 1000 ppm (e). Operating conditions: Biogas=60/40 CH_4/CO_2 vol.%; T=600 ºC; S/CH_4=6 mol/mol; GHSV=1969 $mL_{CH4}\ g_{cat}^{-1}\ h^{-1}$; sorbent/catalyst ratio=20 g/g; Pd/Ni-Co HT catalyst and dolomite sorbent.

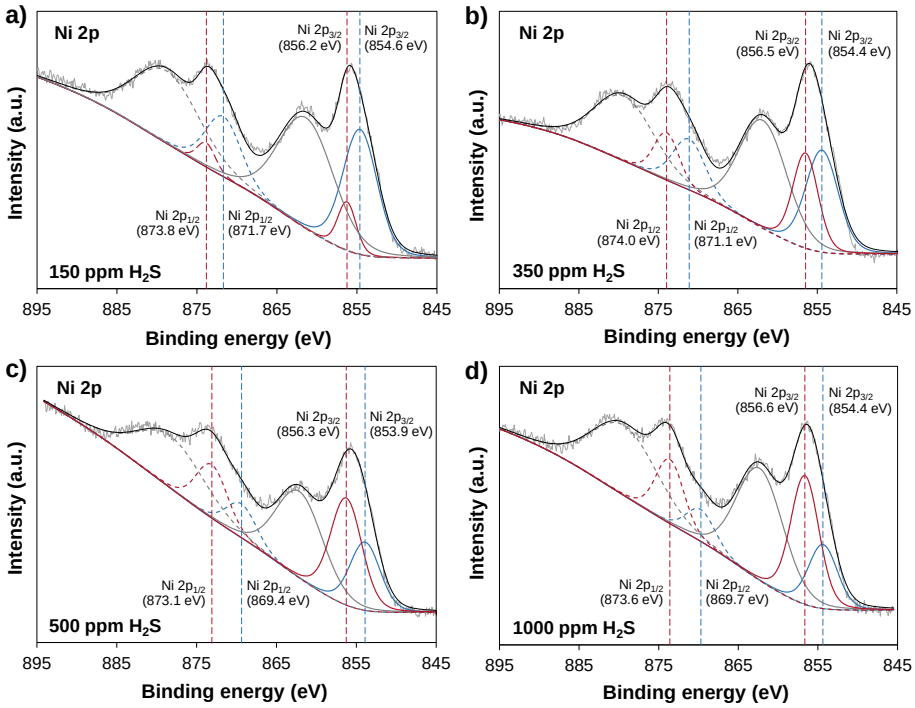

Figure 4.13: XPS surface spectra for Ni 2p of the spent Pd/Ni-Co HT catalyst after five cycles of the SESR process for biogas H_2S concentrations of 150 (a), 350 (b), 500 (c), and 1000 ppm (d). Operating conditions: Biogas=60/40 CH_4/CO_2 vol.%; T=600 C; S/CH_4=6 mol/mol; GHSV=1969 $mL_{CH4}g_{cat}^{-1}h^{-1}$; sorbent/catalyst ratio=20 g/g; Pd/Ni-Co HT catalyst and dolomite sorbent.

Figure 4.14 shows the Co 2p XPS spectra of the spent catalyst after five cycles of the SESR process for all biogas H_2S concentrations. Two peaks can be seen corresponding to Co $2p_{3/2}$ and Co $2p_{1/2}$ around 778.7 and 791.9 eV, respectively. In addition, two other peaks corresponding to Co $2p_{3/2}$ and Co $2p_{1/2}$ are seen around 781.4 and 797.1 eV, respectively. Moreover, two shake-up satellite peaks (around 786.2 and 802.7 eV) are detected. A peak at low values of binding energy is detected due to the use of non-monochromatic radiation.

Peaks around 779.5 eV and 781.4 eV are due to the presence of surface Co^{3+} and Co^{2+} species, respectively [183]. Co $2p_{3/2}$ binding energy around 778.0 eV has been associated to the metallic cobalt [184]. Co 2p binding energy around 782.8 eV has been associated to the Co^{2+} species in $CoSO_4$ [182], while Co 2p binding energy around 783.5 can be associated to the Co^{2+} species in $CoAl_2O_4$ phase. Therefore, in the present work, it is clear the

presence of some Co^{2+} species, although XPS analysis does not clarify the presence of $CoSO_4$.

As explained above, in the present work, spent catalyst and sorbent were subjected to calcination and reduction steps during the last SESR cycle. Therefore, it should be considered that sulphur compounds formed from H_2S during the reforming step could have been later converted under calcination and reduction conditions.

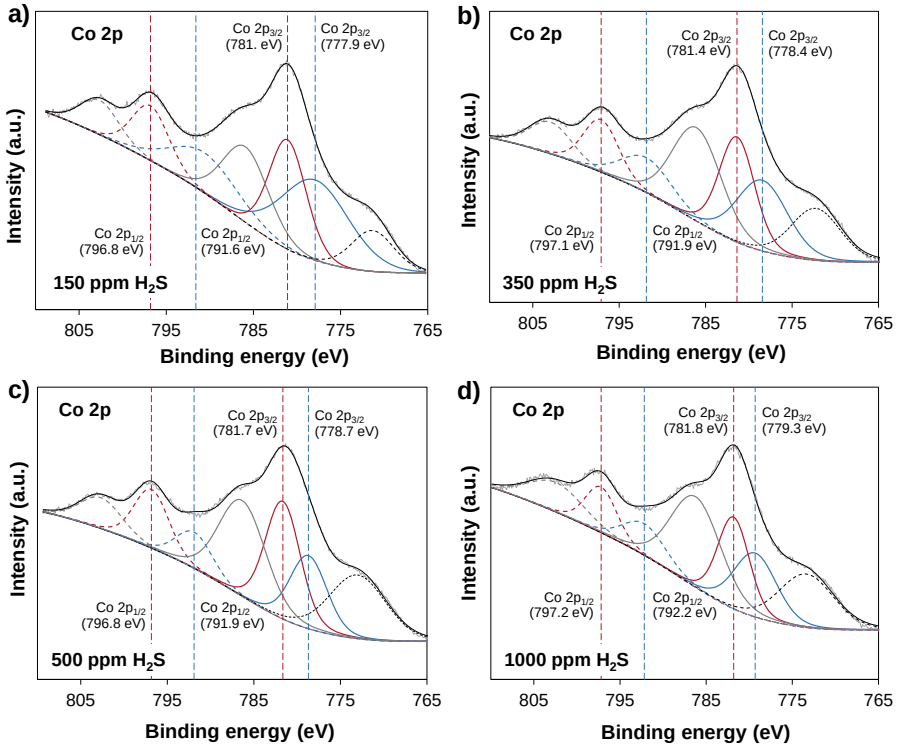

Figure 4.14: XPS surface spectra for Co 2p of the spent Pd/Ni-Co HT catalyst after five cycles of the SESR process for biogas H_2S concentrations of 150 (a), 350 (b), 500 (c), and 1000 ppm (d). Operating conditions: Biogas=60/40 CH_4/CO_2 vol.%; T=600 ^oC; S/CH_4=6 mol/mol; GHSV=1969 $mL_{CH4}\ g_{cat}^{-1}\ h^{-1}$; sorbent/catalyst ratio=20 g/g; Pd/Ni-Co HT catalyst and dolomite sorbent.

Thus, Ni–S species in the catalyst can be cracked by increasing the reaction temperature or feeding oxygen. In the presence of oxygen, sulphur on the catalyst surface can be oxidized, while Ni metals can be converted to NiO or $NiSO_4$ by Eq. 4.5 and Eq. 4.6, respectively [185]. Indeed, oxidative

treatments at high temperature are used to remove the adsorbed sulphur by oxidation and regenerate the active Ni sites in steam reforming studies [112].

$$Ni–S + 3/2O_2 \leftrightarrow NiO + SO_2 \quad \text{Eq. 4.5}$$

$$Ni–S + 2O_2 \leftrightarrow NiSO_4 \quad \text{Eq. 4.6}$$

SO_2 was detected in the gas phase in chemical looping reforming (CLR) of biogas from the oxidation of the sulphur compounds attached on the oxygen carrier during the reduction/reforming step (mainly NiS_2) [171]. In addition, it has been reported for chemical looping combustion [179] that Ni_3S_2 was the main sulphide found in the oxygen carrier after the reduction step. These authors found that part of the sulphur retained in the solid as Ni_3S_2 during reforming was later released as SO_2 during oxidation due to Ni_3S_2 oxidation to form $NiSO_4$ (Eq. 4.7) was favoured at high oxygen concentrations (21 vol.%) [179].

$$Ni_3S_2 + 9/2O_2 \rightarrow 2NiSO_4 + NiO \quad \text{Eq. 4.7}$$

After calcination, a reduction step under a mixture of hydrogen and nitrogen was carried out. Under this atmosphere, Ni_3S_2 and $NiSO_4$ can be reduced by Eq. 4.8 and Eq. 4.9, respectively [186].

$$Ni_3S_2 + 2H_2 \rightarrow 3Ni + 2H_2S \quad \text{Eq. 4.8}$$

$$3NiSO_4 + 13H_2 \rightarrow Ni_3S_2 + 12H_2O + 2H_2S \quad \text{Eq. 4.9}$$

Figure 4.13 shows that the contribution at around 854 eV decreases as the H_2S concentration in biogas increases. Conversely, the peak at 864 eV increases with biogas H_2S content. It could indicate that the formation of $NiSO_4$ is higher during the regeneration step, and it is not converted again into sulphide species during reduction. It could contribute to decreasing the catalyst activity as detected for high sulphur concentrations.

XPS analysis was also performed to determine the chemical states of the surface S species present in the spent sorbent after five cycles of the SESR process. Figure 4.15 shows the S 2p XPS spectra of the fresh (Figure 4.15a) and spent (Figure 4.15b) sorbent after five cycles of SESR of biogas containing 1000 ppm H_2S. No sulphur peak was detected in the XPS spectra of the fresh sorbent and spent sorbent for lower H_2S concentrations. Figure 4.15a shows

a small peak at the highest binding energies, which could be associated with a beta satellite peak generated by the excitation of the Al and Mg signals.

A similar XPS spectrum to that shown in Figure 4.15a is observed for all the sorbent samples after SESR with biogas H_2S contends of 150-500 ppm. However, in the case of 1000 ppm H_2S, the XPS spectrum shows a peak at lower binding energy, as shown in Figure 4.15b. This peak was not detected for lower H_2S concentrations probably because sulphur concentration in these samples was below the detection limit of the XPS analyser.

The S 2p XPS spectrum for the 1000 ppm sample shows a peak corresponding to S $2p_{3/2}$ and S $2p_{1/2}$ at 160.7 and 161.9 eV, respectively, suggesting the presence of sulphur as the S^{2-} ion [171,177]. These results suggest that H_2S could have reacted with the surface Ca of the sorbent during the reforming step of the SESR process, which could have contributed to the decrease in the CO_2 capture capacity of the sorbent. Since the ratio of CaO introduced with the calcined dolomite in the reactor to sulphur introduced with the biogas was very high, the conversion of H_2S to CaS (Eq. 2.8) could occur until equilibrium was reached, as previously reported for sorption enhanced gasification experiments [173].

On the other hand, CaS can react with O_2 under the oxidant atmosphere of the regeneration step to form stable $CaSO_4$ by Eq. 4.10, which could form a tight layer on the sorbent surface that reduces the extent of the calcination reaction [187]. This phenomenon could explain the decrease in CO_2 capture capacity during cyclic SESR of H_2S-containing biogas. If $CaSO_4$ is formed during SESR cycles, it could contribute to plugging the pores and hinder the mass transfer of CO_2 to the sorbent particles, reducing the CO_2 removal capacity.

$$CaS + 2O_2 \leftrightarrow CaSO_4 \qquad \text{Eq. 4.10}$$

Sulphur peaks associated with sulphates, which can have formed during the calcination step of the SESR process under air atmosphere, could be found at higher binding energy (around 168-170 eV) [177]. However, these peaks would overlap with the satellite peak shown in Figure 4.15b. In addition, as already mentioned, the sulphur concentration in this sample is probably below the detection limit.

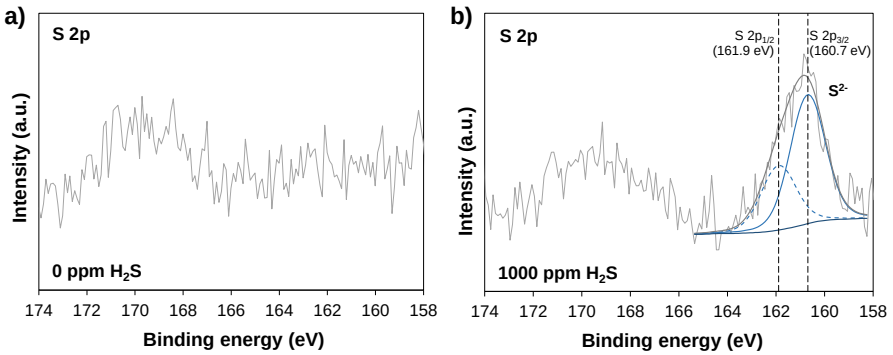

Figure 4.15: XPS surface spectra for S 2p of the spent dolomite sorbent after five cycles of the SESR process for biogas H_2S concentrations of 150 (a), 350 (b), 500 (c), and 1000 ppm (d). Operating conditions: Biogas=60/40 CH_4/CO_2 vol.%; T=600 ^oC; S/CH_4=6 mol/mol; GHSV=1803 $mL_{CH4}\,g_{cat}^{-1}\,h^{-1}$; sorbent/catalyst ratio=20 g/g; Pd/Ni-Co HT catalyst and dolomite sorbent.

4.2.3. Discussion comparing catalyst deactivation during SESR and conventional SR

It has been widely shown in the literature that Ni catalysts are deactivated by the presence of H_2S during conventional reforming processes, even when very low H_2S concentrations are present. Under SR operation, H_2S poisoning resulted in an exponential decrease in catalyst activity, and even at a H_2S concentration of 30 ppm, the reforming catalyst showed an 86% drop in activity after 12 h at 700 ^oC, with the decrease in catalyst activity being much faster at higher sulphur levels. This study remarked that the poisoned Ni catalyst only maintained acceptable residual activity when operating at 900 ^oC (86% of the original methane conversion with 108 ppm H_2S) [112].

It has also been shown in the literature that the H_2S presence (20-100 ppm) led to deactivation of a Ni/Al_2O_3 catalyst in SR experiments of biogas, and higher H_2S concentrations showed faster deactivation [111]. All H_2S concentrations led to almost complete deactivation (98%) of the catalyst at 700 ^oC. However, at 800 ^oC the residual activity retained by the catalyst was 34% of CH_4 conversion for 100 ppm of H_2S in the feed gas, 43% for 50 ppm, and 48% for 20 ppm. H_2S poisoning was also detected by Ashrafi et al. [112] during conventional SR for H_2S concentrations of 15-145 ppm and temperatures of 700-800 ^oC. Almost complete deactivation of a Ni/Al_2O_3 catalyst was also shown in the literature [188] for the dry reforming of biogas

in experiments at 700 and 800 ^{o}C with 5 and 10 ppm of H_2S in the feed gas. It has also been reported that a Ni-MgAl catalyst started deactivating almost instantaneously and lost approximately 80% of the initial CH_4 conversion activity within 1.5 h in the presence of H_2S during dry methane reforming [109].

Therefore, the decrease in activity of the Pd/Ni-Co HT catalyst used for biogas SESR is much lower than that detected in conventional steam reforming studies, demonstrating a higher H_2S tolerance. In addition, steady-state catalytic activity was shown during the sorption enhanced reforming stage.

In the SESR experiments of the present study, CaO breakthrough occurs before the catalyst is completely deactivated. In conventional steam reforming processes, the H_2S poisoning effect varies exponentially with time on stream and the final catalyst activity depends on the uncovered active surface available [189]. From this, it can be deduced that there are still active catalytic sites after cyclic SESR.

Lately, recent developments in sulphur-resilient catalysts highlighted that bimetallic formulations involving nickel and another complementary metal such as cobalt, iron or copper seem to impart variable degrees of sulphur resistance to the catalyst [124]. It has been shown that co-impregnation of cobalt with nickel to obtain a bimetallic catalyst led to increased stability against sulphur poisoning during dry methane reforming (100 ppm of H_2S), suggesting that cobalt played a sacrificial role by intercepting some of the sulphur content in the feed and preventing it from deactivating the nickel sites [115].

Other works in the literature have reported that the addition of cobalt delays the deactivation by H_2S compared to a single Ni catalyst. Thus, it has been shown that catalysts containing both Ni and Co are stable over long periods under dry methane reforming conditions (775 ^{o}C; 20-30 ppm of H_2S), while a Ni-only catalyst deactivated completely after contacting with sulphur [190]. This was attributed to Ni-Co interaction, since the electronic modifications of the Ni in the smaller metal clusters caused by interaction with Co hinders adsorption of H_2S. It was also reported [109] that compared to Ni-MgAl, a NiCo-MgAl catalyst showed much better resistance to the deactivation in H_2S during dry reforming of methane (800 ^{o}C; 20 ppm of H_2S),

and negligible deactivation was observed for 4 h after the introduction of H_2S, with the CH_4 conversion remaining > 90%, which rapidly decreased after that time. The promoting role of Co on sulphur tolerance is attributed to an electronic interaction exerted by Co on Ni that alters sulphur chemisorption kinetics. Likewise, it was found [183] that deactivation by sulphur poisoning of a Ce-doped Co perovskite catalyst was temporary and reversible during the reforming reaction. All these results indicate that the addition of Co can decrease the overall rate of sulphur adsorption on the catalyst.

In this work it is proposed to prevent the Ni poisoning, not only by using a bi-metallic catalyst that includes Co, but also using a CO_2 sorbent which contributes to lower the poisoning of the catalyst, since a significant amount of sulphur was detected in the dolomite.

4.2.4. Conclusions on the effect of H_2S on biogas SESR

The conclusions of the study of the effect of H_2S on biogas SESR are as follows:

- No catalyst deactivation due to H_2S poisoning was detected during cyclic biogas SESR for H_2S concentrations of 150 and 350 ppm at 600 °C. However, H_2S concentrations of 500-1000 ppm slightly reduced H_2 yield (between 4.5% and 10.8% points) and H_2 purity (between 2% and 3% points).

- The results of this study suggest that cleaning the biogas to reduce H_2S levels below 350 ppm could allow the biogas to be used for hydrogen production by the SESR process.

- Sulphur was detected in both spent catalyst and sorbent materials. For 1000 ppm H_2S in the inlet biogas, most of the sulphur introduced into the reactor was retained in the spent sorbent particles after cyclic SESR.

- XPS characterisation of the catalyst revealed that not only S^{2-} species are formed, but also SO_4^{2-} species are present due to the different oxidation/reduction steps involved in the continuous cyclic operation. On the other hand, S^{2-} species are present in the sorbent, but the presence of SO_4^{2-} could not be confirmed and,

therefore, future studies using higher H_2S concentrations are needed.

- Catalyst deactivation during cyclic SESR was notably lower than that usually detected in conventional steam reforming processes, suggesting that, together with the use of a Co-containing bimetallic catalyst, the presence of a sorbent that can react with sulphur compounds could make the SESR process more resistant to H_2S.

Since S chemisorption on nickel is a reversible process, the activity of sulphur-poisoned catalysts could be partly recovered at high temperatures under different atmospheres by gradual sulphur desorption. In future studies, the effect of different sorbent calcination conditions (such as temperature, oxygen concentration or gas flow), and catalyst reduction operating parameters, on the regeneration of the sulphur-poisoned catalyst will be evaluated. The effect of higher biogas H_2S contents on catalyst deactivation, as well as longer continuous operation (i.e., more cycles), will also be studied.

4.3. PROCESS SIMULATIONS OF H_2 PRODUCTION BY SORPTION ENHANCED STEAM REFORMING (SESR) OF BIOGAS

This study is included in *Publication III* of the thesis. This section presents a summary of the results of this work, while the complete document is shown in *Annex II: Publications*.

The main challenge of SESR processes is the heat required for sorbent regeneration. In fact, the optimization of the energy demand in the process and the development and implementation of robust heat and energy recovery systems have recently been highlighted as key existing challenges for the viable production of H_2 by sorption enhanced processes [59].

During the reforming step of the SESR process, the CO_2 sorption reaction (carbonation) is exothermic. However, the sorbent regeneration by the calcination reaction is highly endothermic, which requires extra energy. Biogas is a carbon-neutral source of renewable H_2 that can be especially relevant for the energy integration of the SESR process since, due to the exothermic sorption reaction, the CO_2 contained in the biogas provides extra heat to the system, which can help to balance the energy requirements of the process.

To study the effect of the addition of CO_2 in the feeding, an energy analysis by simulation of the SESR process of biogas is needed to understand the thermodynamic limitations of the system under possible process configurations and optimise the energy efficiency. The process designs studied for the production of renewable hydrogen from biogas SESR aim at recovering the heat released in the reformer while maximizing CO_2 capture.

This work evaluates three process configurations for the energy integration of the SESR process of biogas for high-purity H_2 production: 1) SESR with sorbent regeneration using a portion of the produced H_2 (SESR+REG_H_2), 2) SESR with sorbent regeneration using biogas (SESR+REG_BG), and 3) SESR with sorbent regeneration using biogas and adding a pressure swing adsorption (PSA) unit for hydrogen purification (SESR+REG_BG+PSA). These configurations were studied using air (all) and oxy-fuel combustion (when using biogas as fuel in the calciner) atmospheres, resulting in five case studies. A sensitivity analysis was performed including

the study of the effect of biogas composition, SESR temperature, SESR pressure, and S/CH_4 ratio.

The thermodynamic modelling assumptions used as the base design of the process to develop the different flowsheets are collected in Table 4.6. Biogas is simulated as a mixture of CH_4 and CO_2, while the solid sorbent is simulated as pure CaO. Using the baseline conditions shown in Table 4.6, the range of the different variables studied is shown in Table 4.7.

Table 4.6: Design assumption made to develop the base case flowsheet in Aspen Plus.

Parameters	Value	Unit
Biogas feed	0.76 (13.33)	kg/s (MW*)
Biogas composition (CH_4/CO_2)	60/40	vol.%
Water feed inlet temperature	25	^oC
Water feed inlet pressure	1	bar
Molar Ca/C ratio	1.5	-
Reformer pressure	10	bar
Reformer temperature	600	^oC
Reformer molar steam/CH_4	5.5	-
Reformer heat loss	10	%
Calciner temperature	850	^oC
Calciner pressure	1	bar
Excess oxygen[1]	5	%
Air/oxygen inlet temperature	25	^oC
Air/oxygen pressure	1	bar
Fuel feed inlet temperature[2]	25	^oC
Fuel feed pressure	1	bar
Calcination conversion	100	%
Heat exchanger pinch	20	^oC
Isentropic efficiency of the compressor and water pump efficiency	83	%
Mechanical efficiency of the compressors and pump driver efficiency	98	%

Table 4.7: Range in which the different process variables are analysed.

Parameters	Range	Unit
Biogas composition (CH_4/CO_2)	50/50-80/20	vol%
Reformer temperature	500-675	^oC
Reformer pressure	1.5-25	bar
Reformer molar steam/CH_4	3-6.5	-

The base flowsheet of the process mainly consists of two reactors: a reformer (SESR) and a calciner (REG). The models developed in this work include the extra heat recovery from the SESR unit to achieve an autothermal operation of the system.

4.3.1. Effect of biogas composition

The effect of the biogas composition on H_2 purity, CH_4 conversion, and H_2 yield is shown in Figure 4.16. The range of compositions studied raises up to 80% of CH_4. In Cases 1 and 2 (Figure 4.16a and Figure 4.16b respectively), H_2 purity slightly increases from 97.1 to 97.6% for the high methane concentrations in the feed stream from 50 to 80 vol.%. However, H_2 purity achieves nearly 100 vol.% in Case 3 with the PSA purification unit (Figure 4.16c). This indicates that biogas compositions do not significantly change the H_2 purity obtained after SESR, which is in good agreement with the experimental results previously reported [127].

In addition, the results show that the recovery of the extra heat produced in the SESR step with the proposed designs allows to achieve an autothermal operation of the reformer, regardless of the biogas composition.

For Cases 1 and 2, CH_4 conversion increases slightly from 89.8 to 91.5% with CH_4 content in biogas, similar to the H_2 purity, so the same results are obtained when a fraction of the produced H_2 is used as fuel for sorbent regeneration (Figure 4.16a) as when biogas is used as fuel in the REG reactor (Figure 4.16b). On the other hand, the addition of the PSA unit, and subsequent recycling of the off-gas (PSA-OG) to the REG reactor, i.e., Case 3, increases the CH_4 conversion to 100%, as unreacted CH_4 from the SESR unit is recirculated with the PSA-OG to the REG reactor, where it is combusted (Figure 4.16c).

Finally, the H_2 yield is very low in Case 1 (Figure 4.16a) due to the use of a fraction of the produced hydrogen as renewable fuel to fulfil the energy duty of the sorbent regeneration stage. It increases from 35.2 to 49.1% in the range of the biogas compositions analysed, i.e., 50 to 80 vol.% of CH_4 (balance CO_2). The highest H_2 yield is obtained in Case 2, biogas used as fuel in REG (Figure 4.16b) without the PSA-OG recycle: 89.7 to 91.4% for 50 to 80 vol.% of CH_4 in biogas. When PSA-OG is recycled in Case 3 (Figure 4.16c), the H_2

yield decreases, as the off-gas contains not only the unreacted CH_4 from SESR, but also a small fraction of H_2 (we assume a PSA efficiency of 95%), and increases from 85.3 to 86.9% for 50 to 80 vol.% of CH_4 in biogas. Therefore, the biogas composition has little effect on the H_2 yield, in agreement with the slight increase in CH_4 conversion.

The efficiencies, CGE and NE, for the different configurations and the percentage of fuel consumed for sorbent regeneration are shown in Figure 4.16d-f as a function of biogas composition (50 to 80 vol.% of CH_4, balance CO_2). The process configurations have been evaluated using air (all) and oxy-combustion (when biogas is used as fuel) atmospheres. A decrease in net efficiency due to the additional auxiliary power consumption of the Air Separation Unit (ASU) was observed in the case of oxy-combustion.

In Case 1, where produced H_2 is used as fuel in REG, CGE increases a total of 16.8%, from 42.5 to 59.4%, with CH_4 content in the biogas (Figure 4.16d). In Case 2 (Figure 4.16e), where biogas is directly combusted in the calciner, CGE increases from 63.2 to 70.3% as CH_4 content in the biogas increases, meaning a total increase of 7.1%. Finally, for Case 3 (Figure 4.16f), when a PSA unit is utilized, CGE increases from 66.1 to 73.5%, which means a total increase of 7.4%.

When combustion is carried out under an air atmosphere, in Cases 1 and 2, NE is 1.6% points below CGE due to the electric utility requirement of the auxiliaries considered. However, NE is 3.3% lower than CGE for Case 3 due to the additional compressor needed to match the pressure required by the PSA unit. When combustion in REG is carried out under oxy-combustion conditions, NE is 2.3-2.5% lower than that obtained for the air atmosphere due to the energy penalty of the ASU.

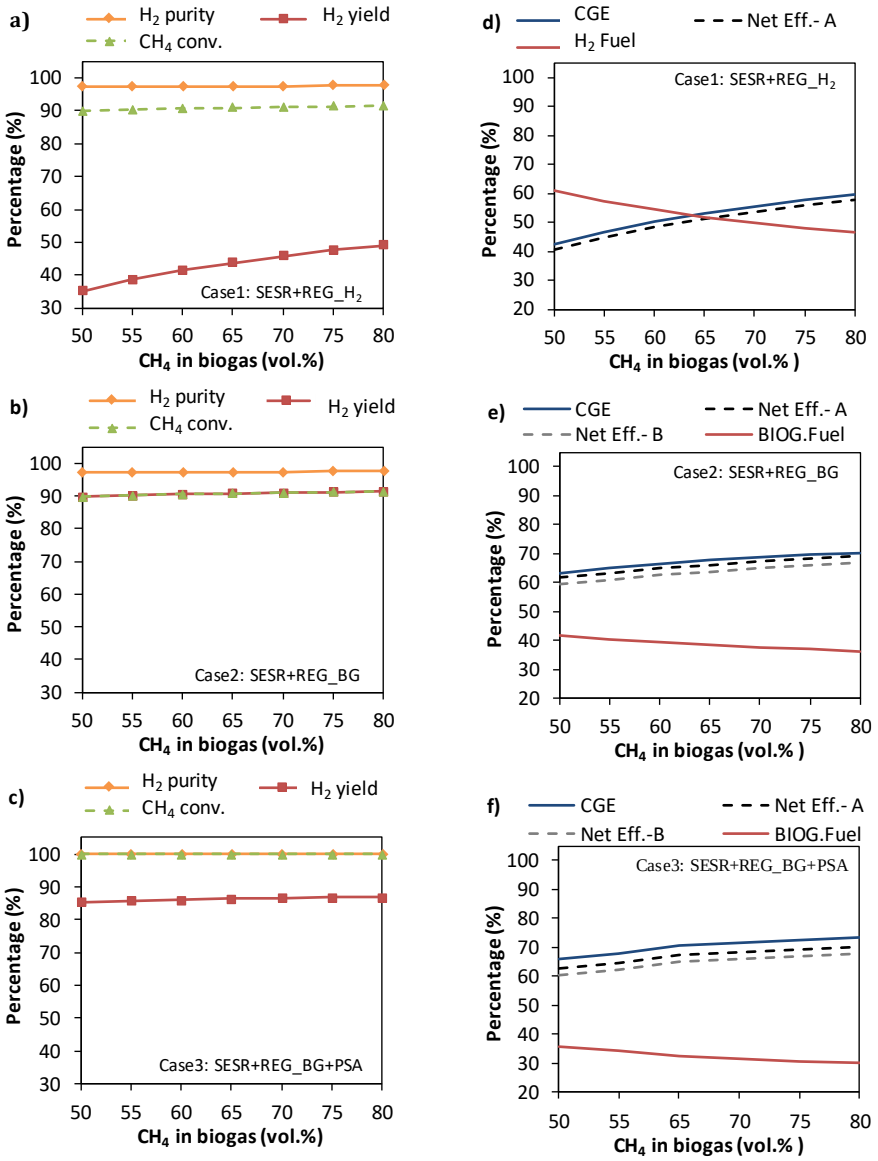

Figure 4.16: Effect of biogas composition on H_2 purity, H_2 yield, and CH_4 conversion (a-c) and on cold gas efficiency (CGE), net efficiency (NE, using both air, Net Eff. A, and oxy-combustion, Net Eff-B, in REG) and fuel consumption for sorbent regeneration (d-f) for the different process configurations studied: (a and d) use of a fraction of the produced hydrogen as fuel for sorbent regeneration (SESR+REG_H_2); (b and e) use of biogas as fuel for sorbent regeneration (SESR+REG_BG); and (c and f) addition of a PSA unit and use of biogas and off-gas (PSA-OG) for sorbent regeneration (SESR+REG_BG+PSA). SESR conditions: S/CH_4 = 5.5, T = 600 ^oC, P = 10 bar, and 50% sorbent excess.

On the other hand, Table 4.8 shows the effect of the biogas composition on the heat recovery from the SESR reactor. The amount of energy recovered from SESR varies from 3.9 MW (50 vol.% CH_4 in biogas) to 2.5 MW (80 vol.% CH_4 in biogas) for the same amount of biogas treated (100 kmol/h). This results from a balance between the carbonation and reforming reactions: when CO_2 content in biogas is higher, the carbonation occurs to a greater extent, and more heat is released in the SESR reactor. These results explain the higher excess heat in the final CO_2 stream for biogas with lower concentrations of CH_4 (see Table 4.9). The excess heat in the outlet CO_2 stream has been calculated as the maximum recoverable heat while ensuring the avoidance of condensation by specifying 5 ^oC of superheat at the outlet of the hot stream. As mentioned above, more heat is available in this stream for the lower CH_4 content in biogas, highlighting the potential interest of using low grade biogas compared to natural gas due to heat recovery from this hot stream.

Therefore, if a waste heat recovery system is employed to recover the heat available in the final CO_2 stream, the overall CGE values of the process could increase for all biogas compositions to values similar to those reached with higher concentrations of methane. This hypothesis is demonstrated for Case 3 with air regeneration, as an example, in Figure 4.17, where the extra heat in the outlet CO_2 stream has been used to preheat the reactants used for sorbent regeneration.

Table 4.8: Effect of biogas composition on the heat recovered from SESR (heat losses considered). SESR conditions: S/CH_4 = 5.5, T = 600 ^oC, P = 10 bar, and 50% sorbent excess.

Biogas composition	Heat recovered from SESR (MW)
50% CH_4 – 50% CO_2	3.9
55% CH_4 – 45% CO_2	3.7
60% CH_4 – 40% CO_2	3.4
65% CH_4 – 35% CO_2	3.2
70% CH_4 – 30% CO_2	3.0
75% CH_4 – 25% CO_2	2.8
80% CH_4 – 20% CO_2	2.5

Table 4.9: Excess of heat not used that is remaining in the CO_2 stream as a function of the biogas composition. SESR conditions: S/CH_4 = 5.5, T = 600 °C, P = 10 bar, and 50% sorbent excess.

Biogas composition	Excess heat not used in the CO_2 stream (MW)		
	Case 1 SESR+REG_H_2	Case 2 SESR+REG_BG	Case 3 SESR+REG_BG + PSA
50% CH_4 – 50% CO_2	1.8	1.7	1.7
55% CH_4 – 45% CO_2	1.5	1.4	1.5
60% CH_4 – 40% CO_2	1.3	1.2	1.2
65% CH_4 – 35% CO_2	1.0	1.0	1.0
70% CH_4 – 30% CO_2	0.7	0.8	0.8
75% CH_4 – 25% CO_2	0.4	0.6	0.6
80% CH_4 – 20% CO_2	0.1	0.4	0.4

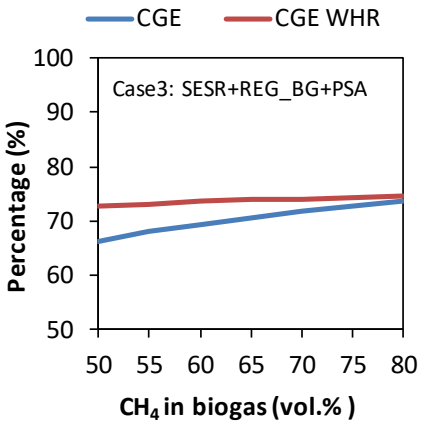

Figure 4.17: Comparison of the CGE with (red line) and without (blue line) waste heat recovery (WHR) from the CO_2 stream for the Case 3 (SESR+REG_BG+PSA).

4.3.2. Effect of SESR temperature

The effect of the reforming temperature on H_2 purity, CH_4 conversion, H_2 yield, CGE, NE, and percentage of fuel consumed by sorbent regeneration is shown in Figure 4.18.

The results for H_2 purity, CH_4 conversion, H_2 yield, CGE and fuel consumption remain unchanged when using air or oxy-combustion atmospheres for the sorbent regeneration, and only NE is affected. In Cases 1 and 2 (Figure 4.18a and Figure 4.18b), H_2 purity increases from 91.0 to 98.3% as the SESR temperature rises from 500 to 625 °C due to the

endothermic SR reaction (Eq. 2.1). When the temperature increases from 625 up to 675 °C, H_2 purity slightly decreases (by ~0.4%) since the enhancement effect of the in situ CO_2 capture is thermodynamically unfavourable at higher temperatures because the carbonation reaction is exothermic [54,67]. In Case 3 (Figure 4.18c), H_2 purity achieves nearly 100 vol.% for all SESR temperatures due to the PSA unit, which performs a further purification of the hydrogen rich stream.

The CH_4 conversion in Cases 1 and 2 increases from 71.8 to 94.5% as SESR temperature increases up to 625 °C, also due to the endothermic SR reaction; afterwards, it increases slightly with further increase in temperature (by ~0.4%). With the addition of the PSA unit and OG recycling (Case 3), the CH_4 conversion reaches a constant value of 100% (Figure 4.18c) since PSA-OG contains the unreacted CH_4 from SESR, which is then burned in the REG reactor.

On the other hand, the lowest H_2 yield is obtained in Case 1 due to the recycling of part of the H_2 produced in SESR as a fuel for the REG reactor. H_2 yield increases from 31.0 to 41.4% with the increase in the SESR temperature from 500 °C to 600 °C since higher temperatures favour the reforming reaction. A faster increase is observed from 600 to 625 °C, and then is kept around 50% above 625 °C. In Cases 2 and 3, H_2 yield also increases faster up to 625 °C, reaching values of 94.4 and 89.7%, respectively. As temperature further increases, a slight increase is seen up to 94.7% in Case 2 and 89.9% in Case 3. As explained before, when PSA-OG is burned (Case 3), the H_2 yield is slightly lower as the off-gas also contains a small fraction of H_2 because the efficiency of the PSA unit is assumed to be 95%.

The faster increase detected in the H_2 yield value from 600 to 625 °C in Case 1 (Figure 4.18a) is related to the formation of solid $Ca(OH)_2$ below 600 °C since its formation is thermodynamically unfavoured above 600 °C due to the lime hydration reaction (Eq. 4.11) is exothermic [191].

$$CaO_{(s)} + H_2O_{(l)} \leftrightarrow Ca(OH)_{2(s)} \qquad \Delta H_r^0 = -67 \text{ kJ mol}^{-1} \qquad \text{Eq. 4.11}$$

Therefore, the unconverted sorbent is found in the form of $Ca(OH)_2$ below 600 °C but in the form of CaO above that temperature (Table 4.10). This means that at lower SESR temperatures, $Ca(OH)_2$ is formed together with $CaCO_3$ and both must be regenerated in the REG reactor, requiring more

energy than necessary when only $CaCO_3$ is formed and the unreacted sorbent remains as CaO.

This also causes a change in the trend of CGE and NE efficiencies. The effect of $Ca(OH)_2$ formation at lower temperatures can be observed not only in Case 1 when H_2 is recycled to REG, but also in Cases 2 and 3 when biogas is used as fuel in REG, affecting the efficiency values. However, the impact for Cases 2 and 3 is lower since the heating value of biogas is higher than that of hydrogen, and the additional amount of biogas needed as fuel in those cases is lower, as observed in the consumption in Figure 4.18d-f.

CGE increases noticeably as the SESR temperature increases up to 625 ^{o}C (Figure 4.18d-f), as a consequence of the increase in methane conversion with temperature. At higher temperatures, only small variations (~0.5%) are observed. This is also in agreement with the decrease in the fuel consumption in REG for Cases 1 and 2 (Figure 4.18d and Figure 4.18f) with the temperature increase due to a narrower temperature window between the reformer and calciner at a higher SESR temperature. However, in Case 3, with PSA-OG use in REG, the fuel consumption increases until 600 ^{o}C (Figure 4.18f), and hence the increase in the efficiency with temperature is less pronounced since it is affected by the change in the PSA-OG composition with the SESR temperature.

As the temperature increases in the reformer, CH_4 conversion also increases and less unreacted CH_4 is present in PSA-OG, which, in turn, enriches the off-gas in H_2. Conversely, at low SESR temperatures the content of CH_4 in the PSA-OG is higher, the calorific value of the PSA-OG increases, and the process requires a lower amount of biogas as fuel for the sorbent regeneration. The CGE values at 625 ^{o}C are 60.7 and 72.0% in Cases 1 and 2, respectively, while it reaches 74.3% at 675 ^{o}C in Case 3. The addition of a PSA unit improves the efficiency due to the utilization of PSA-OG to provide more heat to the system. NE values when using air combustion in REG are lower than CGE values by ~1.80% in Cases 1 and 2, and 3.5% in Case 3, as expected. This is due to the additional compressor needed in Case 3 to match the pressure required by the PSA unit. When using oxy-combustion, NE lowers by 2.4% compared to the use of air due to the penalty associated with the oxygen production in the ASU.

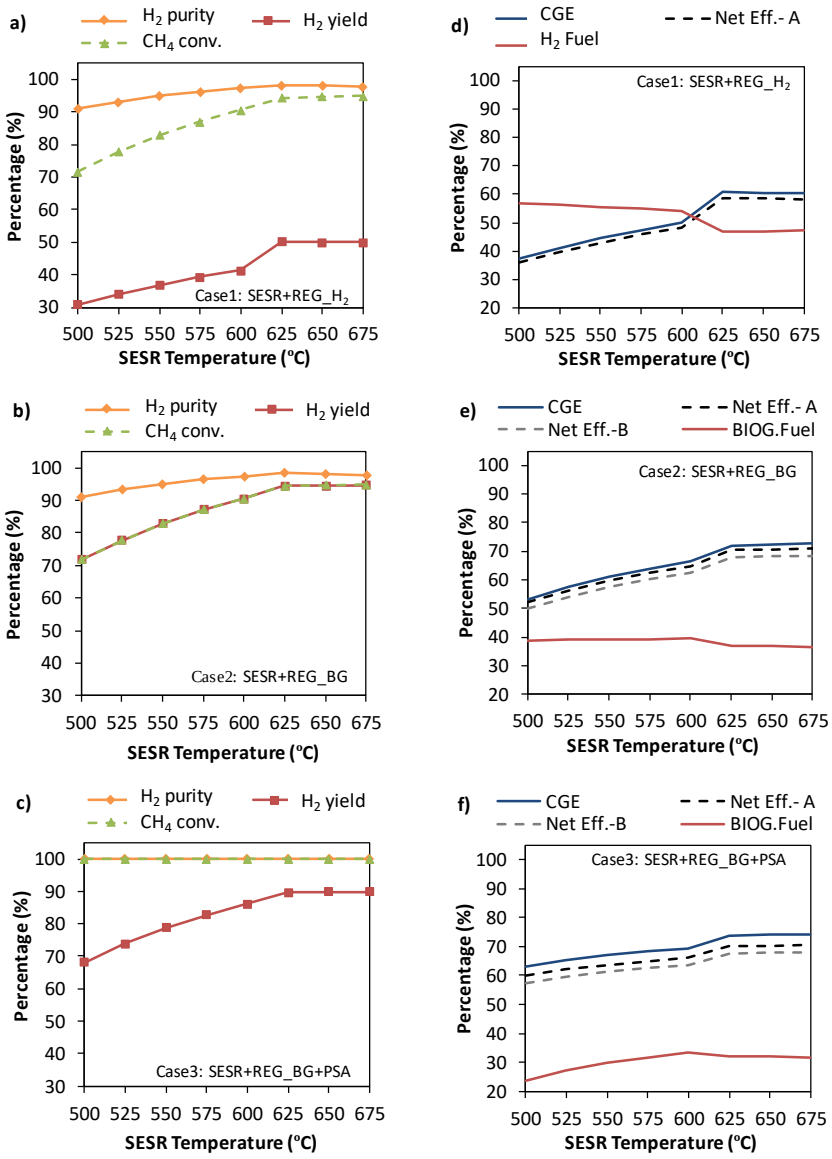

Figure 4.18: Effect of SESR temperature on H_2 purity, H_2 yield, and CH_4 conversion (a-c) and on cold gas efficiency (CGE), net efficiency (NE, using both air, Net Eff. A, and oxy-combustion, Net Eff-B, in REG), and fuel consumption for sorbent regeneration (d-f) for the different process configurations studied: (a and d) use of a fraction of the produced hydrogen as fuel for sorbent regeneration (SESR+REG_H_2); (b and e) use of biogas as fuel for sorbent regeneration (SESR+REG_BG); and (c and f) addition of a PSA unit and use of biogas and off-gas (PSA-OG) for sorbent regeneration (SESR+REG_BG+PSA). SESR conditions: S/CH_4 = 5.5, P = 10 bar, biogas = 60/40 vol.% CH_4/CO_2, and 50% sorbent excess.

Table 4.10: Effect of SESR temperature on the composition of the solids circulating between SESR and REG. SESR conditions: S/CH_4 = 5.5, P = 10 bar, biogas = 60/40 vol.% CH_4/CO_2, and 50% sorbent excess.

SESR Temperature (°C)	Solids composition at SESR outlet (mol %)		
	$CaCO_3$	CaO	$Ca(OH)_2$
500	55.4	0.0	44.6
525	57.7	0.0	42.3
550	59.8	0.0	40.2
575	61.4	0.0	38.6
600	62.7	0.0	37.3
625	64.1	35.9	0.0
650	63.9	36.1	0.0
675	63.4	36.6	0.0

Finally, the amount of energy recovered from the SESR reactor as a function of temperature decreases from 4.0 MW at 500 °C to 1.8 MW at 675 °C (Table 4.11). As the SESR temperature increases, the reforming reaction governs the heat balance, however, at lower temperatures, the carbonation reaction drives the heat balance since reforming is not favoured. Therefore, more heat released by carbonation is available in the SESR reactor. In addition, at lower temperatures not only carbonation releases heat but also lime hydration that is slightly exothermic (Eq. 4.11), and more heat is therefore available in SESR for recovery.

Table 4.11: Effect of SESR temperature on the heat recovered from SESR (heat losses considered). SESR conditions: S/CH_4 = 5.5, P = 10 bar, biogas = 60/40 vol.% CH_4/CO_2, and 50% sorbent excess.

SESR Temperature (°C)	**Heat recovered from SESR (MW)**
500	4.0
525	3.9
550	3.7
575	3.6
600	3.4
625	2.0
650	1.9
675	1.8

4.3.3. Effect of SESR pressure

Since high-pressure operation is a common practice in large-scale applications to reduce the reactor size and cost of H_2 production [88], pressure is an important parameter to evaluate. Furthermore, higher

operating pressures could be of interest for SESR to apply a pressure swing to regenerate the CO_2 sorbent instead of increasing the temperature [192]. The effect of the reforming pressure on H_2 purity, CH_4 conversion, and H_2 yield for the different process configurations is shown in Figure 4.19a-c. In Cases 1 and 2 (Figure 4.19a and Figure 4.19b), H_2 purity has a value of 99.0 vol.% between 1.5 and 5 bar, decreasing until 91.4 vol.% as pressure increases up to 25 bar. In Case 3 (Figure 4.19c), when a PSA unit is included, H_2 purity shows values of 100% along the pressure range since H_2 purity increases due to the additional capture step.

CH_4 conversion slightly decreases from 98.9 to 96.7% as SESR pressure increases from 1.5 to 5 bar in Cases 1 and 2. At higher pressures, CH_4 conversion decreases very sharply as pressure increases from 5 to 25 bar until a value of 73.0%. In agreement with the literature [193], as pressure increases, the CH_4 conversion and H_2 purity decrease since SESR is thermodynamically favoured at lower pressure due to the rise in the number of gas moles associated with the overall reaction which involves SMR and carbonation [194]. In Case 3 (Figure 4.19c), when a PSA unit is added, CH_4 conversion shows values of 100% for all pressures since the unconverted CH_4 from the SESR reactor is later used as fuel in the REG reactor through the PSA-OG combustion.

Regarding H_2 yield, it also shows higher values at pressures of 1.5-5 bar, decreasing as pressure increases up to 25 bar. The highest H_2 yield values are obtained in Case 2 when only biogas is used as fuel in the REG reactor (Figure 4.19b), decreasing H_2 yield values from 98.7% at 1.5 bar to 96.7% at 5 bar (then decreasing until 73.0% at 25 bar). In Case 3 (Figure 4.19c), H_2 yield slightly lowers from 93.8% at 1.5 bar to 91.9% at 5 bar, decreasing down to 69.3% at 25 bar, due to the combustion of a small fraction of H_2 with the PSA-OG. Finally, in Case 1, H_2 yield is much lower, ranging from 51.3% at 1.5 bar to 50.4% at 5 bar, decreasing down to 33.9% at 25 bar (Figure 4.19a), since a fraction of the produced hydrogen is used as fuel in the REG reactor. The decrease in this parameter above 5 bar is in accordance with the trend observed for the CH_4 conversion and H_2 purity.

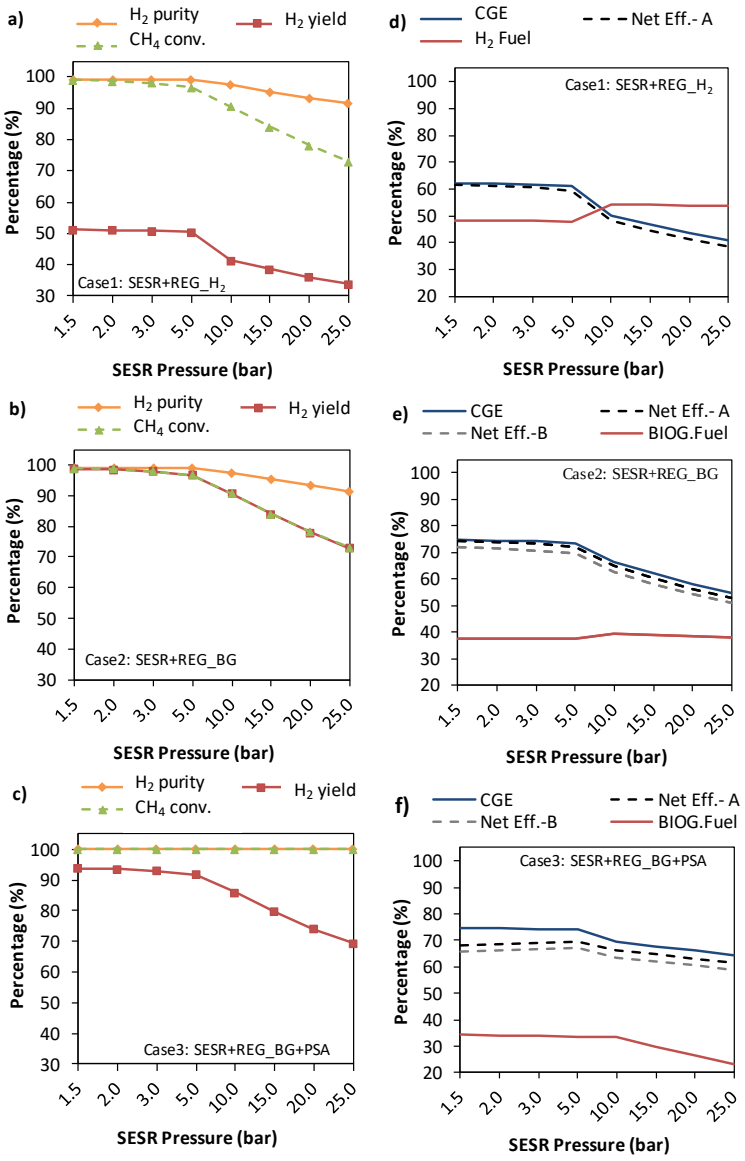

Figure 4.19: Effect of SESR pressure on H_2 purity, H_2 yield, and CH_4 conversion (a-c) and on cold gas efficiency (CGE), net efficiency (NE, using both air, Net Eff. A, and oxy-combustion, Net Eff-B, in REG), and fuel consumption for sorbent regeneration (d-f) for the different configurations: (a and d) use of a fraction of the produced hydrogen as fuel for sorbent regeneration (SESR+REG_H_2); (b and e) use of biogas as fuel (SESR+REG_BG); and (c and f) addition of a PSA unit and use of biogas and off-gas (PSA-OG) for sorbent regeneration (SESR+REG_BG+PSA). SESR conditions: S/CH_4 = 5.5, T = 600 °C, biogas = 60/40 vol.% CH_4/CO_2, and 50% sorbent excess.

Figure 4.19d-f shows that CGE and NE follow a similar trend to H_2 yield. CGE decreases as pressure increases following the decrease in methane conversion and, hence, in hydrogen production. In Cases 1 and 2 (Figure 4.19d and Figure 4.19e), CGE and NE values when air combustion is used in REG are close at low SESR pressures (1.5-5 bar) due to the lower workload required for the compression. At higher operating pressures (5-25 bar), NE for combustion in air is 1.5 to 2.3% lower than CGE as a consequence of the increase in the workload of the auxiliaries with process pressure. In Case 3 (Figure 4.19f), the PSA unit has an apparent impact on the net efficiency of the whole process. When air is used in REG, NE lowers from 6.8 to 4.4% below CGE in the pressure range of 1.5-5 bar, and 3% at higher pressures. The impact of the PSA is more noticeable at low pressures because the gap between the process and PSA pressure is higher, requiring more work in the compressor to match both pressures upstream of the SESR unit.

The slight increase in NE between 1.5 and 5 bar responds to the slightly lower gap as pressure increases. In Case 3, fuel consumption decreases when pressure increases above 5 bar. A higher content of CH_4 in PSA-OG and, hence, a higher calorific value of the off-gas reduces the amount of biogas required as fuel for sorbent regeneration. In the cases using biogas as fuel, a lower value (2.4%) of NE when using oxy-combustion in REG is explained by the penalty of the ASU.

For pressures above 5 bar, the formation of $Ca(OH)_2$ is observed under the simulation conditions (Table 4.12). As shown above, there is a marked change in the analysed variables between 5 and 10 bar, which is explained by the formation of $Ca(OH)_2$. When $Ca(OH)_2$ is formed, more heat is needed for regeneration, which decreases the efficiency of the process and increases the fuel required in the REG reactor.

As explained above, the effect of $Ca(OH)_2$ formation is more pronounced when the hydrogen-rich stream is used as fuel (Figure 4.19a) than when biogas is used (Figure 4.19e and Figure 4.19f) because the heating value of biogas is higher than that of hydrogen.

Table 4.12: Effect of SESR pressure on the composition of the solids circulating between SESR and REG. SESR conditions: S/CH_4 = 5.5, T = 600 °C, biogas = 60/40 vol.% CH_4/CO_2, and 50% sorbent excess.

SESR Pressure (bar)	Solids composition at SESR outlet (mol %)		
	$CaCO_3$	CaO	$Ca(OH)_2$
1.5	65.1	34.9	0.0
2	65.3	34.7	0.0
3	65.3	34.7	0.0
5	65.0	35.0	0.0
10	62.7	0.0	37.3
15	60.1	0.0	39.9
20	57.7	0.0	42.3
25	55.7	0.0	44.3

The amount of energy recovered from the SESR reactor (Table 4.13) is 2.0 MW in the pressure range of 1.5 to 5 bar. As the pressure increases from 5 to 25 bar, the recovered energy increases from 2.0 to 3.7 MW. As the SESR pressure increases, the methane conversion during SESR decreases and less heat is consumed by the reforming reaction, so there is more heat released by carbonation available for recovery.

The process design proposed in Case 3 could be interesting when producing H_2 for fuel cell applications, since the H_2 purity and CH_4 conversion are 100% regardless of the process pressure. However, the negative impact of high pressures on H_2 yield should be carefully considered.

Table 4.13: Effect of SESR pressure on the heat recovered from SESR (heat losses considered). SESR conditions: S/CH_4 = 5.5, T = 600 °C, biogas = 60/40 vol.% CH_4/CO_2, and 50% sorbent excess.

SESR Pressure (bar)	Heat recovered from SESR (MW)
1.5	2.0
2	2.0
3	2.0
5	2.0
10	3.4
15	3.5
20	3.6
25	3.7

4.3.4. Effect of S/CH_4 ratio

Steam is usually fed beyond its stoichiometric limit to promote H_2 production and to prevent coking [65]. Therefore, a wide range of S/CH_4 ratios (3-6.5) was studied. The effect of the S/CH_4 ratio on H_2 purity, CH_4 conversion, and H_2 yield for the different process configurations is shown in Figure 4.20a-c.

For Cases 1 and 2, H_2 purity increases up to 97.9 vol.% for S/CH_4 between 3 and 5 (Figure 4.20a and Figure 4.20b), followed by a slight decrease, and it finally increases up to 98.3 vol.% at a S/CH_4 ratio of 6.5. In Case 3, H_2 purity reaches a value of 100% for all S/CH_4 ratios (Figure 4.20c) due to the PSA unit purifying H_2. The effect of the S/CH_4 ratio on the H_2 purity is in agreement with the literature since higher CH_4 conversion leads to higher H_2 production and less off-gas methane contaminant content [195].

The conversion of CH_4 also increases with the S/CH_4 ratio since higher amounts of steam favour both SR and WGS reactions [65]. In cases 1 and 2, CH_4 conversion increases from 76.5 to 94.0% as S/CH_4 increases from 3 to 6.5. However, for Case 3, CH_4 conversion reaches a value of 100% for all S/CH_4 ratios because of the recycling of PSA-OG allows the unreacted CH_4 from SESR to be burned in the REG reactor.

On the other hand, H_2 yield increases with the S/CH_4 ratio in Cases 2 and 3 (Figure 4.20b and Figure 4.20c). In Case 2 it increases from 76.5 to 94.0% in the 3-6.5 S/CH_4 ratio range, while in Case 3 it increases from 72.6 to 89.3%. This lower value in Case 3 is explained because a small fraction of the H_2 produced is burned while recycling PSA-OG to the REG reactor due to the assumption of 95% separation efficiency of the PSA unit. However, in Case 1 (Figure 4.20a), H_2 yield is lower than in the other two configurations due to hydrogen consumption in REG. Its value is around 50% for S/CH_4 ratios between 3 and 5, and it notably decreases to 39.8% for higher S/CH_4 values due to $Ca(OH)_2$ formation (Table 4.14). This effect, as explained above, is stronger in the case of using H_2 for sorbent regeneration as compared to biogas, since hydrogen has a lower heating value, and hence, a higher amount of fuel is required.

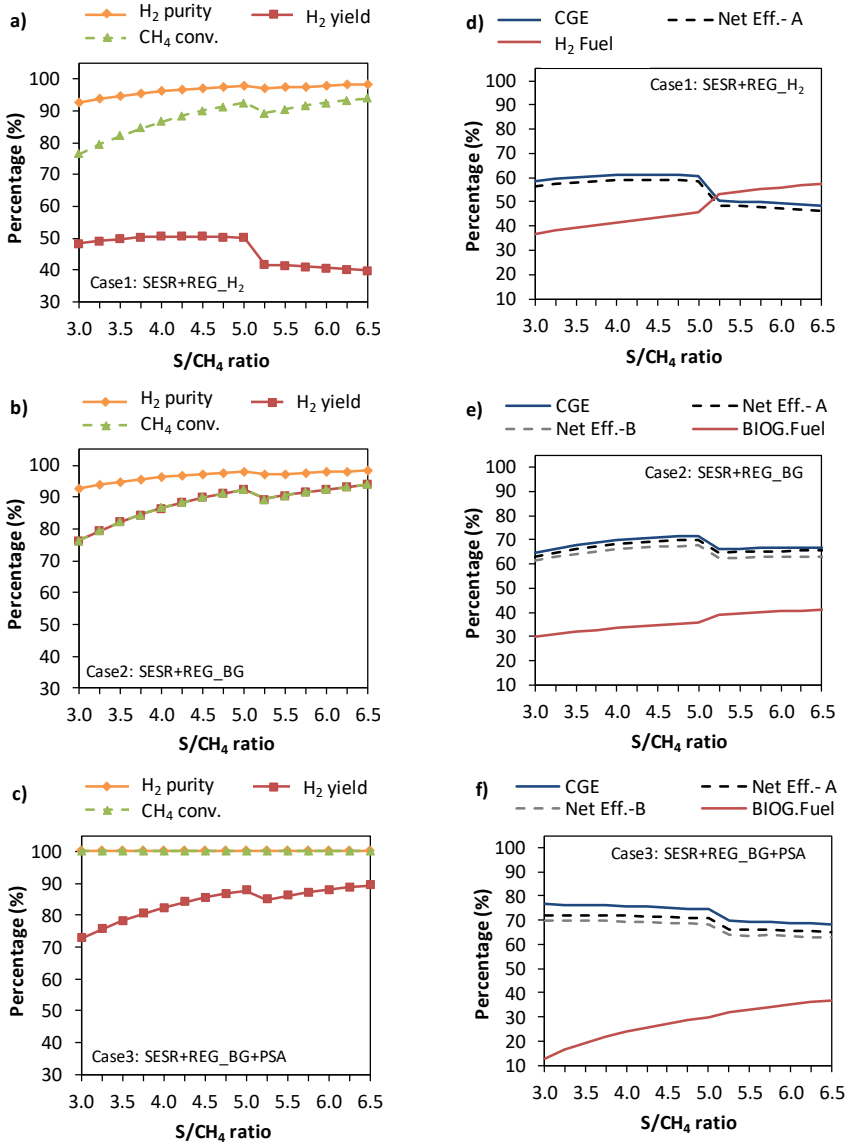

Figure 4.20: Effect of S/CH_4 on H_2 purity, H_2 yield, and CH_4 conversion (a-c) and on cold gas efficiency (CGE), net efficiency (NE, using both air, Net Eff. A, and oxy-combustion, Net Eff-B, in REG), and fuel consumption for sorbent regeneration (d-f) for the different process configurations studied: (a and d) use of a fraction of the produced hydrogen as fuel for sorbent regeneration (SESR+REG_H2); (b and e) use of biogas as fuel for sorbent regeneration (SESR+REG_BG); and (c and f) addition of a PSA unit and use of biogas and off-gas (PSA-OG) for sorbent regeneration (SESR+REG_BG+PSA). SESR conditions: 600 °C, P = 10 bar, biogas = 60/40 vol.% CH_4/CO_2, and 50% sorbent excess.

Table 4.14: Effect of S/CH_4 on the composition of the solids circulating between SESR and REG. SESR conditions: 600 °C, P = 10 bar, biogas = 60/40 vol.% CH_4/CO_2, and 50% sorbent excess.

S/CH_4 ratio	Solids composition at SESR outlet (mol %)		
	$CaCO_3$	CaO	$Ca(OH)_2$
3.00	57.1	42.9	0.0
3.50	59.4	40.6	0.0
4.00	61.2	38.8	0.0
4.50	62.5	37.5	0.0
5.00	63.5	36.5	0.0
5.25	62.3	0.0	37.7
5.50	62.7	0.0	37.3
6.00	63.5	0.0	36.5
6.50	64.1	0.0	35.9

The results corresponding to CGE and NE, as well as fuel consumption for sorbent regeneration, are shown in Figure 4.20d-f. The effect of the $Ca(OH)_2$ formation is also apparent in those figures at S/CH_4 ratios higher than 5.25 (see Table 4.14). The lowest fuel consumption in REG is achieved when a PSA unit is added due to the PSA-OG recycling (Figure 4.20f), which corresponds to the highest process efficiencies. It should be highlighted that the heat content of PSA-OG can reduce significantly the fuel consumption at low S/CH_4 ratios. In Case 3, CGE decreases from 76.5 to 74.4% as S/CH_4 increases from 3 to 5, then to 68.3% at a S/CH_4 ratio of 6.5. When using a lower S/CH_4 ratio, the content of CH_4 in the PSA-OG is higher, due to the lower methane conversion in SESR, which decreases the consumption of biogas for regeneration. CGE has lower values in Cases 1 and 2 than in Case 3. In Case 1, CGE increases from 58.4 to 60.7% for S/CH_4 values between 3 and 5 according to the higher methane conversion but then decreases to 48.2% at a S/CH_4 ratio of 6.5. In Case 2, CGE decreases from 64.6 to 71.6% as S/CH_4 increases from 3 to 5, and then to 66.9% at S/CH_4 ratio of 6.5. In Cases 1 and 2, when using air in REG, NE is 1.5-2.2% lower than CGE, whereas when oxy-combustion is used in REG, NE reduces an additional 2.2% in Case 2 due to the ASU penalty. In Case 3, when using air in REG, NE is 3.1-4.4% lower than CGE, whereas when oxy-combustion is used in REG, NE reduces an additional 2.4% due to the ASU penalty.

The amount of energy recovered from the SESR reactor is 2.1 MW when the S/CH_4 ratio is lower than 5, while it grows to 3.4 MW when S/CH_4 is higher than 5.25 (Table 4.15). The increase in heat recovery can be ascribed to the

heat released upon the formation of $Ca(OH)_2$ at higher S/CH_4 ratios, according to Eq. 4.11.

Table 4.15: Effect of S/CH_4 ratio on the heat recovered from SESR (heat losses considered). SESR conditions: 600 °C, P = 10 bar, biogas = 60/40 vol.% CH_4/CO_2, and 50% sorbent excess.

S/CH_4 ratio	Heat recovered from SESR (MW)
3.00	2.1
4.00	2.1
5.00	2.1
5.25	3.4
5.50	3.4
6.00	3.4
6.50	3.4

4.3.5. Discussion on SESR designs to optimise H_2 purity and captured CO_2

From the sensitivity analysis discussed above we can deduce that, in general, the CGE values depend largely on the amount of fuel used in REG, which indicates that the use of biogas as renewable fuel for sorbent regeneration (Case 2) gives better results than the use of the produced H_2 (Case 1). On the other hand, Case 3 has the highest CGE value due to the positive effect of the additional H_2 purification with the PSA unit and the subsequent recycling of the off-gas to the REG reactor. This is explained because recycling allows a decrease in fuel consumption compared to other configurations. Therefore, the addition of a PSA unit improves efficiency due to the utilization of PSA-OG to provide some additional fuel to the system.

After evaluating five case studies, the optimal operating conditions to achieve maximum H_2 purity based on the sensitivity analysis are shown in Table 4.16.

The differences between air and oxy-fuel combustion in REG can be seen in the net efficiency and CO_2 captured for cases 2 and 3. Case 1 is only evaluated with air combustion in REG. For Cases 1 and 2, the captured CO_2 is 98-99%, while in Case 3, the PSA unit boosts the captured CO_2 to ~100%. The CO_2 captured using air for regeneration means zero global emissions for the process since, although a renewable feedstock such as biogas is used, the outlet CO_2 stream is diluted with N_2 from the air. However, in oxy-combustion, the captured CO_2 translates into negative emissions from the process since in these cases a pure CO_2 outlet stream is obtained.

Comparing Cases 1 and 2, higher efficiency is achieved when using biogas as fuel for sorbent regeneration in REG (Case 2) compared to H_2 (Case 1), as expected. In Case 2, NE is 74.5% when air is used and 72.0% oxy-fuel combustion is used, along with H_2 purity of 98.5 vol.%, CH_4 conversion of 95.8%, and H_2 yield of 95.6%, operating at 625 ^{o}C, 5 bar, and S/CH_4 = 5. In this case, zero carbon emissions are achieved if air is used in REG, while negative emissions are achieved with 98.9% captured CO_2 for oxy-fuel combustion.

In Case 3, biogas is used for sorbent regeneration combined with a PSA unit at the end. Its NE is 72.5% when air is used and 70.2% when oxy-fuel combustion is used, i.e., 2% and 1.8% points less than in Case 2. However, the H_2 purity and CH_4 conversion reach almost 100%, with H_2 yield of 90.8%, when operating at 675 ^{o}C, 5 bar and S/CH_4 = 5. In this case, zero carbon emissions are achieved if air is used in REG, while negative emissions with ~100% captured CO_2 are achieved for oxy-fuel combustion. Therefore, assuming a slightly lower net efficiency by incorporating a PSA unit into the system, Case 3 can produce a high purity H_2 that meets the high requirements of, for example, fuel cells, both under air and oxy-fuel combustion conditions.

In summary, biogas SESR with sorbent regeneration using biogas (SESR+REG_BG) (Case 2) could be the best option if a H_2 purity of 98.5 vol.% fulfils the hydrogen requirements needed (with a CGE of 75.7%). For this configuration, oxy-fuel combustion sorbent regeneration delivers negative emissions with 98.9% captured CO_2. On the other hand, the addition of a PSA unit to the biogas SESR system that also uses biogas for sorbent regeneration (SESR+REG_BG+PSA) (Case 3) is needed if a H_2 purity of nearly 100 vol.% is required (with a CGE of 77.3%). Additionally, negative CO_2 captured of ~100% could be reached if oxy-fuel combustion is used in REG.

As can be seen in Figure 4.21, the efficiency obtained in the proposed biogas SESR+PSA configuration is higher than that the reported in the literature for other biogas reforming processes and comparable to that obtained for biogas chemical looping technology, which is one of the state of the art CO_2 CCS technologies.

Table 4.16: Optimal operating conditions with maximum H_2 purity for the biogas SESR configurations evaluated. SESR conditions: biogas = 60/40 vol.% CH_4/CO_2, and 50% sorbent excess.

Case No.	T (°C)	P (bar)	S/CH_4	H_2 purity (vol%)	CH_4 conversion (%)	H_2 yield (%)	CGE (%)	NE (%)	CO_2 captured (%)
Case 1-Air	625	5	5	98.5	95.8	53.8	65.1	63.5	98.0 (zero)
Case 2-Air	625	5	5	98.5	95.8	95.6	75.7	74.5	97.7 (zero)
Case 2-Oxy	625	5	5	98.5	95.8	95.6	75.7	72.0	98.9 (negat.)
Case 3-Air	675	5	5	100	100	90.8	77.3	72.5	100 (zero)
Case 3-Oxy	675	5	5	100	100	90.8	77.3	70.2	100 (negat.)

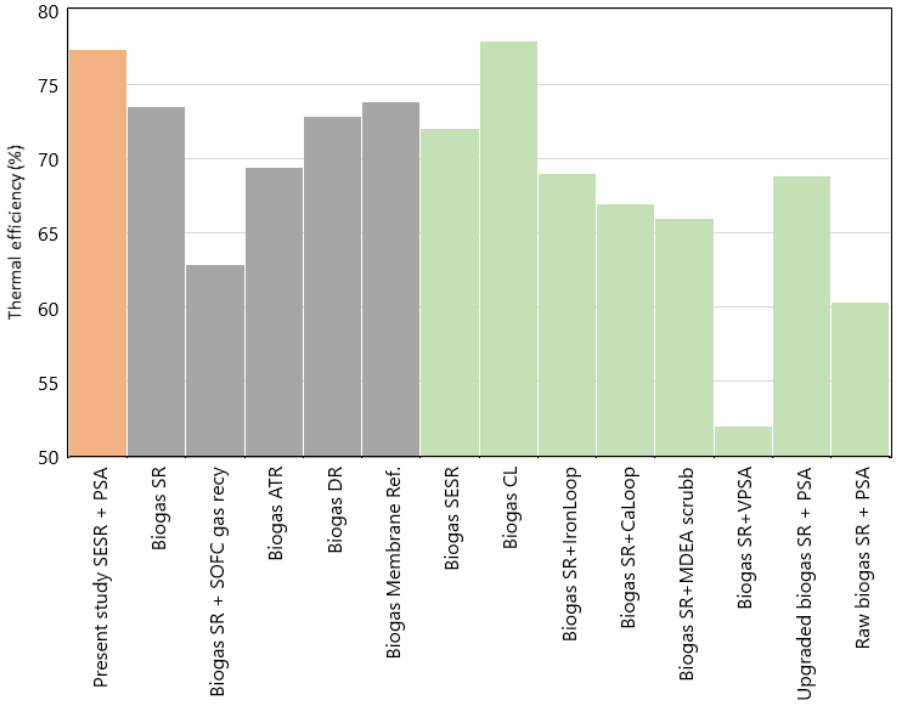

Figure 4.21: Comparison of the proposed biogas SESR + PSA (orange column) with different literature biogas reforming processes without CCS (grey columns; conventional SR [196], SR+SOFC [197], ATR: autothermal reforming [196,198], DR: dry reforming [199], membrane reformer [140]) and with CCS or PSA/VPSA (green columns; SESR [136], SR+CL: chemical looping [160], SR+Iron looping/Ca looping/MDEA scrubbing [200], SR+ VPS/PSA [160,201]).

4.3.6. Conclusions on process simulation of H_2 production by SESR of biogas

The conclusions of the process simulation of H_2 production by biogas SESR are as follows:

- The SESR+REG_BG configuration, which uses biogas to meet the energy requirements of sorbent regeneration, delivers a H_2 purity of 98.5 vol.% at 625 ^{o}C, 5 bar and S/CH_4 = 5, with a CGE of 75.7% and zero carbon emissions in the air regeneration operation. A captured CO_2 of 98.9% can be achieved in oxy-fuel combustion sorbent regeneration, and potentially negative emissions could be achieved.

- The SESR+REG_H_2 configuration, where part of the H_2 produced by the system is used to heat the calciner reactor, can produce a H_2 purity of 98.5 vol.% at 625 ^{o}C, 5 bar and S/CH_4 = 5, but with lower efficiency (CGE = 65.1%) than in case of biogas.

- The SESR+REG_BG+PSA configuration can produce ~100% H_2 purity at 675 ^{o}C, 5 bar, and S/CH_4 = 5, with a CGE of 77.3% and zero carbon emissions if an air-fired calciner is used. However, negative emissions and ~100% CO_2 captured are feasible if regeneration is performed in an oxy-fuel combustion atmosphere.

- The use of oxy-combustion in the regeneration stage represents a penalty of 2.3% points in the net efficiency of the process, although it allows a process with negative carbon emissions.

Overall, the results of this equilibrium study demonstrate the thermodynamic feasibility of the biogas SESR process and provide the optimal process configurations and operating conditions to maximise the cold gas efficiency of the process.

4.4. TECHNO-ECONOMIC ANALYSIS OF H_2 PRODUCTION BY SORPTION ENHANCED STEAM REFORMING (SESR) OF BIOGAS

This section presents the results of the techno-economic analysis of H_2 production from biogas using the SESR process. Firstly, the effect of changing the feedstock from natural gas to biogas on the process performance is studied. Secondly, the techno-economic evaluation of this process is carried out.

4.4.1. Technical performance of the SESR process of biogas and natural gas

A techno-economic analysis has been carried out for three case studies: 1) Case 1_BIOG_ IndAIR, 2) Case 2_BIOG_DirOXY, 3) Case 3_NG_ IndAIR. The latter case is based on the use of natural gas and is performed for comparison purposes. The techno-economic analysis is based on the following points:

- Technical analysis → a first technical analysis is conducted in order to evaluate the differences in SESR performance between the use of natural gas and biogas.
- Estimation of CAPEX and OPEX → the capital and operational costs are estimated and compared for all cases.
- Estimation of the levelised cost of hydrogen → the levelised cost of hydrogen is calculated and compared for all cases.

The general assumptions of the thermodynamic modelling used for the techno-economic analysis are the same as those defined for the simulation of the SESR process in section 4.3 (see Table 4.6). Among the configurations studied, the design that includes a PSA unit for further purification of H_2 and recycling of off-gas to an external burner was selected.

The specific operating conditions for the biogas and natural gas cases are shown in Table 4.17. For the techno-economic evaluation, a fixed production capacity of 50 MW of H_2 was set using a design specification that varies the amount of feedstock fed to achieve the desired production target. In the case of biogas , the temperature and pressure of the reformer were selected as the optimal values from the previous sensitivity analysis. In the case of natural gas, the pressure and temperature of the reformer are the optimal values according to the literature [131].

Table 4.18 shows the compositions of biogas [29,202] and natural gas [203] used in the simulations, which were selected based on the values reported in the literature.

Table 4.17: Operating conditions used in the simulations for the techno-economic analysis.

Parameter	Unit	Biogas	Natural gas
		Value	Value
H_2 out	MW	50	
Reformer P	bar	5	25
Reformer T	ºC	675	611
Molar S/CH_4	Molar ratio	5	5
Calciner T	ºC	900	900
Calciner P	bar	1	1
Burner T	ºC	1000	1000
PSA compressor P	bar	25	25
Pure CO_2 compressor	bar	110	110

Table 4.18: Biogas and natural gas compositions used for the techno-economic analysis.

	CH_4	CO_2	N_2	C_2H_6	C_3H_8	C_{4+}
Biogas composition (mol%)	58.9	38.1	3.0	-	-	-
Natural gas composition (mol%)	92.0	-	0.5	5.8	1.3	0.5

The three case studies were simulated using the AspenPlus software. Table 4.19 shows the main results of the simulations.

Table 4.19: Simulation results obtained for the three case studies proposed for the techno-economic analysis.

Parameter	Units	**Case 1** BIOG_ IndAIR	**Case 2** BIOG_ DirOXY	**Case 3** NG_ IndAIR
Reformer feed	ton/hr	9.5	9.5	3.7
Fuel calciner/burner	ton/hr	4.5	3.5	1.7
Boiler feed water	ton/hr	18.5	18.5	21.0
CO_2 compressor (110bar)	MW_{th}	2.1	6.4	1.3
H_2 compressor (to PSA at 25bar)	MW_{th}	1.4	1.4	0.0
Air separation unit (ASU)	MW_{th}	0.0	1.0	0.0
Calciner capacity (LHV based)	MW_{th}	18.2	16.9	12.4
Burner capacity (LHV based)	MW_{th}	20.2	-	13.6
H_2 product flowrate	tonne/hr	1.5	1.5	1.5
Plant capacity - H_2 product (LHV based)	MW_{th}	50.0	50.0	50.0

As shown in Table 4.18, the main element contained in natural gas is CH_4 (92%), while the CH_4 content in biogas is around 60% and the rest is mainly CO_2. Therefore, to achieve the target production capacity (50 MW_{th}), it is necessary to supply a larger amount of biogas (9.5 ton/hr) compared to that of natural gas (3.7 ton/hr), as shown in Table 4.19. This is also reflected in the fuel demand of the calciner, which is lower in the case of using natural gas (1.7 ton/hr) than when using biogas (4.5 ton/hr in Case 1, and 3.5 ton/hr in Case 2).

The difference in the calciner fuel demand between the two biogas case studies (Cases 1 and 2) is due to the strategy for supplying heat to the calciner. In Case 1, heat is supplied by indirect heating by heat transfer from an external burner to the calciner. Air combustion occurs at 1000 ^oC, 100 ^oC higher than the calciner. Therefore, a slightly higher amount of fuel is needed in Case 1 compared to Case, 2 where direct oxy-combustion is performed at 900 ^oC.

The results of the technical analysis are also affected by different optimal operating conditions of the reformer for biogas and natural gas (see Table 4.17). For example, an important difference can be found in the work required by the CO_2 compressor. In order to store the pure CO_2 captured, it is necessary to previously compress the gas (110 bar is assumed). Comparing the two biogas cases, oxy-combustion requires greater compression work (6.4 MW_{th}), since it is performed using a mixture of 30% O_2 and 70% CO_2 to avoid extreme operation conditions (see section 3.2.1). Comparing biogas and natural gas, the use of biogas requires more work due to the higher CO_2 content.

The results of the SESR performance for the three case studies proposed for the techno-economic analysis are shown in Table 4.20. The results of CO_2 capture and emissions for these case studies are shown in Table 4.21.

Regarding the main KPI's (see Table 4.20), the feedstock conversion in SESR is slightly lower when using natural gas due to the lower optimal temperature. The highest efficiency is obtained with natural gas but CO_2 emissions are unabated, as will be discussed later. When biogas is used, oxy-combustion (Case 2) provides a 6 % higher CGE that air combustion (Case 1), because the oxy-combustion reactor operates at a lower temperature (900 ^{o}C) than the external burner used for air combustion (1000 ^{o}C).

Furthermore, in biogas cases all CO_2 can potentially be considered as captured CO_2 and some of it could even be negative. On the contrary, in the case of natural gas (Case 3), it is estimated that CO_2 capture is around 67.8%. This corresponds to 2.8 kg CO_2/kg H_2 avoided if biogas is used. The CO_2 emissions only apply to the Case 3, when natural gas is used, and are calculated as the CO_2 mass flow in the flue gas of the external burner divided by the mass flow of H_2 produced in the 50MW plant.

Table 4.20: Results for the main KPIs obtained for the three case studies proposed for the techno-economic analysis.

Parameter	Units	Case 1 BIOG_ IndAIR	Case 2 BIOG_DirO XY	Case 3 NG_ IndAIR
H_2 purity (%)	%	100.0	100.0	100.0
SESR feedstock conversion	%	96.27	96.27	86.3
Cold gas efficiency (CGE)	%	74.1	80.2	82.2
Net efficiency (NE - including CO_2 compression)	%	66.1	61.6	76.7

Table 4.21: Results of CO_2 capture and emissions obtained for the three case studies proposed for the techno-economic analysis.

Parameter	Units	Case 1 BIOG_ IndAIR	Case 2 BIOG_DirO XY	Case 3 NG_ IndAIR
Captured CO_2	%	100.0	100.0	67.8
Capt. CO_2 from the sorbent reg. (negative for biogas)	(kg CO_2 /kg H_2)	9.3	27.1	5.9
Capt. CO_2 from the flue gas when using biomass feedstock in the combustor (zero)	(kg CO_2 /kg H_2)	5.4	0.0	0.0
CO_2 emissions	(kg CO_2 /kg H_2)	0.0	0.0	2.8

4.4.2. Economic analysis of biogas and natural gas SESR

4.4.2.1. Estimation of CAPEX and OPEX

The main assumptions for the economic analysis are shown in Table 4.22. Costs, such as design and engineering, maintenance, supervision, etc., were assumed as a percentage of other costs, as reported by Y. Yan et al. [138]. The complete assumptions are included in *Annex I: Techno-economic analysis*.

To estimate CAPEX and OPEX, the chemical plant cost estimation methodology developed by Sinnott et al. [162] was used, as explained in section 3.3.2.

Table 4.22: Main assumptions for the economic analysis.

Parameter	Units	Value	Ref.
Main equipment			
Cost of reformer	€m	39.0	[138]
Cost of calciner and burner	€m	31.5	[138]
Cost of PSA unit	€m	45.0	[138]
Cost of ASU	€m	43.2	[138]
SOx Sulphur removal unit	€m	0.7	[142]
CO_2 storage			
Cost of CO_2 compressor	€m	15.4	[138]
Cost of CO_2 storage	€/ton	21.7	[138]
Materials			
Natural gas price	€/ton	159.4	[139]
Biogas price	€/GJ	1.5	[140]
Water price	€/ton	3.5	[138]
Electricity cost	€ MWh^{-1}	120.0	[141]
Ni catalyst (life span: 5 years)	€/ton	50000.0	[141]
Ni catalyst: CaO weight ratio	-	0.5	[138]
Spent catalyst landfill	€/ton	26.7	[204]
Limestone (life span 500h)	€/ton	96.9	[138]
Design, engineering and operation			
Chemical Engineering Plant Cost Index (CEPCI)2021 - A	-	708.0	[205]
Chemical Engineering Plant Cost Index (CEPCI)2019 - B	-	607.5	[205]
Chemical Engineering Plant Cost Index (CEPCI)2011 - B	-	585.7	[206]
Plant staff	-	20.0	Based on [138]
Burdened labour cost	€/hr	29.1	[207]
Plant life	year	30.0	Based on [138]
Working hours per year	hr/year	8760.0	Based on [138]
Capacity factor	-	0.95	[138]

Table 4.23 shows the total CAPEX and OPEX values obtained from the economic analysis. The complete set of results is included in *Annex I: Techno-economic analysis*.

Table 4.23: Total CAPEX and OPEX obtained for the SESR of biogas and natural gas.

	Units	**Case 1** BIOG_ IndAIR	**Case 2** BIOG_DirOXY	**Case 3** NG_ IndAIR
Total capital costs - CAPEX	€m	55.4	69.6	42.3
Total operating costs - OPEX	€m	27.9	40.3	27.5

In addition, Figure 4.22 shows the breakdown of the CAPEX and variable OPEX.

The highest CAPEX (69.6 €m) is obtained for Case 2 (biogas with direct oxy-combustion), as well as the highest OPEX (40.3 €m). On the other hand, the lowest CAPEX (42.3 €m) is obtained for Case 3 (natural gas with indirect air combustion), while an intermediate value (55.4 €m) is obtained for Case 1 (biogas with indirect air combustion). The use of air combustion decreases the CAPEX value compared to oxy-combustion, since the O_2/CO_2 mixture used in oxy-combustion increases the cost of the CO_2 compressor due to the higher amount of CO_2. The ASU also represents an additional cost in oxy-combustion. For the same reason, oxy-combustion results in higher OPEX due to higher electricity and CO_2 storage costs.

In terms of CAPEX, when using air combustion in an external burner (Cases 1 and 3), the main contributors to the total CAPEX are the reformer, the calciner and the burner, as expected. The reformer contributes 39% (biogas) and 29% (natural gas), while the calciner and burner have a similar contribution when biogas and natural gas are used (19% of total CAPEX approx.).

In the case of oxy-combustion (Case 2), the contribution of the ASU (15%) is much higher than that of the calciner (9%), representing an important cost in this case. In terms of variable OPEX, the largest contribution is related to water and electricity costs when biogas is used (40 and 46% in cases 1 and 2, respectively), while the largest contribution

is associated with the cost of natural gas (60%) when natural gas is used (Case 3).

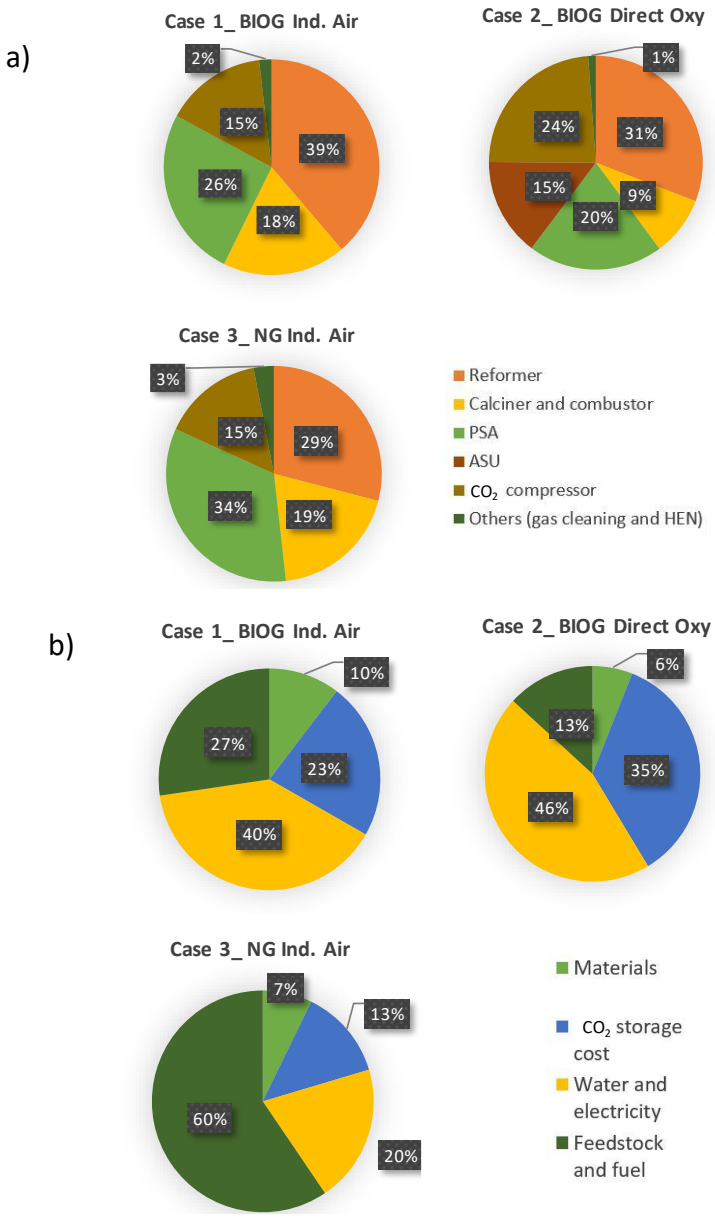

Figure 4.22: Breakdown of CAPEX (a) and variable OPEX (b) for the SESR of biogas (BIOG) and natural gas (NG).

4.4.2.2. Estimation of the levelised cost of hydrogen – LCOH

The levelised cost of hydrogen is useful for comparing different scenarios, as it represents all the costs required to build and operate a plant over its economic life, normalized over the net electricity generated (50MW for this study, based on the LHV of H_2).

Figure 4.23 shows the distribution of the different costs contributing to the LCOH with CO_2 storage (Figure 4.23a) and without CO_2 storage (Figure 4.23b).

The lowest LCOH is obtained in Case 3 (2.6 €/kg H_2 including CO_2 storage), which corresponds to the natural gas case. Moreover, this is also the only case with positive CO_2 emissions (2.8 kg CO_2/kg H_2, see Table 4.21). Among the biogas case studies, the lowest LCOH is obtained when using an indirectly heated calciner boosted by air combustion in an external burner (Case 1; 2.8 €/kg H_2 including CO_2 storage). The difference between the use of natural gas and biogas is only 0.2 €/kg H_2, suggesting that biogas could be a potential economically competitive substitutive for natural gas and that it also promotes the mitigation of CO_2 emissions by being a carbon neutral option. However, if the objective is to achieve negative emissions (Case 2), the LCOH increases considerably (3.8 €/kg H_2), which makes this option less attractive from an economic point of view.

The LCOH is greatly affected by different technical and economic factors [138]. As shown in Figure 4.22, the case of natural gas is particularly affected by the cost of the feedstock. In fact, the price of natural gas has recently been influenced by different social and political reasons (e.g., the recent military conflict in Ukraine). In this work, a reasonable price has been assumed (159.4 €/ton [139]), but it should be noted that the price of natural gas could reach very high values such as those reached in 2022 of approximately 0.065 €/kwh, which corresponds to 900.8 €/ton (based on the LHV of CH_4) [208]. If this natural gas price is considered, the LCOH of Case 3 (including CO_2 storage) would increase by approximately 51% , reaching a value of 5.2 €/ton. In this situation, the biogas option would be clearly more advantageous.

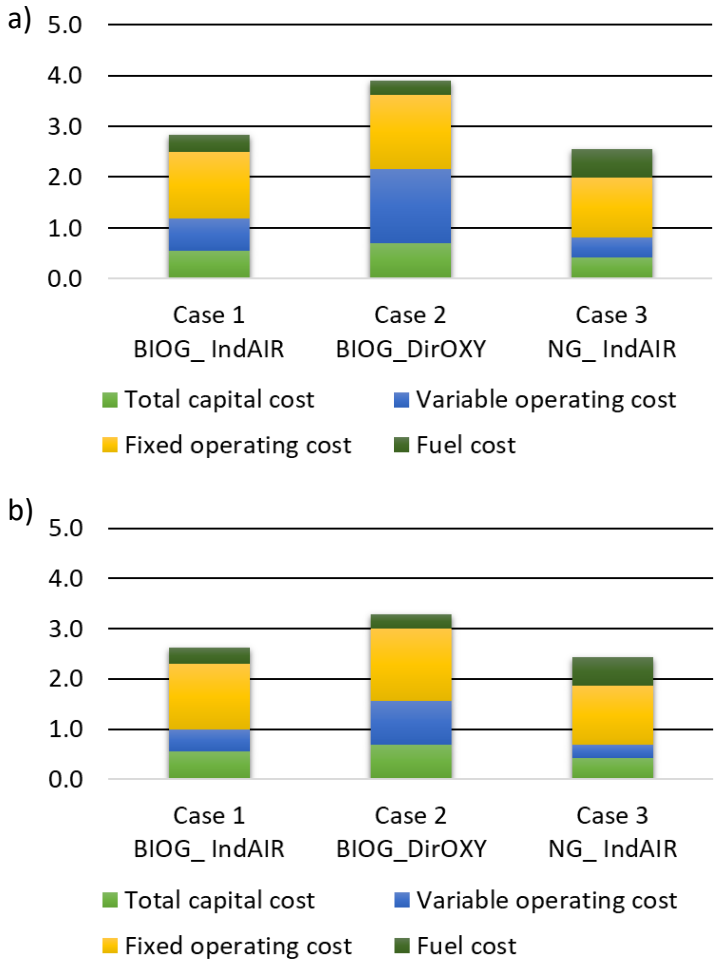

Figure 4.23: Splitting of the different costs of LCOH for the SESR of biogas (BIOG) and natural gas (NG) with CO_2 storage (a) and without CO_2 storage (b).

The results obtained in this economic analysis are in good agreement with those reported recently by the European Biogas Association (EBA) in the report *Decarbonising Europe's hydrogen production with biohydrogen* (2023) [209], where the cost associated to MSR (with or without CCS) is expected to be in the range 1.15-7.34 €/kg H_2.

4.4.3. Conclusions on the techno-economic analysis of biogas SESR

The conclusions from the techno-economic analysis of a SESR plant producing 50MW of H_2 using biogas and natural gas are as follows:

- When comparing the CGE of the biogas case studies, a higher efficiency is obtained in the case of direct oxy-combustion in the calciner (80.2%) than in indirect air combustion (74.1%). The main reason is that a larger amount of fuel is needed in the external burner compared to the calciner. The highest efficiency is obtained in the case of natural gas (82.2%). However, the biogas cases are not far from this value.

- In the biogas case studies, all CO_2 is captured, while the part coming from the calciner can be considered as negative emissions. In contrast, only 67.8% of CO_2 is captured when natural gas is used, corresponding to 2.8 $kgCO_2/kg\ H_2$ of CO_2 emissions. Therefore, even if CCS is included in the case of natural gas, this option cannot be considered totally carbon neutral.

- The lowest LCOH is obtained when using natural gas (2.6 €/kg H_2 including CO_2 storage), and this is also the only case with positive CO_2 emissions. Among the biogas case studies, the lowest LCOH is obtained when using indirect air combustion in an external burner (2.8 €/kg H_2 including CO_2 storage). The difference between both feedstocks is only 0.2 €/kg H_2, suggesting that biogas could be a potential economically competitive substitutive for natural gas.

Overall, although the use of natural gas is more efficient and gives a lower LCOH, the use of biogas is very close and competitive in terms of both efficiency and cost. In addition, the biogas case studies would be carbon neutral, while the natural gas case would emit 2.8 kg $CO_2/kg\ H_2$.

4.5. PRODUCTION OF BIO-DME AS HYDROGEN CARRIER: PROCESS SIMULATION OF THE INTEGRATION OF BIOGAS SESR AND SEDMES

This section presents the results of the study of the integration of the SESR process of biogas with the SEDMES process to produce bio-DME.

4.5.1. Simulation of the integration of biogas SESR and SEDMES to efficiently produce low-carbon bio-DME

The assumptions for the biogas SESR process in this study are shown in Table 4.24.

Table 4.24: Thermodynamic assumptions of the biogas SESR unit.

Variable	Units	Value
Biogas composition	molar	60/40
S/CH_4	molar	5
Reformer T	^oC	675.0
Reformer P	bar	5.0
Reformer and burner heat loss	%	10
Calciner T	^oC	900
Burner T	^oC	965
Calciner and burner P	bar	1
Calcination conversion	%	100
Excess of oxygen in external burner	%	5
H_2 production SESR	MW	40.0

On the other hand, Table 4.25 shows the assumptions for the SEDMES unit. The SEDMES temperature was set at 250 ^oC since the direct synthesis of DME is usually performed at this temperatures [33]. On the other hand, 50 bar was set as the pressure for the SEDMES process since this is the usual pressure for the DME reaction [148]. Regarding the water removal percentage, the ratio CO/CO_2 in the outlet gas should be around 2 based on previous experimental experience [146]. Therefore, to define the percentage of water removal according to this ratio, a sensitivity analysis was performed. The results are shown in Table 4.26, where it can be seen that for 98.7% of H_2O removed, a ratio CO/CO_2 of 2 is achieved, so this was the selected H_2O removal value.

Table 4.25: Assumption of the three blocks that conform the SEDMES unit.

Variable	Units	Value
M-module	-	2
SEDMES T	^{o}C	250
SEDMES P	bar	50
Stoichiometric reactor conversion of CO_2 and CO to DME	molar	0.99
H_2O removal in the separator	%	98.7
Inert gases in the RGibbs reactor	-	CH_4, C, C_2H_4 and C_2H_6

The final step in the SEDMES unit is the purification of the DME. To meet the purity requirements stablished in ISO 16861:2015 (purity > 99.5%), two distillation columns were used for the distillation train. In both distillation columns, the feed stage and the number of stages were defined based on previous knowledge of shortcut models, which were then set up in RadFrac distillation models. In addition, the distillate ratio in both columns was calculated with a calculator block.

In the first distillation column, the light components such as H_2, CO, CH_4 and specially CO_2 are separated from DME/MetOH. The separation of CO_2 from DME is the most energy-consuming process in the purification train [147]. The product specification of this column implies a CO_2 concentration of less than 0.1 wt.%. Therefore, the pressure was reduced to 30 bar to minimize the reflux ratio needed to achieve the target CO_2 separation in this column, improving the duty requirement. All specifications for the first distillation column are shown in Table 4.27.

On the other hand, the bottom product from the first distillation column is treated in the second distillation column. The objective in this distillation column is to separate as much MetOH (and water) as possible from the DME, achieving the purity requirements of ISO 16861:2015. Therefore, the reflux ratio is chosen to achieve the product specification, i.e., methanol < 0.05 wt.%, while minimizing the duty requirement of this column. The pressure is set at 5 bar, as previously reported in the literature [148]. All specifications for the second distillation column are shown in Table 4.28.

Table 4.26: Sensitivity analysis of the percentage of water removal in the SEDMES unit and outlet gas composition.

%H_2O removed	Outlet gas composition SEDMES (mol% dry basis)						
	CH_4	H_2	CO	CO_2	DME	METOH	CO/CO_2
98.0	4.5	15.4	3.9	2.9	72.5	0.8	1.4
98.5	4.6	13.8	4.1	2.2	74.7	0.7	1.8
98.7	**4.6**	**13.1**	**4.1**	**2.0**	**75.6**	**0.6**	**2.1**
99.0	4.7	12.0	4.2	1.6	77.1	0.5	2.6
99.5	4.8	9.9	4.2	0.9	79.7	0.4	4.6

Table 4.27: Specifications for the first distillation column of the DME purification train.

Variable	Units	Value
Number of stages/Feed	-	9/4
Pressure and pressure drop	bar	30/0.01
Reflux ratio	-	1.1
Distillate rate	kmol/hr	30.7
DME losses in D1	wt.%	1.6
Condenser temperature	^oC	-58.3
Reboiler temperature	^oC	94.8

Table 4.28: Specifications for the second distillation column of the DME purification train.

Variable	Units	Value
Number of stages/Feed	-	9/4
Pressure and pressure drop	bar	5/0.01
Reflux ratio	-	0.5
Distillate rate	kmol/hr	95.6
DME purity	wt.%	99.9
Condenser temperature	^oC	19.4
Reboiler temperature	^oC	75.9

The main objective of this work is to integrate biogas SESR and SEDMES. The basic diagram without any integration is shown in Figure 4.24. For the basic design a CGE of 63.8% is obtained with a global yield of 39.0%.

The integration of both processes will be carried out through the exploitation of three synergies found between both processes, which are the following:

- Synergy 1 → a heat integration between the two units can be stablished (Figure 4.25).
- Synergy 2 → the by-products from the SEDMES unit can be recycled in the external burner used to supply heat to the calciner of the biogas SESR unit (Figure 4.26).
- Synergy 3 → since a purge step is necessary to recover the adsorbent used in SEDMES to remove the retained steam, the steam can be recycled from the SEDMES unit to the biogas SESR unit (Figure 4.27).

Based on these synergies, three strategies for the integration of both processes were studied. Table 4.29 shows the results in terms of efficiencies and global yield of bio-DME for the different strategies studied.

The SEDMES process operates at 250 ^{o}C, while the reformer operates at 675 ^{o}C, and the calciner and burner at 900 and 965^{o}C, respectively. Although a HEN was designed to recover as much heat as possible from the gases in the SESR unit, when mixing H_2 and CO_2 to feed the SEDMES unit, the temperature of this stream would be around 580 ^{o}C and a cooler would be required between the SESR and SEDMES units.

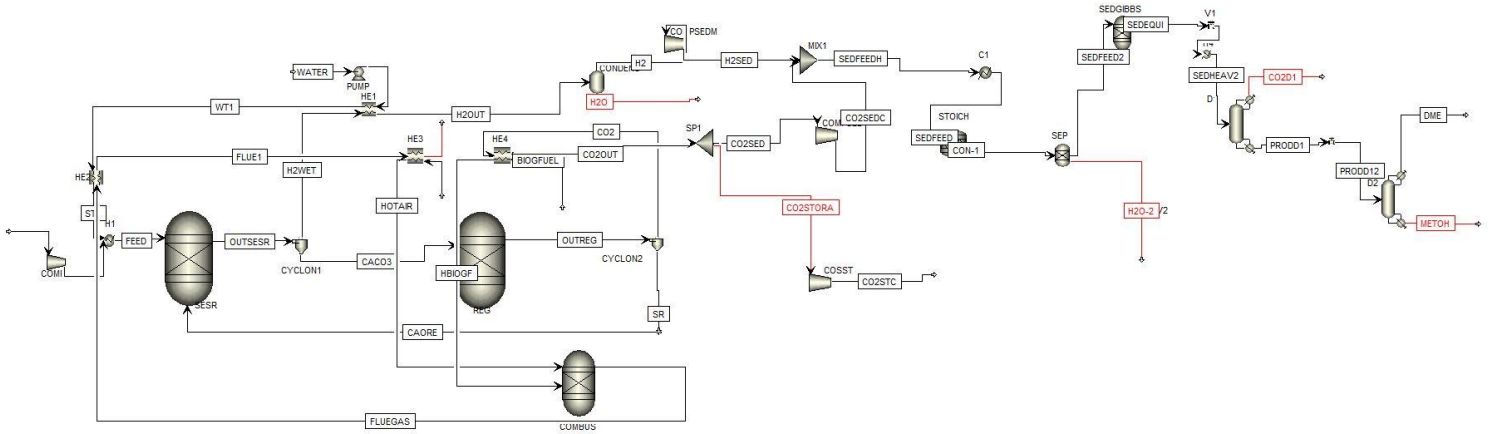

Figure 4.24: AspenPlus diagram of the basic bio-DME production plant from biogas coupling biogas SESR and SEDMES.

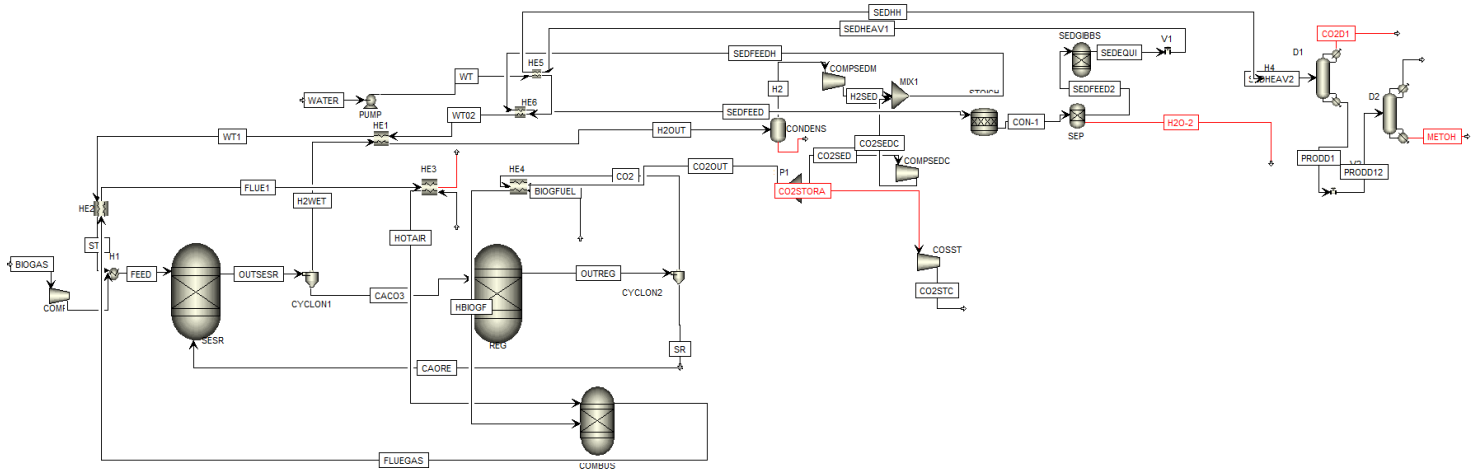

Figure 4.25: AspenPlus diagram of the heat integration between biogas SESR and SEDMES.

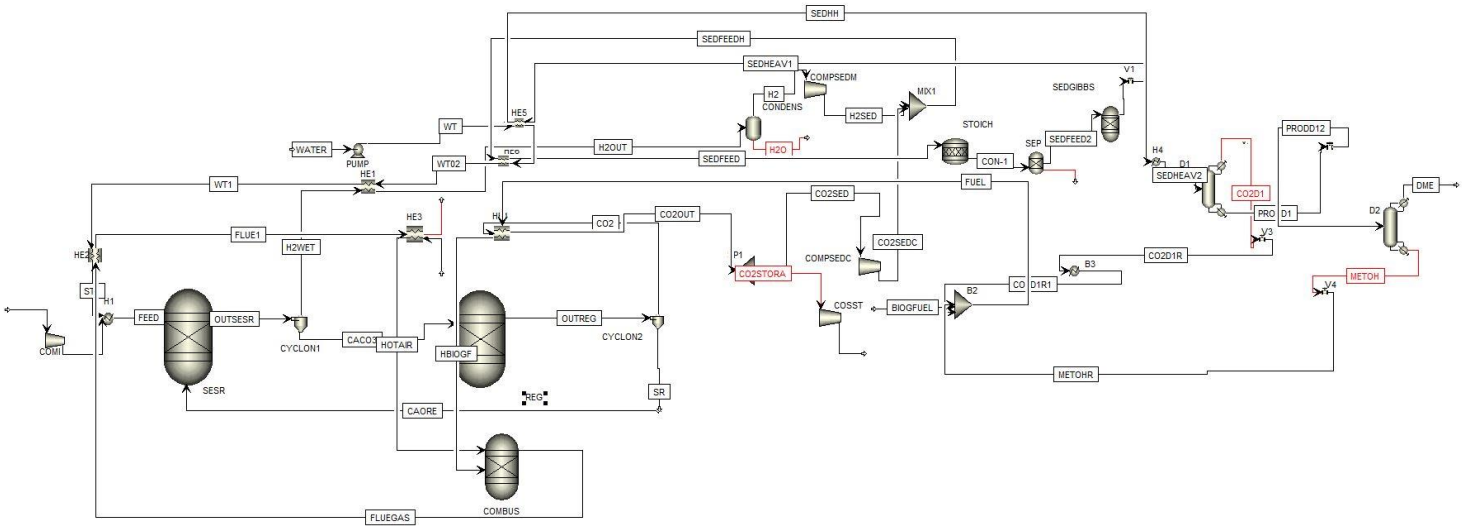

Figure 4.26: AspenPlus diagram of the second synergy; the recycling of SEDMES by-products to the external burner of SESR unit.

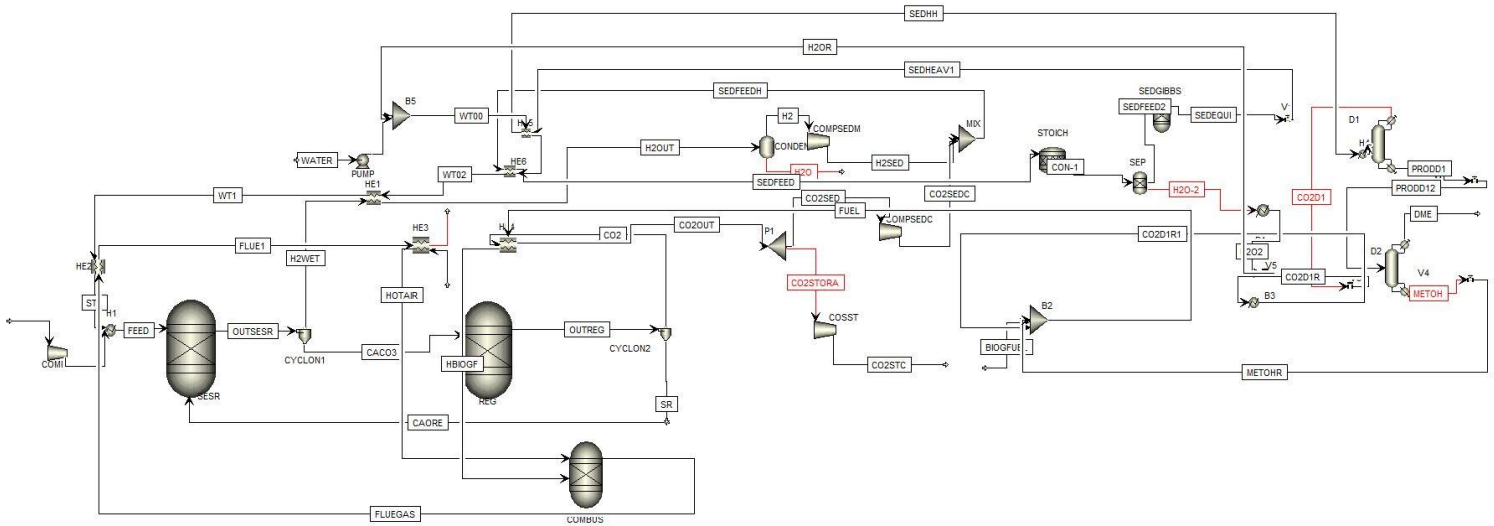

Figure 4.27: AspenPlus diagram of the last strategy included; the recycling of the steam from SEDMES to SESR.

Therefore, in the first strategy, the cooler is replaced by a heat exchanger to take advantage of this heat to support steam production in the SESR unit. Secondly, the first distillation column requires a low temperature feed stream (around 10ºC) in order to separate CO_2 from the main product. Therefore, a cooler is needed between the RGibbs reactor and the first distillation column. This cooler is replaced in this strategy by another heat exchanger to support also the steam production in the SESR unit. Due to this heat integration between units, the CGE increased by 3% and the global yield by almost 2% (Table 4.29).

The second strategy includes recycling the SEDMES by-products to be used as fuel for the external burner of the SESR unit, which supplies heat to the calciner. With this strategy, the biogas demand in the burner decreases by 4% and the overall CGE of the plant increases by 4.3%. The overall yield increases to 43.5%.

Finally, the third strategy mimics the use of the steam recovered in the SEDMES unit during a purge step to be used in the SESR unit to carry out the steam reforming reaction. By re-using steam, some of the heat required for its production is saved. This heat can be used to preheat other streams, increasing the overall efficiency of the plant. In addition, since a close water loop is created, some of the water required is also saved. By adding this third synergy, the highest efficiency of 74.1% is achieved, as well as the highest yield of 45.3% is reached. In addition, 38% of water consumption is saved.

Table 4.29: Results of the three synergies in terms of efficiencies and global yield of bio-DME production from the integration of biogas SESR and SEDMES.

Strategy	CGE (%)	NE (%)	Global yield (%)
Basic design	63.8	47.1	39.0
Heat integration between units	67.0	53.6	40.9
By-products recycling from SEDMES to the external burner in SESR	71.3	56.2	43.5
Steam recycling from SEDMES (purge step for adsorbent recovery) to SESR	74.1	56.3	45.3

As can be observed in Figure 4.28, the carbon balance improves with integration strategies, as more carbon ends up in the DME as used carbon (almost 54%).

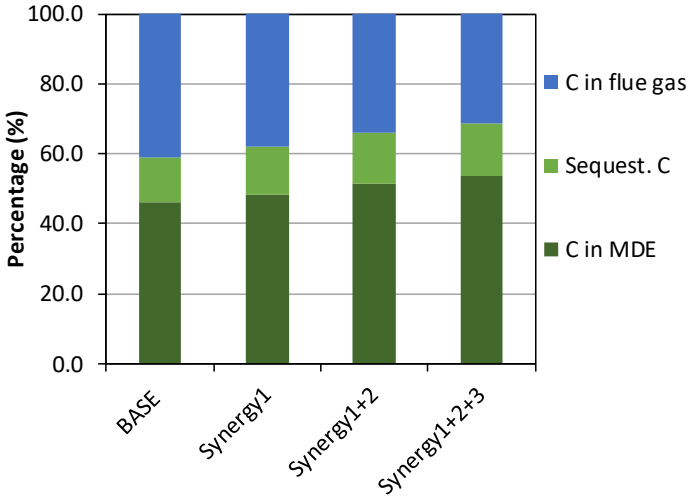

Figure 4.28: Carbon balance of the different strategies studied for the integration of biogas SESR and SEDMES for bio-DME production.

4.5.2. Conclusions on the integration of biogas SESR and SEDMES for the production of bio-DME

The conclusions on the integration of biogas SESR and SEDMES for the production of bio-DME as hydrogen carrier are as follows:

- The results of this study demonstrate that it is possible to convert biogas to DME efficiently with a net zero approach.

- Three synergies between the two processes were exploited to increase the global CGE to a value of 74% compared to approximately 64% before the integration.

- The overall yield of the process was improved from 39% to 45% due to the integration of both process with the different strategies studied.

- The carbon balance was also improved during the integration of biogas SESR and SEDMES and more carbon ended up in the DME when all the synergies were included in the design. Carbon in the DME increased from 46% to 53.5%.

Chapter 5

CONCLUSIONS

The work presented in this thesis dissertation results from three published papers and two international collaborations.

In relation to the experimental work on the effect of biogas composition, it can be concluded that:

- The production of renewable H_2 by the sorption enhanced steam reforming (SESR) of biogas has been demonstrated both thermodynamic and experimentally.

- High-purity (98.4 vol.%) and high-yield (91%) hydrogen can be obtained by SESR of biogas (CH_4+CO_2) on a Pd/Ni-Co catalyst and using Arctic dolomite as carbon dioxide sorbent.

- The catalyst did not deactivate due to H_2S poisoning during cyclic SESR of biogas for H_2S concentrations of 150 and 350 ppm at 600 ^oC. However, a H_2S concentration of 1000 ppm slightly reduced H_2 yield (between 4.5% and 10.8% points) and H_2 purity (between 2 vol.% and 3 vol.% points).

- Nevertheless, catalyst deactivation during cyclic SESR was notably lower than that usually detected in conventional steam reforming processes, which suggests that, together with the use of a bimetallic catalyst containing Co, the presence of a sorbent that can react with sulphur compounds could make the SESR process more resistant to H_2S.

In relation to the process simulations of H_2 production by SESR of biogas, it was found that:

- A flowsheet configuration that includes regeneration using biogas as fuel and a PSA for the purification of the H_2 can produce ~100% H_2 purity at 675 ^oC, 5 bar, and S/CH_4 = 5, with a CGE of 77.3% and zero carbon emissions if air-fired calciner is applied. However, negative emissions and ~100% CO_2 captured are feasible if regeneration is performed in an oxy-fuel combustion atmosphere. Partial negative emission can be also achieved if the air combustion is performed in an external burner.

- In an optimised biogas SESR process, higher efficiency is obtained in the case of direct oxy-combustion in the calciner (80.2%) than in indirect air combustion (74.1%). The main reason is the higher amount of fuel needed for the indirect combustion due to the necessity of higher temperature in the external burner than in the calciner to boost the heat transfer between the units.

Regarding the techno-economic analysis comparing biogas and natural gas SESR, the following should be highlighted:

- The lowest levelised cost of hydrogen (LCOH) is obtained when using natural gas (2.6 €/kg H_2 including CO_2 storage), but this is also the only case with CO_2 emissions (2.8 kgCO_2/kg H_2).

- Among the biogas cases, the lowest LCOH corresponds to the case with indirect air combustion in an external burner (2.8 €/kg H_2 with CO_2 storage). When switching natural gas to biogas (in the indirectly heated calciner) the LCOH increases by just 0.2 €/kg H_2, suggesting that biogas could be a potential substitute for natural gas and economically competitive.

Finally, from the integration of biogas SESR and DME production by SEDMES, it can be concluded that:

- It is possible to convert biogas into DME in an efficient way with a net zero approach through the integration of biogas SESR and SEDMES technologies. Exploiting the synergies between the two processes it was possible to increase the global CGE to the value of 74% starting at 63.8%.

- The carbon balance was also improved during the integration, meaning that more carbon ended in the DME when the synergies were considered in the design. The carbon that ended in the DME increased from 46% to 53.5%.

CONCLUSIONES

El trabajo presentado en esta tesis doctoral se deriva de tres artículos publicados y dos colaboraciones internacionales.

En relación con el trabajo experimental sobre el efecto de la composición del biogás, se puede concluir lo siguiente:

- Se ha demostrado tanto termodinámicamente como experimentalmente la producción de H_2 renovable mediante el proceso de reformado mejorado con captura in situ de CO_2 (SESR) de biogás.
- Es posible obtener hidrógeno de alta pureza (98.4% vol.) y alto rendimiento (91%) mediante SESR de biogás (CH_4+CO_2) utilizando un catalizador de Pd/Ni-Co y dolomía ártica como sorbente de CO_2.
- El catalizador no se desactivó por envenenamiento por H_2S durante ciclos de SESR para concentraciones de H_2S en el biogás de 150 y 350 ppm a 600 °C. Sin embargo, una concentración de H_2S de 1000 ppm redujo ligeramente el rendimiento de H_2 (entre 4.5 y 10.8%) y la pureza (entre 2 y 3% vol.).
- A pesar de ello, la desactivación del catalizador durante el proceso SESR fue notablemente menor que la generalmente detectada en procesos convencionales de reformado de vapor, lo que sugiere que, junto con el uso de un catalizador bimetálico que contiene Co, la presencia de un sorbente que pueda reaccionar con compuestos de azufre podría hacer que el proceso SESR sea más resistente al H_2S.

En relación con las simulaciones del proceso de producción de H_2 mediante SESR del biogás, se encontró que:

- Un diseño de proceso que incluye la regeneración del sorbente utilizando biogás como combustible y una unidad PSA para la purificación de H_2 puede producir ~100% de pureza de H_2 a 675 °C, 5 bares y S/CH_4 = 5, con una eficiencia CGE del 77.3% y emisiones de carbono cero si se utilizada un calcinador con combustión en aire. Sin embargo, emisiones negativas y ~100% de captura de CO_2 son factibles si la regeneración se realiza en

una atmósfera de combustión con oxígeno. También se pueden lograr emisiones parcialmente negativas si la combustión con aire se realiza en un quemador externo.

- En el proceso SESR de biogás se obtiene una eficiencia más alta en el caso de la combustión directa con oxígeno en el calcinador (80.2%) que en la combustión indirecta con aire (74.1%). Esto de debe a la mayor cantidad de combustible necesaria para la combustión indirecta debido a la necesidad de una temperatura más alta en el quemador externo que en el calcinador para aumentar la transferencia de calor entre las unidades.

Con respecto al análisis tecno-económico que compara SESR de biogás y gas natural, se concluye lo siguiente:

- El menor coste de hidrógeno (LCOH) se obtiene al utilizar gas natural (2.6 €/kg H_2, incluido el almacenamiento de CO_2), pero éste es también el único caso que presenta emisiones de CO_2 (2.8 kgCO_2/kg H_2).
- Cuando se utiliza biogás, el LCOH más bajo corresponde al caso de combustión indirecta con aire en un quemador externo (2.8 €/kg H_2 con almacenamiento de CO_2). Al cambiar de gas natural a biogás (en el calcinador calentado indirectamente), el LCOH aumenta solo 0.2 €/kg H_2, lo que sugiere que el biogás podría ser un potencial sustituto del gas natural económicamente competitivo.

Finalmente, en la integración de SESR de biogás y la producción de DME mediante SEDMES, se puede concluir que:

- Es posible convertir el biogás en DME de manera eficiente con un enfoque de emisiones netas cero mediante la integración de las tecnologías SESR de biogás y SEDMES. Explotando las sinergias entre los dos procesos, es posible aumentar la eficiencia energética hasta 74% partiendo de 63.8%.
- El balance de carbono también mejoró durante esta integración, lo que significa que una mayor cantidad de carbono terminó en el DME cuando se consideraron las sinergias en el diseño. El carbono que acabó en el DME aumentó del 46% al 53.5%.

REFERENCES

[1] D. Lee, H. Nam, M. Won Seo, S. Hoon Lee, D. Tokmurzin, S. Wang, Y.K. Park, Recent progress in the catalytic thermochemical conversion process of biomass for biofuels, Chem. Eng. J. 447 (2022) 137501. https://doi.org/10.1016/j.cej.2022.137501.

[2] UNFCCC, United Nations Framework on Climate Change Kyoto Protocol, Conf. Parties. (1997) 1–24.

[3] World Meteorological Organization, WMO Greenhouse Gas Bulletin (GHG Bulletin) - No. 17, WMO Greenh. Gas Bull. 17 (2021) 1–10. https://library.wmo.int/doc_num.php?explnum_id=10904.

[4] A.N. Antzaras, A.A. Lemonidou, Recent advances on materials and processes for intensified production of blue hydrogen, Renew. Sustain. Energy Rev. 155 (2022). https://doi.org/10.1016/j.rser.2021.111917.

[5] C.D. Keeling, Ralph F; Keeling, Atmospheric Monthly In Situ CO2 Data., Mauna Loa Obs. Hawaii (Archive 2023-06-04).In Scripps CO2 Progr. Data. UC San Diego Libr. Digit. Collect. Https//Doi.Org/10.6075/J08W3BHW. (2017).

[6] MITECO - Ministerio para la Transición Ecológica, Guía para el cálculo de la huella de carbono y para la elaboración de un plan de mejora de una organización, (2019). https://www.miteco.gob.es/es/cambio-climatico/temas/mitigacion-politicas-y-medidas/guia_huella_carbono_tcm30-479093.pdf.

[7] H. Ritchie, Sector by sector: where do global greenhouse gas emissions come from?, Our World Data. (2020). https://ourworldindata.org/ghg-emissions-by-sector#article-licence.

[8] J. Delbeke, A. Runge-Metzger, Y. Slingenberg, J. Werksman, The paris agreement, Towar. a Clim. Eur. Curbing Trend. (2019) 24–45. https://doi.org/10.4324/9789276082569-2.

[9] European Commission, European Climate Law, Off. J. Eur. Union. 2021 (2021) 17. https://eur-lex.europa.eu/legal-content/EN/TXT/?uri=CELEX:32021R1119.

[10] International Energy Agency, Net Zero by 2050: A Roadmap for the Global Energy Sector, (2021) 70. https://www.iea.org/reports/net-zero-by-2050.

[11] International Energy Agency, Energy Technology Perspectives 2020 -

Special Report on Carbon Capture Utilisation and Storage, Energy Technol. Perspect. 2020 - Spec. Rep. Carbon Capture Util. Storage. (2020). https://doi.org/10.1787/208b66f4-en.

[12] A. Dubey, A. Arora, Advancements in carbon capture technologies: A review, J. Clean. Prod. 373 (2022) 133932. https://doi.org/10.1016/j.jclepro.2022.133932.

[13] A. Mukherjee, J.A. Okolie, A. Abdelrasoul, C. Niu, A.K. Dalai, Review of post-combustion carbon dioxide capture technologies using activated carbon, J. Environ. Sci. 83 (2019) 46–63. https://doi.org/10.1016/j.jes.2019.03.014.

[14] S. Kammerer, I. Borho, J. Jung, M.S. Schmidt, Review: CO2 capturing methods of the last two decades, Int. J. Environ. Sci. Technol. 20 (2023) 8087–8104. https://doi.org/10.1007/s13762-022-04680-0.

[15] C.C. et al. J.C. Abanades, R.M. Alonso, B. Arias, Captura de CO2: tecnologías para cumplir el Acuerdo de París, 2019. https://pteco2.es/documentos/captura-de-co2-tecnologias-para-cumplir-el-acuerdo-de-paris/.

[16] X. Wang, F. Zhang, L. Li, H. Zhang, S. Deng, Carbon dioxide capture and storage, Int. Panel Clim. Chang. 58 (2005) 297–348. https://doi.org/10.1016/bs.ache.2021.10.005.

[17] A. Arenillas, S. Eguilior, P. Fernández-Canteli, J. García, A. Hurtado, J.F. Mediato, R. Nita, F. Recreo, M.J. Rovira, El almacenamiento de CO2: mitigación del cambio climático, Plataforma Tecnológica Española Del CO2. (2018). https://www.pteco2.es/es/publicaciones/el-almacenamiento-de-co2:-mitigacion-del-cambio-climatico.

[18] I. Ghiat, T. Al-Ansari, A review of carbon capture and utilisation as a CO2abatement opportunity within the EWF nexus, J. CO2 Util. 45 (2021) 101432. https://doi.org/10.1016/j.jcou.2020.101432.

[19] E. Catizzone, G. Bonura, M. Migliori, F. Frusteri, G. Giordano, CO2 recycling to dimethyl ether: State-of-the-art and perspectives, Molecules. 23 (2017) 1–28. https://doi.org/10.3390/molecules23010031.

[20] M. Shahbaz, A. AlNouss, I. Ghiat, G. Mckay, H. Mackey, S. Elkhalifa, T. Al-Ansari, A comprehensive review of biomass based thermochemical

conversion technologies integrated with CO2 capture and utilisation within BECCS networks, Resour. Conserv. Recycl. 173 (2021) 105734. https://doi.org/10.1016/j.resconrec.2021.105734.

[21] Z. Abdin, A. Zafaranloo, A. Rafiee, W. Mérida, W. Lipiński, K.R. Khalilpour, Hydrogen as an energy vector, Renew. Sustain. Energy Rev. 120 (2020). https://doi.org/10.1016/j.rser.2019.109620.

[22] J.P. Dees, W.J. Sagues, E. Woods, H.M. Goldstein, A.J. Simon, D.L. Sanchez, Leveraging the bioeconomy for carbon drawdown, Green Chem. 25 (2023) 2930–2957. https://doi.org/10.1039/d2gc02483g.

[23] S.E. Tanzer, K. Blok, A. Ramírez, Decarbonising Industry via BECCS: Promising Sectors, Challenges, and Techno-economic Limits of Negative Emissions, Curr. Sustain. Energy Reports. 8 (2021) 253–262. https://doi.org/10.1007/s40518-021-00195-3.

[24] H.K. Jeswani, D.M. Saharudin, A. Azapagic, Environmental sustainability of negative emissions technologies: A review, Sustain. Prod. Consum. 33 (2022) 608–635. https://doi.org/10.1016/j.spc.2022.06.028.

[25] O.W. Awe, Y. Zhao, A. Nzihou, D.P. Minh, O.W. Awe, Y. Zhao, A. Nzihou, D.P. Minh, N. Lyczko, A. Review, A Review of Biogas Utilisation, Purification And Upgrading Technologies, Waste and Biomass Valorization. 8 (2018) 11–12.

[26] D.G. Avraam, T.I. Halkides, D.K. Liguras, O.A. Bereketidou, M.A. Goula, An experimental and theoretical approach for the biogas steam reforming reaction, in: Int. J. Hydrogen Energy, 2010: pp. 9818–9827. https://doi.org/10.1016/j.ijhydene.2010.05.106.

[27] S.H. Kim, G. Kumar, W.H. Chen, S.K. Khanal, Renewable hydrogen production from biomass and wastes (ReBioH2-2020), Bioresour. Technol. 331 (2021). https://doi.org/10.1016/j.biortech.2021.125024.

[28] I.E. Agency, Global Hydrogen Review 2021, 2021. https://doi.org/10.1787/39351842-en.

[29] D.P. Minh, T.J. Siang, D.V.N. Vo, T.S. Phan, C. Ridart, A. Nzihou, D. Grouset, Hydrogen production from biogas reforming: An overview of steam reforming, dry reforming, dual reforming, and tri-reforming of methane, 2018. https://doi.org/10.1016/B978-0-12-811197-

0.00004-X.

[30] N. Scarlat, J.F. Dallemand, F. Fahl, Biogas: Developments and perspectives in Europe, Renew. Energy. 129 (2018) 457–472. https://doi.org/10.1016/j.renene.2018.03.006.

[31] D. Liuzzi, C. Peinado, M.A. Peña, J. Van Kampen, J. Boon, S. Rojas, Increasing dimethyl ether production from biomass-derived syngas: via sorption enhanced dimethyl ether synthesis, Sustain. Energy Fuels. 4 (2020) 5674–5681. https://doi.org/10.1039/d0se01172j.

[32] M. Fedeli, F. Negri, F. Manenti, Biogas to advanced biofuels: Techno-economic analysis of one-step dimethyl ether synthesis, J. Clean. Prod. 376 (2022) 134076. https://doi.org/10.1016/j.jclepro.2022.134076.

[33] J. Van Kampen, J. Boon, J. Vente, M. Van Sint Annaland, Sorption enhanced dimethyl ether synthesis under industrially relevant conditions: Experimental validation of pressure swing regeneration, React. Chem. Eng. 6 (2021) 244–257. https://doi.org/10.1039/d0re00431f.

[34] R.S. El-Emam, H. Özcan, Comprehensive review on the techno-economics of sustainable large-scale clean hydrogen production, J. Clean. Prod. 220 (2019) 593–609. https://doi.org/10.1016/j.jclepro.2019.01.309.

[35] V. Stenberg, V. Spallina, T. Mattisson, M. Rydén, Techno-economic analysis of H2 production processes using fluidized bed heat exchangers with steam reforming – Part 1: Oxygen carrier aided combustion, Int. J. Hydrogen Energy. 45 (2020) 6059–6081. https://doi.org/10.1016/j.ijhydene.2019.10.202.

[36] H. Zhang, Z. Sun, Y.H. Hu, Steam reforming of methane: Current states of catalyst design and process upgrading, Renew. Sustain. Energy Rev. 149 (2021). https://doi.org/10.1016/j.rser.2021.111330.

[37] J. R. Rostrup-Nielsen, Catalytic Steam Reforming, Catal. - Sci. Technol. (1984) 7–69.

[38] M.L. Heilig, United States Patent Office, 28 (1930) 131–134. https://doi.org/10.1145/178951.178972.

[39] W.B.R. E. Gorin, Method for the production of hydrogen, U.S. Pat. 3,108,857 (1963).

[40] A. Di Giuliano, K. Gallucci, Sorption enhanced steam methane reforming based on nickel and calcium looping: a review, Chem. Eng. Process. - Process Intensif. 130 (2018) 240–252. https://doi.org/10.1016/j.cep.2018.06.021.

[41] R. Cherbanski, E. Molga, Sorption-enhanced steam methane reforming (SE-SMR) – A review: Reactor types, catalyst and sorbent characterization, process modeling, Chem. Process Eng. 39 (2018) 427–448. https://doi.org/10.24425/122961.

[42] D.P. Harrison, Sorption-enhanced hydrogen production: A review, in: Ind. Eng. Chem. Res., 2008: pp. 6486–6501. https://doi.org/10.1021/ie800298z.

[43] B. Balasubramanian, A.L. Ortiz, S. Kaytakoglu, D.P. Harrison, Hydrogen from methane in a single-step process, Chem. Eng. Sci. 54 (1999) 3543–3552. https://doi.org/10.1016/S0009-2509(98)00425-4.

[44] A.L. Ortiz, D.P. Harrison, Hydrogen production using sorption-enhanced reaction, in: Ind. Eng. Chem. Res., 2001: pp. 5102–5109. https://doi.org/10.1021/ie001009c.

[45] M. V. Gil, K.R. Rout, D. Chen, Production of high pressure pure H2 by pressure swing sorption enhanced steam reforming (PS-SESR) of byproducts in biorefinery, Appl. Energy. 222 (2018) 595–607. https://doi.org/10.1016/j.apenergy.2018.03.181.

[46] V. Manovic, E.J. Anthony, Lime-based sorbents for high-temperature co2 capture-a review of sorbent modification methods, Int. J. Environ. Res. Public Health. 7 (2010) 3129–3140. https://doi.org/10.3390/ijerph7083129.

[47] M. Shokrollahi Yancheshmeh, H.R. Radfarnia, M.C. Iliuta, High temperature CO2 sorbents and their application for hydrogen production by sorption enhanced steam reforming process, Chem. Eng. J. 283 (2016) 420–444. https://doi.org/10.1016/j.cej.2015.06.060.

[48] M. Kavosh, K. Patchigolla, E.J. Anthony, J.E. Oakey, Carbonation performance of lime for cyclic CO2 capture following limestone calcination in steam/CO2 atmosphere, Appl. Energy. 131 (2014) 499–

507. https://doi.org/10.1016/j.apenergy.2014.05.020.

[49] A.M. Parvez, S. Hafner, M. Hornberger, M. Schmid, G. Scheffknecht, Sorption enhanced gasification (SEG) of biomass for tailored syngas production with in-situ CO2 capture: Current status, process scale-up experiences and outlook, Renew. Sustain. Energy Rev. 141 (2021). https://doi.org/10.1016/j.rser.2021.110756.

[50] M.T. Dunstan, F. Donat, A.H. Bork, C.P. Grey, C.R. Müller, CO2Capture at Medium to High Temperature Using Solid Oxide-Based Sorbents: Fundamental Aspects, Mechanistic Insights, and Recent Advances, Chem. Rev. 121 (2021) 12681–12745. https://doi.org/10.1021/acs.chemrev.1c00100.

[51] A.I. Lysikov, A.N. Salanov, A.G. Okunev, Change of CO2 carrying capacity of CaO in isothermal recarbonation-decomposition cycles, Ind. Eng. Chem. Res. 46 (2007) 4633–4638. https://doi.org/10.1021/ie0702328.

[52] G.S. Grasa, J.C. Abanades, CO2 capture capacity of CaO in long series of carbonation/calcination cycles, Ind. Eng. Chem. Res. 45 (2006) 8846–8851. https://doi.org/10.1021/ie0606946.

[53] J.M. Valverde, P.E. Sanchez-Jimenez, L.A. Perez-Maqueda, Ca-looping for postcombustion CO2 capture: A comparative analysis on the performances of dolomite and limestone, Appl. Energy. 138 (2015) 202–215. https://doi.org/10.1016/j.apenergy.2014.10.087.

[54] L. He, H. Berntsen, De Chen, Approaching sustainable H2 production: Sorption enhanced steam reforming of ethanol, J. Phys. Chem. A. 114 (2010) 3834–3844. https://doi.org/10.1021/jp906146y.

[55] A. De La Calle Martos, J.M. Valverde, P.E. Sanchez-Jimenez, A. Perejón, C. García-Garrido, L.A. Perez-Maqueda, Effect of dolomite decomposition under CO2 on its multicycle CO2 capture behaviour under calcium looping conditions, Phys. Chem. Chem. Phys. 18 (2016) 16325–16336. https://doi.org/10.1039/c6cp01149g.

[56] K. Phuakpunk, B. Chalermsinsuwan, S. Putivisutisak, S. Assabumrungrat, Simulations of sorbent regeneration in a circulating fluidized bed system for sorption enhanced steam reforming with dolomite, Particuology. 50 (2020) 156–172.

https://doi.org/10.1016/j.partic.2019.08.005.

[57] S. Wang, S.A. Nabavi, P.T. Clough, A review on bi/polymetallic catalysts for steam methane reforming, Int. J. Hydrogen Energy. 48 (2023) 15879–15893. https://doi.org/10.1016/j.ijhydene.2023.01.034.

[58] J.G. Jakobsen, Noble metal catalysts for methane steam reforming, Dep. Phys. PhD (2010) 119. https://backend.orbit.dtu.dk/ws/portalfiles/portal/5126159/thesis_vers_final-JonGeestJakobsen.pdf.

[59] S. Masoudi Soltani, A. Lahiri, H. Bahzad, P. Clough, M. Gorbounov, Y. Yan, Sorption-enhanced Steam Methane Reforming for Combined CO2 Capture and Hydrogen Production: A State-of-the-Art Review, Carbon Capture Sci. Technol. 1 (2021) 100003. https://doi.org/10.1016/j.ccst.2021.100003.

[60] J. Xu, W. Zhou, Z. Li, J. Wang, J. Ma, Biogas reforming for hydrogen production over nickel and cobalt bimetallic catalysts, Int. J. Hydrogen Energy. 34 (2009) 6646–6654. https://doi.org/10.1016/j.ijhydene.2009.06.038.

[61] B.W.L. Jang, R. Gläser, M. Dong, C.J. Liu, Towards efficient hydrogen production from glycerol by sorption enhanced steam reforming, Energy Environ. Sci. 3 (2010) 253. https://doi.org/10.1039/b922355j.

[62] L. He, H. Berntsen, E. Ochoa-Fernández, J.C. Walmsley, E.A. Blekkan, D. Chen, Co-Ni catalysts derived from hydrotalcite-like materials for hydrogen production by ethanol steam reforming, Top. Catal. 52 (2009) 206–217. https://doi.org/10.1007/s11244-008-9157-1.

[63] J. Fermoso, M. V. Gil, F. Rubiera, D. Chen, Multifunctional Pd/Ni-Co catalyst for hydrogen production by chemical looping coupled with steam reforming of acetic acid, ChemSusChem. 7 (2014) 3063–3077. https://doi.org/10.1002/cssc.201402675.

[64] M. V. Gil, J. Fermoso, C. Pevida, D. Chen, F. Rubiera, Production of fuel-cell grade H2 by sorption enhanced steam reforming of acetic acid as a model compound of biomass-derived bio-oil, Appl. Catal. B Environ. 184 (2016) 64–76. https://doi.org/10.1016/j.apcatb.2015.11.028.

[65] T. Noor, M. V. Gil, D. Chen, Production of fuel-cell grade hydrogen by

sorption enhanced water gas shift reaction using Pd/Ni-Co catalysts, Appl. Catal. B Environ. 150–151 (2014) 585–595. https://doi.org/10.1016/j.apcatb.2014.01.002.

[66] G. Esteban-Díez, M. V. Gil, C. Pevida, D. Chen, F. Rubiera, Effect of operating conditions on the sorption enhanced steam reforming of blends of acetic acid and acetone as bio-oil model compounds, Appl. Energy. 177 (2016) 579–590. https://doi.org/10.1016/j.apenergy.2016.05.149.

[67] M. V. Gil, J. Fermoso, F. Rubiera, D. Chen, H2 production by sorption enhanced steam reforming of biomass-derived bio-oil in a fluidized bed reactor: An assessment of the effect of operation variables using response surface methodology, Catal. Today. 242 (2015) 19–34. https://doi.org/10.1016/j.cattod.2014.04.018.

[68] L. He, D. Chen, Single-stage production of highly concentrated hydrogen from biomass-derived syngas, ChemSusChem. 3 (2010) 1169–1171. https://doi.org/10.1002/cssc.201000167.

[69] R. García, M. V. Gil, F. Rubiera, D. Chen, C. Pevida, Renewable hydrogen production from biogas by sorption enhanced steam reforming (SESR): A parametric study, Energy. 218 (2021) 119491. https://doi.org/10.1016/j.energy.2020.119491.

[70] J. Fermoso, L. He, D. Chen, Sorption enhanced steam reforming (SESR): A direct route towards efficient hydrogen production from biomass-derived compounds, J. Chem. Technol. Biotechnol. 87 (2012) 1367–1374. https://doi.org/10.1002/jctb.3857.

[71] Z. Yong, V. Mata, A.E. Rodrigues, Adsorption of carbon dioxide at high temperature - A review, Sep. Purif. Technol. 26 (2002) 195–205. https://doi.org/10.1016/S1383-5866(01)00165-4.

[72] J. Ashok, Y. Kathiraser, M.L. Ang, S. Kawi, Bi-functional hydrotalcite-derived NiO-CaO-Al2O3 catalysts for steam reforming of biomass and/or tar model compound at low steam-to-carbon conditions, Appl. Catal. B Environ. 172–173 (2015) 116–128. https://doi.org/10.1016/j.apcatb.2015.02.017.

[73] R. Dębek, M. Motak, T. Grzybek, M.E. Galvez, P. Da Costa, A short review on the catalytic activity of hydrotalcite-derived materials for

dry reforming of methane, Catalysts. 7 (2017) 1–25. https://doi.org/10.3390/catal7010032.

[74] K.O. Christensen, D. Chen, R. Lødeng, A. Holmen, Effect of supports and Ni crystal size on carbon formation and sintering during steam methane reforming, Appl. Catal. A Gen. 314 (2006) 9–22. https://doi.org/10.1016/j.apcata.2006.07.028.

[75] E. Ochoa-Fernández, C. Lacalle-Vilà, K.O. Christensen, J.C. Walmsley, M. Rønning, A. Holmen, D. Chen, Ni catalysts for sorption enhanced steam methane reforming, Top. Catal. 45 (2007) 3–8. https://doi.org/10.1007/s11244-007-0231-x.

[76] H. Shen, H. Li, Z. Yang, C. Li, Magic of hydrogen spillover: Understanding and application, Green Energy Environ. 7 (2022) 1161–1198. https://doi.org/10.1016/j.gee.2022.01.013.

[77] G. Jacobs, J.A. Chaney, P.M. Patterson, T.K. Das, B.H. Davis, Fischer-Tropsch synthesis: Study of the promotion of Re on the reduction property of Co/Al2O3 catalysts by in situ EXAFS/XANES of Co K and Re LIII edges and XPS, Appl. Catal. A Gen. 264 (2004) 203–212. https://doi.org/10.1016/j.apcata.2003.12.049.

[78] A. Di Giuliano, K. Gallucci, S.S. Kazi, F. Giancaterino, A. Di Carlo, C. Courson, J. Meyer, L. Di Felice, Development of Ni- and CaO-based mono- and bi-functional catalyst and sorbent materials for Sorption Enhanced Steam Methane Reforming: Performance over 200 cycles and attrition tests, Fuel Process. Technol. 195 (2019) 106160. https://doi.org/10.1016/j.fuproc.2019.106160.

[79] A. Di Giuliano, K. Gallucci, P.U. Foscolo, C. Courson, Effect of Ni precursor salts on Ni-mayenite catalysts for steam methane reforming and on Ni-CaO-mayenite materials for sorption enhanced steam methane reforming, Int. J. Hydrogen Energy. 44 (2019) 6461–6480. https://doi.org/10.1016/j.ijhydene.2019.01.131.

[80] M. Aissaoui, O.A. Zadeh Sahraei, M.S. Yancheshmeh, M.C. Iliuta, Development of a Fe/Mg-bearing metallurgical waste stabilized-CaO/NiO hybrid sorbent-catalyst for high purity H2 production through sorption-enhanced glycerol steam reforming, Int. J. Hydrogen Energy. 45 (2020) 18452–18465. https://doi.org/10.1016/j.ijhydene.2019.08.216.

[81] Y. Wang, M.Z. Memon, M.A. Seelro, W. Fu, Y. Gao, Y. Dong, G. Ji, A

review of CO2 sorbents for promoting hydrogen production in the sorption-enhanced steam reforming process, Int. J. Hydrogen Energy. 46 (2021) 23358–23379. https://doi.org/10.1016/j.ijhydene.2021.01.206.

[82] C. Dang, J. Long, H. Li, W. Cai, H. Yu, Pd-promoted Ni-Ca-Al bi-functional catalyst for integrated sorption-enhanced steam reforming of glycerol and methane reforming of carbonate, Chem. Eng. Sci. 230 (2021). https://doi.org/10.1016/j.ces.2020.116226.

[83] M. Broda, A.M. Kierzkowska, D. Baudouin, Q. Imtiaz, C. Copéret, C.R. Müller, Sorbent-enhanced methane reforming over a Ni-Ca-based, bifunctional catalyst sorbent, ACS Catal. 2 (2012) 1635–1646. https://doi.org/10.1021/cs300247g.

[84] X. Chen, L. Yang, Z. Zhou, Z. Cheng, Core-shell structured CaO-Ca9Al6O18@Ca5Al6O14/Ni bifunctional material for sorption-enhanced steam methane reforming, Chem. Eng. Sci. 163 (2017) 114–122. https://doi.org/10.1016/j.ces.2017.01.036.

[85] R. Aniruddha, S.A. Singh, B.M. Reddy, I. Sreedhar, Sorption enhanced reforming: A potential route to produce pure H2 with in-situ carbon capture, Fuel. 351 (2023) 128925. https://doi.org/10.1016/j.fuel.2023.128925.

[86] J. Wang, Y. Wang, H.A. Jakobsen, The modeling of circulating fluidized bed reactors for SE-SMR process and sorbent regeneration, Chem. Eng. Sci. 108 (2014) 57–65. https://doi.org/10.1016/j.ces.2013.12.012.

[87] J.P. Jakobsen, E. Halmøy, Reactor modeling of sorption enhanced steam methane reforming, Energy Procedia. 1 (2009) 725–732. https://doi.org/10.1016/j.egypro.2009.01.096.

[88] G. Diglio, D.P. Hanak, P. Bareschino, F. Pepe, F. Montagnaro, V. Manovic, Modelling of sorption-enhanced steam methane reforming in a fixed bed reactor network integrated with fuel cell, Appl. Energy. 210 (2018) 1–15. https://doi.org/10.1016/j.apenergy.2017.10.101.

[89] Y.J. Wu, P. Li, J.G. Yu, A.F. Cunha, A.E. Rodrigues, Progress on sorption-enhanced reaction process for hydrogen production, Rev. Chem. Eng. 32 (2016) 271–303. https://doi.org/10.1515/revce-2015-0043.

[90] A.N. Antzaras, A.A. Lemonidou, Recent advances on materials and processes for intensified production of blue hydrogen, Renew. Sustain. Energy Rev. 155 (2022) 111917. https://doi.org/10.1016/j.rser.2021.111917.

[91] S. Masoudi Soltani, A. Lahiri, H. Bahzad, P. Clough, M. Gorbounov, Y. Yan, Sorption-enhanced Steam Methane Reforming for Combined CO2 Capture and Hydrogen Production: A State-of-the-Art Review, Carbon Capture Sci. Technol. 1 (2021) 100003. https://doi.org/10.1016/j.ccst.2021.100003.

[92] J. Boon, Sorption-enhanced reactions as enablers for CO2 capture and utilisation, Curr. Opin. Chem. Eng. 40 (2023) 100919. https://doi.org/10.1016/j.coche.2023.100919.

[93] K.D. Dewoolkar, P.D. Vaidya, Tailored hydrotalcite-based hybrid materials for hydrogen production via sorption-enhanced steam reforming of ethanol, Int. J. Hydrogen Energy. 41 (2016) 6094–6106. https://doi.org/10.1016/j.ijhydene.2015.10.034.

[94] C. Dang, H. Yu, H. Wang, F. Peng, Y. Yang, A bi-functional Co-CaO-Ca12Al14O33 catalyst for sorption-enhanced steam reforming of glycerol to high-purity hydrogen, Chem. Eng. J. 286 (2016) 329–338. https://doi.org/10.1016/j.cej.2015.10.073.

[95] J. Fermoso, L. He, D. Chen, Production of high purity hydrogen by sorption enhanced steam reforming of crude glycerol, Int. J. Hydrogen Energy. 37 (2012) 14047–14054. https://doi.org/10.1016/j.ijhydene.2012.07.084.

[96] S. Assabumrungrat, P. Sonthisanga, W. Kiatkittipong, N. Laosiripojana, A. Arpornwichanop, A. Soottitantawat, W. Wiyaratn, P. Praserthdam, Thermodynamic analysis of calcium oxide assisted hydrogen production from biogas, J. Ind. Eng. Chem. 16 (2010) 785–789. https://doi.org/10.1016/j.jiec.2010.07.001.

[97] D. Saebea, S. Authayanun, Y. Patcharavorachot, A. Arpornwichanop, Thermodynamic analysis of hydrogen production from the adsorption-enhanced steam reforming of biogas, in: Energy Procedia, Elsevier B.V., 2014: pp. 2254–2257. https://doi.org/10.1016/j.egypro.2014.12.120.

[98] H. Liu, Z. Yang, S. Wu, The Evaluation of Reactive Sorption Enhanced Biogas Steam Reforming Process for Hydrogen Production Using

Nano-Sized CaO Adsorbents, J. Nanosci. Nanotechnol. 19 (2019) 3244–3251. https://doi.org/10.1166/jnn.2019.16608.

[99] J. Phromprasit, J. Powell, S. Wongsakulphasatch, W. Kiatkittipong, P. Bumroongsakulsawat, S. Assabumrungrat, Activity and stability performance of multifunctional catalyst (Ni/CaO and Ni/Ca12Al14O33-CaO) for bio-hydrogen production from sorption enhanced biogas steam reforming, Int. J. Hydrogen Energy. 41 (2016) 7318–7331. https://doi.org/10.1016/j.ijhydene.2016.03.125.

[100] J. Phromprasit, J. Powell, S. Wongsakulphasatch, W. Kiatkittipong, P. Bumroongsakulsawat, S. Assabumrungrat, H2 production from sorption enhanced steam reforming of biogas using multifunctional catalysts of Ni over Zr-, Ce- and La-modified CaO sorbents, Chem. Eng. J. 313 (2017) 1415–1425. https://doi.org/10.1016/j.cej.2016.11.051.

[101] J. Phromprasit, J. Powell, A. Arpornwichanop, A.E. Rodrigues, S. Assabumrungrat, Hydrogen production from sorption enhanced biogas steam reforming using nickel-based catalysts, Eng. J. 17 (2013) 19–34. https://doi.org/10.4186/ej.2013.17.4.19.

[102] J. Meyer, J. Mastin, C.S. Pinilla, Sustainable hydrogen production from biogas using sorption- enhanced reforming, Energy Procedia. 63 (2014) 6800–6814. https://doi.org/10.1016/j.egypro.2014.11.714.

[103] O. Jönsson, E. Polman, J.K. Jensen, R. Eklund, H. Schyl, S. Ivarsson, Sustainable gas enters the european gas distribution system, Danish Gas Technol. Cent. (2003) 1–9. http://members.igu.org/html/wgc2003/WGC_pdffiles/10042_10453 03060_28611_1.pdf.

[104] Y. Gao, J. Jiang, Y. Meng, F. Yan, A. Aihemaiti, A review of recent developments in hydrogen production via biogas dry reforming, Energy Convers. Manag. 171 (2018) 133–155. https://doi.org/10.1016/j.enconman.2018.05.083.

[105] J.R. Rostrup-Nielsen, J. Sehested, J.K. Nørskov, Hydrogen and synthesis gas by steam- and C02 reforming, Adv. Catal. 47 (2002) 65–139. https://doi.org/10.1016/s0360-0564(02)47006-x.

[106] J.R. Rostrup-Nielsen, Chemisorption of hydrogen sulfide on a supported nickel catalyst, J. Catal. 11 (1968) 220–227.

https://doi.org/10.1016/0021-9517(68)90035-3.

[107] C.H. Bartholomew, P.K. Agrawal, J.R. Katzer, Sulfur Poisoning of Metals, Adv. Catal. 31 (1982) 135–242. https://doi.org/10.1016/S0360-0564(08)60454-X.

[108] K.P. Kepp, A quantitative scale of oxophilicity and thiophilicity, Inorg. Chem. 55 (2016) 9461–9470. https://doi.org/10.1021/acs.inorgchem.6b01702.

[109] S. Das, K.H. Lim, T.Z.H. Gani, S. Aksari, S. Kawi, Bi-functional CeO2 coated NiCo-MgAl core-shell catalyst with high activity and resistance to coke and H2S poisoning in methane dry reforming, Appl. Catal. B Environ. 323 (2023) 122141. https://doi.org/10.1016/j.apcatb.2022.122141.

[110] O. Iyoha, R. Enick, R. Killmeyer, B. Morreale, The influence of hydrogen sulfide-to-hydrogen partial pressure ratio on the sulfidization of Pd and 70 mol% Pd-Cu membranes, J. Memb. Sci. 305 (2007) 77–92. https://doi.org/10.1016/j.memsci.2007.07.032.

[111] S. Appari, V.M. Janardhanan, R. Bauri, S. Jayanti, Deactivation and regeneration of Ni catalyst during steam reforming of model biogas: An experimental investigation, Int. J. Hydrogen Energy. 39 (2014) 297–304. https://doi.org/10.1016/j.ijhydene.2013.10.056.

[112] M. Ashrafi, C. Pfeifer, T. Pröll, H. Hofbauer, Experimental study of model biogas catalytic steam reforming: 2. Impact of sulfur on the deactivation and regeneration of Ni-based catalysts, Energy and Fuels. 22 (2008) 4190–4195. https://doi.org/10.1021/ef8000828.

[113] V. Chiodo, S. Maisano, G. Zafarana, F. Urbani, Effect of pollutants on biogas steam reforming, Int. J. Hydrogen Energy. 42 (2017) 1622–1628. https://doi.org/10.1016/j.ijhydene.2016.07.251.

[114] X. Chen, J. Jiang, F. Yan, K. Li, S. Tian, Y. Gao, H. Zhou, Dry Reforming of Model Biogas on a Ni/SiO2 Catalyst: Overall Performance and Mechanisms of Sulfur Poisoning and Regeneration, ACS Sustain. Chem. Eng. 5 (2017) 10248–10257. https://doi.org/10.1021/acssuschemeng.7b02251.

[115] B. Saha, A. Khan, H. Ibrahim, R. Idem, Evaluating the performance of non-precious metal based catalysts for sulfur-tolerance during the dry reforming of biogas, Fuel. 120 (2014) 202–217.

https://doi.org/10.1016/j.fuel.2013.12.016.

[116] R.Y. Chein, Y.C. Chen, W.H. Chen, Experimental study on sulfur deactivation and regeneration of ni-based catalyst in dry reforming of biogas, Catalysts. 11 (2021) 777. https://doi.org/10.3390/catal11070777.

[117] U. Izquierdo, I. García-García, Á.M. Gutierrez, J.R. Arraibi, V.L. Barrio, J.F. Cambra, P.L. Arias, Catalyst deactivation and regeneration processes in biogas tri-reforming process. The effect of hydrogen sulfide addition, Catalysts. 8 (2018). https://doi.org/10.3390/catal8010012.

[118] P. Wachter, C. Gaber, J. Raic, M. Demuth, C. Hochenauer, Experimental investigation on H2S and SO2 sulphur poisoning and regeneration of a commercially available Ni-catalyst during methane tri-reforming, Int. J. Hydrogen Energy. 46 (2021) 3437–3452. https://doi.org/10.1016/j.ijhydene.2020.10.214.

[119] D.L. Keairns, R.A. Newby, E.P. O'Neill, D.H.Archer, High Temperature Sulfur Removal System Development for the westinghouse fluidized bed coal gasification process, ACS Div. Fuel Chem. Prepr. (1976). https://www.osti.gov/biblio/7350271.

[120] J. Weldon, G.B. Haldipur, D.A. Lewandowski, K.J. Smith, Advanced coal gasification and desulfurization with calcium based sorbents, in: ACS Div. Fuel Chem. Prepr., 1986: pp. 244–252.

[121] M. Husmann, C. Zuber, V. Maitz, T. Kienberger, C. Hochenauer, Comparison of dolomite and lime as sorbents for in-situ H2S removal with respect to gasification parameters in biomass gasification, Fuel. 181 (2016) 131–138. https://doi.org/10.1016/j.fuel.2016.04.124.

[122] J. Abbasian, A. Rehmat, D. Leppin, D.D. Banerjee, Desulfurization of fuels with calcium-based sorbents, Fuel Process. Technol. 25 (1990) 1–15. https://doi.org/10.1016/0378-3820(90)90091-6.

[123] L.A. Fenouil, S. Lynn, Study of Calcium-Based Sorbents for High-Temperature H2S Removal. 2. Kinetics of H2S Sorption by Calcined Limestone, ACS, Am. Chem. Soc. (1995) 2334–2342. https://doi.org/https://doi.org/10.1021/ie00046a015.

[124] T.Y. Yeo, J. Ashok, S. Kawi, Recent developments in sulphur-resilient

catalytic systems for syngas production, Renew. Sustain. Energy Rev. 100 (2019) 52–70. https://doi.org/10.1016/j.rser.2018.10.016.

[125] D.K. Binte Mohamed, A. Veksha, Q.L.M. Ha, W.P. Chan, T.T. Lim, G. Lisak, Advanced Ni tar reforming catalysts resistant to syngas impurities: Current knowledge, research gaps and future prospects, Fuel. 318 (2022) 123602. https://doi.org/10.1016/j.fuel.2022.123602.

[126] J. Sehested, Four challenges for nickel steam-reforming catalysts, in: Catal. Today, Elsevier, 2006: pp. 103–110. https://doi.org/10.1016/j.cattod.2005.10.002.

[127] A. Capa, R. García, D. Chen, F. Rubiera, C. Pevida, M. V Gil, On the effect of biogas composition on the H2 production by sorption enhanced steam reforming (SESR), Renew. Energy. 160 (2020) 575–583. https://doi.org/10.1016/j.renene.2020.06.122.

[128] X. Tian, S. Wang, J. Zhou, Y. Xiang, F. Zhang, B. Lin, S. Liu, Z. Luo, Simulation and exergetic evaluation of hydrogen production from sorption enhanced and conventional steam reforming of acetic acid, Int. J. Hydrogen Energy. 41 (2016) 21099–21108. https://doi.org/10.1016/j.ijhydene.2016.09.184.

[129] K.F. Tzanetis, C.S. Martavaltzi, A.A. Lemonidou, Comparative exergy analysis of sorption enhanced and conventional methane steam reforming, in: Int. J. Hydrogen Energy, 2012: pp. 16308–16320. https://doi.org/10.1016/j.ijhydene.2012.02.191.

[130] S. Alam, J.P. Kumar, K.Y. Rani, C. Sumana, Self-sustained process scheme for high purity hydrogen production using sorption enhanced steam methane reforming coupled with chemical looping combustion, J. Clean. Prod. 162 (2017) 687–701. https://doi.org/10.1016/j.jclepro.2017.05.136.

[131] Y. Yan, D. Thanganadar, P.T. Clough, S. Mukherjee, K. Patchigolla, V. Manovic, E.J. Anthony, Process simulations of blue hydrogen production by upgraded sorption enhanced steam methane reforming (SE-SMR) processes, Energy Convers. Manag. 222 (2020). https://doi.org/10.1016/j.enconman.2020.113144.

[132] A. Antzara, E. Heracleous, D.B. Bukur, A.A. Lemonidou, Thermodynamic analysis of hydrogen production via chemical looping steam methane reforming coupled with in situ CO2 capture, in:

Energy Procedia, 2014: pp. 6576–6589. https://doi.org/10.1016/j.egypro.2014.11.694.

[133] A. Phuluanglue, W. Khaodee, S. Assabumrungrat, Simulation of intensified process of sorption enhanced chemical-looping reforming of methane: Comparison with conventional processes, Comput. Chem. Eng. 105 (2017) 237–245. https://doi.org/10.1016/j.compchemeng.2017.02.031.

[134] A. Ebneyamini, J.R. Grace, C.J. Lim, N. Ellis, S.S.E.H. Elnashaie, Simulation of Limestone Calcination for Calcium Looping: Potential for Autothermal and Hydrogen-Producing Sorbent Regeneration, Ind. Eng. Chem. Res. 58 (2019) 8636–8655. https://doi.org/10.1021/acs.iecr.9b00668.

[135] L. Barelli, G. Bidini, A. Corradetti, U. Desideri, Study of the carbonation-calcination reaction applied to the hydrogen production from syngas, Energy. 32 (2007) 697–710. https://doi.org/10.1016/j.energy.2006.04.016.

[136] L. Barelli, G. Bidini, A. Corradetti, U. Desideri, Production of hydrogen through the carbonation-calcination reaction applied to CH4/CO2 mixtures, Energy. 32 (2007) 834–843. https://doi.org/10.1016/j.energy.2006.06.008.

[137] G. Diglio, D.P. Hanak, P. Bareschino, E. Mancusi, F. Pepe, F. Montagnaro, V. Manovic, Techno-economic analysis of sorption-enhanced steam methane reforming in a fixed bed reactor network integrated with fuel cell, J. Power Sources. 364 (2017) 41–51. https://doi.org/10.1016/j.jpowsour.2017.08.005.

[138] Y. Yan, V. Manovic, E.J. Anthony, P.T. Clough, Techno-economic analysis of low-carbon hydrogen production by sorption enhanced steam methane reforming (SE-SMR) processes, Energy Convers. Manag. 226 (2020) 196–8904. https://doi.org/10.1016/j.enconman.2020.113530.

[139] T.N. Do, H. Kwon, M. Park, C. Kim, Y.T. Kim, J. Kim, Carbon-neutral hydrogen production from natural gas via electrified steam reforming: Techno-economic-environmental perspective, Energy Convers. Manag. 279 (2023) 116758. https://doi.org/10.1016/j.enconman.2023.116758.

[140] G. Di Marcoberardino, S. Foresti, M. Binotti, G. Manzolini, Potentiality of a biogas membrane reformer for decentralized hydrogen production, Chem. Eng. Process. - Process Intensif. 129 (2018) 131–141. https://doi.org/10.1016/j.cep.2018.04.023.

[141] S. Bock, B. Stoppacher, K. Malli, M. Lammer, V. Hacker, Techno-economic analysis of fixed-bed chemical looping for decentralized, fuel-cell-grade hydrogen production coupled with a 3 MWth biogas digester, Energy Convers. Manag. 250 (2021) 114801. https://doi.org/10.1016/j.enconman.2021.114801.

[142] I.D. Dumbrava, C.C. Cormos, Techno-economical evaluations of decarbonized hydrogen production based on direct biogas conversion using thermo-chemical looping cycles, Int. J. Hydrogen Energy. 46 (2021) 23149–23163. https://doi.org/10.1016/j.ijhydene.2021.04.142.

[143] E. Catizzone, C. Freda, G. Braccio, F. Frusteri, G. Bonura, Dimethyl ether as circular hydrogen carrier: Catalytic aspects of hydrogenation/dehydrogenation steps, J. Energy Chem. 58 (2021) 55–77. https://doi.org/10.1016/j.jechem.2020.09.040.

[144] J. Boon, J. van Kampen, R. Hoogendoorn, S. Tanase, F.P.F. van Berkel, M. van Sint Annaland, Reversible deactivation of Γ-alumina by steam in the gas-phase dehydration of methanol to dimethyl ether, Catal. Commun. 119 (2019) 22–27. https://doi.org/10.1016/j.catcom.2018.10.008.

[145] J. Van Kampen, J. Boon, J. Vente, M. Van Sint Annaland, Sorption enhanced dimethyl ether synthesis for high efficiency carbon conversion: Modelling and cycle design, J. CO2 Util. 37 (2020) 295–308. https://doi.org/10.1016/j.jcou.2019.12.021.

[146] J. van Kampen, J. Overbeek, J. Boon, M. van Sint Annaland, Continuous multi-column sorption-enhanced dimethyl ether synthesis (SEDMES): Dynamic operation, Front. Chem. Eng. 5 (2023) 1–10. https://doi.org/10.3389/fceng.2023.1055896.

[147] G. Skorikova, M. Saric, S.N. Sluijter, J. van Kampen, C. Sánchez-Martínez, J. Boon, The Techno-Economic Benefit of Sorption Enhancement: Evaluation of Sorption-Enhanced Dimethyl Ether Synthesis for CO2 Utilization, Front. Chem. Eng. 2 (2020) 1–11. https://doi.org/10.3389/fceng.2020.594884.

[148] L.P. Merkouri, H. Ahmet, T. Ramirez Reina, M.S. Duyar, The direct synthesis of dimethyl ether (DME) from landfill gas: A techno-economic investigation, Fuel. 319 (2022). https://doi.org/10.1016/j.fuel.2022.123741.

[149] J. Fermoso, F. Rubiera, D. Chen, Sorption enhanced catalytic steam gasification process: A direct route from lignocellulosic biomass to high purity hydrogen, Energy Environ. Sci. 5 (2012) 6358–6367. https://doi.org/10.1039/c2ee02593k.

[150] S. Brunauer, P.H. Emmett, E. Teller, Adsorption of gases in multimolecular layers, J. Am.Chem.Soc. 60 (1938) 309–319. https://doi.org/https://doi.org/10.1021/ja01269a023.

[151] N.H. Florin, A.T. Harris, Hydrogen production from biomass coupled with carbon dioxide capture: The implications of thermodynamic equilibrium, Int. J. Hydrogen Energy. 32 (2007) 4119–4134. https://doi.org/10.1016/j.ijhydene.2007.06.016.

[152] A. Capa, R. García, F. Rubiera, C. Pevida, M. V. Gil, Energy analysis on the effect of biogas composition in the sorption enhanced steam reforming (SESR) for green hydrogen production, Eur. Biomass Conf. Exhib. Proc. (2021) 1366–1370.

[153] P. Marín, F. V. Díez, S. Ordóñez, Reverse flow reactors as sustainable devices for performing exothermic reactions: Applications and engineering aspects, Chem. Eng. Process. - Process Intensif. 135 (2019) 175–189. https://doi.org/10.1016/j.cep.2018.11.019.

[154] V. Stenberg, M. Rydén, T. Mattisson, A. Lyngfelt, Exploring novel hydrogen production processes by integration of steam methane reforming with chemical-looping combustion (CLC-SMR) and oxygen carrier aided combustion (OCAC-SMR), Int. J. Greenh. Gas Control. 74 (2018) 28–39. https://doi.org/10.1016/j.ijggc.2018.01.008.

[155] M. Junk, M. Reitz, J. Strohle, B. Epple, Technical and economical assessment of the indirectly heated carbonate looping process, J. Energy Resour. Technol. Trans. ASME. 138 (2016) 1–8. https://doi.org/10.1115/1.4033142.

[156] D. Hoeftberger, J. Karl, The indirectly heated carbonate looping process for CO2 capture A concept with heat pipe heat exchanger, J.

Energy Resour. Technol. Trans. ASME. 138 (2016) 1–7. https://doi.org/10.1115/1.4033302.

[157] M. Reitz, M. Junk, J. Ströhle, B. Epple, Design and operation of a 300 kWth indirectly heated carbonate looping pilot plant, Int. J. Greenh. Gas Control. 54 (2016) 272–281. https://doi.org/10.1016/j.ijggc.2016.09.016.

[158] M. Rydén, P. Ramos, H 2 production with CO 2 capture by sorption enhanced chemical-looping reforming using NiO as oxygen carrier and CaO as CO 2 sorbent, Fuel Process. Technol. 96 (2012) 27–36. https://doi.org/10.1016/j.fuproc.2011.12.009.

[159] K. Johnsen, J.R. Grace, S.S.E.H. Elnashaie, L. Kolbeinsen, D. Eriksen, Modeling of sorption-enhanced steam reforming in a dual fluidized bubbling bed reactor, Ind. Eng. Chem. Res. 45 (2006) 4133–4144. https://doi.org/10.1021/ie0511736.

[160] F. Kong, J. Swift, Q. Zhang, L.S. Fan, A. Tong, Biogas to H2 conversion with CO2 capture using chemical looping technology: Process simulation and comparison to conventional reforming processes, Fuel. 279 (2020) 118479. https://doi.org/10.1016/j.fuel.2020.118479.

[161] M. Broda, V. Manovic, Q. Imtiaz, A.M. Kierzkowska, E.J. Anthony, C.R. Müller, High-purity hydrogen via the sorption-enhanced steam methane reforming reaction over a synthetic CaO-based sorbent and a Ni catalyst, Environ. Sci. Technol. 47 (2013) 6007–6014. https://doi.org/10.1021/es305113p.

[162] R.K. Sinnott, Costing and Project Evaluation, Coulson Richardson's Chem. Eng. (1993) 209–244. https://doi.org/10.1016/b978-0-08-041865-0.50014-3.

[163] S.M. Nazir, J.H. Cloete, S. Cloete, S. Amini, Pathways to low-cost clean hydrogen production with gas switching reforming, Int. J. Hydrogen Energy. 46 (2021) 20142–20158. https://doi.org/10.1016/j.ijhydene.2020.01.234.

[164] F. Pruvost, S. Cloete, C. Arnaiz del Pozo, A. Zaabout, Blue, green, and turquoise pathways for minimizing hydrogen production costs from steam methane reforming with CO2 capture, Energy Convers. Manag. 274 (2022). https://doi.org/10.1016/j.enconman.2022.116458.

[165] J. Reeve, O. Grasham, T. Mahmud, V. Dupont, Advanced Steam Reforming of Bio-Oil with Carbon Capture: A Techno-Economic and CO2 Emissions Analysis, Clean Technol. 4 (2022) 309–328. https://doi.org/10.3390/cleantechnol4020018.

[166] C. Arnaiz del Pozo, S. Cloete, Á. Jiménez Álvaro, Carbon-negative hydrogen: Exploring the techno-economic potential of biomass co-gasification with CO2 capture, Energy Convers. Manag. 247 (2021). https://doi.org/10.1016/j.enconman.2021.114712.

[167] D.A. Chisalita, C.C. Cormos, Techno-economic assessment of hydrogen production processes based on various natural gas chemical looping systems with carbon capture, Energy. 181 (2019) 331–344. https://doi.org/10.1016/j.energy.2019.05.179.

[168] E. Rubin, G. Booras, J. Davison, C. Ekstrom, M. Matuszewski, S. McCoy, C. Short, Toward a common method of cost estimation for co2 capture and storage at fossil fuel power plants, Glob. CCS Inst. (2013) 1–36. http://cdn.globalccsinstitute.com/sites/default/files/publications/85761/toward-common-method-cost-estimation-ccs-fossil-fuel-power-plants-white-paper.pdf.

[169] S. Ahmed, S.H.D. Lee, M.S. Ferrandon, Catalytic steam reforming of biogas - Effects of feed composition and operating conditions, Int. J. Hydrogen Energy. 40 (2015) 1005–1015. https://doi.org/10.1016/j.ijhydene.2014.11.009.

[170] H.J. Alves, C. Bley Junior, R.R. Niklevicz, E.P. Frigo, M.S. Frigo, C.H. Coimbra-Araújo, Overview of hydrogen production technologies from biogas and the applications in fuel cells, Int. J. Hydrogen Energy. 38 (2013) 5215–5225. https://doi.org/10.1016/j.ijhydene.2013.02.057.

[171] T. Zheng, M. Li, D. Mei, J. Ma, B. Wang, Z. Xu, Effect of H2S presence on chemical looping reforming (CLR) of biogas with a firebrick supported NiO oxygen carrier, Fuel Process. Technol. 226 (2022). https://doi.org/10.1016/j.fuproc.2021.107088.

[172] F. Dashtestani, M. Nusheh, V. Siriwongrungson, J. Hongrapipat, V. Materic, S. Pang, Effect of H2S and NH3 in biomass gasification producer gas on CO2 capture performance of an innovative CaO and Fe2O3 based sorbent, Fuel. 295 (2021).

https://doi.org/10.1016/j.fuel.2021.120586.

[173] I. Martínez, M.S. Callén, G. Grasa, J.M. López, R. Murillo, Sorption-enhanced gasification (SEG) of agroforestry residues: Influence of feedstock and main operating variables on product gas quality, Fuel Process. Technol. 226 (2022) 378–3820. https://doi.org/10.1016/j.fuproc.2021.107074.

[174] J.H. Wang, M. Liu, Computational study of sulfur-nickel interactions: A new S-Ni phase diagram, Electrochem. Commun. 9 (2007) 2212–2217. https://doi.org/10.1016/j.elecom.2007.06.022.

[175] J. Wang, J. Guo, R. Parnas, B. Liang, Calcium-based regenerable sorbents for high temperature H2S removal, Fuel. 154 (2015) 17–23. https://doi.org/10.1016/j.fuel.2015.02.105.

[176] Y. Hu, S. Wu, Y. Li, J. Zhao, S. Lu, H2S removal performance of Ca3Al2O6-stabilized carbide slag from CO2 capture cycles using calcium looping, Fuel Process. Technol. 218 (2021). https://doi.org/10.1016/j.fuproc.2021.106845.

[177] B. Guan, Y. Li, B. Yin, K. Liu, D. Wang, H. Zhang, C. Cheng, Synthesis of hierarchical NiS microflowers for high performance asymmetric supercapacitor, Chem. Eng. J. 308 (2017) 1165–1173. https://doi.org/10.1016/j.cej.2016.10.016.

[178] K. Taira, T. Sugiyama, H. Einaga, K. Nakao, K. Suzuki, Promoting effect of 2000 ppm H2S on the dry reforming reaction of CH4 over pure CeO2, and in situ observation of the behavior of sulfur during the reaction, J. Catal. 389 (2020) 611–622. https://doi.org/10.1016/j.jcat.2020.06.040.

[179] C. Dueso, M.T. Izquierdo, F. García-Labiano, L.F. de Diego, A. Abad, P. Gayán, J. Adánez, Effect of H2S on the behaviour of an impregnated NiO-based oxygen-carrier for chemical-looping combustion (CLC), Appl. Catal. B Environ. 126 (2012) 186–199. https://doi.org/10.1016/j.apcatb.2012.07.011.

[180] T. Fan, L. Dou, H. Zhang, Nonprecious mixed oxide catalysts Co3AlO and Co2NiAlO derived from nanoflowerlike cobalt-based hydrotalcites for highly efficient oxidation of nitric oxide, RSC Adv. 6 (2016) 110274–110287. https://doi.org/10.1039/c6ra23704e.

[181] J. Ashok, S. Das, N. Dewangan, S. Kawi, Steam reforming of surrogate

diesel model over hydrotalcite-derived MO-CaO-Al2O3 (M = Ni & Co) catalysts for SOFC applications, Fuel. 291 (2021) 120194. https://doi.org/10.1016/j.fuel.2021.120194.

[182] S.O. Grim, W.E. Swartz, L.J. Matienzo, I. Yin, X-Ray Photoelectron Spectroscopy of Nickel Compounds, Inorg. Chem. 12 (1973) 2762–2769. https://doi.org/10.1021/ic50130a005.

[183] J. Ashok, S. Das, N. Dewangan, S. Kawi, H2S and NOx tolerance capability of CeO2 doped La1−xCexCo0.5Ti0.5O3−Δ perovskites for steam reforming of biomass tar model reaction, Energy Convers. Manag. X. 1 (2019) 100003. https://doi.org/10.1016/j.ecmx.2019.100003.

[184] Z. Ferencz, E. Varga, R. Puskás, Z. Kónya, K. Baán, A. Oszkó, A. Erdőhelyi, Reforming of ethanol on Co/Al2O3 catalysts reduced at different temperatures, J. Catal. 358 (2018) 118–130. https://doi.org/10.1016/j.jcat.2017.12.003.

[185] L. Li, C. Howard, D.L. King, M. Gerber, R. Dagle, D. Stevens, Regeneration of sulfur deactivated Ni-based biomass syngas cleaning catalysts, Ind. Eng. Chem. Res. 49 (2010) 10144–10148. https://doi.org/10.1021/ie101032x.

[186] F. García-Labiano, L.F. De Diego, P. Gayán, J. Adánez, A. Abad, C. Dueso, Effect of fuel gas composition in chemical-looping combustion with ni-based oxygen carriers. 1. Fate of sulfur, Ind. Eng. Chem. Res. 48 (2009) 2499–2508. https://doi.org/10.1021/ie801332z.

[187] X. Meng, W. De Jong, R. Pal, A.H.M. Verkooijen, In bed and downstream hot gas desulphurization during solid fuel gasification: A review, Fuel Process. Technol. 91 (2010) 964–981. https://doi.org/10.1016/j.fuproc.2010.02.005.

[188] V. Pawar, S. Appari, D.S. Monder, V.M. Janardhanan, Study of the Combined Deactivation Due to Sulfur Poisoning and Carbon Deposition during Biogas Dry Reforming on Supported Ni Catalyst, Ind. Eng. Chem. Res. 56 (2017) 8448–8455. https://doi.org/10.1021/acs.iecr.7b01662.

[189] S. Appari, V.M. Janardhanan, R. Bauri, S. Jayanti, O. Deutschmann, A detailed kinetic model for biogas steam reforming on Ni and catalyst

deactivation due to sulfur poisoning, Appl. Catal. A Gen. 471 (2014) 118–125. https://doi.org/10.1016/j.apcata.2013.12.002.

[190] C. Jiang, E. Loisel, D.A. Cullen, J.A. Dorman, K.M. Dooley, On the enhanced sulfur and coking tolerance of Ni-Co-rare earth oxide catalysts for the dry reforming of methane, J. Catal. 393 (2021) 215–229. https://doi.org/10.1016/j.jcat.2020.11.028.

[191] E.J. Anthony, E.M. Bulewicz, L. Jia, Reactivation of limestone sorbents in FBC for SO2 capture, Prog. Energy Combust. Sci. 33 (2007) 171–210. https://doi.org/10.1016/j.pecs.2006.10.001.

[192] S. Rodríguez, A. Capa, R. García, D. Chen, F. Rubiera, C. Pevida, M. V. Gil, Blends of bio-oil/biogas model compounds for high-purity H2 production by sorption enhanced steam reforming (SESR): Experimental study and energy analysis, Chem. Eng. J. 432 (2022). https://doi.org/10.1016/j.cej.2021.134396.

[193] R. Habibi, F. Pourfayaz, M. Mehrpooya, H. Kamali, A natural gas-based eco-friendly polygeneration system including gas turbine, sorption-enhanced steam methane reforming, absorption chiller and flue gas CO2 capture unit, Sustain. Energy Technol. Assessments. 52 (2022) 101984. https://doi.org/10.1016/j.seta.2022.101984.

[194] L. Zhu, L. Li, J. Fan, A modified process for overcoming the drawbacks of conventional steam methane reforming for hydrogen production: Thermodynamic investigation, Chem. Eng. Res. Des. 104 (2015) 792–806. https://doi.org/10.1016/j.cherd.2015.10.022.

[195] A. Ebneyamini, J.R. Grace, C.J. Lim, N. Ellis, Simulation of Sorbent-Enhanced Steam Methane Reforming and Limestone Calcination in Dual Turbulent Fluidized Bed Reactors, Energy and Fuels. 34 (2020) 7743–7755. https://doi.org/10.1021/acs.energyfuels.0c01093.

[196] M. Minutillo, A. Perna, A. Sorce, Green hydrogen production plants via biogas steam and autothermal reforming processes: energy and exergy analyses, Appl. Energy. 277 (2020). https://doi.org/10.1016/j.apenergy.2020.115452.

[197] S. Ma, G. Loreti, L. Wang, F. Maréchal, J. Van herle, C. Dong, Comparison and optimization of different fuel processing options for biogas-fed solid-oxide fuel cell plants, Int. J. Hydrogen Energy. 47 (2022) 551–564. https://doi.org/10.1016/j.ijhydene.2021.10.025.

[198] N. et. a. Montenegro Camacho, Y. S., Bensaid, S., Lorentzou, S., Vlachos, Development of a robust and efficient biogas processor for hydrogen production. Part 2: Experimental campaign, Int. J. Hydrogen Energy. 43 (2018) 161–177. https://doi.org/10.1016/j.ijhydene.2017.10.177.

[199] A. Hajizadeh, M. Mohamadi-Baghmolaei, N.M. Cata Saady, S. Zendehboudi, Hydrogen production from biomass through integration of anaerobic digestion and biogas dry reforming, Appl. Energy. 309 (2022). https://doi.org/10.1016/j.apenergy.2021.118442.

[200] C.C. Cormos, A.M. Cormos, L. Petrescu, S. Dragan, Techno-economic assessment of decarbonized biogas catalytic reforming for flexible hydrogen and power production, Appl. Therm. Eng. 207 (2022) 118218. https://doi.org/10.1016/j.applthermaleng.2022.118218.

[201] G. Di Marcoberardino, D. Vitali, F. Spinelli, M. Binotti, G. Manzolini, Green hydrogen production from raw biogas: A techno-economic investigation of conventional processes using pressure swing adsorption unit, Processes. 6 (2018). https://doi.org/10.3390/pr6030019.

[202] B. Aghel, S. Behaein, F. Alobiad, CO2 capture from biogas by biomass-based adsorbents: A review, Fuel. 328 (2022) 125276. https://doi.org/10.1016/j.fuel.2022.125276.

[203] F. Denys, W. de Vries, Gas Composition Transition Agency Report, Gas Compos. Transit. Agency Assen. Netherlands. (2013) 1–18.

[204] A. Cabello, T. Mendiara, A. Abad, J. Adánez, Techno-economic analysis of a chemical looping combustion process for biogas generated from livestock farming and agro-industrial waste, Energy Convers. Manag. 267 (2022) 115865. https://doi.org/10.1016/j.enconman.2022.115865.

[205] C. Maxwell, Cost Indices – Towering Skills, 2021 Towering Ski. LLC. (2021). https://www.toweringskills.com/financial-analysis/cost-indices/#chemical-engineering-plant-cost-index-cepci.

[206] Department of Labor's Bureau of Labor Statistics, Chemical Engineering Plant Cost Index, (2011).

https://es.scribd.com/doc/111518047/cepci-2011-py#.

[207] Statista, EU hourly labor cost by country, Statista.Com. (2021). https://www.statista.com/statistics/1211601/hourly-labor-cost-in-europe.

[208] Eurostat, Natural gas price statistics, Eur. Comm. (2022) 1–12. https://ec.europa.eu/eurostat/statistics-explained/index.php?title=Natural_gas_price_statistics.

[209] EBA, Decarbonising Europe's hydrogen production with biohydrogen, (2023) 45. https://www.europeanbiogas.eu/wp-content/uploads/2023/06/Decarbonising-Europes-hydrogen-production-with-biohydrogen.pdf.

[210] M. Erans, M. Jeremias, L. Zheng, J.G. Yao, J. Blamey, V. Manovic, P.S. Fennell, E.J. Anthony, Pilot testing of enhanced sorbents for calcium looping with cement production, Appl. Energy. 225 (2018) 392–401. https://doi.org/10.1016/j.apenergy.2018.05.039.

ANNEXES

Flowsheet diagram used in the techno-economic analysis

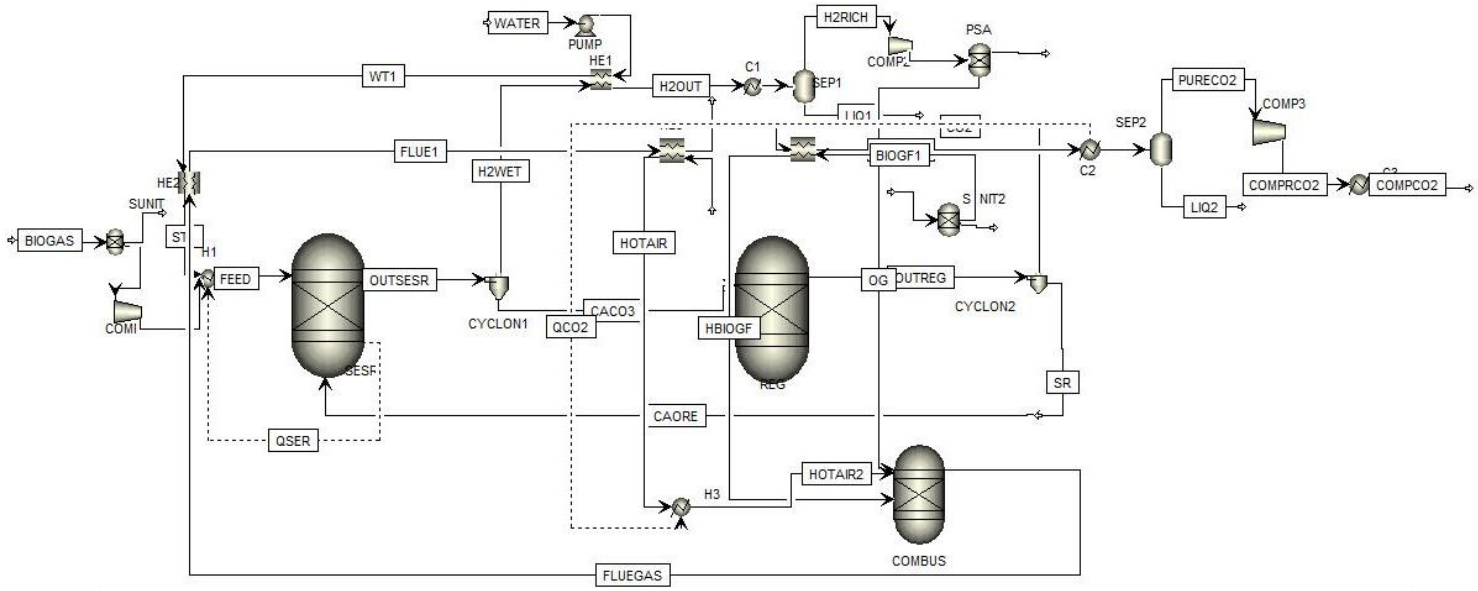

Fig. II: AspenPlus diagram of the flowsheet design for biogas SESR with an indirectly heated calciner.

Annex I

Assumptions for the techno-economic analysis

Some extra assumptions used in the techno-economic analysis are collected in Table I.1.

Table I.1: Extra economic assumptions.

Parameter	Value
Design and engineering	20% of total direct capital cost
Contractor's fees	5% of total direct capital cost
Contingency allowance	5% of total direct capital cost
Land	2% of total direct and indirect capital costs
Maintenance	10% of capital cost
Laboratory costs	20% of operating labour cost
Supervision	10% of operating labour cost
Plant overheads	60% of labour cost
Local taxes	1% of total capital cost
Insurance rate	1% of total capital cost
Miscellaneous materials	10% of maintenance cost

The discussion of the results relative to the OPEX and CAPEX calculations was done based on the representation of the main results (see in section 4.4.2.1 the Figure 4.22). Nevertheless, the complete results set is collected in Table I.2.

Table I.2: Complete results sets for the estimation of the CAPEX and OPEX of biogas and natural gas SESR.

	Units	**Case 1** BIOG_ IndAIR	**Case 2** BIOG_DirO XY	**Case 3** NG_ IndAIR
Capital Cost - CAPEX				
Direct capital costs				
Reformer	€m	16.2	16.2	9.3
Calciner and combustor	€m	7.7	4.7	6.1
PSA	€m	10.7	10.7	10.7
ASU	€m	-	7.8	-
CO_2 compressor	€m	6.4	12.5	4.8
Sulphur removal unit	€m	0.3	0.2	0.2

	Units	Case 1 BIOG_ IndAIR	Case 2 BIOG_DirO XY	Case 3 NG_ IndAIR
Heat exchangers	€m	0.5	0.4	0.7
Indirect capital costs				
Design and engineering	€m	8.4	10.5	6.4
Contractor's fees	€m	2.1	2.6	1.6
Contingency allowance	€m	2.1	2.6	1.6
Non-depreciable capital costs				
Land	€m	1.1	1.4	0.8
Total capital costs - CAPEX	**€m**	**55.4**	**69.6**	**42.3**
Operating cost				
Fixed operating costs				
Maintenance	€m	5.5	7.0	4.2
Operating labour cost	€m	5.1	5.1	5.1
Laboratory costs	€m	1.0	1.0	1.0
Supervision	€m	0.5	0.5	0.5
Plant overheads	€m	3.1	3.1	3.1
Local taxes	€m	0.6	0.7	0.4
Insurance rate	€m	0.6	0.7	0.4
Variable operating costs				
Limestone[1]	€m	0.2	0.2	0.1
Ni Catalyst	€m	0.5	0.5	0.4
Spent Ni catalyst landfill disposal	€m	0.00025	0.00025	0.00019

[1] Landfill cost of limestone is not considered since the end-used of the material can be done in the cement industry following a circular economy approach [210].

	Units	**Case 1** BIOG_ IndAIR	**Case 2** BIOG_DirO XY	**Case 3** NG_ IndAIR
CO_2 storage cost	€m	2.7	7.9	1.7
Boiler feed water	€m	0.3	0.3	0.3
Electricity	€m	4.3	9.9	2.3
Miscellaneous materials	€m	0.6	0.7	0.4
Fuel costs				
Biogas / NG	€m	3.2	2.9	7.6
Total operating costs - OPEX	**€m**	**27.9**	**40.3**	**27.5**

Paper I

Renewable Energy 160 (2020) 575–583

Contents lists available at ScienceDirect

Renewable Energy

journal homepage: www.elsevier.com/locate/renene

On the effect of biogas composition on the H_2 production by sorption enhanced steam reforming (SESR)

A. Capa [a], R. García [a], D. Chen [b], F. Rubiera [a], C. Pevida [a, *], M.V. Gil [a, **]

[a] Instituto de Ciencia y Tecnología del Carbono, INCAR-CSIC, Francisco Pintado Fe, 26, 33011, Oviedo, Spain
[b] Department of Chemical Engineering, Norwegian University of Science and Technology, Sem Sælands vei 4, Trondheim, NO-7491, Norway

ARTICLE INFO

Article history:
Received 29 April 2020
Received in revised form
23 June 2020
Accepted 24 June 2020
Available online 5 July 2020

Keywords:
Biogas
CH_4/CO_2 composition
Hydrogen
Sorption enhanced steam reforming
Pd/Ni–Co catalyst
CO_2 capture
Dolomite

ABSTRACT

Biogas is a valuable source of renewable energy produced from biodegradable organic materials via anaerobic digestion. The production of H_2 by sorption enhanced steam reforming (SESR) of biogas has been studied thermodynamic and experimentally. A Pd/Ni–Co catalyst and dolomite as CO_2 sorbent were used. The effect of biogas composition (CH_4/CO_2 vol.%) on the process was evaluated at 600 and 650 °C in a fluidized bed reactor using biogas CO_2 concentrations of 5–50 vol.%. During conventional biogas steam reforming (SR), high CH_4 partial pressures in the feed favor the process, producing high H_2 concentrations. During biogas SESR, CO_2 was effectively removed from the gas phase by the sorbent for all the biogas compositions, and it did not alter the process compared to pure methane. Steam methane reforming (SMR) and water-gas shift (WGS), together with carbonation, were the main reactions occurring during biogas SESR. Dry (or CO_2) methane reforming did not occur under the conditions studied due to the relatively low temperature and the presence of steam. High H_2 purity (98.4 vol.%) and H_2 yield (91%) were experimentally obtained, pointing out the biogas SESR as a promising technology for the efficient production of high-purity, high-yield hydrogen from a renewable source.

1. Introduction

Global warming and climate change are two of the most important challenges that our society faces nowadays. Nevertheless, there is still a high dependence on traditional fossil fuels (such as coal, petroleum and natural gas) as energy sources, which cause serious greenhouse gas (GHG) emissions during their combustion [1]. In addition, energy consumption is expected to continue increasing in the future, since it is closely associated with industrialization and the rapid growth of the population. Therefore, the utilization of renewable energy is urgently needed to reduce GHG emissions to the atmosphere.

Biogas is a promising source of renewable bioenergy, which can be produced by the anaerobic digestion process from different types of biomass or biodegradable materials. Thus, it is produced in different environments, such as landfills and both sewage sludge and biowaste digesters, during the anaerobic degradation of organic materials [2]. Depending on the type of biomass used, the composition of the obtained biogas varies. However, methane is usually a major component of biogas, which can be a valuable renewable energy source, but also a harmful greenhouse gas if emitted to the atmosphere. In general, raw biogas is mainly composed of methane (CH_4) (35–75%) and CO_2 (25–55%) [1]. There are other minor components in biogas, including nitrogen (N_2), oxygen (O_2), hydrogen (H_2), hydrogen sulfide (H_2S), water vapor (H_2O), carbon monoxide (CO), ammonia (NH_3), siloxanes and aromatics, as well as some dust particles. Purification or cleaning technologies (such as physical and chemical absorption, biological desulphurization or membrane separation) are commonly applied to control the levels of impurities in biogas and to remove harmful and toxic compounds such as H_2S, N_2, O_2, CO, and NH_3 that can affect the end-users, grid transmission, machineries or storage facilities.

Biogas contains variable concentrations of carbon dioxide, depending on the biogas source. However, the presence of carbon dioxide reduces the biogas calorific value. Biogas from sewage sludge digesters usually contains 55–75% of CH_4, 20–40% of CO_2 and <1% of nitrogen, whereas the composition of biogas from organic waste digesters is usually 45–75% of CH_4, 25–55% of CO_2 and <1% of nitrogen. On the other hand, in landfills, CH_4 content often varies from 35% to 55%, CO_2 from 15% to 40% and nitrogen from 5% to 25% [1,2].

Heat and steam production is the traditional method of biogas

* Corresponding author.
** Corresponding author.
E-mail addresses: cpevida@incar.csic.es (C. Pevida), victoria.gil@incar.csic.es (M.V. Gil).

https://doi.org/10.1016/j.renene.2020.06.122
0960-1481/

utilization, while the combined heat and power (CHP) generation has attracted increasing attention over the past decades, although the high CO_2 content of biogas decreases the heating value and flame stability of the gas mixture and prevents the use of biogas as a common energy source [3]. The conversion of biogas into higher-value products by catalytic reforming methods (dry reforming, steam reforming, and partial oxidative reforming) for producing syngas/hydrogen is, therefore, becoming an attractive option in recent years because it is commercially produced in large quantities and the availability of CO_2 and CH_4 is relatively inexpensive [4]. Syngas is an attractive and valuable gas, consisting of H_2 and CO, which has many potential applications (production of methanol, Fischer-Tropsch oil, gasoline), while hydrogen is a clean energy carrier that can be used for power and fuel generation, in industry and transport. Hydrogen is considered as a critical player in future energy scenarios, although most hydrogen currently derives from non-renewable resources, mainly natural gas [5]. The true environmental benefit of hydrogen use requires that it is produced from renewable sources, like biomass.

Between the catalytic reforming methods, the sorption enhanced steam reforming (SESR) process has recently emerged as an attractive novel technology that has received much attention during the last years to produce high purity hydrogen. This process combines the reforming reaction for hydrogen production with the in situ CO_2 separation in a single step. During the steam reforming (SR) process of methane, the steam reforming reaction, shown in Eq. (1), coexists with the water-gas shift (WGS) reaction, shown in Eq. (2).

$$CH_4 + H_2O \leftrightarrow CO + 3H_2 \; \Delta H_r^0 = +206 \text{ kJ mol}^{-1} \quad (1)$$

$$CO + H_2O \leftrightarrow CO_2 + H_2 \; \Delta H_r^0 = -41 \text{ kJ mol}^{-1} \quad (2)$$

For the carbon dioxide separation, natural CaO based materials are widely used in CO_2 sorption at high temperatures due to their high CO_2 capture capacity, fast CO_2 carbonation/calcination kinetics, low cost, and wide availability. Therefore, CaO sorbents are typically used in SESR processes, despite their lower reactivity after multiple carbonation/calcination cycles. CO_2 reacts with CaO and it is converted to a solid calcium carbonate by the carbonation reaction (Eq. (3)), giving the overall sorption enhanced steam reforming (SESR) reaction of methane, shown in Eq. (4):

$$CaO_{(s)} + CO_2 \leftrightarrow CaCO_{3(s)} \; \Delta H_r^0 = -178 \text{ kJ mol}^{-1} \quad (3)$$

$$CH_4 + 2H_2O + CaO_{(s)} \rightarrow 4H_2 + CaCO_{3(s)} \; \Delta H_r^0 = -13 \text{ kJ mol}^{-1} \quad (4)$$

During SESR, as CO_2 is being removed in situ from the gas phase by the sorbent (Eq. (3)), the thermodynamic equilibrium of the steam reforming of methane (Eq. (1)) and water-gas shift (Eq. (2)) reactions shift towards the production of H_2 according to the Le Chatelier's principle, which enhances the hydrogen production in one single reactor. It allows using lower reaction temperatures (typically 550–650 °C) than in conventional steam reforming processes whilst achieving high H_2 purities.

Furthermore, SR (Eq. (1)) is a highly endothermic reaction whereas the carbonation reaction (Eq. (3)) is exothermic. When they are combined in a single unit, together with the WGS reaction (Eq. (2)), during the SESR process, the enthalpy of the reforming process and hence the external energy demand in the reforming stage are reduced, and the overall reaction (Eq. (4)) results slightly exothermic. Besides, if biogas is reformed in the presence of a sorbent, the overall process is expected to be more exothermic than the SESR of pure methane. That is, if the amount of CO_2 contained in the biogas is removed from the gas phase by Eq. (3), it will provide additional heat to the system. This entails an additional advantage of the process regarding the global energy demand since the subsequent sorbent regeneration stage requires energy.

Recent research studies have focused on the SESR process of different biomass materials to generate renewable hydrogen such as ethanol [6], glycerol [7,8] or bio-oil from biomass fast pyrolysis [9–13]. However, the SESR of biogas is a topic scarcely studied in the literature. Assabumrungrat et al. [14] performed a thermodynamic analysis of the combined sorption enhanced steam reforming and partial oxidation of biogas (50/50 CH_4/CO_2 vol.%), studying the effects of the steam/CH_4, CaO/CH_4 and O_2/CH_4 ratios on the equilibrium hydrogen production. Saebea et al. [15] carried out a thermodynamic analysis of the SESR of biogas (60/40 CH_4/CO_2 vol.%) to study the effects of the temperature and steam/CH_4 ratio on the equilibrium hydrogen production. Both works concluded that the use of a CO_2 sorbent clearly enhances the production of hydrogen compared to the conventional steam reforming of biogas based on the predicted equilibrium results. Liu et al. [16] reported the simulation of a biogas steam reforming process for hydrogen production using nano-sized CaO sorbents, showing their advantages compared to conventional steam reforming and micro-sized CaO sorbents. On the other hand, an experimental study of the SESR of biogas (60/40 CH_4/CO_2 vol.%) was performed by Phromprasit et al. [17,18] with the objective of comparing the activity of different catalysts based on Ni and CaO under a selected operating condition. Moreover, Phromprasit et al. [19] studied different bed arrangements of catalyst and sorbent for the biogas SESR in a fixed bed reactor, demonstrating that the best results are obtained when the catalyst is physically mixed with the sorbent. Finally, preliminary batch tests under a fixed condition have been performed on a sorption enhanced reforming dual fluidized bed reactor system using upgraded biogas, obtaining a hydrogen concentration of 94 vol.% [20].

A main characteristic of the biogas is that it may contain variable concentrations of CH_4 and CO_2 as a function of its origin. However, the works in the literature on the sorption enhanced steam reforming of biogas have usually used a representative biogas composition (mainly 60/40 CH_4/CO_2 vol.%). Therefore, the objective of the present work is to carry out a comprehensive study on the effect of the biogas composition on the SESR process. With this aim, the influence of CH_4 and CO_2 concentrations (vol.%) in biogas on the process performance will be assessed. The process parameters under study include H_2 yield, H_2 selectivity, CH_4 conversion, H_2 purity, and CH_4, CO and CO_2 concentrations in the effluent gas. The results from biogas SESR will be compared with the conventional biogas steam reforming process. A thermodynamic analysis of the process will also be conducted to determine the theoretical feasibility of the process under the selected conditions and to compare the equilibrium values obtained with the experimental results.

2. Experimental

2.1. Catalyst and CO_2 sorbent

A 1%Pd/20%Ni–20%Co hydrotalcite-like material (Pd/Ni–Co HT) catalyst was selected. It was prepared by the incipient wetness impregnation method from a 20%Ni–20%Co hydrotalcite-like material (Ni–Co HT) precursor. The Ni–Co HT precursor was previously synthesized by co-precipitation of $Ni(NO_3)_2{\cdot}6H_2O$, $Co(NO_3)_2{\cdot}6H_2O$, $Mg(NO_3)_2{\cdot}6H_2O$ and $Al(NO_3)_3{\cdot}9H_2O$. A stoichiometric ratio of cations was chosen so as to yield a 40 wt% total metal load of Ni and Co, resulting in a material with a nominal composition of 20%Ni–20%Co. The precipitate obtained was filtered, washed, dried overnight and then calcined at 600 °C for 6 h. A detailed description of the precursor preparation procedure has

been reported elsewhere [21]. The Ni–Co HT precursor was then impregnated with a Pd solution to yield a 1 wt.% load of Pd. The Pd solution was prepared by dissolving $PdCl_2$ into two equivalents of HCl and diluting them in ethanol to the desired concentration. The sample was then dried for 14 h at 100 °C and calcined in airflow at 500 °C for 1 h in a muffle oven using a heating rate of 5 °C min^{-1}. The calcined catalyst was pelletized, ground and sieved to obtain a particle size of 250–500 μm. It was then reduced at 670 °C (heating rate of 2 °C min^{-1}) for 10 h in a mixed flow of H_2 (50 NmL min^{-1}) and N_2 (50 NmL min^{-1}). A detailed description of the preparation procedure of the Pd/Ni–Co HT catalyst as well as its characterization has been reported elsewhere [10].

Arctic dolomite was supplied by Franefoss Miljøkalk A/S, Norway. It has a purity of approximately 98.5 wt.% $CaMg(CO_3)_2$ and no sulfur according to X-ray fluorescence analysis. The dolomite was used as a precursor of CaO for the capture of CO_2. Its initial maximum CO_2 capture capacity was estimated as being 0.46 g CO_2/g sorbent. The BET surface area and pore volume of the calcined dolomite were 11.0 m^2 g^{-1} and 0.16 cm^3 g^{-1}, respectively [10]. It was calcined in airflow (200 mL min^{-1}) at 800 °C for 4 h and stored in an airtight desiccator for later use.

2.2. Experimental procedure

Fig. 1 shows the schematic flow diagram of the experimental setup used for the SESR experiments with biogas. It consists of an updraft bubbling fluidized bed stainless steel reactor (i.d. 21.5 mm), which was loaded with a 10.5 g mixture of calcined dolomite and Pd/Ni–Co HT catalyst, at a sorbent-to-catalyst ratio of 20 g/g. The reactor is located inside a tubular electric furnace and the reaction temperature is controlled by a K-type thermocouple which is inserted into the catalyst/sorbent bed and connected to a temperature controller and data recorder. The gases are delivered by Bronkhorst® mass flow controllers. The water is fed in by means of a Gilson® high-performance liquid chromatography (HPLC) pump.

The SESR experiments for biogas (mixtures of CH_4 and CO_2) were performed at atmospheric pressure and isothermally, at temperatures of 600 and 650 °C. SESR experiments using 100% CH_4 were also carried out for comparison purposes. The reactor was heated to the desired reaction temperature under N_2 atmosphere (100 NmL min^{-1}). Once the operating temperature was reached, the CH_4/CO_2 mixture (or CH_4), together with steam and N_2 (25 NmL min^{-1} flow, used as internal standard), was introduced updraft to the reactor through the catalyst/sorbent bed. Liquid H_2O was firstly evaporated in an evaporator and then mixed with the gas stream. This mixture was heated to 200 °C in a preheating zone before being fed into the reactor. The CH_4 concentration in the biogas was varied between 50 and 95 vol.% (in CO_2). The biogas compositions studied are shown in Table 1.

Two sets of biogas SESR experiments were performed: (i) the CH_4 flow in the feed gas was maintained constant, i.e., constant steam/CH_4 molar ratio of 6 and $GHSV_{CH4}$ value of 1969 mL CH_4 g_{cat}^{-1} h^{-1} were used, and (ii) the biogas flow in the feed gas was maintained constant, i.e., constant steam/C molar ratio of 3 and $GHSV_{biogas}$ value of 3937 mL biogas g_{cat}^{-1} h^{-1} were used. Table 2 shows the range of experimental conditions used in the experiments. The SESR process proceeded until the calcined dolomite became saturated (pre-breakthrough) and lost its capacity for CO_2 removal. Afterwards, CO_2 capture by the sorbent is negligible (post-breakthrough) and the conventional catalytic steam reforming (i.e., SR) process is assumed to occur, which was allowed to reach the

Table 1
Composition of the biogas mixtures studied.

Biogas mixture	CH_4 (vol.%)	CO_2 (vol.%)	CH_4/CO_2 molar ratio
50/50	50	50	1.00
60/40	60	40	1.50
70/30	70	30	2.33
80/20	80	20	4
90/10	90	10	9
95/5	95	5	19

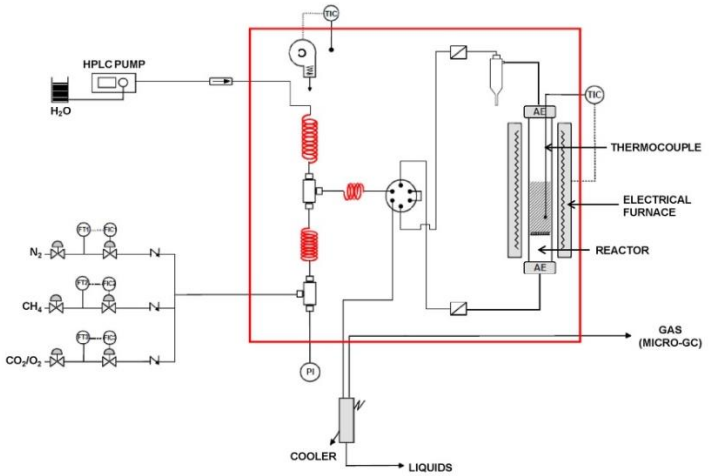

Fig. 1. Schematic flow diagram of the experimental setup used for the experiments.

Table 2
Experimental conditions used in the SESR experiments with biogas.

Parameter	Constant CH_4 flow	Constant biogas (CH_4+CO_2) flow
CH_4 in feed gas (vol.%)	50–100	50–100
Temperature	600 °C, 650 °C	600 °C, 650 °C
Steam/CH_4, H_2O/CH_4 molar ratio	6.0	3.2–6.0
Steam/C, $H_2O/(CH_4+CO_2)$ molar ratio	3.0–5.7	3.0
$GHSV_{CH4}$ (mL CH_4 g_{cat}^{-1} h^{-1})	1969	1969–3740
$GHSV_{biogas}$ (mL biogas g_{cat}^{-1} h^{-1})	2072–3937	3937

steady-state in the present work to compare the results with the SESR process.

The effluent gas from the reactor was cleaned of solid particles that may have been elutriated from the bed by means of a cyclone. The excess steam and other liquids that may have formed were separated from the exiting gas by condensation in a thermoelectric cooling tank. The composition of the dried gas was analyzed using an on-line dual-channel Varian® CP-4900 Micro GC, equipped with both molecular sieve Molsieve 5 Å and PPQ columns, and with a thermal conductivity detector (TCD). Helium was used as the carrier gas. The species detected were H_2, CH_4, CO, and CO_2. The product distribution was calculated on the basis of the nitrogen-free and dry composition of the gas effluent. The flow rates of the species generated during the experiment were calculated by means of a nitrogen balance since the amount of nitrogen fed in and the composition of the nitrogen evolved are known.

The H_2 yield, H_2 selectivity, CH_4 conversion, H_2 purity, and CH_4, CO, and CO_2 concentrations were calculated from Eqs. (5)–(9), respectively:

$$H_2\ \text{yield}\ (\%) = 100\cdot(F_{H2,out}/4\cdot F_{CH4,in}) \quad (5)$$

$$H_2\ \text{selectivity}\ (\%) = 100\cdot[2\cdot y_{H2}/(2\cdot y_{H2}+4\cdot y_{CH4})] \quad (6)$$

$$CH_4\ \text{conversion}\ (\%) = 100\cdot((F_{CH4,in} - F_{CH4,out})/F_{CH4,in}) \quad (7)$$

$$H_2\ \text{purity}\ (\text{vol.}\%) = 100\cdot(y_{H2}/\Sigma_i\, y_i) \quad (8)$$

$$CH_4/CO/CO_2\ (\text{vol.}\%) = 100\cdot(y_{CH4/CO/CO2}/\Sigma_i\, y_i) \quad (9)$$

where $F_{H2,out}$ is the molar flow rate of H_2 produced (mol min^{-1}), $F_{CH4,in}$ is the molar flow rate of methane fed in (mol min^{-1}), y_i is the molar content (N_2 free and on a dry basis) of each species i (H_2, CH_4, CO and CO_2) in the outlet gas, and $F_{CH4,out}$ is the molar flow rate of CH_4 produced (mol min^{-1}). H_2 yield calculation is based on Eq. (4), i.e., considering that only methane steam reforming (Eq. (1)) and WGS (Eq. (2)) reactions occur.

The gas hourly space velocity (GHSV) is defined as the ratio of the reactant volumetric flow rate to the mass of catalyst, according to Eq. (10):

$$GHSV\ (mL\ CH_4\,/\,biogas\ g_{cat}^{-1}\ h^{-1}) = \frac{Volumetric\ flow\ rate\ of\ inlet\ methane\,/\,biogas\ (mL\ CH_4\,/\,biogas\ h^{-1})}{Mass\ of\ catalyst\ (g)} \quad (10)$$

2.3. Thermodynamic equilibrium calculations

Thermodynamic analysis of the SESR process of biogas was conducted taking into account a wide range of reaction conditions so that the equilibrium results can be evaluated and compared with the experimental values. The equilibrium composition was estimated by minimizing the Gibbs free energy of the system since this non-stoichiometric approach offers greater flexibility when tackling complex problems where the reaction pathways are unclear [22]. Aspen Plus V10 software (Aspentech) was used to predict the thermodynamic behavior of the system. The RGibbs reactor was specified as the reaction system and the Peng-Robinson thermodynamic package as the property method. The species produced in concentrations higher than 10^{-4} mol% were H_2, CH_4, CO, CO_2, H_2O, CaO and $CaCO_3$. C_2H_4, C_2H_6 and C (graphite as solid carbon) were also included in the products pool, but their concentrations in the equilibrium stream were null or not high enough to be considered relevant products [23]. The product mole fractions were calculated on a dry basis. See Supporting Information.

3. Results and discussion

3.1. Effect of CH_4/CO_2 composition on the SESR of biogas

Effect of biogas composition considering CH_4 as the only reactant gas. To study the effect of biogas composition, i.e., CH_4/CO_2 vol.%, on the SESR and SR processes, a first set of experiments was performed at 600 and 650 °C, where the CH_4 flow in the feed gas was maintained constant, i.e., a constant steam/CH_4 molar ratio of 6 and a $GHSV_{CH4}$ value of 1969 mL CH_4 g_{cat}^{-1} h^{-1} were used. In this way, only CH_4 is considered as reactant gas in the process and so the steam to carbon molar ratio and the space velocity regarding methane are kept constant. Fig. 2 shows the concentrations of gases obtained from these experiments. The equilibrium values obtained from thermodynamic analysis for the experimental conditions used are also presented in Fig. 2.

For the SESR process, H_2 (Fig. 2a), CH_4 (Fig. 2b), CO (Fig. 2c) and CO_2 (Fig. 2d) concentrations have an approximately constant value for all the biogas compositions studied (50–95 vol.% of CH_4). These values are similar to those obtained from the SESR of pure methane (100 vol.% CH_4 in the plots), which indicates that the sorbent removes from the gas phase all the extra CO_2 added with the biogas compared to pure methane by the carbonation reaction (Eq. (3)). On the other hand, the experimental values for the gas concentrations are quite close to those of the equilibrium under all the conditions. As was evidenced from the thermodynamic analysis (see Supporting Information), the experimental results of the SESR of biogas also indicate that there is no particular effect of the CO_2 contained in the biogas on the SESR performance compared to pure methane. CO_2 is effectively removed from the gas phase by reaction

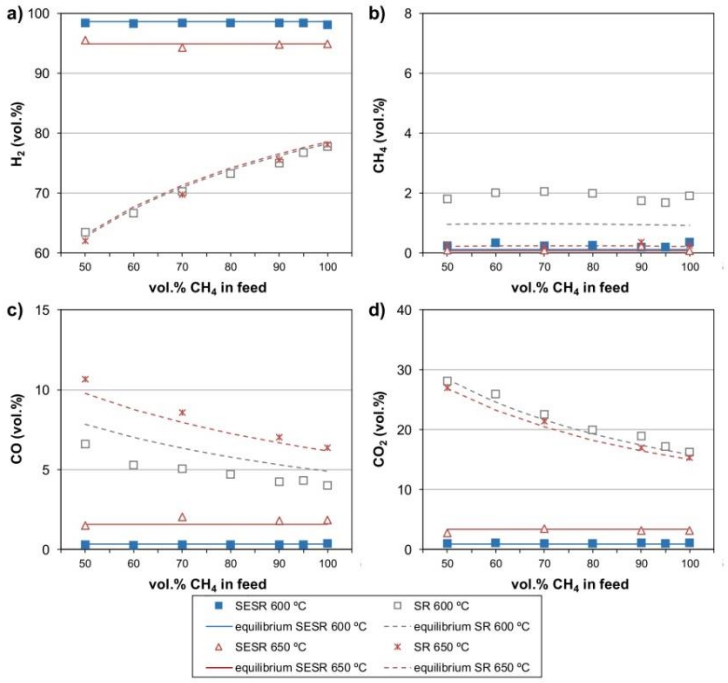

Fig. 2. Effect of methane content in biogas on the H_2 (a), CH_4 (b), CO (c) and CO_2 (d) concentrations during SESR and SR at 600 and 650 °C. Reaction conditions: steam/CH_4 = 6 mol/mol, $GHSV_{CH4}$ = 1969 mL CH_4 g_{cat}^{-1} h^{-1}, sorbent/catalyst ratio = 20 g/g, Pd/Ni–Co HT catalyst and dolomite sorbent.

with the sorbent under the studied conditions. This provides great flexibility to the SESR process when it comes to the use of biogas with different compositions derived from a wide range of sources. Besides, the presence of CO_2 in the feed gas could have a positive effect on the thermal equilibrium of the overall process, since heat is released by the carbonation reaction as the CO_2 is removed.

For the SR process, H_2 concentration (Fig. 2a) gradually increases with the increase in the methane content of biogas. CH_4 concentration (Fig. 2b) does not significantly vary, while CO and CO_2 concentrations (Fig. 2c and d, respectively) decrease as the methane content in biogas increases. The higher CO_2 concentrations obtained with lower methane content in biogas are due to the higher amount of CO_2 added with the biogas, which is not removed by any sorbent under SR conditions. The increase in H_2 concentration with the methane content in biogas is in accordance with the lower concentration of CO_2 for the highest methane contents in biogas, together with the lower CO concentrations obtained. These results suggest that higher CO_2 concentrations in the gas phase supplied by the biogas prevent the WGS reaction from occurring to a higher extent (or the equilibrium between CO and CO_2 could tend to favor the reverse WGS), resulting in higher CO contents, and in turn lower H_2 concentrations. Therefore, higher CH_4 partial pressures in the feed favor the steam methane reforming process. It has been highlighted in the literature that the presence of CO_2 in biogas is advantageous for the SR process when the desired product is syngas (H_2+CO), which is used to produce higher-value products such as synthetic liquid fuels or other chemicals. However, when the desired product is hydrogen, CO needs to be converted to CO_2 by the WGS reaction and, therefore, the CO_2 in biogas adds no benefit [24]. For hydrogen production, the lower the CO_2 content in biogas, the more efficient the CH_4 conversion in the desired product, which facilitates obtaining high purity H_2 by SR of biogas [25]. These results are also predicted by the equilibrium analysis. It can be seen that H_2 and CO_2 concentrations closely follow the equilibrium pattern, while slightly higher experimental values of CH_4 and lower values of CO are obtained compared to equilibrium (Fig. 2).

Fig. 3 shows the H_2 yield (Fig. 3a), H_2 selectivity (Fig. 3b) and CH_4 conversion (Fig. 3c) as a function of methane content in biogas. For SESR, their values are quite similar, independently of the biogas composition, and very close to the equilibrium in the case of the H_2 selectivity and CH_4 conversion. However, H_2 yield values are below those predicted by the thermodynamic equilibrium under all the conditions studied.

For SR, a slight increase in the H_2 yield, H_2 selectivity, and CH_4 conversion is detected as the methane content in biogas increases

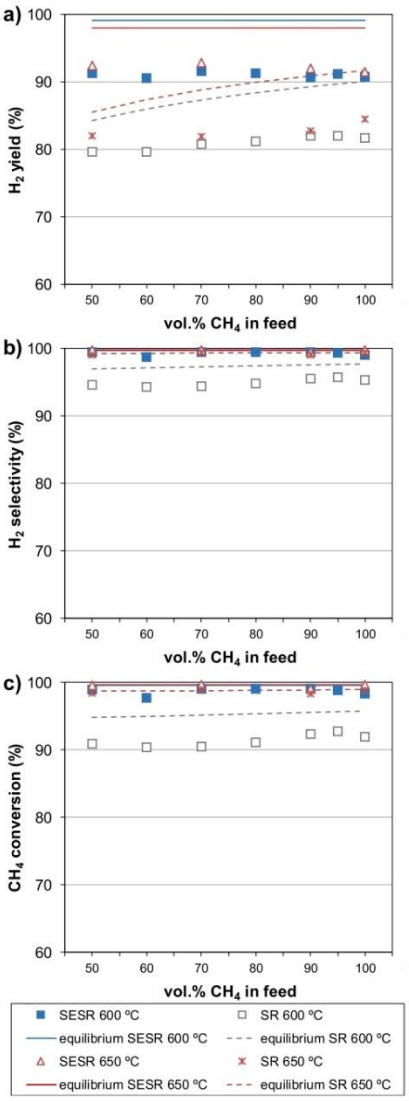

Fig. 3. Effect of methane content in biogas on the H_2 yield (a), H_2 selectivity (b) and CH_4 conversion (c) during SESR and SR at 600 and 650 °C. Reaction conditions: steam/CH_4 = 6 mol/mol, $GHSV_{CH4}$ = 1969 mL CH_4 g_{cat}^{-1} h^{-1}, sorbent/catalyst ratio = 20 g/g, Pd/Ni–Co HT catalyst and dolomite sorbent.

and their values are below those of the equilibrium calculations.

During biogas steam reforming, given that CO_2 is supplied to the process with the feed, a combination of steam reforming of methane (Eq. (1)) and dry methane reforming (Eq. (11)) could be considered to occur:

$$CH_4 + CO_2 \leftrightarrow 2CO + 2H_2 \quad \Delta H_r^0 = +247 \text{ kJ mol}^{-1} \tag{11}$$

However, the dry methane reforming reaction is a highly endothermic reaction that occurs at high temperatures (>700 °C) [26] and plays a minor role when enough H_2O is available [27]. The water-gas shift reaction is typically faster than dry methane reforming in the presence of reforming catalysts [28]. In the present work, the absence of dry methane reforming is evidenced because CH_4 conversion is not significantly enhanced during the SR of biogas compared to pure methane under the conditions studied. Moreover, no excess amount of CO in relation to the amount of CH_4 converted was detected, which could have derived from CO_2-reforming by Eq. (11) according to Ahmed et al. [24]. If the steam/C ratio is relatively high, it has been reported that the steam methane reforming and WGS reactions are predominant, resulting in the production of CO_2 and H_2 [29].

On the other hand, the results regarding the methane content in biogas follow similar tendencies for both temperatures studied, 600 and 650 °C. Furthermore, the effect of temperature on the process is in accordance with the equilibrium predictions. Thus, for the SESR process, the H_2 concentration is higher when using lower temperatures (Fig. 2a). The CO concentration is lower at lower temperatures (Fig. 2c) due to the favored exothermic WGS reaction. The CO_2 concentration is also lower at lower temperatures (Fig. 2d) due to the favored exothermic carbonation reaction. These results support the higher H_2 concentration at lower temperatures. The CH_4 concentration is lower at higher temperatures (Fig. 2b) due to the methanation reaction being thermodynamically unfavorable at high temperatures, when the steam methane reforming reaction is favored, as previously commented in literature for the sorption enhanced process [23,30].

For the SR process, the H_2 concentration is quite similar for both temperatures studied (Fig. 2a). The CO concentration is higher at higher temperatures (Fig. 2c) due to the WGS reaction being unfavorable, which leads to a slightly lower CO_2 concentration at higher temperatures (Fig. 2d). The CH_4 concentration is markedly lower at higher temperatures (Fig. 2b) since the methanation reaction is unfavorable and the steam methane reforming reaction is favored, at high temperatures.

Effect of biogas composition considering CH_4 and CO_2 as reactant gases. The second set of experiments was also performed at 600 and 650 °C to study the effect of biogas composition, i.e., CH_4/CO_2 vol.%, on the SESR and SR processes. In this case, the biogas flow in the feed gas was maintained constant, i.e., a constant steam/C molar ratio of 3.0 and a $GHSV_{biogas}$ value of 3937 mL biogas g_{cat}^{-1} h^{-1} were used. In this way, both CH_4 and CO_2 are considered as possible reactant gases in the process and so the steam to carbon molar ratio and the space velocity regarding biogas are kept constant. For this set, the steam/CH_4 molar ratio changed from 3.2 to 6.0, while the $GHSV_{CH4}$ changed from 1969 to 3740 mL CH_4 g_{cat}^{-1} h^{-1} (Table 2). The results for the SESR and SR processes are shown in Figs. 4 and 5, together with the equilibrium values obtained for the experimental conditions used.

For the SESR process, H_2 concentration (Fig. 4a) very slightly decreases as methane content in biogas increases. The CH_4 (Fig. 4b)

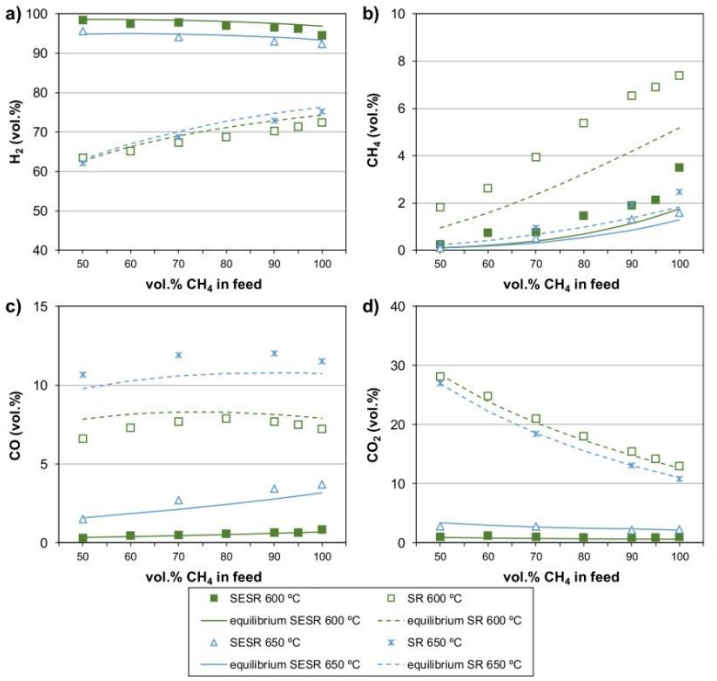

Fig. 4. Effect of methane content in biogas on the H_2 (a), CH_4 (b), CO (c) and CO_2 (d) concentrations during SESR and SR at 600 and 650 °C. Reaction conditions: steam/C = 3 mol/mol, $GHSV_{biogas}$ = 3937 mL biogas g_{cat}^{-1} h^{-1}, sorbent/catalyst ratio = 20 g/g, Pd/Ni–Co HT catalyst and dolomite sorbent.

and CO (Fig. 4c) concentrations slightly increase with methane content in biogas, while CO_2 concentration (Fig. 4d) does not change significantly under the studied conditions. Moreover, the experimental gas concentrations are quite close to the equilibrium values. On the other hand, H_2 yield (Fig. 5a), H_2 selectivity (Fig. 5b) and CH_4 conversion (Fig. 5c) decrease as methane content in biogas increases and they are slightly below the equilibrium values. These results (Figs. 4 and 5) differ from those obtained for the experiments with constant CH_4 flow in the feed gas (Figs. 2 and 3) where no effect of biogas composition on the SESR performance was observed (i.e., when CO_2 is removed from the gas phase by the carbonation reaction). It has to be borne in mind that for the experiments with constant biogas flow (Figs. 4 and 5), as methane content in biogas increases the steam/CH_4 molar ratio decreases from 6.0 to 3.0 and, correspondingly, the space velocity related to methane, $GHSV_{CH4}$, increases from 1969 to 3937 mL CH_4 g_{cat}^{-1} h^{-1} (Table 2). Therefore, the lower steam content reduces both the steam methane reforming and WGS reactions, which accounts for the higher CH_4 and CO contents and the lower H_2 concentration obtained for methane-enriched biogas compositions. The CO_2 concentration should also decrease if the steam methane reforming and WGS reactions are hampered, but it is somehow kept unchanged with methane content in biogas, which indicates that the carbonation reaction is effectively occurring under the conditions studied. Furthermore, higher H_2 production and fuel conversion might be expected at low space velocities due to longer contact times of gas and solid phases, i.e., with lower methane contents in biogas. The results indicate that H_2 yield is more affected by lower steam concentrations and/or higher space velocity values than H_2 purity, as it has been suggested in the literature [8].

For the SR process, H_2 and CH_4 concentrations (Fig. 4a and b, respectively) increase with methane content in biogas. The CO concentration (Fig. 4c) slightly increases as methane content in biogas increases until 80 vol.% and then slightly decreases with a further increase in methane content of biogas. Finally, the CO_2 concentration (Fig. 4d) decreases as methane content in biogas increases. All these results agree with the values predicted by the thermodynamic equilibrium for the SR process. H_2 yield (Fig. 5a), H_2 selectivity (Fig. 5b) and CH_4 conversion (Fig. 5c) decrease as methane content in biogas increases and they are slightly below the equilibrium values. If the gas concentrations are compared to those obtained for SR with constant CH_4 flow in the feed gas (Fig. 2), it can be seen that with constant biogas flow in the feed (Fig. 4) the CO_2 concentration decreases when methane content in biogas increases due to the lower amount of CO_2 in the biogas, together with the lower steam/C molar ratios that could reduce the steam methane

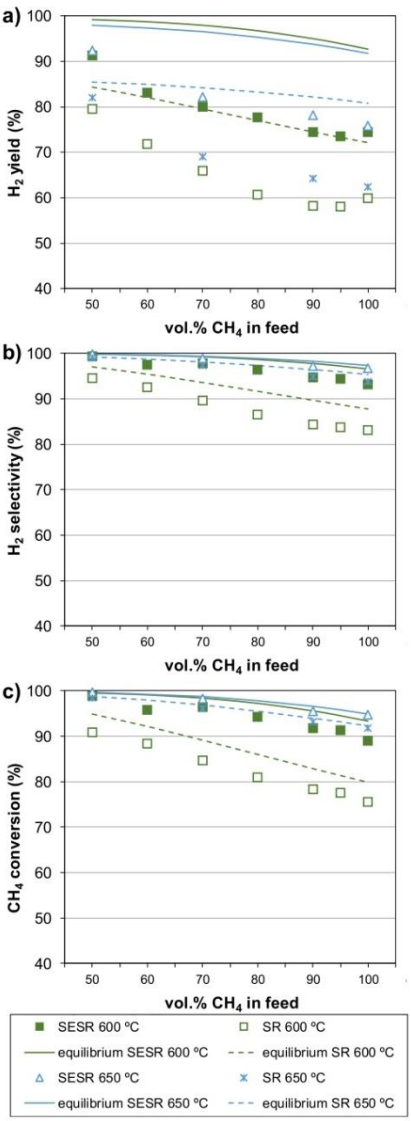

Fig. 5. Effect of methane content in biogas on the H_2 yield (a), H_2 selectivity (b) and CH_4 conversion (c) during SESR and SR at 600 and 650 °C. Reaction conditions: steam/C = 3 mol/mol, $GHSV_{biogas}$ = 3937 mL biogas g_{cat}^{-1} h^{-1}, sorbent/catalyst ratio = 20 g/g, Pd/Ni–Co HT catalyst and dolomite sorbent.

reforming and WGS reactions. In Fig. 4, an increase in the H_2 concentration with methane content in biogas is also detected, which is in accordance with the lower concentration of CO_2 that is added with biogas at these conditions. However, this is a minor increase compared to the case of constant methane content (Fig. 2) since higher concentrations of CO and CH_4 are detected under constant biogas flow conditions (Fig. 4). This suggests that besides hindering the WGS reaction due to the higher CO_2 concentrations in the gas phase at SR conditions, the associated decrease in the steam/CH_4 molar ratio and the increase in the space velocity under constant biogas flow conditions would have worsened the results. This effect is especially remarkable for the H_2 yield, H_2 selectivity and CH_4 conversion, which experienced a marked decrease with methane content in biogas that was not observed for the experiments with constant CH_4 flow. These results are predicted by the equilibrium, although higher values of CH_4 and lower values of H_2 purity, H_2 yield, H_2 selectivity, and CH_4 conversion are obtained experimentally compared to equilibrium.

On the other hand, the effect of temperature on the process performance for the experiments with a constant biogas flow (Figs. 4 and 5) is also in accordance with the equilibrium predictions and follows the same tendency as that for the experiments with a constant CH_4 flow (Figs. 2 and 3).

For the experiments with constant biogas flow, the absence of dry methane reforming (Eq. (11)) is confirmed by the absence of excess CO derived from CO_2-reforming with respect to the converted CH_4 [24]. This fact can be explained because the temperature used in these experiments (600–650 °C) does not promote the endothermic dry methane reforming reaction. On the other hand, the presence of steam favors the steam methane reforming and WGS reactions at the expense of the dry methane reforming reaction. Therefore, these results confirm that the CO_2 supplied with the biogas is effectively removed from the gas phase by the sorbent during the SESR of biogas and it does not influence the sorption enhanced reforming process compared to pure methane since it does not act as a reactant in the process. Thus, considering CH_4 as the only reactant gas in the process, i.e., using a constant CH_4 flow in the feed gas (and so constant steam/CH_4 and $GHSV_{CH4}$), seems more appropriate to study the effect of biogas composition on the SESR process under the evaluated conditions.

4. Conclusions

The production of renewable H_2 by the sorption enhanced steam reforming of biogas has been demonstrated both thermodynamic and experimentally. High-purity high-yield hydrogen can be obtained by SESR of biogas (CH_4+CO_2) on a Pd/Ni–Co catalyst and using Arctic dolomite as carbon dioxide sorbent. During the SESR of biogas of different compositions (from 50 to 95 vol.% of CH_4), all the CO_2 supplied with the biogas is effectively removed from the gas phase by the sorbent and it does not affect the sorption enhanced steam reforming process compared to pure methane. However, higher CH_4 partial pressures in the biogas favor the steam methane reforming reaction and give higher concentrations of H_2 during the conventional steam reforming of biogas.

No dry methane reforming has been found to occur under the conditions studied due to the relatively low temperature and the presence of steam. On the contrary, steam methane reforming, water-gas shift and carbonation are the main reactions taking place during the SESR of biogas.

High H_2 purity (98.4 vol.%) and H_2 yield (91%) have been

obtained from the SESR of biogas containing 50–95 vol.% of CH_4 balance CO_2. The results of the present study demonstrate that the sorption enhanced steam reforming of biogas is a promising process for the production of green hydrogen from renewable energy sources.

CRediT authorship contribution statement

A. Capa: Investigation, Writing - review & editing. **R. García:** Investigation, Methodology, Writing - review & editing. **D. Chen:** Writing - review & editing. **F. Rubiera:** Supervision, Writing - review & editing. **C. Pevida:** Conceptualization, Supervision, Writing - review & editing, Funding acquisition. **M.V. Gil:** Conceptualization, Methodology, Writing - original draft, Supervision.

Declaration of competing interest

The authors declare that they have no known competing financial interests or personal relationships that could have appeared to influence the work reported in this paper.

Acknowledgments

The authors thank Franefoss Miljøkalk A/S (Norway) for supplying Arctic dolomite. This work was carried out with financial support from the Spanish MICINN (Project ENE2017-83530-R) and from the Gobierno del Principado de Asturias (PCTI, Ref. IDI/2018/000115), both co-financed by the European Regional Development Fund (ERDF). M.V. Gil acknowledges support from a Ramón y Cajal grant (RYC-2017-21937) of the Spanish government, co-financed by the European Social Fund (ESF). A. Capa acknowledges a fellowship awarded by the Spanish MICINN (FPI program, PRE2018-083634), co-financed by the European Social Fund (ESF).

Appendix A. Supplementary data

Supplementary data to this article can be found online at https://doi.org/10.1016/j.renene.2020.06.122.

References

[1] O. Jönsson, E. Polman, J.K. Jensen, R. Eklund, H. Schyl, S. Ivarsson, Sustainable gas enters the European gas distribution system, Danish Gas Technology Center, 2003. http://www.dgc.eu/sites/default/files/filarkiv/documents/C0301_sustainable_gas.pdf. (Accessed 18 December 2019).
[2] Y. Gao, J. Jiang, Y. Meng, F. Yan, A. Aihemaiti, A review of recent developments in hydrogen production via biogas dry reforming, Energy Convers. Manag. 171 (2018) 133–155, https://doi.org/10.1016/j.enconman.2018.05.083.
[3] M.P. Kohn, M.J. Castaldi, R.J. Farrauto, Biogas reforming for syngas production: the effect of methyl chloride, Appl. Catal. B Environ. 144 (2014) 353–361, https://doi.org/10.1016/j.apcatb.2013.07.031.
[4] O.W. Awe, Y. Zhao, A. Nzihou, D.P. Minh, N. Lyczko, A review of biogas utilisation, purification and upgrading technologies, Waste Biomass Valorization 8 (2017) 267–283, https://doi.org/10.1007/s12649-016-9826-4.
[5] D.G. Avraam, T.I. Halkides, D.K. Liguras, O.A. Bereketidou, M.A. Goula, An experimental and theoretical approach for the biogas steam reforming reaction, Int. J. Hydrogen Energy 35 (2010) 9818–9827, https://doi.org/10.1016/j.ijhydene.2010.05.106.
[6] K.D. Dewoolkar, P.D. Vaidya, Tailored hydrotalcite-based hybrid materials for hydrogen production via sorption-enhanced steam reforming of ethanol, Int. J. Hydrogen Energy 41 (2016) 6094–6106, https://doi.org/10.1016/j.ijhydene.2015.10.034.
[7] C. Dang, H. Yu, H. Wang, F. Peng, Y. Yang, A bi-functional Co–CaO–$Ca_{12}Al_{14}O_{33}$ catalyst for sorption-enhanced steam reforming of glycerol to high-purity hydrogen, Chem. Eng. J. 286 (2016) 329–338, https://doi.org/10.1016/j.cej.2015.10.073.
[8] J. Fermoso, L. He, D. Chen, Production of high purity hydrogen by sorption enhanced steam reforming of crude glycerol, Int. J. Hydrogen Energy 37 (2012) 14047–14054, https://doi.org/10.1016/j.ijhydene.2012.07.084.
[9] G. Esteban-Díez, M.V. Gil, C. Pevida, D. Chen, F. Rubiera, Effect of operating conditions on the sorption enhanced steam reforming of blends of acetic acid and acetone as bio-oil model compounds, Appl. Energy 177 (2016) 579–590, https://doi.org/10.1016/j.apenergy.2016.05.149.
[10] J. Fermoso, M.V. Gil, F. Rubiera, D. Chen, Multifunctional Pd/Ni–Co catalyst for hydrogen production by chemical looping coupled with steam reforming of acetic acid, ChemSusChem 7 (2014) 3063–3077, https://doi.org/10.1002/cssc.201402675.
[11] M.V. Gil, J. Fermoso, C. Pevida, D. Chen, F. Rubiera, Production of fuel-cell grade H_2 by sorption enhanced steam reforming of acetic acid as a model compound of biomass-derived bio-oil, Appl. Catal. B Environ. 184 (2016) 64–76, https://doi.org/10.1016/j.apcatb.2015.11.028.
[12] M.V. Gil, J. Fermoso, F. Rubiera, D. Chen, H_2 production by sorption enhanced steam reforming of biomass-derived bio-oil in a fluidized bed reactor: an assessment of the effect of operation variables using response surface methodology, Catal. Today 242 (Part A) (2015) 19–34, https://doi.org/10.1016/j.cattod.2014.04.018.
[13] M.V. Gil, K.R. Rout, D. Chen, Production of high pressure pure H_2 by pressure swing sorption enhanced steam reforming {PS-SESR} of byproducts in bio-refinery, Appl. Energy 222 (2018) 595–607, https://doi.org/10.1016/j.apenergy.2018.03.181.
[14] S. Assabumrungrat, P. Sonthisanga, W. Kiatkittipong, N. Laosiripojana, A. Arpornwichanop, A. Soottitantawat, et al., Thermodynamic analysis of calcium oxide assisted hydrogen production from biogas, J. Ind. Eng. Chem. 16 (2010) 785–789, https://doi.org/10.1016/j.jiec.2010.07.001.
[15] D. Saebea, S. Authayanun, Y. Patcharavorachot, A. Arpornwichanop, Thermodynamic analysis of hydrogen production from the adsorption-enhanced steam reforming of biogas, Energy Procedia 61 (2014) 2254–2257, https://doi.org/10.1016/j.egypro.2014.12.120.
[16] H. Liu, Z. Yang, S. Wu, The evaluation of reactive sorption enhanced biogas steam reforming process for hydrogen production using nano-sized CaO adsorbents, J. Nanosci. Nanotechnol. 19 (2019) 3244–3251, https://doi.org/10.1166/jnn.2019.16608.
[17] J. Phromprasit, J. Powell, S. Wongsakulphasatch, W. Kiatkittipong, P. Bumroongsakulsawat, S. Assabumrungrat, Activity and stability performance of multifunctional catalyst (Ni/CaO and Ni/$Ca_{12}Al_{14}O_{33}$CaO) for bio-hydrogen production from sorption enhanced biogas steam reforming, Int. J. Hydrogen Energy 41 (2016) 7318–7331, https://doi.org/10.1016/j.ijhydene.2016.03.125.
[18] J. Phromprasit, J. Powell, S. Wongsakulphasatch, W. Kiatkittipong, P. Bumroongsakulsawat, S. Assabumrungrat, H_2 production from sorption enhanced steam reforming of biogas using multifunctional catalysts of Ni over Zr-, Ce- and La-modified CaO sorbents, Chem. Eng. J. 313 (2017) 1415–1425, https://doi.org/10.1016/j.cej.2016.11.051.
[19] J. Phromprasit, J. Powell, A. Arpornwichanop, A.E. Rodrigues, S. Assabumrungrat, Hydrogen production from sorption enhanced biogas steam reforming using nickel-based catalysts, Eng. J. 17 (2013) 19–34, https://doi.org/10.4186/ej.2013.17.4.19.
[20] J. Meyer, J. Mastin, C.S. Pinilla, Sustainable hydrogen production from biogas using sorption-enhanced reforming, Energy Procedia 63 (2014) 6800–6814, https://doi.org/10.1016/j.egypro.2014.11.714.
[21] L. He, H. Berntsen, E. Ochoa-Fernández, J. Walmsley, E. Blekkan, D. Chen, Co–Ni catalysts derived from hydrotalcite-like materials for hydrogen production by ethanol steam reforming, Top. Catal. 52 (2009) 206–217, https://doi.org/10.1007/s11244-008-9157-1.
[22] N.H. Florin, A.T. Harris, Hydrogen production from biomass coupled with carbon dioxide capture: the implications of thermodynamic equilibrium, Int. J. Hydrogen Energy 32 (2007) 4119–4134, https://doi.org/10.1016/j.ijhydene.2007.06.016.
[23] L. He, H. Berntsen, D. Chen, Approaching sustainable H_2 production: sorption enhanced steam reforming of ethanol, J. Phys. Chem. 114 (2010) 3834–3844, https://doi.org/10.1021/jp906146y.
[24] S. Ahmed, S.H.D. Lee, M.S. Ferrandon, Catalytic steam reforming of biogas – effects of feed composition and operating conditions, Int. J. Hydrogen Energy 40 (2015) 1005–1015, https://doi.org/10.1016/j.ijhydene.2014.11.009.
[25] H.J. Alves, C. Bley Junior, R.R. Niklevicz, E.P. Frigo, M.S. Frigo, C.H. Coimbra-Araújo, Overview of hydrogen production technologies from biogas and the applications in fuel cells, Int. J. Hydrogen Energy 38 (2013) 5215–5225, https://doi.org/10.1016/j.ijhydene.2013.02.057.
[26] V.P. Rathod, P. Bansal, P.V. Bhale, Analytical and experimental investigations for hydrogen rich syngas production by biogas reforming processes, Energy Procedia 75 (2015) 728–733, https://doi.org/10.1016/j.egypro.2015.07.501.
[27] P. Kolbitsch, C. Pfeifer, H. Hofbauer, Catalytic steam reforming of model biogas, Fuel 87 (2008) 701–706, https://doi.org/10.1016/j.fuel.2007.06.002.
[28] M. Ashrafi, C. Pfeifer, T. Pröll, H. Hofbauer, Experimental study of model biogas catalytic steam reforming: 2. Impact of sulfur on the deactivation and regeneration of Ni-based catalysts, Energy Fuels 22 (2008) 4190–4195, https://doi.org/10.1021/ef8000828.
[29] U. Izquierdo, V.L. Barrio, J. Requies, J.F. Cambra, M.B. Güemez, P.L. Arias, Tri-reforming: a new biogas process for synthesis gas and hydrogen production, Int. J. Hydrogen Energy 38 (2013) 7623–7631, https://doi.org/10.1016/j.ijhydene.2012.09.107.
[30] L. He, D. Chen, Hydrogen production from glucose and sorbitol by sorption-enhanced steam reforming: challenges and promises, ChemSusChem 5 (2012) 587–595, https://doi.org/10.1002/cssc.201100566.

Thermodynamic equilibrium results for the SESR and SR of biogas with different composition

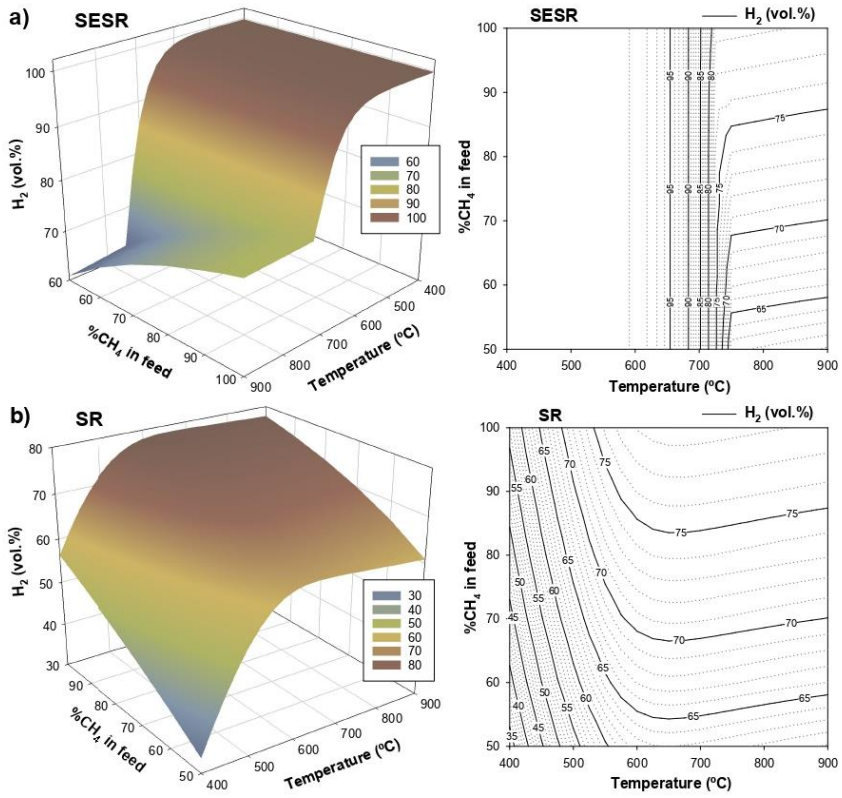

Fig. 1S. Thermodynamic equilibrium H_2 concentrations for the SESR (a) and SR (b) of biogas as a function of feed composition (vol.% of CH_4) and reaction temperature. Reaction conditions: 1 bar, steam/CH_4=6 mol/mol.

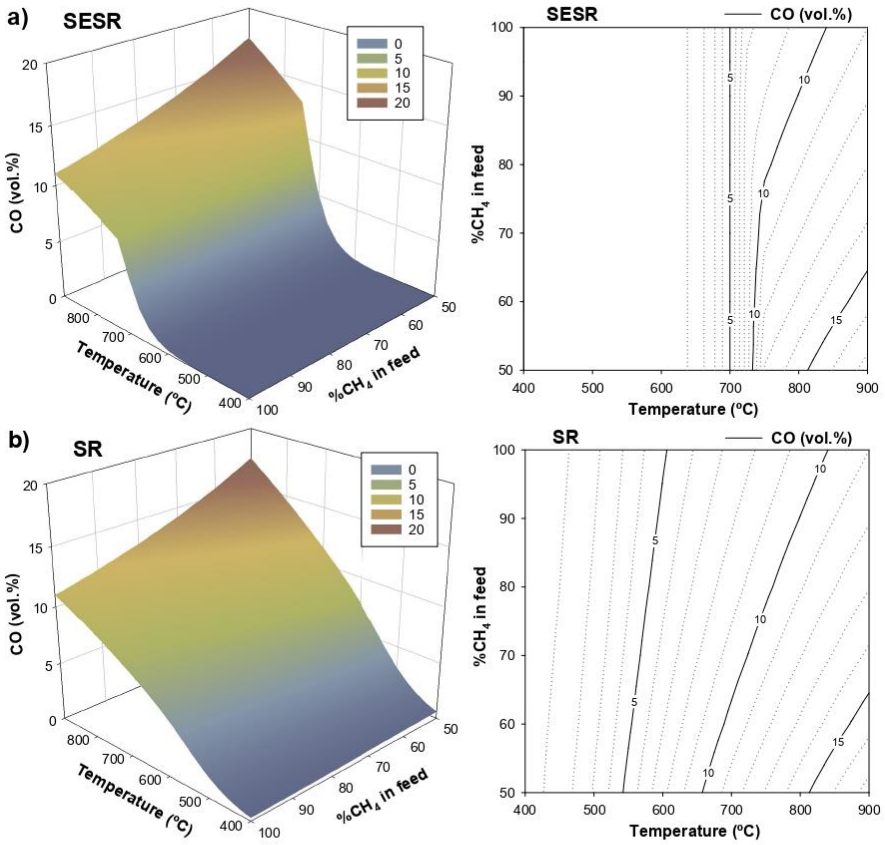

Fig. 2S. Thermodynamic equilibrium CO concentrations for the SESR (a) and SR (b) of biogas as a function of feed composition (vol.% of CH_4) and reaction temperature. Reaction conditions: 1 bar, steam/CH_4=6 mol/mol.

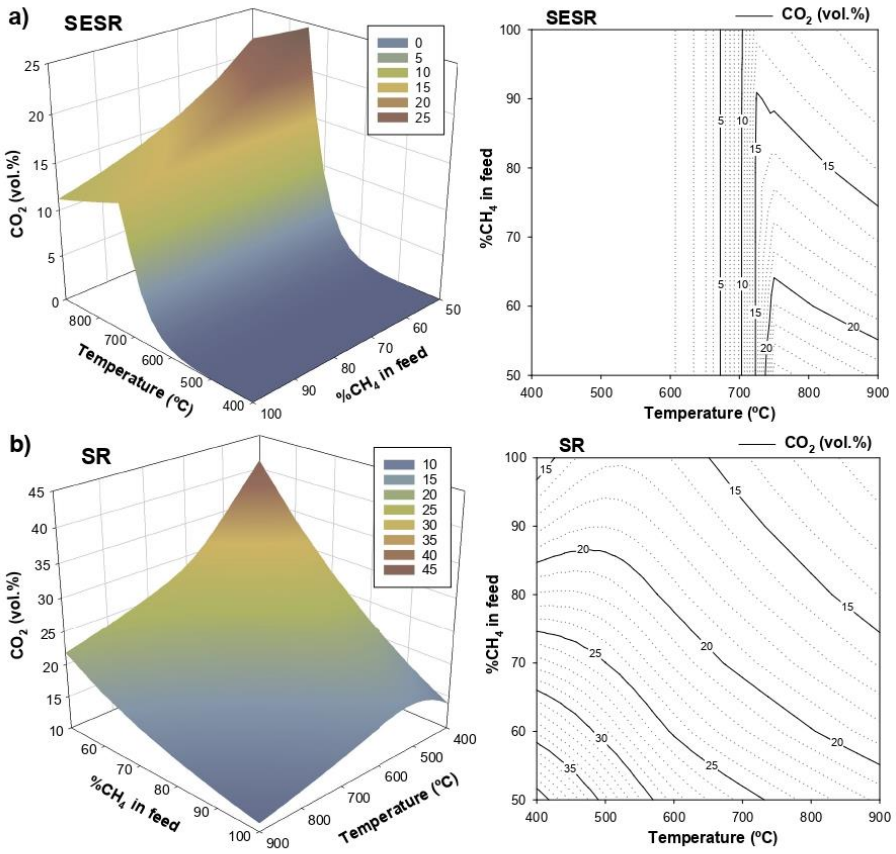

Fig. 3S. Thermodynamic equilibrium CO_2 concentrations for the SESR (a) and SR (b) of biogas as a function of feed composition (vol.% of CH_4) and reaction temperature. Reaction conditions: 1 bar, steam/CH_4=6 mol/mol.

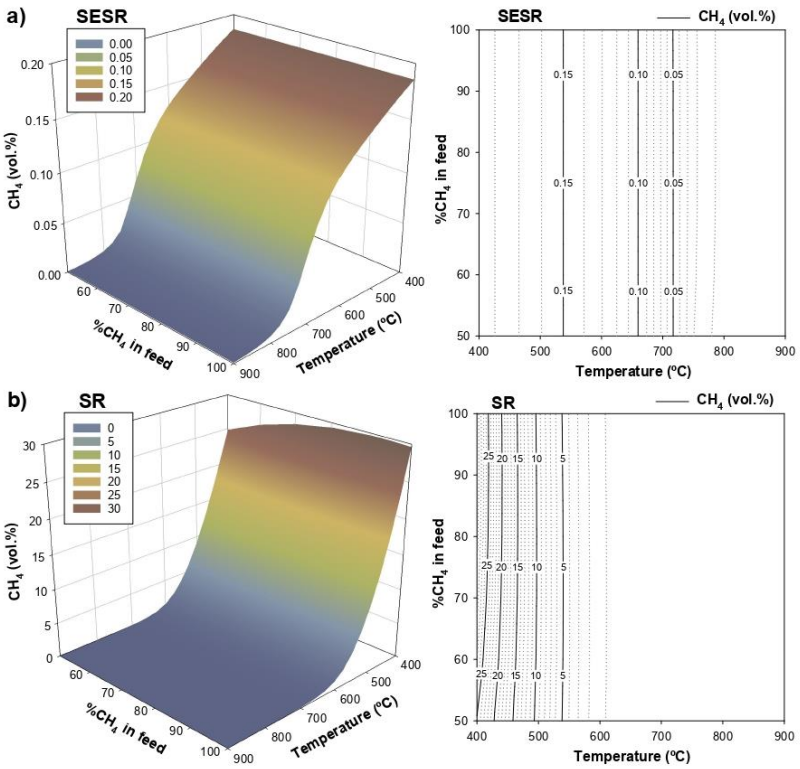

Fig. 4S. Thermodynamic equilibrium CH_4 concentrations for the SESR (a) and SR (b) of biogas as a function of feed composition (vol.% of CH_4) and reaction temperature. Reaction conditions: 1 bar, steam/CH_4=6 mol/mol.

Figs. 1S-4S show the thermodynamic equilibrium results for the SESR and SR of biogas as a function of feed composition (CH_4/CO_2 vol.%) at reaction temperatures between 400 and 900 ºC. The CH_4 concentration in biogas varied between 50 and 95 vol.%, and pure methane (100% CH_4) was also assessed for comparison purposes. For these calculations, the CH_4 flow in the feed gas was maintained constant, i.e., constant steam/CH_4 molar ratio of 6 was used.

If the equilibrium results for SESR and SR are compared, it can easily be observed in the contour plots on the right-hand side in Figs. 1S-4S that the concentration profiles

of the outlet gases (H_2, CO, CO_2, and CH_4) are identical for both SESR and SR processes between 750 and 900 °C when the CH_4 content in biogas takes values between 50-80 vol.%. Likewise, the SESR and SR results are similar between approximately 725 and 900 °C for CH_4 contents in biogas higher than 90 vol.%. This means that when SESR is carried out, CO_2 in the gas phase is removed by the carbonation reaction, between 400 and 725-750 °C, and that the CO_2 in the biogas and/or produced during the process is not captured at higher temperatures.

As mentioned above, for the lowest range of concentrations of CH_4 in biogas (50-80 vol.%), an effective CO_2 removal takes place up to 750 °C. This is due to the higher CO_2 content of biogas in these cases, which implies a higher CO_2 partial pressure in the gas phase that shifts the carbonation reaction to a slightly higher temperature. The carbonation reaction rate on CaO sorbents depends on the partial pressure of CO_2 in the gas phase. In fact, the carbonation is achieved by increasing the partial pressure of CO_2 in the gas phase above the CaO-$CaCO_3$ equilibrium value, which depends on temperature. A CO_2 partial pressure in the gas stream higher than the CO_2 equilibrium pressure for a given temperature is the driving force for the removal of CO_2 by reaction with the sorbent [1].

Furthermore, when comparing the equilibrium results of SESR and SR, it can be seen in Fig. 1S that between 400 and 725-750 °C the H_2 concentration is significantly higher when the sorption enhanced reforming process is occurring. Besides, the CO, CO_2 and CH_4 concentrations are lower, for all the biogas compositions and temperatures studied. This is due to the shift of the steam reforming and WGS equilibrium towards H_2 production by the in-situ CO_2 removal. These results clearly demonstrate the advantages of the sorption enhanced reaction compared to the conventional steam reforming process.

On the other hand, the results for SESR (Figs. 1Sa, 2Sa, 3Sa, and 4Sa) show that the variability in biogas composition, i.e., $\%CH_4$ in the feed, does not influence the equilibrium concentrations of the gases in the 400-700 °C temperature range. It means that the SESR results for methane ($\%CH_4$ in feed=100%) and for all the biogas compositions are identical under such conditions. This indicates that all the extra CO_2 added with the biogas compared to pure methane is removed from the gas phase by the sorbent. The carbonation reaction clearly occurs at temperatures below 700 °C during the SESR of biogas until complete removal of the CO_2 present in the gas phase. As mentioned above, the carbonation reaction would also occur between 700 and 750 °C for biogas, but the extra CO_2 added with the biogas would not be removed completely by the sorbent in this case. At temperatures higher than 750 °C, conventional SR takes place since CO_2 is not removed by the sorbent by the carbonation reaction. Therefore, the results indicate that, according to the thermodynamic equilibrium, there is no effect of the CO_2 contained in biogas on the SESR performance when the CO_2 is effectively removed from the gas phase by reaction with the sorbent, i.e., between 400 and 700 °C.

In the case of the SR process, the CH_4 concentration in the feed influences the equilibrium concentration of gases in all the temperature range studied. H_2 concentration (Fig. 1Sb) increases as methane concentration in biogas increases, conversely to CO (Fig. 2Sb) and CO_2 (Fig. 3Sb) contents that decrease with methane concentration in biogas. CH_4 content in the outlet gas (Fig. 4Sb) does not change significantly for the different biogas compositions, and it only shows a slight increase with methane concentration in biogas at low temperatures. This means that the H_2 concentration is lower, while CO and CO_2 concentrations are higher, for any biogas blend than for pure methane. The CO_2 in the biogas, which is not removed by a sorbent under these conditions, would be responsible for the higher CO_2 concentration, which in turn would hinder the WGS

reaction, increasing the CO content in the outlet gas. The dilution effect of higher CO and CO_2 concentrations then explains the lower H_2 concentration for lower methane concentrations in biogas. Higher CO content in the gas phase could also decrease the steam reforming of methane, reducing its conversion.

Regarding the effect of temperature on the SESR process of biogas (50-95 vol.% CH_4) and pure methane, the thermodynamic results indicate that the H_2 concentration is higher than 99 vol.% in the temperature range of 400-575 ºC and then gradually decreases with further temperature increase (Fig. 1Sa). CO concentration increases with temperature (Fig. 2Sa) due to the fact that the exothermic WGS reaction is thermodynamically favorable at low temperatures. CO_2 concentration also increases with temperature (Fig. 3Sa), since the exothermic carbonation reaction is thermodynamically favorable at low temperatures. CO_2 sorption shifts the equilibrium of the steam reforming and WGS reactions to the product side, promoting H_2 production, which explains the decrease in the H_2 concentration with temperature. Finally, CH_4 concentration decreases with temperature (Fig. 4Sa) due to the joint effect of thermodynamically favorable methanation reaction at low temperatures, and the steam methane reforming reaction being thermodynamically enhanced at higher temperatures. In any case, the effect of temperature is similar for all the biogas compositions studied when the sorption enhanced process is occurring, i.e., between 400 and 700 ºC.

Regarding the effect of temperature on the SR of biogas (50-100 vol.% CH_4), the thermodynamic results indicate that the H_2 concentration increases with temperature until approximately 650 ºC, and then gradually decreases at a slow rate (Fig. 1Sb). This increase is explained because the endothermic steam methane reforming reaction is favored with temperature. CO concentration also increases with temperature (Fig. 2Sb) mainly due to the WGS reaction being thermodynamically unfavorable at high

temperatures. Thus, CO_2 concentration decreases with temperature (Fig. 3Sb). CH_4 concentration also decreases with temperature (Fig. 4Sb) since the methanation reaction is thermodynamically unfavorable at high temperatures when the steam methane reforming reaction is thermodynamic favored. In general, the trends observed in the SR results as a function of temperature are similar for all the biogas compositions evaluated, although the gas concentrations vary, as explained above.

References:

[1] Sun P, Grace JR, Lim CJ, Anthony EJ. Determination of intrinsic rate constants of the $CaO–CO_2$ reaction. Chem Eng Sci 2008;63:47-56. https://doi.org/10.1016/j.ces.2007.08.055.

Paper II

ACS Sustainable Chemistry & Engineering

pubs.acs.org/journal/ascecg

Research Article

Process Simulations of High-Purity and Renewable Clean H_2 Production by Sorption Enhanced Steam Reforming of Biogas

Alma Capa, Yongliang Yan, Fernando Rubiera, Covadonga Pevida,* María Victoria Gil,* and Peter T. Clough

Cite This: ACS Sustainable Chem. Eng. 2023, 11, 4759−4775

Read Online

ACCESS | Metrics & More | Article Recommendations | Supporting Information

ABSTRACT: Renewable clean H_2 has a very promising potential for the decarbonization of energy systems. Sorption enhanced steam reforming (SESR) is a novel process that combines the steam reforming reaction and the simultaneous CO_2 removal by a solid sorbent, such as CaO, which significantly enhances hydrogen generation, enabling high-purity H_2 production. The CO_2 sorption reaction (carbonation) is exothermic, but the sorbent regeneration by calcination is highly endothermic, which requires extra energy. Biogas is one of the available carbon-neutral renewable H_2 production sources. It can be especially relevant for the energy integration of the SESR process since, due to the exothermic sorption reaction, the CO_2 contained in the biogas provides extra heat to the system, which can help to balance the energy requirements of the process. This work studies different process configurations for the energy integration of the SESR process of biogas for high-purity renewable H_2 production: (1) SESR with sorbent regeneration using a portion of the produced H_2 (SESR+REG_H_2), (2) SESR with sorbent regeneration using biogas (SESR+REG_BG), and (3) SESR with sorbent regeneration using biogas and adding a pressure swing adsorption (PSA) unit for hydrogen purification (SESR+REG_BG+PSA). When using biogas as fuel (Cases 2 and 3), these configurations were studied using air and oxy-fuel combustion atmospheres in the sorbent regeneration step, resulting in five case studies. A thermodynamic approach for process modeling can provide the optimal process operating conditions and configurations that maximize the energy efficiency of the process, which are the basis for subsequent optimization of the process at the practical level needed to scale up this technology. For this purpose, process simulations were performed using a steady-state plant model developed in Aspen Plus, incorporating a complex heat exchanger network (HEN) to optimize heat integration. A comprehensive parametric study assessed the effects of biogas composition, temperature, pressure, and steam to methane (S/CH_4) ratio on the process performance represented by the selected key performance indicators, i.e., H_2 purity, H_2 yield, CH_4 conversion, cold gas efficiency (CGE), net efficiency (NE), fuel consumption for the sorbent regeneration step, and CO_2 capture efficiency. H_2 with a purity of 98.5 vol % and a CGE of 75.7% with zero carbon emissions can be achieved. When adding a PSA unit, nearly 100% H_2 purity and CO_2 capture efficiency were achieved with a CGE of 77.3%. The use of oxy-fuel combustion during regeneration lowered the net efficiency of the process by 2.3% points (since it requires an air separation unit) but allowed the process to achieve negative carbon emissions.

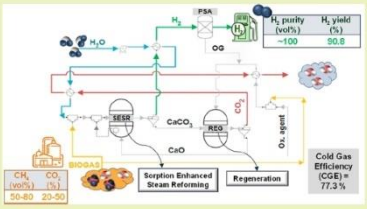

KEYWORDS: *Biogas, CH_4/CO_2 composition, Hydrogen, Sorption enhanced steam reforming, Process simulation, CO_2 capture*

INTRODUCTION

Hydrogen is a versatile feedstock and an attractive energy carrier, positioned as one of the main pillars for the imminent energy transition toward climate change mitigation.[1] However, most of the produced hydrogen comes from fossil resources, either by steam reforming (SR) of methane/natural gas and oil/naphtha or from coal gasification without CO_2 capture.[2] For instance, ~90 Mt of H_2 was used in 2020 and around 80% was produced from fossil fuels (all the remaining came from residual gases), mostly unabated, which resulted in 900 Mt CO_2 emitted in the production of H_2.[3] The conventional SR process usually performs at high temperatures (700−1000 °C) and pressures (15−40 bar). In this process, the endothermic reforming reaction takes place in high-alloy reformer tubes where the catalyst is placed, which in most cases is Ni based. The reformer operates using typical steam to carbon (S/C) ratios from 2 to 6, and external gas burners heat the reformer

Received: December 8, 2022
Revised: February 27, 2023
Published: March 11, 2023

https://doi.org/10.1021/acssuschemeng.2c07316
ACS Sustainable Chem. Eng. 2023, 11, 4759−4775

tubes.[4,5] The process is endothermic and renders low H_2 yield and purity prompting the need for a series of high- and low-temperature water−gas shift (WGS) reactors and hydrogen purification units.

Sorption enhanced steam reforming (SESR) is emerging as a novel intensification process of the conventional SR technology.[6] In the case of the sorption enhanced steam methane reforming (SESMR), in situ CO_2 capture by a solid sorbent material, such as CaO, is performed by eq 1, together with steam methane reforming (SMR, eq 2) and WGS (eq 3) reactions. Due to the addition of the sorbent, the equilibrium of SMR and WGS is shifted toward the forward direction according to Le Chatelier's principle, favoring not solely the increase in the H_2 productivity but also the H_2 purity and reactants conversion.[7] In addition, the overall reaction of SESMR is slightly exothermic (eq 4), which could entail a reduction in the external utility demand (i.e., external gas burners that are necessary for conventional SR reactors). Regeneration of the sorbent occurs through the reverse carbonation reaction of CaO (reverse of eq 1).

$$CaO_{(s)} + CO_2 \leftrightarrow CaCO_{3(s)} \quad \Delta H_r^0 = -178\,kJ\,mol^{-1} \tag{1}$$

$$CH_4 + H_2O \leftrightarrow CO + 3H_2 \quad \Delta H_r^0 = +206\,kJ\,mol^{-1} \tag{2}$$

$$CO + H_2O \leftrightarrow CO_2 + H_2 \quad \Delta H_r^0 = -41\,kJ\,mol^{-1} \tag{3}$$

$$CH_4 + 2H_2O + CaO_{(s)} \rightarrow 4H_2 + CaCO_{3(s)} \quad \Delta H_r^0 = -13\,kJ\,mol^{-1} \tag{4}$$

Hydrogen gains higher interest when produced using low- or zero-carbon energy sources,[1] which is imperative to fulfill climate change mitigation objectives. Indeed, different biomass resources have been proposed for the SESR process. Experimental works in the literature have studied bioethanol,[8−10] glycerol,[11−13] bio-oil from biomass pyrolysis,[14−17] or biogas[18,19] as feedstock. Biogas is a versatile raw material with a high potential to be utilized in reforming processes since it can be used as an alternative renewable source of CH_4.[20,21] Increasing interest in biogas also arises from reducing the dependence on fossil fuels and greenhouse gas emissions;[22] therefore, hydrogen production from biogas has great potential in a future-to-be CO_2 neutral or negative economy.[23] Biogas is produced from biomass, residues, or wastes by anaerobic digestion, being the gas generated in landfill sites also named biogas. Depending on its origin, it has a wide range of CH_4 (35−75 vol %) and CO_2 (25−55 vol %) contents, which are its major constituents, although it could contain other minority compounds such as H_2S, NH_3, siloxanes, and aromatics.[24] High CH_4 content biogas can directly generate heat or electricity, but low-grade biogas (low CH_4 content) is inappropriate for such purposes; hence, large quantities of poor-quality biogases are wasted by venting into the atmosphere.[25]

The main challenge of the SESR processes is the heat required for sorbent regeneration. In fact, the optimization of the energy demand in the process and the development and implementation of robust heat and energy recovery systems have been recently highlighted as key existing challenges for viable H_2 production by sorption enhanced processes.[26] As mentioned above, the SR reaction of methane is highly endothermic, but the WGS and the carbonation reactions are exothermic. Thus, the heat generated by the carbonation and WGS reactions balances the heat demand for reforming, so the reactor where the SESR step occurs is thermally neutral or slightly exothermic (eq 4). However, the subsequent sorbent regeneration step by the calcination reaction is endothermic, so overall the process requires energy.

Theoretically, the SESR of biogas is more exothermic than the SESR of pure methane since CO_2 in the biogas is also removed from the gas phase by the carbonation reaction[18] and provides additional heat into the system. It could be an advantage regarding the energy demand of the process. The CO_2 content in biogas can also have some drawbacks for the SESR process, such as a higher sorbent demand, a lower H_2 yield, or an increase in the equipment size, but these issues are out of the scope of the present work and need to be analyzed in a future techno-economic study of the process. However, to study the effect of the addition of CO_2 in the feeding, an energy analysis by simulation of the SESR process of biogas is needed to understand the thermodynamic limitations of the system under possible process configurations and optimize the energy efficiency.

Some works have performed simulation studies of the SESR process showing its advantages over SR regarding exergy efficiency. Tian et al.[27] reported the exergetic evaluation of the hydrogen production comparing SESR and conventional SR of acetic acid, finding a better performance (98.67% H_2 purity at 450−600 °C) and a 5% higher exergy efficiency in the SESR system. Tzanetis et al.[28] also compared the SESR with conventional SR of methane, finding an increase of 17.3% in the H_2 purity and 3.2% in the exergy efficiency. However, to optimize the energy efficiency of SESR processes, some works have proposed the coupling of SESMR with chemical looping combustion (CLC) for hydrogen production from methane. Alam et al.[29] proposed an efficient process for high purity hydrogen production by integrating SESMR with CLC obtaining an energy efficiency of 70.3%. Yan et al.[30] reported energy efficiency values of 72% for a process integrating SESMR with CLC and 74% for SESMR with oxy-fuel combustion integration. However, the CO_2 capture was higher when coupling CLC or oxy-fuel combustion to the SESMR process using air in the calcination reactor. Other authors have compared SESR and sorption enhanced chemical looping reforming (SECLR) of methane for hydrogen production, reporting higher H_2 yield and purity values in the case of SESMR, but lower energy requirements and higher CO_2 capture in the case of SECLR.[31,32] On the other hand, an autothermal sorbent regeneration process using combined combustion, methane reforming, and a hydrogen-selective membrane in the regenerator has been simulated by Ebneyamini et al.[33] Despite the possible improvements in energy efficiency by SESR integration with CLC or selective membranes use, those processes require additional devices, such as membrane reactors or separate reactors for reoxidation of the oxygen carrier. These unavoidably increase the equipment costs and provide less efficient heat integration.[34] A techno-economic evaluation of the overall processes should therefore be considered. In the case of the SESR of biogas for high purity hydrogen production, little work has been done on the topic, and studies addressing thermodynamic analysis and process simulations are very limited in the literature. Barelli et al.[35,36] performed a thermodynamic study of the hydrogen production with CO_2 capture of different gas mixtures, such as

https://doi.org/10.1021/acssuschemeng.2c07316
ACS Sustainable Chem. Eng. 2023, 11, 4759−4775

ACS Sustainable Chemistry & Engineering pubs.acs.org/journal/ascecg Research Article

syngas and biogas, reaching adiabatic reforming for methane contents in the feed gas of 55%−65% and obtaining hydrogen purity higher than 99% and energy efficiency of 72%. However, a simulation of the SESR process using biogas is still needed to understand the energy utilization under different process configurations, taking advantage of the additional heat that CO_2 in the biogas may provide to the system.

For this purpose, a thermodynamic approach to process modeling is needed to demonstrate the thermodynamic feasibility of the process and provide the optimal process operating conditions and configurations that maximize energy efficiency when using biogas as feedstock. These results will be crucial for future work on the dynamic analysis of the process under the optimal SESR configuration that enables the scaling-up of the technology. The present work hence proposes different process layouts for renewable hydrogen production from biogas SESR, targeting the recovery of the heat released in the reformer while maximizing CO_2 capture. The process has been designed to be energy self-sufficient, hence avoiding the use of external utilities. This work aims to investigate the thermodynamic limitations of the different case studies on a wide range of process conditions, being the kinetic limitations and detailed reactor/auxiliaries design out of the simulation scope. The SESR process was simulated in Aspen Plus, including sorbent regeneration for a cyclic operation and using a heat exchanger network (HEN) to recover the waste heat from the process. With the further ambition to reduce the CO_2 emissions, we have also addressed oxy-combustion capture. Thus, five possible cases studies using three different process configurations have been evaluated to address the potential energy efficiency of the SESR process for a wide range of biogas compositions while maximizing the CO_2 capture. A detailed parametric analysis on biogas compositions, reforming temperature, pressure, and steam to methane (S/CH_4) ratio effect on the process performance is included. Different key performance indicators (KPIs) are discussed for all cases, such as H_2 purity, H_2 yield, CH_4 conversion, cold gas efficiency (CGE), net efficiency (NE), fuel consumption for the sorbent regeneration, and CO_2 capture efficiency.

MODEL DEVELOPMENT AND PROCESS CONFIGURATIONS

Herein, an autothermal SESR process of biogas that includes a first stage of steam reforming coupled with in situ CO_2 capture and a second stage of sorbent regeneration is built in Aspen Plus V11 software (AspenTech). The equilibrium model developed assumes steady-state conditions. The model includes a HEN to recover all the possible heat from the process streams. Three different SESR flowsheet base configurations (Figure 1) are comprehensively analyzed in this section alongside the model design and the different case studies (i.e., using different atmospheres for sorbent recovery). The detailed Aspen Plus flowsheets for the five case studies are shown in the Supporting Information (SI).

Model Development. The thermodynamic modeling assumptions used as the base design of the process to develop the different flowsheets are collected in Table 1. Biogas is simulated as a mixture of CH_4 and CO_2, while the solid sorbent is simulated as pure CaO.

Using the baseline conditions shown in Table 1, the range of the different variables studied is shown in Table 2.

The base flowsheet of the process mainly consists of two reactors: a reformer (SESR) and a calciner (REG). In the SESR reactor, biogas is the feedstock, and H_2 is rich in the product due to coexistence of the SR (eq 2), WGS (eq 3), and carbonation for CO_2 capture (eq 1) reactions. Due to the CO_2 removal, the equilibrium of SR and WGS reactions shifts toward a higher H_2 production according to Le Chatelier's principle. Furthermore, owing to the extra content of CO_2 in the biogas, the carbonation reaction turns pivotal in the overall duty of the SESR unit, which could be highly exothermic when biogas is used as feedstock.[37] The model developed in this work includes the extra heat recovery from the SESR unit to achieve an autothermal operation, assuming in the flowsheet design a 10% of heat loss during the heat transfer.[30] This value agrees with the thermal efficiency of reverse flow reactors,

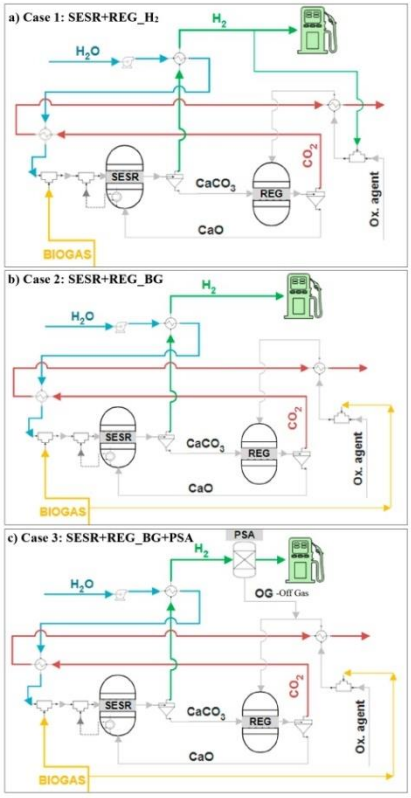

Figure 1. Simplified flow diagrams of the three base configurations proposed for the biogas SESR process. In Case 1 (SESR+REG_H_2), a fraction of the produced H_2 is used as fuel for the sorbent regeneration (a). In Case 2 (SESR+REG_BG), biogas is utilized as fuel for the sorbent regeneration (b). Finally, in Case 3 (SESR +REG_BG+PSA), biogas is used as fuel for the sorbent regeneration, and a PSA unit is included (c).

https://doi.org/10.1021/acssuschemeng.2c07316
ACS Sustainable Chem. Eng. 2023, 11, 4759−4775

Table 1. Design Assumption Made to Develop the Base Case Flowsheet in Aspen Plus

Parameters	Value	Unit
Biogas feed	0.76 (13.33)	kg/s (MW[a])
Biogas composition (CH_4/CO_2)	60/40	vol %
Water feed inlet temperature	25	°C
Water feed inlet pressure	1	bar
Molar Ca/C ratio	1.5	–
Reformer pressure	10	bar
Reformer temperature	600	°C
Reformer molar steam/CH_4	5.5	–
Reformer heat loss	10	%
Calciner temperature	850	°C
Calciner pressure	1	bar
Excess oxygen[b]	5	%
Air/oxygen inlet temperature	25	°C
Air/oxygen pressure	1	bar
Fuel feed inlet temperature[c]	25	°C
Fuel feed pressure	1	bar
Calcination conversion	100	%
Heat exchanger pinch	20	°C
Isentropic efficiency of compressors and water pump efficiency	83	%
Mechanical efficiency of compressors and pump driver efficiency	98	%

[a]Based on LHV of CH_4 (800 MJ/kmol) and H_2 (242 MJ/kmol). [b]This refers to the excess oxygen (vol %) used in the REG reactor for the combustion of the fuel for sorbent regeneration. [c]Unless H_2 is used as fuel, in which case it enters the REG reactor at the reforming temperature.

Table 2. Range in Which the Different Process Variables Are Analyzed

Parameters	Range	Unit
Biogas composition (CH_4/CO_2)	50/50–80/20	vol %
Reformer temperature	500–675	°C
Reformer pressure	1.5–25	bar
Reformer molar steam/CH_4	3–6.5	–

which is a reactor type suggested to be sustainable for exothermic reactions.[38] From a practical point of view, to recover the heat released from the SESR reactor, a fluidized bed heat exchanger, consisting of a fluidized bed with heat exchanger tubes immersed in it, could be used.[5,39] Likewise, heat pipes have been suggested for indirect heating of the calciner in the chemical looping technology[40−42] and recently also for SESMR.[30]

On the other hand, the spent sorbent, forming $CaCO_3$, is separated from the H_2-rich gas stream and sent to the REG reactor, where the sorbent is regenerated to CaO to ensure process operation in a cyclic fashion. The spent sorbent is calcined, which is an endothermic reaction (reverse of eq 1) favored at high temperatures and low pressures (i.e., >800 °C and ∼1 bar).[43] Therefore, the calciner requires a high amount of heat to regenerate the sorbent. The desired temperature for the decomposition of $CaCO_3$ to CaO can be achieved by supplying heat by either burning a fuel in the calciner or indirect heating.[44,45] As shown in Figure 1, this work focuses on the direct combustion of renewable fuel to cover the duty required of the REG reactor using two fuel options: hydrogen and biogas. Moreover, two combustion atmospheres are under study: air and oxy-fuel combustion. In the case of using biogas, it matches the composition of the biogas feeding the SESR reactor for each particular simulation. The direct combustion of additional fuel in the calcination reactor seems to be the most practical option for providing the necessary heat.[15] The extra fuel feeding REG corresponds to the minimum needed to fulfill the duty of this unit. Hence, combustion proceeds without incomplete oxidation products (i.e., CO, H_2, or elemental C) leaving the REG reactor.[23] This is controlled by using different design specifications. The regeneration temperature used is 850 °C unless otherwise specified, ensuring that the regeneration of CaO is performed at 1 bar since low pressures are favorable for the calcination reaction (reverse of eq 1).

It is well-known that CaO-based sorbents suffer from conversion decay over cycles due to sintering.[46,47] Similarly to calcium looping systems, sorbent deactivation in SESR is handled by more often replacing the sorbent and controlling the particle size of the sorbent material. However, this is a practical issue that does not apply to evaluate the thermodynamic feasibility, which is the purpose of the present work. In the simulation, an average carbonation conversion of 50% was assumed for the CaO-based sorbent, according to the results of cyclic SESR experiments shown in the literature.[48,49] It can be maintained by ensuring an efficient makeup flow of the fresh/spent sorbent particles under the experimental operation of the process. Besides, this value has been used to estimate the molar Ca/C ratio in the reformer during the simulation following the Ca/C ratio in the reformer in a recent simulation study on blue hydrogen production by SESMR.[30] Therefore, a molar Ca/C ratio of 1.5 is selected, where C refers to the carbon contained in both CH_4 and CO_2 in the biogas fed to the SESR unit. All the calcium accounted for the Ca/C molar ratio comes from the CaO, initially added in excess, circulating between SESR and REG.

The reformer (SESR) and calciner (REG) were simulated using RGibbs blocks, as suggested in other modeling studies in the literature.[23,30] The Aspen Plus flowsheets are shown in Figures S1−S6 of the Supporting Information. In this work, it is assumed that all the reactions in both reactors, SESR and REG, reach chemical equilibrium, and the entire process operates under a steady state. The chemical equilibrium of the reforming and regeneration reactors is calculated by minimization of the Gibbs free energy. The species considered were H_2, CH_4, CO, CO_2, H_2O, O_2, N_2, CaO, $Ca(OH)_2$, and $CaCO_3$. C_2H_4, C_2H_6, and C (solid carbon graphite to account for the possible formation of coke) were also in the product pool, but their concentrations at equilibrium were negligible under the studied conditions. Physicochemical properties of all the components included in the process are determined using Peng−Robinson's equation of state.

Furthermore, a HEN was designed to recover the maximum heat from the process streams with a minimum number of heat exchangers (Figures S1−S5 of Supporting Information). It aims not only to preheat the reactants but also to produce the steam needed for the reforming avoiding the energy penalty of its production. In the HEN, water is preheated in HE1 using the maximum heat extracted from the hydrogen stream from the SESR reactor while avoiding condensation by specifying 5 °C of superheat at the outlet of the hot stream. Any heat produced during steam condensation is considered non-recoverable heat.[23] Then, the evaporation continues in HE2 using the CO_2 stream from the REG reactor; another heat exchanger, H1 (which uses the heat released from the SESR

https://doi.org/10.1021/acssuschemeng.2c07316
ACS Sustainable Chem. Eng. 2023, 11, 4759−4775

Table 3. Case Studies Evaluated for Energy Integration of SESR Process of Biogas

Process configuration	Sorbent regeneration atmosphere	Sorbent regeneration fuel	H_2 purification
Case 1: SESR+REG_H2	Air	H_2	–
Case 2: SESR+REG_BG	Air	Biogas	–
	Oxy-fuel	Biogas	–
Case 3: SESR+REG_BG+PSA	Air	Biogas + PSA off-gas	PSA
	Oxy-fuel	Biogas + PSA off-gas	PSA

reactor), is used to complete the steam production when needed and to preheat the SESR reactants to reach the reaction temperature. A design specification calculates the minimum amount of energy required in HE2 from the CO_2-rich stream to force the duty of H1 to equal the amount of energy available from SESR (assuming 10% of heat losses). By doing this, the energy balance of the process is matched. Finally, the energy that remains in the CO_2 stream is used to preheat the inlet streams of the REG reactor, using a heat exchanger pinch of 20 °C to maximize the heat recovery from this stream. The exhausted hydrogen-rich gas is cooled down in a cooler (C1) to 25 °C to condensate and separate most of the water in a separation unit (SEP1). The dry H_2 stream is then ready for the downstream processing (i.e., purification, compression, etc.) according to the application.

Process Configurations. Three process configurations were designed (simplified diagrams shown in Figure 1) and five case studies compared (Aspen Plus flowsheets shown in Figures S1−S5 of Supporting Information). The description of each case study is summarized in Table 3. In the first configuration (Figure 1a), the use of a fraction of the produced H_2 as a renewable fuel to supply energy for sorbent regeneration through calcination is studied (SESR +REG_H_2), whereas in the second process configuration (Figure 1b) biogas is used for this purpose (SESR+REG_BG). In Case 1, SESR+REG_H_2, the recycled H_2 contains mainly hydrogen, unreacted CH_4, and trace quantities of CO and CO_2. The amount of hydrogen recycled to the REG reactor is calculated with a design specification to fulfill the energy requirement of the unit and to avoid incomplete oxidation products, as previously explained. In Case 2, SESR+REG_BG, the amounts of fuel (i.e., biogas) and oxidant agent needed are calculated similarly using design specifications. Moreover, in the third configuration, represented by Case 3 (Figure 1c), the dry hydrogen product (H2RICH) is further purified using a pressure swing adsorption (PSA) unit (SESR+REG_BG+PSA) to increase the hydrogen product purity up to levels that allow its use in applications as fuel cells. A compressor is placed before the PSA unit to maintain the inlet stream at a pressure higher than 25 bar, which is the typical operating pressure for PSA. In this work we have set a fixed backup pressure of 30 bar. The off-gas from the PSA unit (PSA-OG) contains mainly H_2 and CH_4 and trace quantities of CO and CO_2, and it is sent to the calciner to reduce the amount of additional biogas required as fuel. The separation efficiency of the PSA unit is set at 95%.[30] In practice, the recovery rate and purity of H_2 after PSA purification will depend on a range of factors (i.e., gas volume handled, adsorption material, temperature and pressure differences, etc.) and should take into account the presence of trace gases (i.e., CO) depending on the final H_2 application, but detailed modeling of the PSA unit is out of the scope of this work.

In all cases, a compressor with 83% isentropic efficiency and 98% mechanical efficiency[30] is placed to match the operating pressure of the reactor (which varies in the different simulations). Similarly, a water pump with the same efficiencies matches the pressure of the water stream used to produce the steam. Furthermore, the flow of oxidant agent used in the REG unit is controlled to meet a 5% excess of oxygen.[30] Thus, in the calciner, not only direct combustion using air is analyzed (Figures S1, S2, and S4 of Supporting Information), but also oxy-fuel combustion (30% O_2 and 70% CO_2 mole fraction gas supplied to REG reactor) is studied (Figures S3 and S5 of Supporting Information) to evaluate the reduction in CO_2 emissions. This resulted in a total of five scenarios: Cases 2 and 3 with direct oxy-fuel and air combustion and Case 1 with direct air combustion in the calciner. Due to the challenges associated with hydrogen in oxy-combustion (high temperatures and overheating, flame instability, flame blowout) derived from its broader flammability range, much higher adiabatic flame temperature, and higher flame propagation rate, the oxy-fuel scenarios have been restricted to biogas used as fuel.

Data Evaluation. Thermodynamic performance of the process is evaluated in terms of H_2 purity, H_2 yield, CH_4 conversion, cold gas efficiency (CGE), net efficiency (NE), fuel consumption in REG unit, and CO_2 capture efficiency. These parameters have been selected as the key process performance indicators (KPIs) of the biogas SESR process to compare all the case studies in this research work. H_2 purity is calculated by eq 5, where y_i is the molar content (N_2 free and on dry basis) of each species i in the outlet gas. H_2 yield represents the percentage of H_2 produced in the plant to the maximum H_2 production according to the SESR reaction stoichiometry, and it is calculated by eq 6, where $F_{H2,out}$ is the molar flow rate of hydrogen produced, and $F_{CH4,in}$ is the molar flow rate of methane fed in. CH_4 conversion is calculated by eq 7, where $F_{CH4,in}$ and $F_{CH4,out}$ are the molar flow rates of CH_4 in the inlet (BIOGAS) or outlet (H_2) streams, respectively.

$$H_2 \text{ purity (vol \%)} = 100 \cdot (y_{H2}/\Sigma y_i) \quad (5)$$

$$H_2 \text{ yield (\%)} = 100 \cdot (F_{H2,out}/(4 \cdot F_{CH4,in})) \quad (6)$$

$$CH_4 \text{ conversion (\%)} = 100 \cdot ((F_{CH4,in} - F_{CH4,out})/F_{CH4,in}) \quad (7)$$

CH_4, CO_2, and CO concentrations are also calculated by eq 8.

$$CH_4/CO_2/CO \text{(vol \%)} = 100 \cdot (y_{CH4/CO2/CO}/\Sigma y_i) \quad (8)$$

On the other hand, the CGE is calculated as the ratio between the chemical energy of the produced H_2 stream to the sum of the feed thermal input (chemical energy of the CH_4 feed consumed in the SESR reactor and the additional CH_4 required to meet the heat requirements of the REG reactor). CGE is calculated by eq 9, where $F_{CH_4,\text{additional}}$ is the molar flow rate of methane contained in the additional biogas fed in the calciner to meet the duty requirement of the REG unit. The

https://doi.org/10.1021/acssuschemeng.2c07316
ACS Sustainable Chem. Eng. 2023, 11, 4759−4775

ACS Sustainable Chemistry & Engineering pubs.acs.org/journal/ascecg Research Article

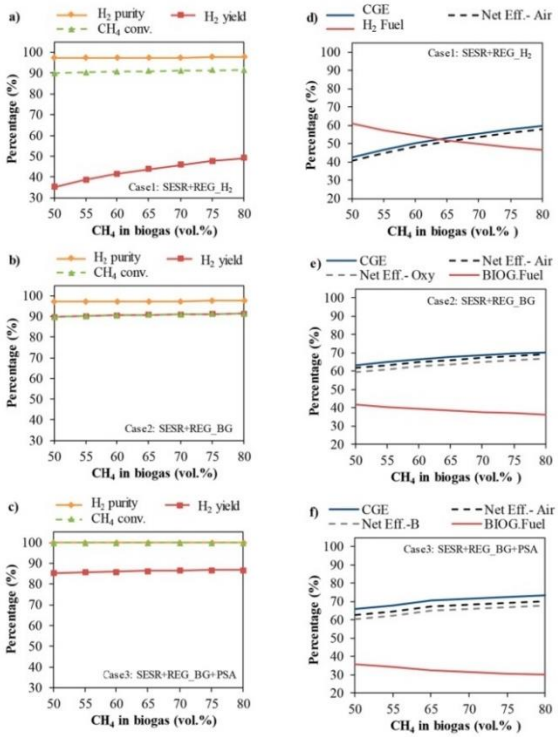

Figure 2. Effect of biogas composition on H_2 purity, H_2 yield, and CH_4 conversion (a–c) and on cold gas efficiency (CGE), net efficiency (NE, using both air, Net Eff. A, and oxy-combustion, Net Eff-B, in REG), and fuel consumption for sorbent regeneration (d–f) for the different process configurations studied: (a, d) use of a fraction of the produced hydrogen as fuel for sorbent regeneration (SESR+REG_H_2), (b, e) use of biogas as fuel for sorbent regeneration (SESR+REG_BG), and (c, f) addition of a PSA unit and use of biogas and off-gas (PSA-OG) for sorbent regeneration (SESR+REG_BG+PSA). SESR conditions: S/CH_4 = 5.5, T = 600 °C, P = 10 bar, and 50% sorbent excess.

LHV_{H_2} and LHV_{CH_4} are the lower heating value of hydrogen (242 MJ/kmol) and methane (800 MJ/kmol), respectively. NE is calculated by eq 10, where the electric utility requirement of the auxiliaries (P_e) is added to the CGE equation where a thermal to electric conversion efficiency (η_{elect}) of 50% is applied, and for the oxy-combustion scenarios, 160 kWh/t of oxygen is assumed as the auxiliary power consumption of the air separation unit (ASU).[30] The fuel consumption in Case 1 (SESR+REG_H_2) is calculated by eq 11, whereas in Case 2 (SESR+REG_BG) and Case 3 (SESR +REG_BG+PSA) it is calculated by eq 12.

$$\mathrm{CGE}\ (\%) = \left(\frac{F_{H_2,out}\cdot LHV_{H_2}}{(F_{CH_4,in} + F_{CH_4,additional})\cdot LHV_{CH_4}}\right)\cdot 100 \quad (9)$$

$$\mathrm{NE}\ (\%) = \left(\frac{F_{H_2,out}\cdot LHV_{H_2}}{(F_{CH_4,in} + F_{CH_4,additional})\cdot LHV_{CH_4} + \frac{P_e}{\eta_{elect}}}\right)\cdot 100 \quad (10)$$

$$\mathrm{Fuel}_{H_2,recycled}(\%) = \left(\frac{F_{H_2,recycled\ to\ REG}}{F_{H_2,recycled\ to\ REG} + F_{H_2,out}}\right)\cdot 100 \quad (11)$$

$$\mathrm{Fuel}_{Biogas}(\%) = \left(\frac{F_{Biogas\ fed\ to\ SESR}}{F_{Biogas\ fed\ to\ SESR} + F_{Biogas\ fed\ to\ REG}}\right)\cdot 100 \quad (12)$$

Finally, the CO_2 capture efficiency is calculated by eq 13, where $F_{CO2,captured}$ is the molar flow of CO_2 in the outlet CO_2 stream.

https://doi.org/10.1021/acssuschemeng.2c07316
ACS Sustainable Chem. Eng. 2023, 11, 4759−4775

$$\text{CO}_2 \text{ capture efficiency (\%)} = \left(\frac{F_{\text{CO}_2,\text{captured}}}{F_{\text{CH}_4,\text{in}} + F_{\text{CH}_4,\text{additional}} + F_{\text{CO}_2,\text{in}} + F_{\text{CO}_2,\text{additional}}} \right) \cdot 100 \quad (13)$$

RESULTS AND DISCUSSION

A sensitivity analysis has been performed for the three process configurations studied: (1) SESR with a H_2-fired calciner (SESR+REG_H_2), (2) SESR realized using biogas for the sorbent regeneration (SESR+REG_BG), and (3) SESR realized using biogas for the sorbent regeneration and with a pressure swing adsorption (PSA) unit (SESR+REG_BG +PSA); the cases were analyzed under air (all) and oxy-fuel combustion (when using biogas as fuel in the calciner), respectively, resulting in five case studies.

Effect of Biogas Compositions. The effects of the biogas compositions on H_2 purity, CH_4 conversion, and H_2 yield are shown in Figure 2a–c. The range of compositions studied increases to 80% of CH_4 since a high concentration of methane could be obtained after a slight biogas purification step, so this case is included for comparison purposes. In Cases 1 and 2 (Figure 2a and b, respectively), H_2 purity slightly increases from 97.1% to 97.6% for the high methane concentrations in the feed stream from 50 to 80 vol %. However, H_2 purity achieves nearly 100 vol % in Case 3 with the PSA purification unit (Figure 2c). This indicates biogas compositions do not significantly change the H_2 purity obtained after SESR, in good agreement with the experimental results reported in our previous proof of concept.[18] Furthermore, the results show that the recovery of the extra heat produced in the SESR step with the proposed designs allows for achieving autothermal operation of the reformer, independently of the biogas composition.

For Cases 1 and 2, CH_4 conversion increases slightly from 89.8% to 91.5% with CH_4 content in biogas, similarly to the H_2 purity, so the same results are obtained when a fraction of the produced H_2 is used as fuel for sorbent regeneration (Figure 2a) than when biogas is used as fuel in the REG reactor (Figure 2b). On the other hand, the addition of the PSA unit and the subsequent recycling of the off-gas (PSA-OG) to the REG reactor, i.e., Case 3, increase the CH_4 conversion to 100% since the unreacted CH_4 from the SESR unit is recirculated with PSA-OG to the REG reactor where it burns off (Figure 2c).

Finally, H_2 yield is very low in Case 1 (Figure 2a) due to the use of a fraction of the produced hydrogen as a renewable fuel to fulfill the energy duty of the sorbent regeneration stage. It increases from 35.2% to 49.1% in the range of the biogas compositions analyzed, i.e., 50 to 80 vol % of CH_4 (balance CO_2). The highest H_2 yield is obtained in Case 2, biogas used as fuel in REG (Figure 2b) without the PSA-OG recycle: 89.7% to 91.4% for 50 to 80 vol % of CH_4 in biogas. When recycling the PSA-OG in Case 3 (Figure 2c), the H_2 yield lowers since the off-gas contains not only the unreacted CH_4 from SESR but also a small fraction of H_2 (we assumed a PSA efficiency of 95%), and it increases from 85.3% to 86.9% for 50 to 80 vol % of CH_4 in biogas. Therefore, the composition of biogas has little effect on the H_2 yield, in agreement with the slight increase in CH_4 conversion.

The efficiencies, CGE and NE, for the different configurations and the percentage of fuel consumed for sorbent regeneration are shown in Figure 2d–f as a function of the biogas composition (50 to 80 vol % of CH_4, balance CO_2). Process configurations have been evaluated using air (all) and oxy-combustion (when using biogas as fuel) atmospheres. The only differences detected in the results between both combustion atmospheres are in the net efficiency of the overall process, due to the additional auxiliary power consumption of the air separation unit (ASU) in the case of oxy-fuel combustion. This small difference in NE is explained because the direct heating approach relies on a sorbent regeneration by decreasing the CO_2 partial pressure during the direct combustion of the fuel in the calciner at a temperature <900 °C.

In Case 1, where produced H_2 is used as fuel in REG, CGE increases a total of 16.8%, from 42.5% to 59.4%, with CH_4 content in the biogas (Figure 2d). In Case 2 (Figure 2e), where biogas is directly combusted in the calciner, CGE increases from 63.2% to 70.3% as CH_4 content in the biogas increases, meaning a total increase of 7.1%. Finally, for Case 3 (Figure 2f), when a PSA unit is utilized, CGE increases from 66.1% to 73.5%, which means a total increase of 7.4%. The increasing tendency in the CGE value with CH_4 content in the biogas agrees with the results reported by Kong et al.[23] for biogas conversion to H_2 using chemical looping (CL) technology. CGE values are dependent on the amount of fuel used in REG, so they indicate that the use of biogas as renewable fuel for sorbent regeneration (Case 2) renders better results than the use of produced H_2 (Case 1). On the other hand, Case 3 has the highest CGE value due to the positive effect of the further H_2 purification with the PSA unit and the subsequent recycling of the off-gas to the REG reactor. It is explained because the recycle allows a notable decrease in the fuel consumption (Figure 2f) compared to other configurations. NE values follow the same increasing tendency with the CH_4 content in the biogas as those for CGE. When combustion is carried out under an air atmosphere, in Cases 1 and 2, NE is 1.6% points below CGE due to the electric utility requirement of the auxiliaries considered. However, NE is 3.3% lower than CGE for Case 3 due to the additional compressor needed to match the pressure required by the PSA unit. When combustion in REG is carried out under oxy-combustion conditions, NE is 2.3%–2.5% lower than that obtained for the air atmosphere due to the energy penalty of the ASU.

On the other hand, Table 4 shows the effect of the biogas composition on the heat recovery from the SESR reactor. The amount of energy recovered from SESR varies from 3.9 MW (50 vol % CH_4 in biogas) to 2.5 MW (80 vol % CH_4 in biogas) for the same amount of biogas treated (100 kmol/h). This

Table 4. Effect of Biogas Composition on Heat Recovered from SESR (Heat Losses Considered)[a]

Biogas composition	Heat recovered from SESR (MW)
50% CH_4–50% CO_2	3.9
55% CH_4–45% CO_2	3.7
60% CH_4–40% CO_2	3.4
65% CH_4–35% CO_2	3.2
70% CH_4–30% CO_2	3.0
75% CH_4–25% CO_2	2.8
80% CH_4–20% CO_2	2.5

[a]SESR conditions: S/CH_4 = 5.5, T = 600 °C, P = 10 bar, and 50% sorbent excess.

https://doi.org/10.1021/acssuschemeng.2c07316
ACS Sustainable Chem. Eng. 2023, 11, 4759–4775

ACS Sustainable Chemistry & Engineering pubs.acs.org/journal/ascecg Research Article

Table 5. Excess of Heat Not Used That Is Remaining in CO_2 Stream as a Function of Biogas Composition[a]

	Excess heat not used in CO_2 stream (MW)		
Biogas composition	Case 1: SESR+REG_H_2	Case 2: SESR+REG_BG	Case 3: SESR+REG_BG + PSA
50% CH_4–50% CO_2	1.8	1.7	1.7
55% CH_4–45% CO_2	1.5	1.4	1.5
60% CH_4–40% CO_2	1.3	1.2	1.2
65% CH_4–35% CO_2	1.0	1.0	1.0
70% CH_4–30% CO_2	0.7	0.8	0.8
75% CH_4–25% CO_2	0.4	0.6	0.6
80% CH_4–20% CO_2	0.1	0.4	0.4

[a]SESR conditions: S/CH_4 = 5.5, T = 600 °C, P = 10 bar, and 50% sorbent excess.

results from a balance between the carbonation and reforming reactions: when CO_2 content in biogas is higher, carbonation occurs to a greater extent, and more heat is released in the SESR reactor. These results explain the higher excess heat in the final CO_2 stream for biogas with lower concentrations of CH_4 that is shown in Table 5; more heat is recovered from the SESR reactor, and hence more heat remains in the CO_2 stream. The excess heat in the outlet CO_2 stream has been calculated as the maximum recoverable heat while ensuring the avoidance of condensation by specifying 5 °C of superheat at the outlet of the hot stream; i.e., any heat produced during steam condensation is considered nonrecoverable heat.[23] As mentioned above, more heat is available in this stream for the lower CH_4 content in biogas, highlighting the potential interest of using low grade biogas compared to natural gas due to heat recovery from this hot stream.

Therefore, if a waste heat recovery system was employed to recover the heat available in the final CO_2 stream, the overall CGE values of the process could increase for all biogas compositions to similar values to those reached with higher methane concentrations. It has been demonstrated as an example for Case 3 with air regeneration and shown in Figure 3, where the surplus heat in the outlet CO_2 stream has been employed in the regeneration reactants preheating.

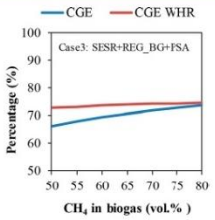

Figure 3. Comparison of the CGE with (red line) and without (blue line) waste heat recovery (WHR) from the CO_2 stream for the Case 3 (SESR+REG_BG+PSA).

Effect of SESR Reactor Temperature. The effects of the reforming temperature on H_2 purity, CH_4 conversion and H_2 yield, CGE, NE, and percentage of fuel consumed by sorbent regeneration are shown in Figure 4a–f. The results for H_2 purity, CH_4 conversion, H_2 yield, CGE, and fuel consumption remain unchanged when using air or oxy-combustion atmospheres for the sorbent regeneration, and only NE is affected. In Cases 1 and 2 (Figure 4a and b), where H_2 and biogas are used as fuels for regeneration, respectively, without a PSA unit, H_2 purity increases from 91.0% to 98.3% as the SESR temperature rises from 500 to 625 °C due to the endothermic nature of the SR reaction (eq 2). When the temperature further increases from 625 up to 675 °C, H_2 purity slightly decreases (by ∼0.4%) since the enhancement effect of the in situ CO_2 capture is thermodynamically unfavorable at higher temperatures because the carbonation reaction is exothermic (eq 1).[16,50] In Case 3 (Figure 4c), where biogas is used as fuel for regeneration but adding a PSA step, H_2 purity achieves nearly 100 vol % for all SESR temperatures due to the PSA unit, which performs a further purification of the hydrogen rich stream.

CH_4 conversion in Cases 1 and 2 significantly increases from 71.8% to 94.5% as SESR temperature increases up to 625 °C, also due to the endothermic SR reaction; afterward, it only slightly increases with a further increase in temperature (by ∼0.4%). With the addition of the PSA unit and the use of the off-gas (PSA-OG) in REG (Case 3), the CH_4 conversion reaches a constant value of 100% for all SESR temperatures (Figure 4c) since PSA-OG contains the unreacted CH_4 from SESR, which then burns in the REG reactor.

On the other hand, the lowest H_2 yield is obtained in Case 1 due to the recycling of part of the H_2 produced in SESR as a fuel for the REG reactor. H_2 yield increases from 31.0% to 41.4% with the increase in the SESR temperature from 500 to 600 °C since higher temperatures favor the reforming reaction and, consequently, the methane conversion and hydrogen production. A faster increase is observed from 600 to 625 °C and then is kept around 50% above 625 °C. In Cases 2 and 3, H_2 yield also increases faster up to 625 °C, reaching values of 94.4% and 89.7%, respectively. As temperature further increases, a slight increase is seen up to 94.7% in Case 2 and 89.9% in Case 3. As explained above, when PSA-OG is combusted (Case 3), the H_2 yield is slightly lower, since the off-gas also contains a small fraction of H_2 because the PSA unit efficiency is 95%.

The higher increase detected in the H_2 yield value from 600 to 625 °C in Case 1 (Figure 4a) is related to the formation of solid $Ca(OH)_2$ below 600 °C since its formation is thermodynamically disfavored above 600 °C because the lime hydration reaction (eq 14) is exothermic.[51]

$$CaO_{(s)} + H_2O_{(l)} \leftrightarrow Ca(OH)_{2(s)} \quad \Delta H_r^0 = -67\,\mathrm{kJ\,mol^{-1}} \tag{14}$$

As can be seen in Table 6, the excess sorbent not converted to $CaCO_3$ is in the form of $Ca(OH)_2$ below 600 °C but in the form of CaO above that temperature. It means that at lower SESR temperatures, $Ca(OH)_2$ is formed alongside $CaCO_3$ by carbonation, and both need to be regenerated and converted to CaO in the REG reactor. It requires more energy than that

https://doi.org/10.1021/acssuschemeng.2c07316
ACS Sustainable Chem. Eng. 2023, 11, 4759–4775

ACS Sustainable Chemistry & Engineering pubs.acs.org/journal/ascecg Research Article

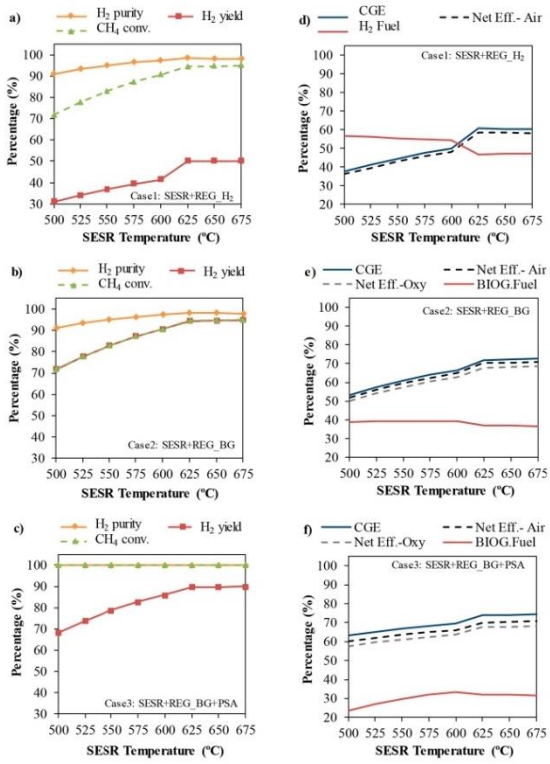

Figure 4. Effect of SESR temperature on H_2 purity, H_2 yield, and CH_4 conversion (a–c) and on cold gas efficiency (CGE), net efficiency (NE, using both air, Net Eff. A, and oxy-combustion, Net Eff-B, in REG), and fuel consumption for sorbent regeneration (d–f) for the different process configurations studied: (a, d) use of a fraction of the produced hydrogen as fuel for sorbent regeneration (SESR+REG_H_2), (b, e) use of biogas as fuel for sorbent regeneration (SESR+REG_BG), and (c, f) addition of a PSA unit and use of biogas and off-gas (PSA-OG) for sorbent regeneration (SESR+REG_BG+PSA). SESR conditions: S/CH_4 = 5.5, P = 10 bar, biogas = 60/40 vol % CH_4/CO_2, and 50% sorbent excess.

Table 6. Effect of SESR Temperature on Composition of Solids Circulating between SESR and REG[a]

	Solids composition at SESR outlet (%)		
SESR Temperature (°C)	$CaCO_3$	CaO	$Ca(OH)_2$
500	55.4	0.0	44.6
525	57.7	0.0	42.3
550	59.8	0.0	40.2
575	61.4	0.0	38.6
600	62.7	0.0	37.3
625	64.1	35.9	0.0
650	63.9	36.1	0.0
675	63.4	36.6	0.0

[a]SESR conditions: S/CH_4 = 5.5, P = 10 bar, biogas = 60/40 vol % CH_4/CO_2, and 50% sorbent excess.

needed when only $CaCO_3$ is formed and the unreacted sorbent remains as CaO. Therefore, more energy needs for REG means more H_2 needs to be recycled to cover the duty of the REG reactor at lower temperatures which, in turn, has a negative impact on H_2 yield.

Figure 4d–f shows that CGE and NE follow a similar tendency than H_2 yield. The effect of the $Ca(OH)_2$ formation at lower temperatures can be observed not only in Case 1 when recycling H_2 to REG but also in Cases 2 and 3 when using biogas as fuel in REG, affecting the efficiency values. However, the impacts for Cases 2 and 3 are lower because the heating value of biogas is higher than that of hydrogen, and the additional amount of biogas needed as fuel in those cases is lower, as observed in the fuel consumption in Figure 4d–f. On the other hand, low operating temperatures below 625 °C favor CO_2 removal according to the thermodynamics leading

https://doi.org/10.1021/acssuschemeng.2c07316
ACS Sustainable Chem. Eng. 2023, 11, 4759–4775

to a very low CO_2 content in the SESR outlet gas (Figure 5b). As reported by He et al.,[50] in the low temperature range, the

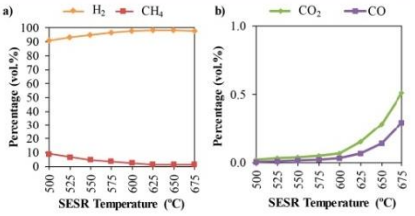

Figure 5. Effect of SESR temperature on H_2 and CH_4 concentrations (a) and CO_2 and CO concentrations (b) in the outlet gas from the SESR reactor in Case 1. SESR conditions: S/CH_4 = 5.5, P = 10 bar, biogas = 60/40 vol % CH_4/CO_2, and 50% sorbent excess.

endothermic reaction of methanation is favored by thermodynamics and might make an important contribution to CH_4 formation. Consequently, a higher content of CH_4 can be seen in the product gas of the SESR reactor at lower temperatures (Figure 5a).

Figure 4d–f shows that CGE increases noticeably as the SESR temperature increases up to 625 °C, as a consequence of the increase in methane conversion with temperature. At higher temperatures, only small variations (~0.5%) are observed. This is also in agreement with the decrease in the fuel consumption in REG for Cases 1 and 2 (Figure 4d and 4f) with the temperature increase due to a narrower temperature window between the reformer and calciner at a higher SESR temperature. However, in Case 3, with PSA-OG use in REG, the fuel consumption increases up to 600 °C (Figure 4f), and hence, the increase in the efficiency with temperature is less pronounced since it is affected by the change in the PSA-OG composition with the SESR temperature. As the temperature increases in the reformer, CH_4 conversion also increases, and less unreacted CH_4 is present in PSA-OG, which, in turn, enriches the off-gas in H_2. Conversely, at low SESR temperatures, the content of CH_4 in the PSA-OG is higher, the calorific value of the PSA-OG increases, and the process requires a lower amount of biogas as fuel for the sorbent regeneration. The overall positive tendency in the efficiency would result from the overall energy balance since, at higher SESR temperature, the solids circulating between SESR and REG are at closer temperature boosting the fulfilment of the REG energy requirement. Besides, it has been suggested in the literature that an increase in the carbonation reactor temperature could improve the efficiency of a plant involving carbonation–calcination cycles.[36] The CGE values at 625 °C are 60.7% and 72.0% in Cases 1 and 2, respectively, while it reaches 74.3% at 675 °C in Case 3. The addition of a PSA unit improves the efficiency due to the utilization of PSA-OG to provide more heat to the system. NE values when using air combustion in REG are lower than CGE values by ~1.80% in Cases 1 and 2 and 3.5% in Case 3. This is due to the additional compressor needed in Case 3 to match the pressure required by the PSA unit. When using oxy-combustion, the NE lowers (2.4% points) compared to the use of air due to the penalty associated with the oxygen production in the ASU.

The amount of energy recovered from the SESR reactor as a function of temperature decreases from 4.0 MW at 500 °C to 1.8 MW at 675 °C (see Table S1 of the Supporting Information). As the SESR temperature increases, so does the methane conversion, and the reforming reaction governs the heat balance. However, at lower temperatures, the carbonation reaction drives the heat balance since reforming is not favored; therefore, more heat released by carbonation is available in the SESR reactor. In addition, at lower temperatures, not only carbonation releases heat but also lime hydration that is slightly exothermic, and more heat is therefore available in SESR for recovery.

Effect of Pressure. Since high-pressure operation is a common practice in large-scale applications to reduce the reactor size and cost of H_2 production,[52] pressure is an important parameter to address. Furthermore, higher operating pressures could be of interest for SESR to apply a pressure swing to regenerate the CO_2 sorbent instead of increasing the temperature.[53] The effects of the reforming pressure on H_2 purity, CH_4 conversion, and H_2 yield for the different process configurations are shown in Figure 6a–c. In Cases 1 and 2 (Figure 6a and b), H_2 purity has a value of 99.0 vol % between 1.5 and 5 bar, decreasing until 91.4 vol % as pressure increases up to 25 bar. In Case 3 (Figure 6c), when a PSA unit is included, H_2 purity shows values of 100% along the pressure range since H_2 purity increases due to the additional capture step.

CH_4 conversion slightly decreases from 98.9% to 96.7% as SESR pressure increases from 1.5 to 5 bar in Cases 1 and 2. At higher pressures, CH_4 conversion decreases very sharply as pressure increases from 5 to 25 bar until a value of 73.0%. In agreement with the literature,[54] as pressure increases, the CH_4 conversion and H_2 purity decrease since SESR is thermodynamically favored at lower pressure due to the rise in the number of gas moles associated with the overall reaction which involves SMR and carbonation.[55] In addition, an increase in pressure promotes the formation of methane by the methanation reaction,[17,53] hence increasing the content of CH_4 in the gas coming out from SESR (Figure 7a). In Case 3 (Figure 6c), when a PSA unit is added, CH_4 conversion shows values of 100% for all pressures since the unconverted CH_4 from the SESR reactor is later used as fuel in the REG reactor through the PSA-OG combustion.

Regarding the H_2 yield, it also shows higher values at pressures of 1.5–5 bar, decreasing as pressure increases up to 25 bar. The highest H_2 yield values are obtained in Case 2 when only biogas is used as fuel in the REG reactor (Figure 6b), decreasing H_2 yield values from 98.7% at 1.5 bar to 96.7% at 5 bar (then decreasing until 73.0% at 25 bar). In Case 3 (Figure 6c), H_2 yield slightly lowers from 93.8% at 1.5 bar to 91.9% at 5 bar, decreasing down to 69.3% at 25 bar, due to the combustion of a small fraction of H_2 with the PSA-OG. Finally, in Case 1, H_2 yield is much lower, ranging from 51.3% at 1.5 bar to 50.4% at 5 bar (decreasing down to 33.9% at 25 bar) (Figure 6a) since a fraction of the produced hydrogen is used as fuel in the REG reactor. The decrease in this parameter above 5 bar is in accordance with the tendency observed for the CH_4 conversion and H_2 purity.

Higher electrical efficiency is expected in a solid oxide fuel cell (SOFC) when using H_2 produced at high pressure, as reported by Diglio et al.[52] Moreover, if the H_2 stream is going to be used in phosphoric acid fuel cells (PAFC) or low-temperature proton exchange membrane fuel cells (LT-

https://doi.org/10.1021/acssuschemeng.2c07316
ACS Sustainable Chem. Eng. 2023, 11, 4759–4775

ACS Sustainable Chemistry & Engineering pubs.acs.org/journal/ascecg Research Article

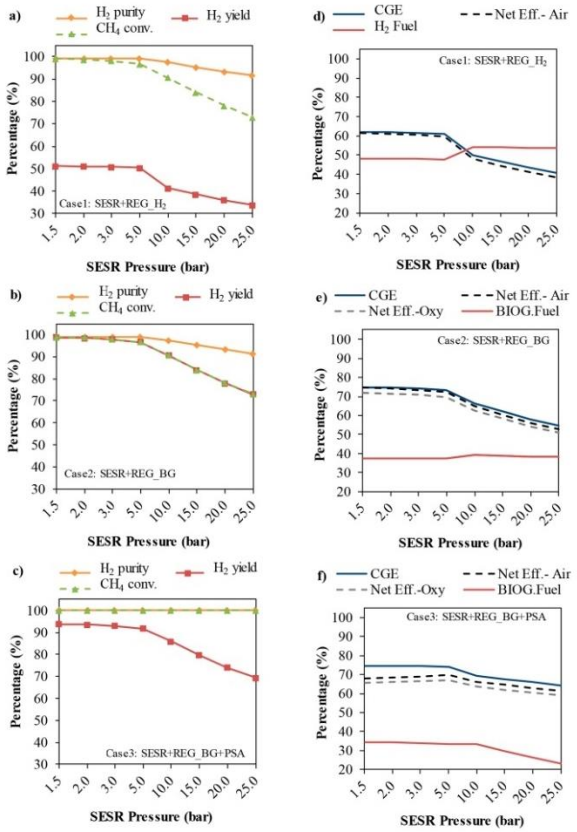

Figure 6. Effect of SESR pressure on H_2 purity, H_2 yield, and CH_4 conversion (a–c) and on cold gas efficiency (CGE), net efficiency (NE, using both air, Net Eff. A, and oxy-combustion, Net Eff-B, in REG), and fuel consumption for sorbent regeneration (d–f) for the different process configurations studied: (a, d) use of a fraction of the produced hydrogen as fuel for sorbent regeneration (SESR+REG_H_2), (b, e) use of biogas as fuel for sorbent regeneration (SESR+REG_BG), and (c, f) addition of a PSA unit and use of biogas and off-gas (PSA-OG) for sorbent regeneration (SESR+REG_BG+PSA). SESR conditions: S/CH_4 = 5.5, T = 600 °C, biogas = 60/40 vol % CH_4/CO_2, and 50% sorbent excess.

PEMFC), where the CO content in the H_2 stream is critical, another way to achieve lower CO concentrations could be to use higher operating pressures.[53] Therefore, the process layout proposed in Case 3 could be interesting when producing H_2 for fuel cell applications, since H_2 purity and CH_4 conversion are 100% regardless the process pressure. However, the negative impact of high pressure values on the H_2 yield should be carefully considered.

Figure 6d–f shows that CGE and NE follow a similar trend to H_2 yield. CGE decreases as pressure increases following the decrease in methane conversion and, hence, in hydrogen production. In Cases 1 and 2 (Figure 6d and 6e), CGE and NE values when air combustion is used in REG are close at low SESR pressures (1.5–5 bar) due to the lower workload required for the compression. At higher operating pressures (5–25 bar), NE for combustion in air is 1.5% to 2.3% lower than CGE as a consequence of the increase in the workload of the auxiliaries with process pressure. In Case 3 (Figure 6f), the PSA unit has an apparent impact on the net efficiency of the whole process. When air is used in REG, NE lowers from 6.8% to 4.4% below CGE in the pressure range of 1.5–5 bar and 3% at higher pressures. The impact of the PSA is more noticeable at low pressures because the gap between the process and PSA pressure is higher, requiring much more work in the compressor to match both pressures upstream of the SESR unit. The slight increase in NE between 1.5 and 5 bar responds

https://doi.org/10.1021/acssuschemeng.2c07316
ACS Sustainable Chem. Eng. 2023, 11, 4759–4775

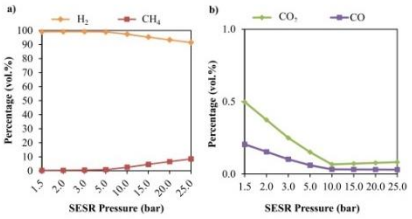

Figure 7. Effect of SESR pressure on H_2 and CH_4 concentrations (a) and CO_2 and CO concentrations (b) in the gas coming out from the SESR reactor. SESR conditions: S/CH_4 = 5.5, T = 600 °C, biogas = 60/40 vol % CH_4/CO_2, and 50% sorbent excess.

to the slightly lower gap as pressure increases. In Case 3, fuel consumption decreases when pressure increases above 5 bar. A higher content of CH_4 in PSA-OG and, hence, a higher calorific value of the off-gas reduces the amount of biogas required as fuel for sorbent regeneration. In the cases using biogas as fuel, a lower value (2.4%) of NE when using oxy-combustion in REG is explained by the penalty of the ASU.

For pressures above 5 bar, the formation of $Ca(OH)_2$ is observed under simulation conditions (Table 7). As reported

Table 7. Effect of SESR Pressure on Composition of Solids Circulating between SESR and REG[a]

	Solids composition at SESR outlet (%)		
SESR pressure (bar)	$CaCO_3$	CaO	$Ca(OH)_2$
1.5	65.1	34.9	0.0
2	65.3	34.7	0.0
3	65.3	34.7	0.0
5	65.0	35.0	0.0
10	62.7	0.0	37.3
15	60.1	0.0	39.9
20	57.7	0.0	42.3
25	55.7	0.0	44.3

[a]SESR conditions: S/CH_4 = 5.5, T = 600 °C, biogas = 60/40 vol % CH_4/CO_2, and 50% sorbent excess.

above (see the Effect of SESR Reactor Temperature section), there is a marked change in the analyzed variables between 5 and 10 bar in Figure 9, which is explained by the formation of $Ca(OH)_2$. When $Ca(OH)_2$ is formed, more heat for regeneration is needed, decreasing the efficiency of the process and increasing the fuel needed in the REG reactor. As explained above, the effect of $Ca(OH)_2$ formation is more pronounced when the hydrogen-rich stream is used as fuel (Figure 6a) than when using biogas (Figure 6e and f) because the heating value of biogas is higher than that of hydrogen.

The amount of energy recovered from the SESR reactor (see Table S2 of the Supporting Information) is 2.0 MW in the 1.5 to 5 bar pressure range. As pressure increases from 5 to 25 bar, the energy recovered increases from 2.0 to 3.7 MW. As the SESR pressure increases, the methane conversion during SESR decreases, and less heat is consumed by the reforming reaction, so there is more heat released by carbonation available for recovery.

Effect of Steam to Methane (S/CH_4) Ratio. Steam is usually fed beyond its stoichiometric limit to promote hydrogen productivity and prevent coking.[56] Therefore, a wide range of S/CH_4 ratios (3–6.5) has been studied. The effects of the S/CH_4 ratio on H_2 purity, CH_4 conversion, and H_2 yield for the different process configurations are shown in Figure 8a–c. For Cases 1 and 2, H_2 purity increases up to 97.9 vol % for S/CH_4 between 3 and 5 (Figure 8a and b), followed by a slight decrease, and finally increases up to 98.3 vol % at a S/CH_4 ratio of 6.5. In Case 3, H_2 purity reaches a value of 100% for all S/CH_4 ratios (Figure 8c) due to the PSA unit purifying H_2. The effect of the S/CH_4 ratio on the H_2 purity is in agreement with the literature since higher CH_4 conversion leads to higher H_2 production and less off-gas methane contaminant content.[57]

CH_4 conversion also increases with the S/CH_4 ratio since higher amounts of steam favor both steam reforming (eq 2) and water–gas shift (eq 3) reactions.[56] In Cases 1 and 2, CH_4 conversion increases from 76.5% to 94.0% as the S/CH_4 ratio increases from 3 to 6.5. However, for Case 3, CH_4 conversion reaches a value of 100% for all S/CH_4 ratios because the recycle of PSA-OG allows burning the unreacted CH_4 from SESR in the REG reactor. Therefore, by increasing the S/CH_4 ratio, the CH_4 conversion significantly increases because the excess steam shifts the reforming equilibrium toward a higher feedstock conversion.

On the other hand, H_2 yield increases with the S/CH_4 ratio in Cases 2 and 3 (Figure 8b and c). In Case 2, it shows higher values, increasing from 76.5% to 94.0% in the 3–6.5 S/CH_4 ratio range, while in Case 3, it increases from 72.6% to 89.3% as the S/CH_4 ratio increases from 3 to 6.5. This lower value in Case 3 is explained because a small fraction of the H_2 produced is burned while recycling PSA-OG to the REG reactor due to the assumption of 95% separation efficiency of the PSA unit. However, in Case 1 (Figure 8a), H_2 yield is lower than in the other two configurations due to hydrogen consumption in REG, as already explained. Its value is around 50% for S/CH_4 ratios between 3 and 5, and it notably decreases to 39.8% for higher S/CH_4 values due to $Ca(OH)_2$ formation (Table 8). This effect, as explained above, is stronger in the case of using H_2 for sorbent regeneration (as compared to biogas) since hydrogen has a lower heating value, and hence, a higher amount of fuel is needed.

The effect of the S/CH_4 molar ratio on the SESR reactor outlet gas composition is shown in Figure 9. Higher S/CH_4 molar ratios increase the H_2 concentration while reducing the CH_4 content (Figure 9a), as it has been previously reported in the literature.[19] On the other hand, the CO_2 and CO concentrations remain almost unchanged for the S/CH_4 range evaluated (Figure 9b), indicating that carbonation proceeds satisfactorily, from a thermodynamic point of view, in an atmosphere with steam excess.

The results corresponding to CGE and NE, as well as fuel consumption for sorbent regeneration, are shown in Figure 8d–f. The effect of the $Ca(OH)_2$ formation is also apparent in those plots since it forms at S/CH_4 ratios higher than 5.25 (Table 8). The lowest fuel consumption in REG is achieved when a PSA unit is added to the process due to the PSA-OG recycling, i.e., Case 3 (Figure 8f), which corresponds to the highest process efficiencies of the three studied designs. It should be highlighted that the heat content of PSA-OG can reduce significantly the fuel consumption at low S/CH_4 ratios. In Case 3, CGE decreases from 76.5% to 74.4% as S/CH_4 increases from 3 to 5, then to 68.3% at a S/CH_4 ratio of 6.5. When using a lower S/CH_4 ratio, the content of CH_4 in the

https://doi.org/10.1021/acssuschemeng.2c07316
ACS Sustainable Chem. Eng. 2023, 11, 4759–4775

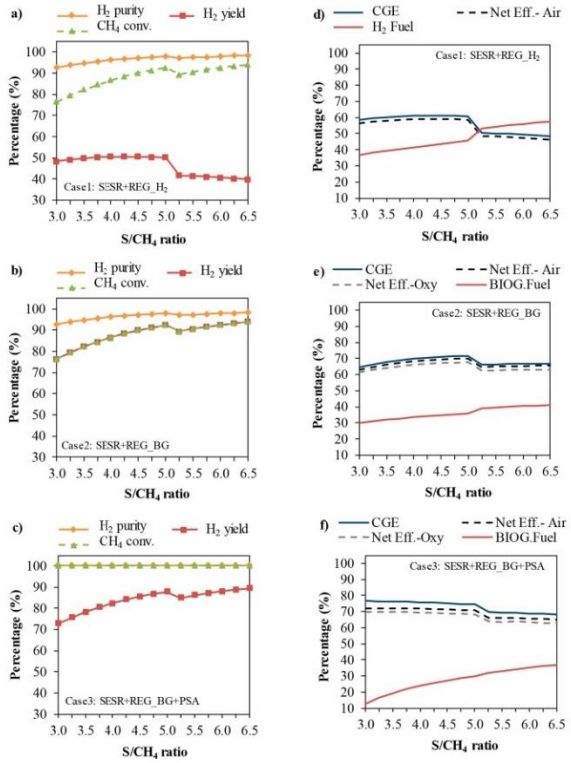

Figure 8. Effect of S/CH_4 on H_2 purity, H_2 yield, and CH_4 conversion (a–c) and on cold gas efficiency (CGE), net efficiency (NE, using both air, Net Eff. A, and oxy-combustion, Net Eff-B, in REG), and fuel consumption for sorbent regeneration (d–f) for the different process configurations studied: (a, d) use of a fraction of the produced hydrogen as fuel for sorbent regeneration (SESR+REG_H_2), (b, e) use of biogas as fuel for sorbent regeneration (SESR+REG_BG), and (c, f) addition of a PSA unit and use of biogas and off-gas (PSA-OG) for sorbent regeneration (SESR +REG_BG+PSA). SESR conditions: 600 °C, P = 10 bar, biogas = 60/40 vol % CH_4/CO_2, and 50% sorbent excess.

Table 8. Effect of S/CH_4 on Composition of Solids Circulating between SESR and REG[a]

	Solids composition at SESR outlet (%)		
S/CH_4 ratio	$CaCO_3$	CaO	$Ca(OH)_2$
3.00	57.1	42.9	0.0
3.50	59.4	40.6	0.0
4.00	61.2	38.8	0.0
4.50	62.5	37.5	0.0
5.00	63.5	36.5	0.0
5.25	62.3	0.0	37.7
5.50	62.7	0.0	37.3
6.00	63.5	0.0	36.5
6.50	64.1	0.0	35.9

[a]SESR conditions: 600 °C, P = 10 bar, biogas = 60/40 vol % CH_4/CO_2, and 50% sorbent excess.

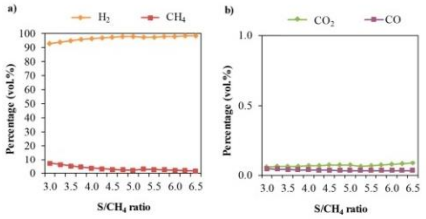

Figure 9. Effect of S/CH_4 on H_2 and CH_4 concentrations (a) and CO_2 and CO concentrations (b) in the gas coming out from the SESR reactor. SESR conditions: 600 °C, P = 10 bar, biogas = 60/40 vol % CH_4/CO_2, and 50% sorbent excess.

https://doi.org/10.1021/acssuschemeng.2c07316
ACS Sustainable Chem. Eng. 2023, 11, 4759−4775

ACS Sustainable Chemistry & Engineering pubs.acs.org/journal/ascecg Research Article

Table 9. Optimal Operating Conditions with Maximum H_2 Purity for Biogas SESR Configurations Evaluated[a]

Case No.	T (°C)	P (bar)	S/CH_4	H_2 purity (vol %)	CH_4 conversion (%)	H_2 yield (%)	CGE (%)	NE (%)	CO_2 capture efficiency (%)	Potential CO_2 capture efficiency in case of indirect heating (%)
Case 1-Air	625	5	5	98.5	95.8	53.8	65.1	63.5	98.0 (zero)	96.5 (negative)
Case 2-Air	625	5	5	98.5	95.8	95.6	75.7	74.5	97.7 (zero)	63.1 (negative)
Case 2-Oxy	625	5	5	98.5	95.8	95.6	75.7	72.0	98.9 (negative)	–
Case 3-Air	675	5	5	100	100	90.8	77.3	72.5	100 (zero)	66.1 (negative)
Case 3-Oxy	675	5	5	100	100	90.8	77.3	70.2	100 (negative)	–

[a]SESR conditions: biogas = 60/40 vol % CH_4/CO_2, and 50% sorbent excess.

PSA-OG is higher, due to the lower methane conversion in SESR, which decreases the consumption of biogas for regeneration, implying a positive impact in the CGE for lower S/CH_4 values. CGE has lower values in Cases 1 and 2 than in Case 3. In Case 1, CGE increases from 58.4% to 60.7% for S/CH_4 values between 3 and 5 according to the higher methane conversion but then decreases to 48.2% at a S/CH_4 ratio of 6.5. In Case 2, CGE decreases from 64.6% to 71.6% as S/CH_4 increases from 3 to 5, then to 66.9% at S/CH_4 ratio of 6.5. In Cases 1 and 2, when using air in REG, NE is 1.5%−2.2% lower than CGE, whereas when oxy-combustion is used in REG, NE reduces an additional 2.2% in Case 2 due to the ASU penalty. In Case 3, when using air in REG, NE is 3.1%−4.4% lower than CGE, whereas when oxy-combustion is used in REG, NE reduces an additional 2.4% due to the ASU penalty.

The amount of energy recovered from the SESR reactor is 2.1 MW when the S/CH_4 ratio is lower than 5, while it grows to 3.4 MW when S/CH_4 is higher than 5.25 (see Table S3 of the Supporting Information). The increase in heat recovery can be ascribed to the heat released upon the formation of $Ca(OH)_2$ at higher S/CH_4 ratios, according to eq 13.

Discussion of SESR Configurations to Optimize H_2 Purity and CO_2 Capture. After evaluating five case studies from the three different process configurations for the SESR of biogas proposed, the optimal operating conditions to reach maximum H_2 purity according to the sensitivity analysis are shown in Table 9. For optimization purposes, the optimal conditions have been selected considering the avoidance of $Ca(OH)_2$ formation and the recovery of waste heat available in the outlet CO_2 stream (assuming 10% of heat losses as in the heat recovered from the SESR reactor). The formation of $Ca(OH)_2$ would not only result in higher energy consumption in the calciner, decreasing the overall efficiency, but also in an extra steam consumption that decreases steam excess and could favor coke deposition in the catalyst surface. The CO_2 capture efficiency is also determined for each configuration. It should be highlighted that the optimal conditions given by this thermodynamic study are in good agreement with those reported in previous experimental works on biogas SESR.[18,19] Under the optimal conditions, the experimental results are very close to those predicted by the thermodynamic equilibrium because the solid sorbent removes separation efficiency in situ CO_2 from the gas phase and shifts the reforming reaction equilibrium toward product formation, increasing the conversion.

The differences between air or oxy-fuel combustion in REG can be seen in the net efficiency and CO_2 capture for Cases 2 and 3. Case 1 is only evaluated in air combustion REG. For Cases 1 and 2, the CO_2 capture efficiency is ∼98% or even above, while in Case 3, the PSA unit boosts the CO_2 capture efficiency to ∼100%. The CO_2 capture using air for regeneration means global zero emissions for the process since, even though we are feeding a renewable feedstock such as biogas, the outlet CO_2 stream is diluted with the N_2 from the air. However, in oxy-fuel combustion conditions for sorbent regeneration, the CO_2 capture translates into negative emissions from the process since in these cases a pure outlet CO_2 stream is obtained.

It would however be possible to reach negative emissions using air combustion for sorbent regeneration if the calciner reactor was indirectly heated. Indirect heating can be achieved by supplying energy to the calciner from an external combustor via a fluidized-bed heat exchanger[5,39] or using heat pipes,[40−42] as recently reported in the literature.[30] The negative emissions that could be reached with indirect heating for the studied cases are shown in Table 9. As it can be seen, comparing Cases 1 and 2, a higher efficiency of the process is reached when biogas is used as fuel for sorbent regeneration in REG (Case 2) compared to H_2 (Case 1). In Case 2, NE is 74.5% when using air and 72.0% when using oxy-fuel combustion, alongside H_2 purity of 98.5 vol %, CH_4 conversion of 95.8%, and H_2 yield of 95.6% operating at 625 °C, 5 bar, and S/CH_4 = 5. In this case, zero carbon emissions are achieved if air is used in REG, while negative emissions with CO_2 capture efficiency of 98.9% are reached for oxy-fuel combustion.

In Case 3, biogas is used for sorbent regeneration combined with a PSA unit at the end. Its NE is 72.5% when using air and 70.2% when using oxy-fuel combustion, i.e., 2% and 1.8% points lower than that in Case 2. However, H_2 purity and CH_4 conversion reach nearly 100%, with H_2 yield of 90.8%, when operating at 675 °C, 5 bar, and S/CH_4 = 5. In this case, zero carbon emissions are achieved if air is used in REG, while negative emissions with CO_2 capture efficiency of ∼100% are reached for oxy-fuel combustion. Therefore, assuming a slightly lower net efficiency by incorporating a PSA unit into the system, Case 3 produces a high-purity H_2 that meets the high requirements of, for example, fuel cells, under both air and oxy-fuel combustion conditions.

In summary, biogas SESR with sorbent regeneration using biogas (SESR+REG_BG) (Case 2) could be the best option if a H_2 purity of 98.5 vol % fulfils the hydrogen requirements needed (with a CGE of 75.7%). For this configuration, oxy-fuel combustion sorbent regeneration delivers negative emissions with CO_2 capture efficiency of 98.9%, whereas indirect air firing would lower the CO_2 capture efficiency to 63.1% but preserve the negative emission. On the other hand, the addition of a PSA unit to the biogas SESR system that also uses biogas for sorbent regeneration (SESR+REG_BG+PSA) (Case 3) is needed if a H_2 purity of nearly 100 vol % is required (with a CGE of 77.3%). Additionally, negative CO_2 capture

https://doi.org/10.1021/acssuschemeng.2c07316
ACS Sustainable Chem. Eng. 2023, 11, 4759−4775

efficiency of ~100% could be reached in oxy-fuel combustion atmosphere or 66.1% in indirect air heating for the calciner.

CONCLUSIONS

This work proposes a novel process to produce renewable high-purity hydrogen from biogas with low-carbon emissions using the SESR technology. Three different process configurations and five case studies have been evaluated using a thermodynamic analysis performed in Aspen Plus to optimize the heat integration of the system, while maximizing the hydrogen production, energy efficiency, and CO_2 capture. A heat exchanger network (HEN) has been designed to recover as much heat as possible from the system. From a parametric analysis, the effects of the operating process conditions on the process performance were studied through the H_2 purity, H_2 yield, CH_4 conversion, energy efficiency, fuel consumption for the sorbent regeneration step, and CO_2 capture.

The results show that the H_2 purity keeps constant for all biogas compositions (50−80 vol % CH_4, balance CO_2). The SESR+REG_BG configuration, using biogas to meet the energy requirements of the sorbent regeneration, delivers a H_2 purity of 98.5 vol % at 625 °C, 5 bar and S/CH_4 = 5, with a CGE of 75.7%, and zero carbon emissions in air regeneration operation. A CO_2 capture efficiency of 98.9% can be achieved in oxy-fuel combustion sorbent regeneration, and the emissions are labeled negative. The SESR+REG_H_2 configuration, where part of the H_2 produced by the system is used to heat the calciner reactor, can produce H_2 purity of 98.5 vol % at 625 °C, 5 bar, and S/CH_4 = 5, but with lower efficiency (CGE = 65.1%) than that in the biogas case. Finally, the SESR +REG_BG+PSA configuration can produce ~100% H_2 purity at 675 °C, 5 bar, and S/CH_4 = 5, with a CGE of 77.3% and zero carbon emissions if an air-fired calciner is applied. However, negative emissions and ~100% CO_2 capture efficiency are feasible if regeneration is performed in an oxy-fuel combustion atmosphere. The use of oxy-fuel combustion in the regeneration stage gives a penalty of 2.3% points in the net efficiency of the process, although it enables a process with negative carbon emissions. The results of this equilibrium study demonstrate the thermodynamic feasibility of the SESR process of biogas and provide the optimal process configurations and operating conditions to maximize the cold gas efficiency of the process. Even though it is outside of the scope of this study, the outcome of this work lays the foundation for subsequent dynamic modeling to design the reactors and heat recovery systems needed to scale up the biogas SESR process.

ASSOCIATED CONTENT

Supporting Information

The Supporting Information is available free of charge at https://pubs.acs.org/doi/10.1021/acssuschemeng.2c07316.

Aspen Plus flowsheets of renewable hydrogen production from biogas SESR for the different process configurations studied (PDF)

AUTHOR INFORMATION

Corresponding Authors

Covadonga Pevida − *Instituto de Ciencia y Tecnología del Carbono, INCAR-CSIC, 33011 Oviedo, Spain*; orcid.org/0000-0002-4662-8448; Email: cpevida@incar.csic.es

María Victoria Gil − *Instituto de Ciencia y Tecnología del Carbono, INCAR-CSIC, 33011 Oviedo, Spain*; orcid.org/0000-0002-2258-3011; Email: victoria.gil@incar.csic.es

Authors

Alma Capa − *Instituto de Ciencia y Tecnología del Carbono, INCAR-CSIC, 33011 Oviedo, Spain; Energy and Sustainability Theme, Cranfield University, Cranfield, Bedfordshire MK43 0AL, United Kingdom*

Yongliang Yan − *Materials, Concept and Reaction Engineering (MatCoRE) Group, School of Engineering, Newcastle University, Newcastle Upon Tyne NE1 7RU, United Kingdom*

Fernando Rubiera − *Instituto de Ciencia y Tecnología del Carbono, INCAR-CSIC, 33011 Oviedo, Spain*; orcid.org/0000-0003-0385-1102

Peter T. Clough − *Energy and Sustainability Theme, Cranfield University, Cranfield, Bedfordshire MK43 0AL, United Kingdom*; orcid.org/0000-0003-1820-0484

Complete contact information is available at: https://pubs.acs.org/10.1021/acssuschemeng.2c07316

Author Contributions

The manuscript was written through contributions of all authors. All authors have given approval to the final version of the manuscript.

Notes

The authors declare no competing financial interest.

ACKNOWLEDGMENTS

This work was carried out with financial support from the Spanish MICINN through Grant PID2020-119539RB-I00, funded by MCIN/AEI/10.13039/501100011033, and from the Gobierno del Principado de Asturias (PCTI, ref. IDI/2021/000060). P.T.C. would like to thank the UK Department for Business, Energy and Industrial Strategy for supporting research into this area through the Bio-HyPER project funded by the H_2 BECCS Phase 1 competition (H2BECCS107). A.C. acknowledges a fellowship awarded by the Spanish MICINN FPI program through Grant PRE2018-083634, funded by MCIN/AEI/10.13039/501100011033 and by "ESF Investing in your future". M.V.G. acknowledges support from the Spanish AEI through the Ramón y Cajal Grant RYC-2017-21937 funded by MCIN/AEI/10.13039/501100011033 and by "ESF Investing in your future".

REFERENCES

(1) El-Emam, R. S.; Özcan, H. Comprehensive Review on the Techno-Economics of Sustainable Large-Scale Clean Hydrogen Production. *Journal of Cleaner Production* **2019**, *220*, 593−609.

(2) Minh, D. P.; Siang, T. J.; Vo, D. V. N.; Phan, T. S.; Ridart, C.; Nzihou, A.; Grouset, D. *Hydrogen Production from Biogas Reforming: An Overview of Steam Reforming, Dry Reforming, Dual Reforming, and Tri-Reforming of Methane*; Elsevier Ltd., 2018. DOI: 10.1016/B978-0-12-811197-0.00004-X.

(3) *Global Hydrogen Review 2021*; International Energy Agency, 2021. DOI: 10.1787/39351842-en.

(4) Abdin, Z.; Zafaranloo, A.; Rafiee, A.; Mérida, W.; Lipiński, W.; Khalilpour, K. R. Hydrogen as an Energy Vector. *Renewable and Sustainable Energy Reviews* **2020**, *120*, 109620.

(5) Stenberg, V.; Spallina, V.; Mattisson, T.; Rydén, M. Techno-Economic Analysis of H2 Production Processes Using Fluidized Bed Heat Exchangers with Steam Reforming − Part 1: Oxygen Carrier

Aided Combustion. *Int. J. Hydrogen Energy* **2020**, *45* (11), 6059–6081.
(6) Di Giuliano, A.; Gallucci, K. Sorption Enhanced Steam Methane Reforming Based on Nickel and Calcium Looping: A Review. *Chemical Engineering and Processing - Process Intensification.* **2018**, *130*, 240.
(7) Cherbanski, R.; Molga, E. Sorption-Enhanced Steam Methane Reforming (SE-SMR) – A Review: Reactor Types, Catalyst and Sorbent Characterization, Process Modeling. *Chem. Process Eng. - Inz. Chem. i Proces.* **2018**, *39* (4), 427–448.
(8) Xu, Y.; Lu, B.; Luo, C.; Chen, J.; Zhang, Z.; Zhang, L. Sorption Enhanced Steam Reforming of Ethanol over Ni-Based Catalyst Coupling with High-Performance CaO Pellets. *Chem. Eng. J.* **2021**, *406*, 126903.
(9) Saupsor, J.; Kasempremchit, N.; Bumroongsakulsawat, P.; Kim-Lohsoontorn, P.; Wongsakulphasatch, S.; Kiatkittipong, W.; Laosiripojana, N.; Gong, J.; Assabumrungrat, S. Performance Comparison among Different Multifunctional Reactors Operated under Energy Self-Sufficiency for Sustainable Hydrogen Production from Ethanol. *Int. J. Hydrogen Energy* **2020**, *45* (36), 18309–18320.
(10) Wang, N.; Feng, Y.; Chen, Y.; Guo, X. Lithium-Based Sorbent from Rice Husk Materials for Hydrogen Production via Sorption-Enhanced Steam Reforming of Ethanol. *Fuel* **2019**, *245*, 263–273.
(11) Fermoso, J.; He, L.; Chen, D. Production of High Purity Hydrogen by Sorption Enhanced Steam Reforming of Crude Glycerol. *Int. J. Hydrogen Energy* **2012**, *37* (19), 14047–14054.
(12) Shokrollahi Yancheshmeh, M.; Radfarnia, H. R.; Iliuta, M. C. Sustainable Production of High-Purity Hydrogen by Sorption Enhanced Steam Reforming of Glycerol over CeO_2-Promoted $Ca_9Al_6O_{18}$-CaO/NiO Bifunctional Material. *ACS Sustain. Chem. Eng.* **2017**, *5* (11), 9774–9786.
(13) Shokrollahi Yancheshmeh, M.; Iliuta, M. C. Embedding Ni in Ni-Al Mixed-Metal Alkoxide for the Synthesis of Efficient Coking Resistant Ni-CaO-Based Catalyst-Sorbent Bifunctional Materials for Sorption-Enhanced Steam Reforming of Glycerol. *ACS Sustain. Chem. Eng.* **2020**, *8* (45), 16746–16756.
(14) Esteban-Díez, G.; Gil, M. V.; Pevida, C.; Chen, D.; Rubiera, F. Effect of Operating Conditions on the Sorption Enhanced Steam Reforming of Blends of Acetic Acid and Acetone as Bio-Oil Model Compounds. *Appl. Energy* **2016**, *177*, 579–590.
(15) Fermoso, J.; Gil, M. V.; Rubiera, F.; Chen, D. Multifunctional Pd/Ni-Co Catalyst for Hydrogen Production by Chemical Looping Coupled with Steam Reforming of Acetic Acid. *ChemSusChem* **2014**, *7* (11), 3063–3077.
(16) Gil, M. V.; Fermoso, J.; Rubiera, F.; Chen, D. H_2 Production by Sorption Enhanced Steam Reforming of Biomass-Derived Bio-Oil in a Fluidized Bed Reactor: An Assessment of the Effect of Operation Variables Using Response Surface Methodology. *Catal. Today* **2015**, *242*, 19–34.
(17) Gil, M. V.; Rout, K. R.; Chen, D. Production of High Pressure Pure H_2 by Pressure Swing Sorption Enhanced Steam Reforming (PS-SESR) of Byproducts in Biorefinery. *Appl. Energy* **2018**, *222*, 595.
(18) Capa, A.; García, R.; Chen, D.; Rubiera, F.; Pevida, C.; Gil, M. V. On the Effect of Biogas Composition on the H2 Production by Sorption Enhanced Steam Reforming (SESR). *Renew. Energy* **2020**, *160*, 575–583.
(19) García, R.; Gil, M. V.; Rubiera, F.; Chen, D.; Pevida, C. Renewable Hydrogen Production from Biogas by Sorption Enhanced Steam Reforming (SESR): A Parametric Study. *Energy* **2021**, *218*, 119491.
(20) Alves, H. J.; Bley Junior, C.; Niklevicz, R. R.; Frigo, E. P.; Frigo, M. S.; Coimbra-Araújo, C. H. Overview of Hydrogen Production Technologies from Biogas and the Applications in Fuel Cells. *Int. J. Hydrogen Energy* **2013**, *38* (13), 5215–5225.
(21) Yang, L.; Ge, X.; Wan, C.; Yu, F.; Li, Y. Progress and Perspectives in Converting Biogas to Transportation Fuels. *Renew. Sustain. Energy Rev.* **2014**, *40*, 1133–1152.
(22) Fontaine, D.; Eriksen, J.; Sørensen, P. Sulfur from Biogas Desulfurization: Fate of S during Storage in Manure and after Application to Plants. *Sci. Total Environ.* **2021**, *754*, 142180.
(23) Kong, F.; Swift, J.; Zhang, Q.; Fan, L. S.; Tong, A. Biogas to H_2 Conversion with CO_2 Capture Using Chemical Looping Technology: Process Simulation and Comparison to Conventional Reforming Processes. *Fuel* **2020**, *279*, 118479.
(24) Gao, Y.; Jiang, J.; Meng, Y.; Yan, F.; Aihemaiti, A. A Review of Recent Developments in Hydrogen Production via Biogas Dry Reforming. *Energy Convers. Manag.* **2018**, *171*, 133–155.
(25) Yentekakis, I. V.; Goula, G. Biogas Management: Advanced Utilization for Production of Renewable Energy and Added-Value Chemicals. *Front. Environ. Sci.* **2017**, *5*, na DOI: 10.3389/fenvs.2017.00007.
(26) Masoudi Soltani, S.; Lahiri, A.; Bahzad, H.; Clough, P.; Gorbounov, M.; Yan, Y. Sorption-Enhanced Steam Methane Reforming for Combined CO_2 Capture and Hydrogen Production: A State-of-the-Art Review. *Carbon Capture Sci. Technol.* **2021**, *1*, No. 100003.
(27) Tian, X.; Wang, S.; Zhou, J.; Xiang, Y.; Zhang, F.; Lin, B.; Liu, S.; Luo, Z. Simulation and Exergetic Evaluation of Hydrogen Production from Sorption Enhanced and Conventional Steam Reforming of Acetic Acid. *Int. J. Hydrogen Energy* **2016**, *41* (46), 21099–21108.
(28) Tzanetis, K. F.; Martavaltzi, C. S.; Lemonidou, A. A. Comparative Exergy Analysis of Sorption Enhanced and Conventional Methane Steam Reforming. *Int. J. Hydrogen Energy* **2012**, *37* (21), 16308–16320.
(29) Alam, S.; Kumar, J. P.; Rani, K. Y.; Sumana, C. Self-Sustained Process Scheme for High Purity Hydrogen Production Using Sorption Enhanced Steam Methane Reforming Coupled with Chemical Looping Combustion. *J. Clean. Prod.* **2017**, *162*, 687–701.
(30) Yan, Y.; Thanganadar, D.; Clough, P. T.; Mukherjee, S.; Patchigolla, K.; Manovic, V.; Anthony, E. J. Process Simulations of Blue Hydrogen Production by Upgraded Sorption Enhanced Steam Methane Reforming (SE-SMR) Processes. *Energy Convers. Manag.* **2020**, *222*, 113144.
(31) Antzara, A.; Heracleous, E.; Bukur, D. B.; Lemonidou, A. A. Thermodynamic Analysis of Hydrogen Production via Chemical Looping Steam Methane Reforming Coupled with in Situ CO_2 Capture. In. *Energy Procedia* **2014**, *63*, 6576.
(32) Phuluanglue, A.; Khaodee, W.; Assabumrungrat, S. Simulation of Intensified Process of Sorption Enhanced Chemical-Looping Reforming of Methane: Comparison with Conventional Processes. *Comput. Chem. Eng.* **2017**, *105*, 237–245.
(33) Ebneyamini, A.; Grace, J. R.; Lim, C. J.; Ellis, N.; Elnashaie, S. S. E. H. Simulation of Limestone Calcination for Calcium Looping: Potential for Autothermal and Hydrogen-Producing Sorbent Regeneration. *Ind. Eng. Chem. Res.* **2019**, *58*, 8636.
(34) Antzara, A.; Heracleous, E.; Bukur, D. B.; Lemonidou, A. A. Thermodynamic Analysis of Hydrogen Production via Chemical Looping Steam Methane Reforming Coupled with in Situ CO2 Capture. *Int. J. Greenh. Gas Control* **2015**, *32*, 115–128.
(35) Barelli, L. Ã.; Bidini, G.; Corradetti, A.; Desideri, U. Study of the Carbonation – Calcination Reaction Applied to the Hydrogen Production from Syngas. *Energy* **2007**, *32*, 697–710.
(36) Barelli, L.; Bidini, G.; Corradetti, A.; Desideri, U. Production of Hydrogen through the Carbonation-Calcination Reaction Applied to CH_4/CO_2 Mixtures. *Energy* **2007**, *32* (5), 834–843.
(37) Capa, A.; García, R.; Rubiera, F.; Pevida, C.; Gil, M. V. Energy Analysis on the Effect of Biogas Composition in the Sorption Enhanced Steam Reforming (SESR) for Green Hydrogen Production. In *29th European Biomass Conference and Exhibition*, 2021; pp 1366–1370.
(38) Marín, P.; Díez, F. V.; Ordóñez, S. Reverse Flow Reactors as Sustainable Devices for Performing Exothermic Reactions: Applications and Engineering Aspects. *Chemical Engineering and Processing - Process Intensification* **2019**, *135*, 175–189.

https://doi.org/10.1021/acssuschemeng.2c07316
ACS Sustainable Chem. Eng. 2023, 11, 4759–4775

(39) Stenberg, V.; Rydén, M.; Mattisson, T.; Lyngfelt, A. Exploring Novel Hydrogen Production Processes by Integration of Steam Methane Reforming with Chemical-Looping Combustion (CLC-SMR) and Oxygen Carrier Aided Combustion (OCAC-SMR). *Int. J. Greenh. Gas Control* **2018**, *74*, 28−39.
(40) Junk, M.; Reitz, M.; Strohle, J.; Epple, B. Technical and Economical Assessment of the Indirectly Heated Carbonate Looping Process. *J. Energy Resour. Technol. Trans. ASME* **2016**, *138* (4), 1−8.
(41) Hoeftberger, D.; Karl, J. The Indirectly Heated Carbonate Looping Process for CO_2 Capture A Concept with Heat Pipe Heat Exchanger. *J. Energy Resour. Technol. Trans. ASME* **2016**, *138* (4), 1−7.
(42) Reitz, M.; Junk, M.; Ströhle, J.; Epple, B. Design and Operation of a 300 KWth Indirectly Heated Carbonate Looping Pilot Plant. *Int. J. Greenh. Gas Control* **2016**, *54*, 272−281.
(43) Rydén, M.; Ramos, P. H2 Production with CO2 Capture by Sorption Enhanced Chemical-Looping Reforming Using NiO as Oxygen Carrier and CaO as CO2 Sorbent. *Fuel Process. Technol.* **2012**, *96* (0), 27−36.
(44) Kavosh, M.; Patchigolla, K.; Anthony, E. J.; Oakey, J. E. Carbonation Performance of Lime for Cyclic CO_2 Capture Following Limestone Calcination in Steam/CO_2 Atmosphere. *Appl. Energy* **2014**, *131*, 499−507.
(45) Johnsen, K.; Grace, J. R.; Elnashaie, S. S. E. H.; Kolbeinsen, L.; Eriksen, D. Modeling of Sorption-Enhanced Steam Reforming in a Dual Fluidized Bubbling Bed Reactor. *Ind. Eng. Chem. Res.* **2006**, *45* (12), 4133−4144.
(46) Shokrollahi Yancheshmeh, M.; Radfarnia, H. R.; Iliuta, M. C. High Temperature CO2 Sorbents and Their Application for Hydrogen Production by Sorption Enhanced Steam Reforming Process. *Chem. Eng. J.* **2016**, *283*, 420−444.
(47) Dunstan, M. T.; Donat, F.; Bork, A. H.; Grey, C. P.; Müller, C. R. CO_2 Capture at Medium to High Temperature Using Solid Oxide-Based Sorbents: Fundamental Aspects, Mechanistic Insights, and Recent Advances. *Chem. Rev.* **2021**, *121*, 12681.
(48) Broda, M.; Manovic, V.; Imtiaz, Q.; Kierzkowska, A. M.; Anthony, E. J.; Müller, C. R. High-Purity Hydrogen via the Sorption-Enhanced Steam Methane Reforming Reaction over a Synthetic CaO-Based Sorbent and a Ni Catalyst. *Environ. Sci. Technol.* **2013**, *47* (11), 6007−6014.
(49) Di Giuliano, A.; Gallucci, K.; Kazi, S. S.; Giancaterino, F.; Di Carlo, A.; Courson, C.; Meyer, J.; Di Felice, L. Development of Ni- and CaO-Based Mono- and Bi-Functional Catalyst and Sorbent Materials for Sorption Enhanced Steam Methane Reforming: Performance over 200 cycles and Attrition Tests. *Fuel Process. Technol.* **2019**, *195*, 106160.
(50) He, L.; Berntsen, H.; Chen, De Approaching Sustainable H_2 Production: Sorption Enhanced Steam Reforming of Ethanol. *J. Phys. Chem. A* **2010**, *114* (11), 3834−3844.
(51) Anthony, E. J.; Bulewicz, E. M.; Jia, L. Reactivation of Limestone Sorbents in FBC for SO_2 Capture. *Prog. Energy Combust. Sci.* **2007**, *33* (2), 171−210.
(52) Diglio, G.; Hanak, D. P.; Bareschino, P.; Pepe, F.; Montagnaro, F.; Manovic, V. Modelling of Sorption-Enhanced Steam Methane Reforming in a Fixed Bed Reactor Network Integrated with Fuel Cell. *Appl. Energy* **2018**, *210*, 1−15.
(53) Rodríguez, S.; Capa, A.; García, R.; Chen, D.; Rubiera, F.; Pevida, C.; Gil, M. V. Blends of Bio-Oil/Biogas Model Compounds for High-Purity H_2 Production by Sorption Enhanced Steam Reforming (SESR): Experimental Study and Energy Analysis. *Chem. Eng. J.* **2022**, *432*, No. 134396.
(54) Habibi, R.; Pourfayaz, F.; Mehrpooya, M.; Kamali, H. A Natural Gas-Based Eco-Friendly Polygeneration System Including Gas Turbine, Sorption-Enhanced Steam Methane Reforming, Absorption Chiller and Flue Gas CO_2 Capture Unit. *Sustain. Energy Technol. Assessments* **2022**, *52*, 101984.
(55) Zhu, L.; Li, L.; Fan, J. A Modified Process for Overcoming the Drawbacks of Conventional Steam Methane Reforming for Hydrogen Production: Thermodynamic Investigation. *Chem. Eng. Res. Des.* **2015**, *104*, 792−806.
(56) Noor, T.; Gil, M. V.; Chen, D. Production of Fuel-Cell Grade Hydrogen by Sorption Enhanced Water Gas Shift Reaction Using Pd/Ni-Co Catalysts. *Appl. Catal. B Environ.* **2014**, *150*−*151*, 585.
(57) Ebneyamini, A.; Grace, J. R.; Lim, C. J.; Ellis, N. Simulation of Sorbent-Enhanced Steam Methane Reforming and Limestone Calcination in Dual Turbulent Fluidized Bed Reactors. *Energy Fuel* **2020**, *34*, 7743−7755.

https://doi.org/10.1021/acssuschemeng.2c07316
ACS Sustainable Chem. Eng. 2023, 11, 4759−4775

Supporting Information

Process Simulations of High-Purity and Renewable Clean H_2 Production by Sorption Enhanced Steam Reforming of Biogas

Alma Capa [a,b], Yongliang Yan[c], Fernando Rubiera[a], Covadonga Pevida [*,a], María Victoria Gil[*,a], Peter T. Clough[b]

[a] Instituto de Ciencia y Tecnología del Carbono, INCAR-CSIC, Francisco Pintado Fe 26, 33011 Oviedo, Spain

[b] Energy and Sustainability Theme, Cranfield University, Cranfield, Bedfordshire MK43 0AL, UK

[c] Materials, Concept and Reaction Engineering (MatCoRE) Group, School of Engineering, Newcastle University, Newcastle Upon Tyne, NE1 7RU, UK

[*]Email: cpevida@incar.csic.es (C. Pevida).

[*]Email: victoria.gil@incar.csic.es (M.V. Gil).

Number of pages: 7

Number of figures: 5

Number of tables: 3

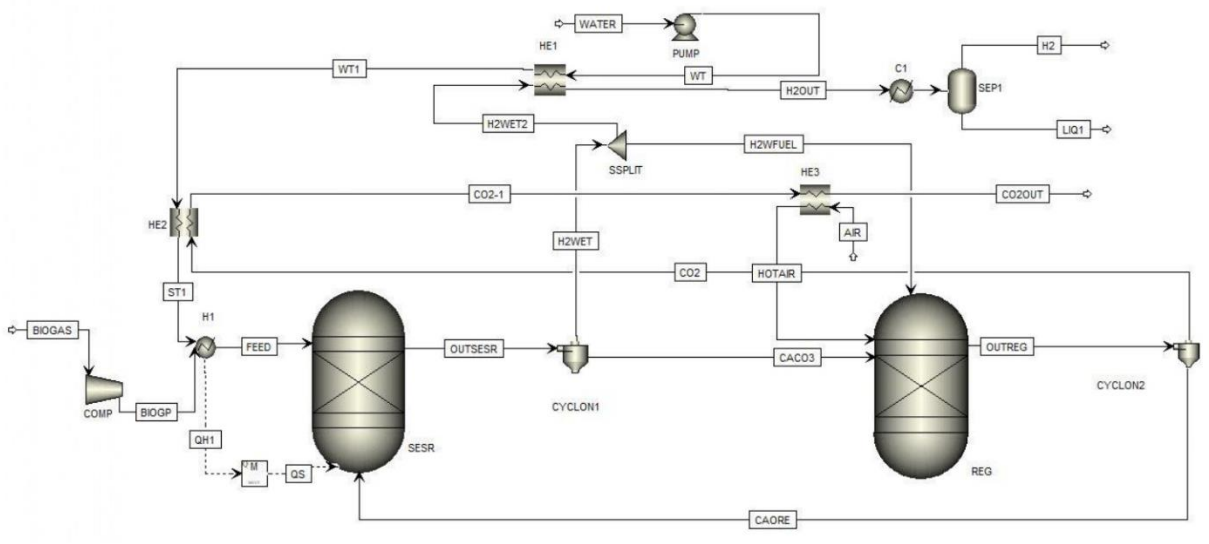

Figure S1. Aspen Plus flowsheet of renewable hydrogen production from biogas SESR using a fraction of the produced hydrogen as fuel for sorbent regeneration in air atmosphere (Case 1 SESR+REG_H_2 - Air).

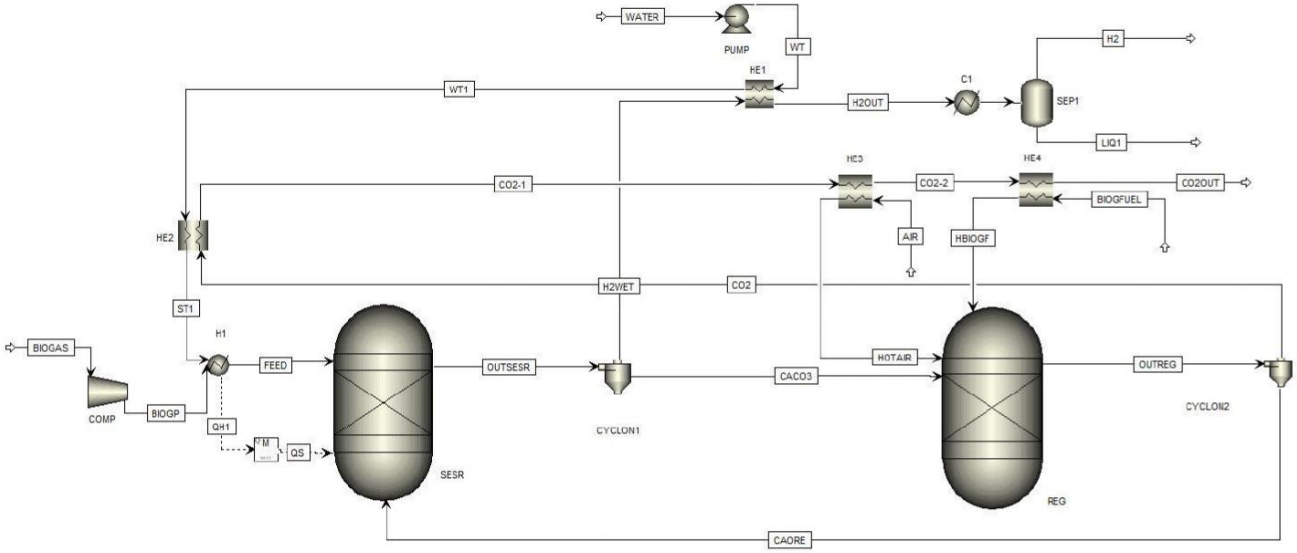

Figure S2. Aspen Plus flowsheet of renewable hydrogen production from biogas SESR using biogas as fuel for sorbent regeneration in air atmosphere (Case 2 SESR+REG_BG - Air).

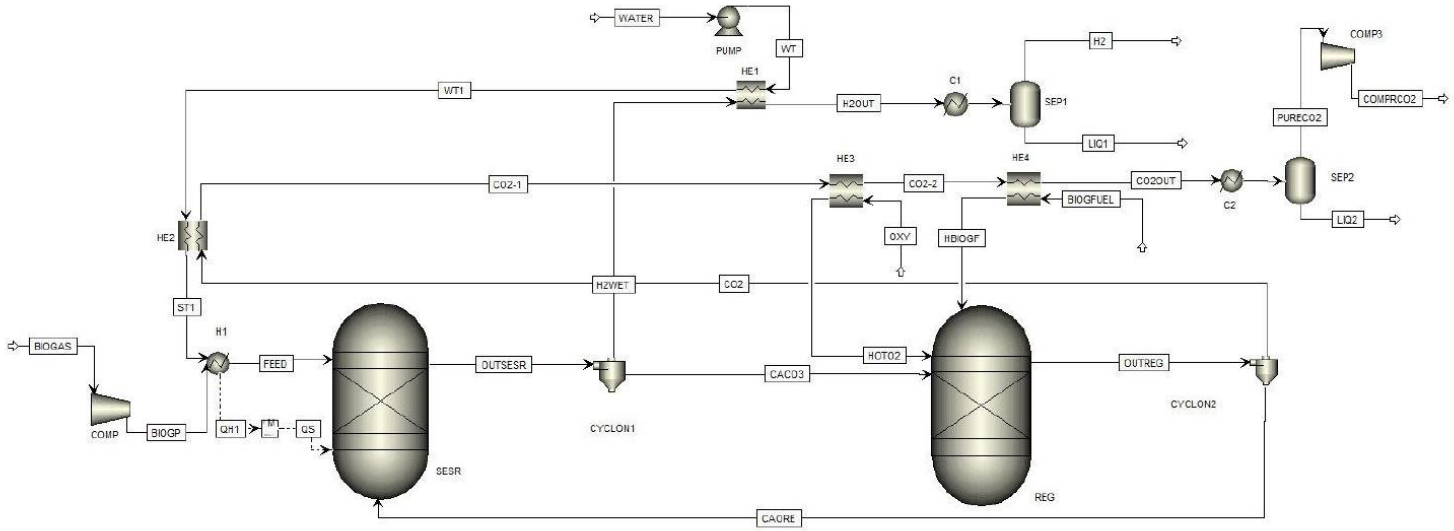

Figure S3. Aspen Plus flowsheet of renewable hydrogen production from biogas SESR using biogas as fuel for sorbent regeneration in air atmosphere (Case 2 SESR+REG_BG - Oxy).

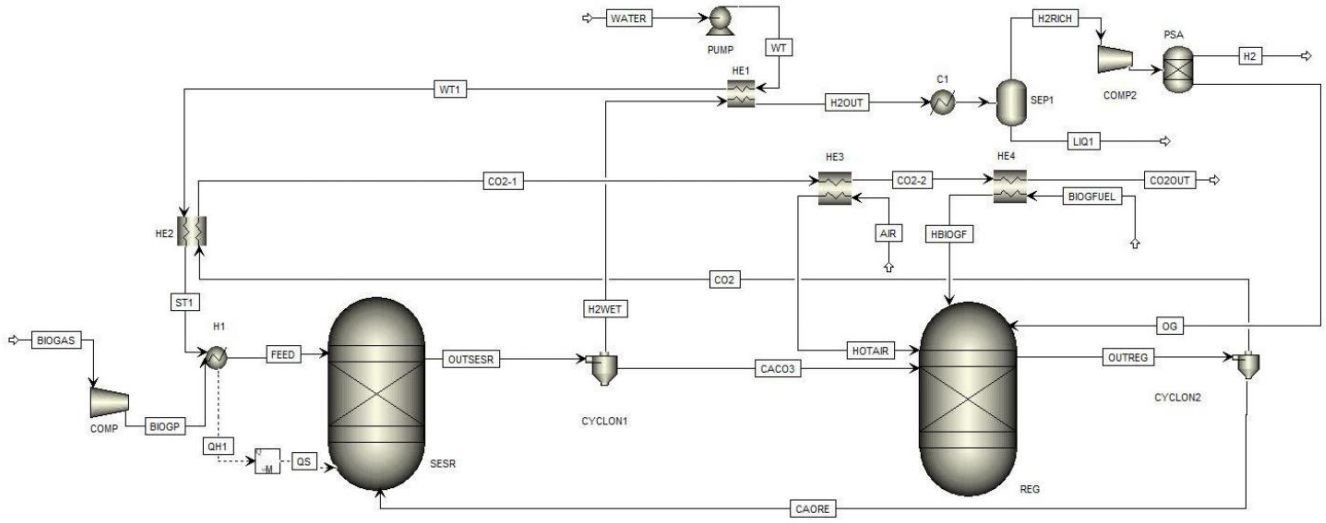

Figure S4. Aspen Plus flowsheet of renewable hydrogen production from biogas SESR using biogas as fuel for sorbent regeneration and recirculating PSA-OG. Combustion performed in air atmosphere in REG reactor (Case 3 SESR+REG_BG+PSA - Air).

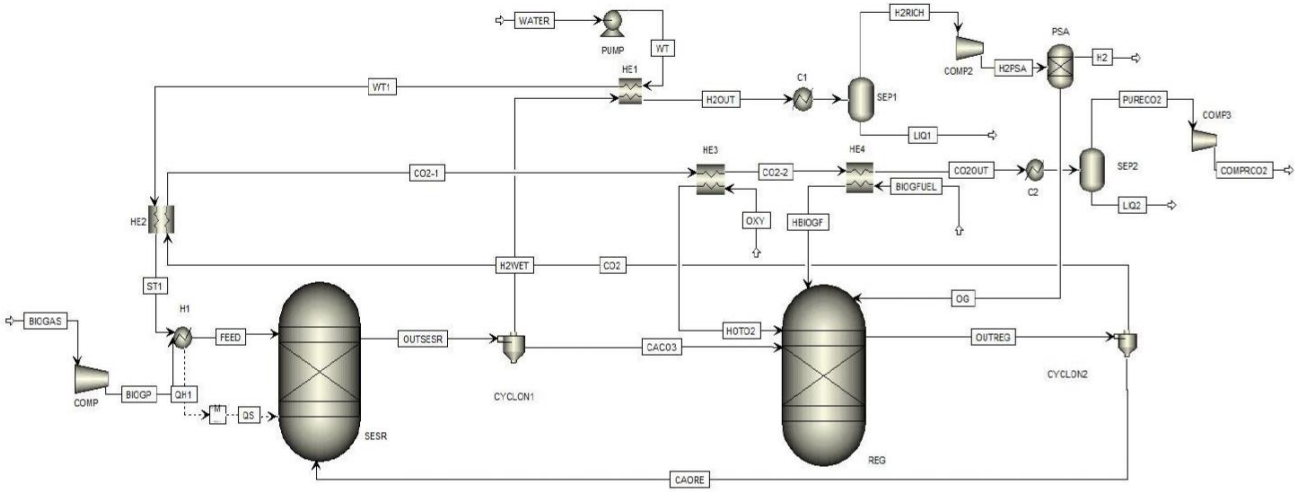

Figure S5. Aspen Plus flowsheet of renewable hydrogen production from biogas SESR using biogas as fuel for sorbent regeneration and recirculating PSA-OG. Oxy-combustion performed in REG reactor (Case 3 SESR+REG_BG+PSA - Oxy).

Table S1. Effect of SESR temperature on the heat recovered from SESR (heat losses considered). SESR conditions: S/CH_4 = 5.5, P = 10 bar, biogas = 60/40 vol.% CH_4/CO_2, and 50% sorbent excess.

SESR Temperature (°C)	Heat recovered from SESR (MW)
500	4.0
525	3.9
550	3.7
575	3.6
600	3.4
625	2.0
650	1.9
675	1.8

Table S2. Effect of SESR pressure on the heat recovered from SESR (heat losses considered). SESR conditions: S/CH_4 = 5.5, T = 600 °C, biogas = 60/40 vol.% CH_4/CO_2, and 50% sorbent excess.

SESR Pressure (bar)	Heat recovered from SESR (MW)
1.5	2.0
2	2.0
3	2.0
5	2.0
10	3.4
15	3.5
20	3.6
25	3.7

Table S3. Effect of S/CH_4 ratio on the heat recovered from SESR (heat losses considered). SESR conditions: 600 °C, P = 10 bar, biogas = 60/40 vol.% CH_4/CO_2, and 50% sorbent excess.

S/CH_4 ratio	Heat recovered from SESR (MW)
3.00	2.1
3.50	2.1
4.00	2.1
4.50	2.1
5.00	2.1
5.25	3.4
5.50	3.4
6.00	3.4
6.50	3.4

Paper III

Chemical Engineering Journal 476 (2023) 146803

Contents lists available at ScienceDirect

Chemical Engineering Journal

journal homepage: www.elsevier.com/locate/cej

Effect of H_2S on biogas sorption enhanced steam reforming using a Pd/Ni-Co catalyst and dolomite as a sorbent

A. Capa [a], M.P. González-Vázquez [a], D. Chen [b], F. Rubiera [a], C. Pevida [a,*], M.V. Gil [a,*]

[a] Instituto de Ciencia y Tecnología del Carbono, INCAR (CSIC), Francisco Pintado Fe 26, 33011 Oviedo, Spain
[b] Department of Chemical Engineering, Norwegian University of Science and Technology, Sem Sælands vei 4, Trondheim NO-7491, Norway

ARTICLE INFO

Keywords:
H_2S
Biogas
Hydrogen
Sorption enhanced steam reforming
Pd/Ni-Co catalyst
CaO sorbent

ABSTRACT

To achieve net zero carbon emissions from energy systems, biogas has become an attractive renewable resource for hydrogen production. The sorption enhanced steam reforming (SESR) process is proposed to produce high-purity hydrogen from biogas, enabled by combining the catalytic reforming reaction with the simultaneous CO_2 removal by sorption in a single reactor. One of the most critical challenges in using biogas in conventional reforming processes is the presence of H_2S since it may deactivate the reforming catalyst. Here we experimentally study the effect of the biogas H_2S concentration on the H_2 production by SESR, i.e., accounting for the presence of a CaO-based solid sorbent. This work was performed in a fixed-bed reactor using a Pd/Ni-Co hydrotalcite-like material (HT) catalyst and dolomite as CO_2 sorbent. Biogas ($60CH_4/40CO_2$ vol.%) with different concentrations of H_2S (150, 350, 500 and 1000 ppm) was evaluated. The catalyst did not deactivate for biogas H_2S concentrations of 150 and 350 ppm during five cycles of the SESR process. However, a slight decrease in the catalyst activity was detected under higher sulfur concentrations after the third SESR cycle. Sulfur was detected in the spent catalyst and sorbent materials, with a higher proportion in the sorbent for the highest H_2S concentration tested (1000 ppm). H_2 yield decreased by 10.8% and 4.5% points for biogas H_2S concentrations of 500 and 1000 ppm after five cycles, respectively, while H_2 purity decreased by only 3 vol.% and 2 vol.% points, respectively.

1. Introduction

Hydrogen is considered a critical player in future energy decarbonization scenarios. However, it still majorly derives from non-renewable resources, mainly natural gas [1]. Many efforts currently focus on the development of processes for the production of clean hydrogen-rich gas. Among the available renewable sources, biogas is versatile to be transformed into hydrogen. Biogas, essentially a mixture of methane and carbon dioxide, is currently mainly used for small- or medium-scale combined heat and power production, even though the high CO_2 content in biogas decreases the calorific value of the gas mixture. Therefore, the conversion of biogas into higher-value products by catalytic reforming methods for producing synthesis gas or hydrogen has become very attractive due to biogas availability and low cost [2].

Biogas is produced by the anaerobic digestion of different biodegradable materials in landfills, and sewage sludge and bio-waste digesters [3]. It mainly contains 35–70% of CH_4 and 30–65% of CO_2, with minor components, such as N_2, O_2, H_2, H_2S, H_2O, CO, NH_3, and siloxanes. Purification or cleaning technologies (physical and chemical absorption, adsorption, biological desulfurization or membrane separation) are commonly applied to remove harmful and toxic compounds such as H_2S, N_2, O_2, CO, and NH_3, which can affect the end-users, grid transmission, machinery or storage facilities. One of the major challenges in using biogas is the presence of H_2S, which may deactivate the catalytic activity of Ni (poisoning), the most commonly used metal in reforming catalysts. Variable H_2S concentrations can be found in the composition of biogas [4,5]: 0–10000 ppm from sewage sludge digesters, 10–2000 ppm from organic waste digesters, and 0–100 ppm from landfills [2].

Nickel has been found as more sensitive to sulfur poisoning than other group VIII metals [6], and nickel-based catalysts are particularly susceptible to deactivation by sulfur compounds. The accepted mechanism of sulfur poisoning is the chemisorption of sulfur on the Ni surface, i.e., the catalyst deactivates through sulfidation of the active Ni particles and formation of Ni–S species that do not take part in the reforming reactions, as shown in Eq. (1) [7].

$$Ni + H_2S \leftrightarrow Ni\text{–}S + H_2 \quad (1)$$

* Corresponding authors.
E-mail addresses: cpevida@incar.csic.es (C. Pevida), victoria.gil@incar.csic.es (M.V. Gil).

https://doi.org/10.1016/j.cej.2023.146803
Received 25 July 2023; Received in revised form 24 September 2023; Accepted 18 October 2023
Available online 20 October 2023

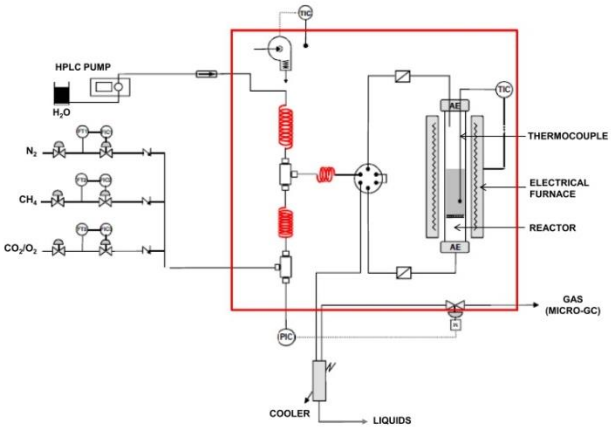

Fig 1. Schematic flow diagram of the experimental setup used for the biogas SESR experiments.

Other metals, such as Ag, Cu, Fe, Co, Mo, Ru, and Pt, can also react with sulfur compounds [8]. Although cobalt metal has a slightly lower affinity for sulfur as compared to nickel [9,10], it could also chemisorb sulfur by Eq. (2).

$$Co + H_2S \leftrightarrow Co\text{–}S + H_2 \quad (2)$$

However, it has been reported that adding Co to a Ni catalyst delays the catalyst deactivation in the presence of H_2S by altering sulfur chemisorption kinetics [10]. On the other hand, Ni is more sensitive to sulfur deactivation than noble metals [8], and catalyst deactivation by sulfur poisoning of Pd is not expected to occur since the p_{H2S}/p_{H2} ratio during the SESR experiments in the present work is lower than the value of this parameter needed for the reaction between Pd and H_2S estimated by Iyoha et al. [11].

To produce high-purity hydrogen from biogas, we propose the sorption enhanced steam reforming (SESR) process, a promising novel technology that combines the reforming reaction for hydrogen production with the in situ CO_2 separation by a sorbent in a single-step. The biogas SESR process involves the methane steam reforming (SR) reaction (Eq. (3)), and the water gas shift (WGS) reaction (Eq. (4)).

$$CH_4 + H_2O \leftrightarrow CO + 3H_2 \; \Delta H_r^0 = +206 \text{ kJ mol}^{-1} \quad (3)$$

$$CO + H_2O \leftrightarrow CO_2 + H_2 \; \Delta H_r^0 = -41 \text{ kJ mol}^{-1} \quad (4)$$

Natural CaO-based materials, such as dolomite, are typically used in SESR processes for carbon dioxide separation due to their high CO_2 capture capacity at high temperatures, fast CO_2 carbonation kinetics, low cost and wide availability, despite their low stability after multiple carbonation/calcination cycles. CO_2 reacts with CaO to form a solid carbonate by the carbonation reaction (Eq. (5)), giving the overall sorption enhanced steam reforming (SESR) reaction of methane, as shown in Eq. (6).

$$CaO + CO_2 \leftrightarrow CaCO_3 \; \Delta H_r^0 = -178 \text{ kJ mol}^{-1} \quad (5)$$

$$CH_4 + 2H_2O + CaO \rightarrow 4H_2 + CaCO_3 \; \Delta H_r^0 = -13 \text{ kJ mol}^{-1} \quad (6)$$

As CO_2 is removed from the gaseous phase by the carbonation reaction, the thermodynamic equilibrium of the SR and WGS reactions shifts towards the production of H_2, according to Le Chatelier's principle, increasing hydrogen production.

Recent research studies have focused on the SESR process of different biomass materials to produce renewable hydrogen, such as ethanol [12], glycerol [13,14], bio-oil from fast pyrolysis of biomass [15–19], and also biogas [20–24]. The effect of the biogas H_2S content on the reforming process has been extensively studied under conventional SR [25–28], dry reforming [29–31], and also for biogas tri-reforming [32,33], although the catalyst deactivation by sulfur poisoning in conventional reforming processes has been mainly studied for low H_2S concentrations (<250 ppm) [25,26,34]. However, to the best of the authors' knowledge, no previous experimental works have studied the effect of biogas H_2S on hydrogen production by the cyclic SESR process, which is a more complex system where different steps under varying gaseous atmospheres are needed due to the presence of a CaO-based CO_2 sorbent (such as reducing conditions during the reforming step, where CaO could react with H_2S to form calcium sulfide by Eq. (7) [35,36]). The use of calcined limestone/dolomite for sulfur capture (H_2S) has been previously studied in gasification processes [37–39].

$$CaO + H_2S \leftrightarrow CaS + H_2O \; \Delta H_r^0 = -59 \text{ kJ mol}^{-1} \quad (7)$$

Although there have been recent efforts focused on the development of sulfur-resistant catalysts (addition of rare-earth, alkaline-earth or noble metals; or use of resilient materials such as alloys, perovskites, and core–shell structures [40,41]), the presence of H_2S is still a challenge in reforming systems and a significant barrier for their commercial implementation. The content of H_2S in biogas can be reduced by employing a desulfurization unit; however, the removal of trace amounts of H_2S is often an economically unattractive option, especially in small-scale applications [25], and sulfur-containing compounds remaining after desulfurization can still reach the catalyst blocking the active sites [29,42]. Therefore, some resistance to sulfur poisoning in reforming processes is crucial to ensure proper operation under industrial conditions [40].

The objective of the present work is to study the effect of the biogas H_2S concentration on the H_2 production by catalytic SESR, which involves using a CaO-based sorbent material. The poisoning and deactivation of a Pd/Ni-Co hydrotalcite-like material (HT) catalyst during cyclic SESR experiments using biogas ($60CH_4/40CO_2$ vol.%) with

different concentrations of H_2S, together with the interaction of sulfur with the CO_2 sorbent, were analyzed. Solid-phase sulfur in catalyst and sorbent materials was characterized using SEM-EDX, XRD, XPS, and ICP-OES analyses.

2. Materials and methods

2.1. Catalyst

The 1%Pd/20%Ni-20%Co hydrotalcite-like material (Pd/Ni-Co HT) catalyst used for the SESR process was synthesized by the incipient wetness impregnation method using a 20%Ni-20%Co hydrotalcite-like material (Ni-Co HT) precursor. The Ni-Co HT precursor was synthesized by co-precipitation of $Ni(NO_3)_2{\cdot}6H_2O$, $Co(NO_3)_3{\cdot}6H_2O$, $Mg(NO_3)_3{\cdot}6H_2O$ and $Al(NO_3)_3{\cdot}9H_2O$. A detailed description of the precursor preparation procedure has been reported elsewhere [43]. The Ni-Co HT precursor was impregnated with a Pd solution to render a 1 wt.% load of Pd in the catalyst. The Pd solution was prepared by dissolving $PdCl_2$ into two equivalents of HCl and diluting them in ethanol to the desired concentration. The calcined catalyst was pelletized, ground and sieved to obtain a particle size of 250–500 μm. It was then reduced at 670 °C (heating rate of 2 °C min^{-1}) for 10 h in a mixed flow of H_2 (50NmL min^{-1}) and N_2 (50 NmL min^{-1}). A detailed description of the preparation procedure of the Pd/Ni-Co HT catalyst, alongside its characterization, has been reported elsewhere [16]. The Pd/Ni-Co HT catalyst has a BET surface area of 144 m^2/g and an average pore size of 12 nm. The metal dispersion estimated by chemisorption of H_2 on the reduced catalyst is 7.8%, while the particle size and the metal surface area are 13 nm and 21 $m^2_{metal}\,g^{-1}_{catalyst}$, respectively.

2.2. CO_2 sorbent

Arctic dolomite was supplied by Franzefoss Minerals AS, Norway, and used as a CO_2 sorbent. It has a purity of approximately 98.5 wt.% $CaMg(CO_3)_2$ and no sulfur, according to X-ray fluorescence analysis. Its estimated initial maximum CO_2 capture capacity was 0.46 g CO_2/g sorbent. It was calcined in an air flow (200 mL min^{-1}) at 800 °C for 4 h prior to use.

2.3. Experimental procedure

The schematic flow diagram of the experimental setup used for the catalytic biogas SESR experiments is shown in Fig. 1. It consists of a purpose-built downdraft fixed bed stainless steel reactor (21.5 mm internal diameter and 35 cm height), which is located inside a tubular electric furnace. The reaction temperature is controlled by a K-type thermocouple inserted into the catalyst/sorbent bed and connected to a temperature controller and data recorder. Bronkhorst® mass flow controllers deliver the gases. Water is fed in with a Gilson® high-performance liquid chromatography (HPLC) pump.

The reactor was loaded with a 10.5 g mixture of calcined dolomite and Pd/Ni-Co HT catalyst (sorbent-to-catalyst ratio = 20 g/g). SESR experiments were carried out using a simulated biogas stream with a composition of 60/40 CH_4/CO_2 vol.% under atmospheric pressure. H_2S was introduced into the reactor from a cylinder containing H_2S (200 ppm) diluted in N_2. Different concentrations of H_2S in the biogas were studied (150, 350, 500, and 1000 ppm), alongside the absence of H_2S for comparison purposes. The experiments were performed at 600 °C, under a steam/CH_4 molar ratio (S/CH_4) of 6 (i.e., three times higher than the stoichiometric value, which was shown as the best condition in previous SESR works [19,23]). Gas hourly space velocity (GHSV) of 1803 $mL_{CH4}\,g^{-1}_{cat}h^{-1}$ was selected to be able to obtain conversion values close to the equilibrium [19,23]. During a typical experiment, the SESR reaction occurs until the calcined dolomite becomes saturated (pre-breakthrough) and losses its capacity to remove CO_2. Afterwards, since the CO_2 capture capacity of the sorbent is negligible (post-breakthrough), a conventional catalytic steam reforming process is assumed to occur. After the reforming stage, the bed was subjected to a regeneration step before the next SESR cycle at 800 °C in air flow (200 NmL min^{-1}) until the CO_2 levels dropped to less than 0.1 vol.%. A reduction step at 670 °C, such as that described in the experimental procedure for the catalyst synthesis, was then carried out after regeneration. The SESR of biogas containing H_2S was evaluated during the pre-breakthrough stage. When the sorbent becomes saturated, which can be detected visually during the experiment by the CO_2 concentration increase in the outlet gas, the operating conditions are changed to perform the regeneration stage. In this work, experiments were carried out during five consecutive SESR cycles for all H_2S concentrations.

The reactor was heated to the desired reaction temperature under a N_2 atmosphere (100 NmL min^{-1}). Once the bed reached the operating temperature, the CH_4/CO_2 mixture, steam, N_2 (used as internal standard), and H_2S were introduced downdraft to the reactor through the catalyst/sorbent bed. Liquid H_2O was first evaporated and then mixed with the gas stream. This mixture was heated to 200 °C in a preheating zone before being fed into the reactor. The effluent gas exiting the reactor was cleaned by a ceramic filter and directed to a thermoelectric cooling tank to condensate the excess steam and other condensable compounds that may have formed. The dry gas composition was analyzed online by a dual channel Varian® CP-4900 Micro GC equipped with Molsieve 5 Å and PPQ columns and a thermal conductivity detector (TCD). Helium was the carrier gas. The species measured were H_2, CH_4, CO, and CO_2. The component distribution was calculated based on the nitrogen-free and dry composition of the gas effluent. The flow rates of the species generated during the experiment were calculated running a nitrogen balance since the amount of nitrogen fed in and evolved is known.

H_2 yield, H_2 selectivity, CH_4 conversion, H_2 purity, and CH_4, CO and CO_2 concentrations were calculated from Eqs. (8)–(12), respectively:

$$H_2\ yield\quad (\%) = 100{\cdot}\left(F_{H2,out}/4{\cdot}F_{CH4,in}\right) \tag{8}$$

$$H_2\quad selectivity\quad (\%) = 100{\cdot}\left[2{\cdot}F_{H2,out}/\left(2{\cdot}F_{H2,out} + 4{\cdot}F_{CH4,out}\right)\right] \tag{9}$$

$$CH_4\quad conversion\quad (\%) = 100{\cdot}\left(\left(F_{CH4,in} - F_{CH4,out}\right)/F_{CH4,in}\right) \tag{10}$$

$$H_2\quad purity\quad (vol.\%) = 100{\cdot}\left(F_{H2,out}/\sum_i F_{i,out}\right) \tag{11}$$

$$CH_4/CO/CO_2 (vol.\%) = 100{\cdot}\left(F_{CH4/CO/CO2,out}/\sum_i F_{i,out}\right) \tag{12}$$

where $F_{i,out}$ is the molar flow rate of each species i produced and $F_{CH4,in}$ is the molar flow rate of methane fed in.

The gas hourly space velocity (GHSV) is defined as the ratio of the methane volumetric flow rate to the mass of catalyst, according to Eq. (13):

$$\mathrm{GHSV}\left(mL_{CH4}\,g_{cat}^{-1}h^{-1}\right) = \frac{\text{Volumetric flow rate of inlet } CH_4\ \left(mL_{CH4/biogas}\ h^{-1}\right)}{\text{Mass of catalyst (g)}} \tag{13}$$

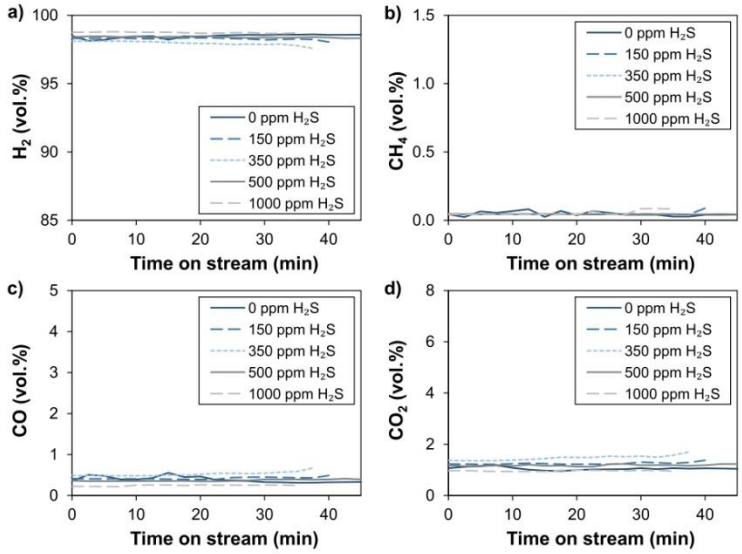

Fig 2. H_2 (a), CH_4 (b), CO (c), and CO_2 (d) concentrations in the outlet gas during the first cycle of biogas SESR as a function of the time on stream for different H_2S concentrations. Operating conditions: Biogas = 60/40 CH_4/CO_2 vol.%; T = 600 °C; S/CH_4 = 6 mol/mol; GHSV = 1803 mL_{CH4} g_{cat}^{-1} h^{-1}; sorbent/catalyst ratio = 20 g/g; Pd/Ni-Co HT catalyst and dolomite sorbent.

2.4. Sulfur analysis and characterization of spent catalyst and sorbent

Inductively coupled plasma optical emission spectrometry (ICP-OES) analysis was used to determine the total sulfur in the spent catalyst and sorbent materials using an Agilent 5110 SVDV ICP-OES analyzer. Before analysis, samples were digested in a mixture of HNO_3, HCl, H_2O_2, and deionized water.

Scanning electron microscopy (SEM) was performed on the spent catalyst and sorbent materials in a Quanta FEG 650 scanning electron microscope coupled to an energy-dispersive X-ray (EDX) detector for detailed elemental mapping.

The fresh and spent sorbents were characterized by physical adsorption of N_2 at − 196 °C using an ASAP 2420 V2.09 analyzer. Samples were outgassed overnight under a vacuum at 120 °C before adsorption measurement. The apparent surface area (S_{BET}) was calculated using the Brunauer-Emmett-Teller (BET) equation in the relative pressure interval of 0.01 to 0.1 [44]. The total pore volume (V_p) was estimated from the amount of nitrogen adsorbed at a relative pressure of 0.99.

The crystalline structure of the spent catalyst and sorbent materials was studied by powder X-ray diffraction (XRD) analysis in a Philips X'Pert diffractometer using Cu-Kα radiation (λ = 0.1541 nm). Samples were scanned in the 2θ range from 10 to 90°.

The surface analysis of the spent catalyst and sorbent materials was performed by X-ray photoelectron spectroscopy (XPS) using a SPECS instrument under a pressure of 10^{-7} Pa and using a non-monochromatic Al Kα X-ray source (14 kV at 175 W). XPS data were analyzed using CasaXPS software. The binding energy (BE) values were referred to the BE of environmental carbon C 1s at 285 eV.

3. Results and discussion

3.1. Effect of the biogas H_2S concentration on the cyclic SESR operation

3.1.1. Catalyst activity and process performance in the presence of H_2S

To study the activity of the catalyst during cyclic SESR of biogas containing H_2S, five carbonation/calcination cycles were performed for different H_2S concentrations in the inlet biogas. Between consecutive SESR cycles, after the reforming stage, a sorbent regeneration step by calcination and a reduction step were carried out. Simulated biogas with 60/40 CH_4/CO_2 vol.% and H_2S concentrations of 150, 350, 500, and 1000 ppm were used for the experimental study. Fig. 2 shows the results of the H_2, CH_4, CO, and CO_2 concentrations in the outlet gas during the first cycle of biogas SESR as a function of the time on stream for all H_2S concentrations and for the complete pre-breakthrough stage before the sorbent saturation. The results for SESR of biogas without H_2S are also shown for comparison.

No catalyst deactivation is detected for biogas H_2S concentrations between 150 and 1000 ppm during the first cycle of SESR since the H_2 purity is similar to that obtained from the SESR of biogas free of H_2S. If some partial catalyst deactivation had occurred due to a slight excess of catalyst for the methane conversion, it still did not influence the results after one cycle. The concentration of produced gases is stable during SESR until the sorbent saturation, indicating that the Pd/Ni-Co HT catalyst keeps its activity during the SESR of biogas over the time of the experiment for any of the H_2S concentrations studied. On the contrary,

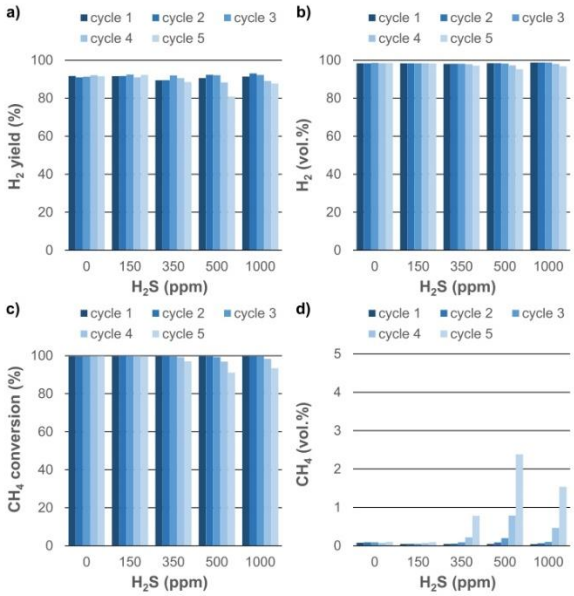

Fig 3. H_2 yield (a), H_2 purity (b), CH_4 conversion (c), and CH_4 concentration (d) during five cycles of SESR for all H_2S concentrations. Operating conditions: Biogas = 60/40 CH_4/CO_2 vol.%; T = 600 °C; S/CH_4 = 6 mol/mol; GHSV = 1803 mL_{CH4} g_{cat}^{-1} h^{-1}; sorbent/catalyst ratio = 20 g/g; Pd/Ni-Co HT catalyst and dolomite sorbent.

previous works in the literature on the biogas conventional SR process have found that the H_2S-poisoning phenomenon usually proceeds quickly depending upon the H_2S concentration in the gas (15–145 ppm) and operating temperature, and they show a steady process after the detected poisoning [26,45]. For example, the catalyst was shown to be almost inactive at 800 °C when using 108 ppm H_2S, whereas it maintained about 55% of its original activity for 31 ppm H_2S. At 700 °C, feeding 108 ppm H_2S, it only kept 8%. It has been suggested that a certain level of sulfur is probably formed on the catalyst particles in the bed, after which the remained poisoning effect is steady and does not increase with time [26].

Fig. 3 shows the H_2 yield, H_2 concentration, CH_4 conversion, and CH_4 concentration during five cycles of SESR for all H_2S concentrations. In the experiments without H_2S and with 150 ppm H_2S, all variables keep constant upon cycling, indicating no detectable catalyst deactivation. However, for higher H_2S concentrations, a decrease in H_2 production is detected during the last cycles. In the case of an H_2S concentration of 350 ppm, a slight decrease in the H_2 production is detected in cycle #5, explained by a slightly lower value of CH_4 conversion (Fig. 3c) and a higher value of CH_4 concentration (Fig. 3d). For H_2S concentrations of 500 and 1000 ppm, the decrease in the H_2 production (Fig. 3a and 3b, respectively) turns more apparent during cycles #4 and #5, producing higher CH_4 concentrations (Fig. 3d) as a result of the lower CH_4 conversion (Fig. 3c). After cycle #4, H_2 yield slightly decreases (~3%) for biogas H_2S concentrations of 500 and 1000 ppm, with a very low decrease in the H_2 purity (~1 vol.%). However, after cycle #5, H_2 yield decreases by 10.8 and 4.5% points for biogas H_2S concentrations of 500 and 1000 ppm, respectively (with much lower H_2 purity decreases of 3 and 2 vol.%, respectively).

There is general agreement in the literature on conventional reforming processes that the main cause of the loss of catalyst activity is the formation of a sulfur layer coating the metal surface. It is assumed that hydrogen sulfide is retained by a chemisorption process (Eq. (1)). The adsorption of H_2S on the metal surface covers the active sites with sulfur, which prevents further adsorption of reactant molecules [7,26]. A faster deactivation of the catalyst and usually lower residual activity with higher H_2S concentration have also been shown in previous studies during biogas dry reforming [41], conventional steam reforming [25] and autothermal biogas reforming [46]. This can be explained because a higher H_2S/H_2 ratio favors the chemisorption of H_2S on active metal and the formation of Ni–S species [47]. The results for the SESR process evaluated in the present study show signs of poisoning on the catalyst for the highest biogas H_2S concentrations studied, even though it is far from complete deactivation.

From a practical point of view, after five SESR cycles, we have found that 150 ppm of H_2S in biogas could be a sufficiently low H_2S concentration to keep the process performance. As suggested in the literature [48], an alternative to obtaining a suitably low H_2S concentration can be the dilution of biogas with steam or cleaning the biogas to lower the H_2S content.

3.1.2. *Sorbent CO_2 capture capacity in the presence of H_2S*

To evaluate how the presence of H_2S in the biogas influences the in situ CO_2 sorption by the dolomite sorbent, we have assessed the CO_2 capture capacity of the sorbent during cyclic SESR of biogas containing different concentrations of H_2S. The CO_2 released during the sorbent

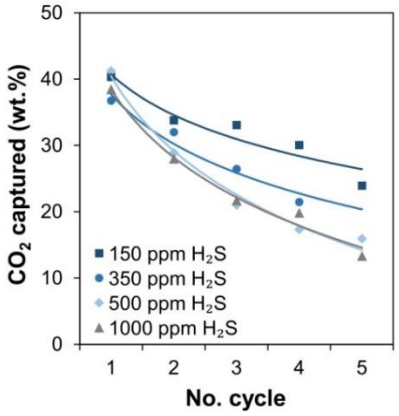

Fig 4. CO_2 captured by the sorbent during five cycles of SESR for all H_2S concentrations. Operating conditions: Biogas = 60/40 CH_4/CO_2 vol.%; $T_{reforming}$ = 600 °C; S/CH_4 = 6 mol/mol; GHSV = 1803 $mL_{CH4}\ g_{cat}^{-1}\ h^{-1}$; sorbent/catalyst ratio = 20 g/g; $T_{regeneration}$ = 800 °C; Pd/Ni-Co HT catalyst and dolomite sorbent.

Table 1
Total sulfur content of the spent Pd/Ni-Co HT catalyst and dolomite sorbent after five cycles of SESR of biogas containing different concentrations of H_2S (normalized by the feeding time).

Biogas H_2S concentration (ppm)	Total S (ppm)	
	Catalyst	Sorbent
150	1209	37
350	3132	76
500	4141	122
1000	3728	552

Operating conditions: Biogas = 60/40 CH_4/CO_2 vol.%; T = 600 °C; S/CH_4 = 6 mol/mol; GHSV = 1803 $mL_{CH_4}\ g_{cat}^{-1}h^{-1}$; sorbent/catalyst ratio = 20 g/g; Pd/Ni-Co HT catalyst and dolomite sorbent.

regeneration step accounts for the CO_2 captured by the sorbent. Fig. 4 shows the CO_2 captured by the sorbent during five carbonation/calcination cycles for all H_2S concentrations studied. As expected, CO_2 captured by the sorbent decreases with the number of cycles for all biogas H_2S concentrations due to a loss in the sorbent capacity. About the H_2S effect, the results show that CO_2 captured during the first SESR cycle is similar for all biogas H_2S contents. This value is close to the theoretical estimated maximum CO_2 capture capacity of 0.46 g CO_2/g sorbent. However, the impact of the H_2S concentration on the CO_2 sorption performance of the sorbent is clearly observed after long cycling. For cycles #2 to #5, a decrease in the CO_2 captured is detected as the H_2S concentration in the inlet biogas increases. The loss rate in CO_2 sorption capacity increases with the biogas H_2S concentration from 150 to 500 ppm, but the values of CO_2 captured along cycles are similar for 500 and 1000 ppm of H_2S.

3.2. Sulfur distribution in spent catalyst and sorbent after cyclic SESR operation

ICP-OES analyses were performed on the spent catalyst and sorbent to determine the total sulfur content. The analyses were carried out immediately after finishing five SESR cycles (including the calcination and reduction steps after cycle #5). The S concentration in the spent catalyst and sorbent materials is shown in Table 1. An increase in the S concentration of the catalyst with biogas H_2S concentration from 150 to 500 ppm is observed. However, a further increase in the biogas H_2S concentration up to 1000 ppm does not have an effect. This indicates that the poisoning effect of the H_2S on the catalyst does not proportionally increase when the biogas H_2S concentration increases from 500 to 1000 ppm, since the accumulated sulfur is slightly lower, which could explain the higher values of hydrogen production for the 1000 ppm H_2S experiment (Fig. 3).

On the other hand, the S concentration in the sorbent increases with the biogas H_2S concentration from 150 to 1000 ppm. It is worth mentioning that the sorbent S content exponentially increases with the biogas H_2S concentration up to 1000 ppm.

The distribution of sulfur from the H_2S between the sorbent, catalyst, and evolved gas was estimated from the total S contents in the sorbent and catalyst materials. The S in the gas phase was calculated by difference. Fig. 5 shows the sulfur distribution between sorbent, catalyst and gas after five cycles of the SESR process for all biogas H_2S concentrations. A similar pattern was observed for the H_2S concentrations of 150 (Fig. 5a), 350 (Fig. 5b), and 500 ppm (Fig. 5c). Almost half of the sulfur introduced (43–48%) was found in the catalyst and 32–37% in the sorbent. Therefore, 19–20% of the sulfur was released with the gas. However, for a biogas H_2S concentration of 1000 ppm (Fig. 5d), 77.5% of the sulfur introduced was found in the sorbent, while a much lower

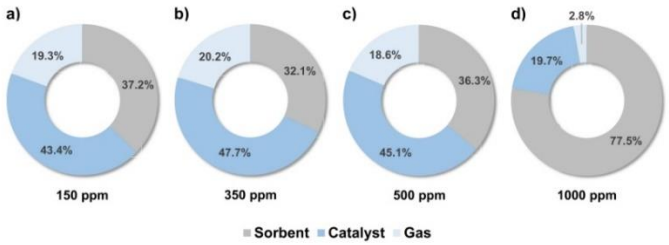

Fig 5. Sulfur distribution (wt.%) between sorbent, catalyst, and evolved gas after five cycles of the SESR process for biogas H_2S concentrations of 150 (a), 350 (b), 500 (c), and 1000 ppm (d). Operating conditions: Biogas = 60/40 CH_4/CO_2 vol.%; T = 600 °C; S/CH_4 = 6 mol/mol; GHSV = 1803 $mL_{CH4}\ g_{cat}^{-1}\ h^{-1}$; sorbent/catalyst ratio = 20 g/g; Pd/Ni-Co HT catalyst and dolomite sorbent.

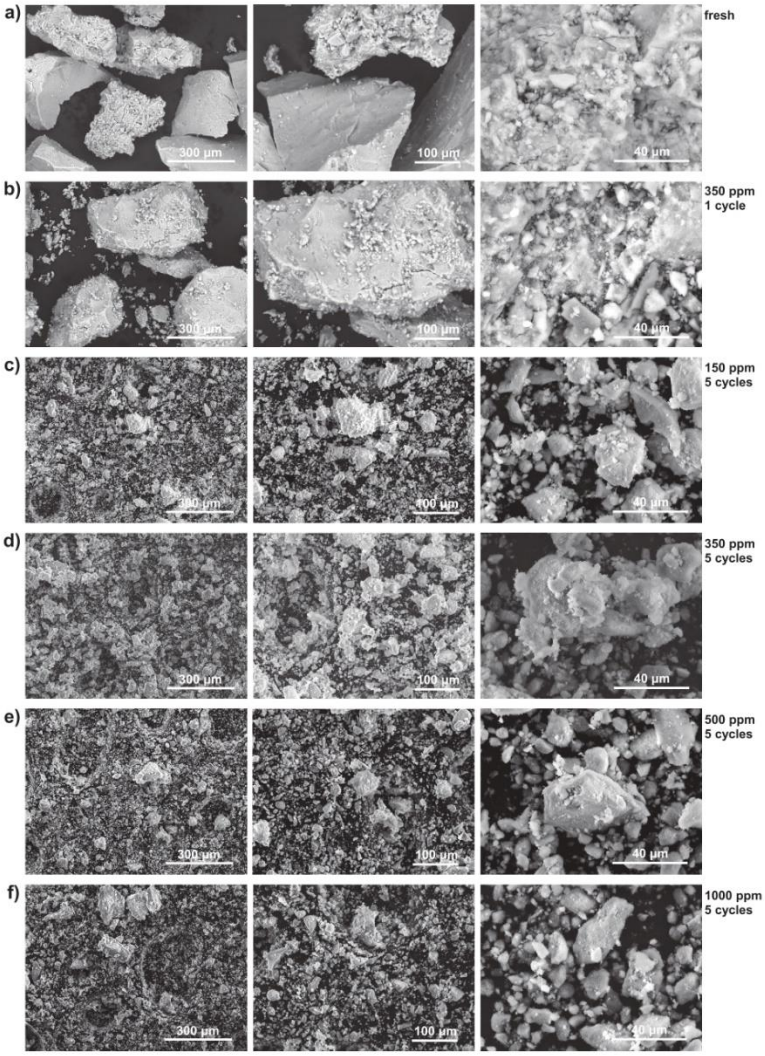

Fig 6. SEM images of the fresh and spent Pd/Ni-Co HT catalyst after one and five cycles of the SESR process for different biogas H_2S concentrations: (a) fresh catalyst; (b) 350 ppm H_2S, 1 cycle; (c) 150 ppm H_2S, 5 cycles; (d) 350 ppm H_2S, 5 cycles; (e) 500 ppm H_2S, 5 cycles; and (f) 1000 ppm H_2S, 5 cycles. Operating conditions: Biogas = 60/40 CH_4/CO_2 vol.%; T = 600 °C; S/CH_4 = 6 mol/mol; GHSV = 1803 $mL_{CH4}\ g_{cat}^{-1}\ h^{-1}$; sorbent/catalyst ratio = 20 g/g; Pd/Ni-Co HT catalyst and dolomite sorbent.

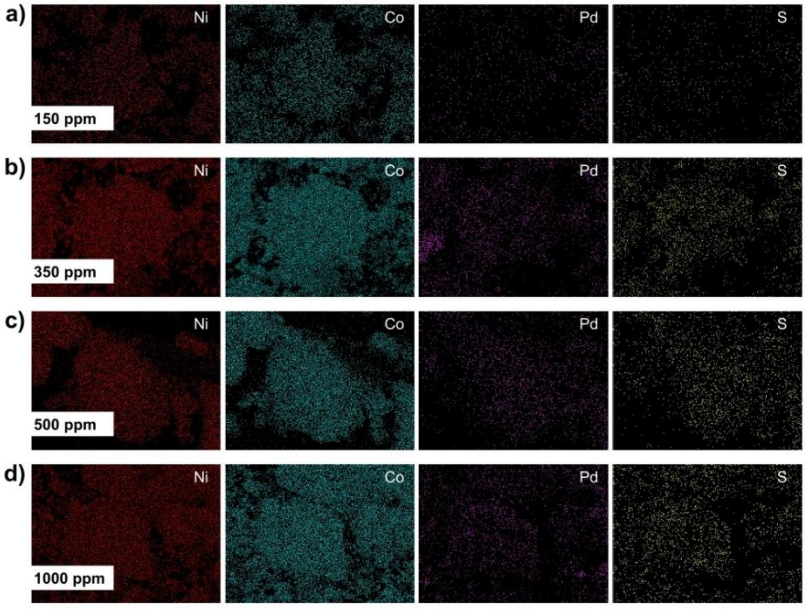

Fig 7. EDX elemental mapping of Ni, Co, Pd and S in the spent Pd/Ni-Co HT catalyst after five cycles of the SESR process for different biogas H_2S concentrations: (a) 150 ppm; (b) 350 ppm; (c) 500 ppm; and (d) 1000 ppm. Operating conditions: Biogas = 60/40 CH_4/CO_2 vol.%; T = 600 °C; S/CH_4 = 6 mol/mol; GHSV = 1803 $mL_{CH4}\ g_{cat}^{-1}\ h^{-1}$; sorbent/catalyst ratio = 20 g/g; Pd/Ni-Co HT catalyst and dolomite sorbent.

percentage, 19.7%, was detected in the catalyst. Therefore, only 2.8% would be released with the outlet gas. It suggests that higher H_2S contents favor the reaction of sulfur with the sorbent. The distribution of sulfur in the spent catalyst and sorbent shown in Fig. 5 could explain the lower catalyst poisoning effect with 1000 ppm H_2S, since higher biogas H_2S concentrations would decrease the reaction of sulfur with the catalyst at the expense of the sorbent. On the other hand, from the results obtained for 1000 ppm of H_2S, we can deduce that removing H_2S from the gas phase is jeopardized when the initial concentration is low.

On the other hand, one important outcome is that these results show that CO_2 and H_2S can be captured simultaneously during SESR under the studied conditions. Previous experiments on sorption enhanced gasification at 640–775 °C have also reported the simultaneous removal of CO_2 and H_2S by CaO [39,49,50]. Martínez et al. found that sulfur in the syngas was around 15% of the total sulfur introduced into the gasification reactor, while 65–85% of the total S was as CaS in the sorbent particles, with the remaining part detected in the unconverted char (no catalyst was used in those experiments) [50]. The present work outlines that a high proportion of sulfur remains in the solid catalyst and sorbent materials after the cyclic SESR process.

3.3. Characterization of spent catalyst after cyclic SESR operation

3.3.1. Catalyst SEM analysis

SEM analysis of the spent Pd/Ni-Co HT catalyst after five cycles of SESR was performed for all biogas H_2S concentrations. The catalyst was also analyzed after the first SESR cycle in the case of the experiment with 350 ppm of H_2S for comparison purposes. Fig. 6 shows the SEM images of the fresh catalyst (Fig. 6a), spent catalyst after cycle #1 (Fig. 6b), and spent catalyst after cycle #5 (Fig. 6c-f) of the SESR process for different biogas H_2S concentrations. The microphotographs of the fresh and the spent catalyst after one cycle are similar. However, the particle size decreases for all the spent catalyst samples after five SESR cycles. No apparent agglomeration of the catalyst particles by sintering after the five cycles is observed. Besides, the spent catalyst shows no appreciable differences for the different biogas H_2S concentrations after the five cycles.

Fig. 7 shows the EDX elemental mapping of Ni, Co, Pd, and S in the spent Pd/Ni-Co HT catalyst after five SESR cycles with biogas containing between 150 and 1000 ppm of H_2S. Elemental mapping by SEM-EDX shows the presence of sulfur in the spent catalyst for all H_2S concentrations, indicating the conversion of H_2S on the catalyst surface during the SESR process. It can be seen that sulfur has a similar distribution in the catalyst than Ni, Co and Pd, suggesting the interaction between sulfur and one (or more) metals. Under the experimental conditions studied nickel/cobalt sulfides could be formed. From a qualitative point of view, EDX mapping shows that the amount of sulfur in the spent catalyst for the experiments with 150 ppm of H_2S is visibly lower than that for the experiments with higher H_2S biogas concentrations.

3.3.2. Catalyst XRD analysis

XRD analysis identified the crystal phase composition of the spent catalyst. Fig. 8 shows the XRD spectra of the fresh and spent catalyst after five cycles of the SESR process for different biogas H_2S

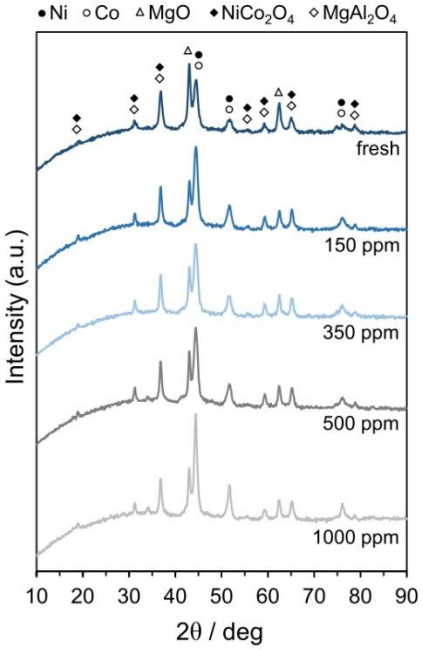

Fig 8. XRD patterns of the fresh and spent Pd/Ni-Co HT catalyst after five cycles of the SESR process for biogas H_2S concentrations of 150, 350, 500, and 1000 ppm. Operating conditions: Biogas = 60/40 CH_4/CO_2 vol.%; T = 600 °C; S/CH_4 = 6 mol/mol; GHSV = 1803 $mL_{CH4}\ g_{cat}^{-1}\ h^{-1}$; sorbent/catalyst ratio = 20 g/g; Pd/Ni-Co HT catalyst and dolomite sorbent.

concentrations. Compared to the fresh catalyst, the diffraction peak intensity of Ni and Co (2θ = 44.5°, 51.8°, and 76.3°, JCPD 87–0712) for the spent catalyst increased after cyclic SESR operation, suggesting the growth of Ni/Co crystallite size. The XRD spectra show no clear evidence of the formation of nickel/cobalt sulfide or sulfate phases, possibly due to these compounds being poorly crystalline or their content below the XRD detection limit.

The chemisorption of hydrogen sulfide on a nickel catalyst has shown to be reversible, while the sulfur coverage is a function of the ratio p_{H2S}/p_{H2}. According to thermodynamic data, a saturation layer has been observed in the 550–645 °C temperature range at p_{H2S}/p_{H2} ratios above $2–5{\cdot}10^{-6}$, whereas bulk nickel sulfide (Ni_3S_2) has been formed (Eq. (14)) at ratios above 10^{-3} [7].

$$3Ni + 2H_2S \leftrightarrow Ni_3S_2 + 2H_2 \quad (14)$$

Formation of bulk sulfide is not favored during the reforming step in SESR since it requires significantly high H_2S partial pressures, but surface-adsorbed sulfur could be expected under the operating conditions [51]. Even if that is the case, the peaks of nickel sulfide are weak and difficult to identify due to overlapping with the diffraction patterns of metal oxide compounds (i.e., MgO periclase and $MgAl_2O_4$ spinel phases) [10].

3.3.3. Catalyst XPS analysis

XPS analysis determined the chemical states of the surface Ni, Co, and S species present in the fresh and spent catalysts after five cycles of the SESR process. Fig. 9 shows the S 2p XPS spectra of the fresh (Fig. 9a) and spent catalyst after five cycles of the SESR process for biogas containing different concentrations of H_2S (Fig. 9b-e). No sulfur was found in the XPS spectra of the fresh catalyst. However, sulfur was detected for all H_2S concentrations in the spent catalyst. We can see two peaks corresponding to S $2p_{3/2}$ and S $2p_{1/2}$ at around 162.1 and 163.4 eV, respectively, which could suggest the presence of sulfur as the S^{2-} ion [48,52]. Moreover, we also see two other peaks corresponding to S $2p_{3/2}$ and S $2p_{1/2}$ at around 168.9 and 170.1 eV, respectively, indicating the presence of sulfur with a higher oxidation state, which could be attributed to sulfur oxides, such as SO_4^{2-} species [52], suggesting the oxidation of hydrogen sulfide or adsorbed sulfur during the calcination step under an air atmosphere [53].

Fig. 10 shows the Ni 2p XPS spectra of the spent catalyst after five cycles of the SESR process for biogas containing different concentrations of H_2S. We can see two peaks corresponding to Ni $2p_{3/2}$ and Ni $2p_{1/2}$ around 854.6 and 871.1 eV, respectively. In addition, two other peaks corresponding to Ni $2p_{3/2}$ and Ni $2p_{1/2}$ are seen around 856.3 and 873.6 eV, respectively. Moreover, two shake-up satellite peaks (around 861.8 and 879.1 eV) are detected. These peaks can indicate the presence of nickel as Ni^{2+}, meaning that one or more nickel-oxygen species can be present [54]. The binding energy of metallic Ni 2p is around 852.0 eV, values around 854.0 eV are characteristic of Ni^{2+} species in NiO, while binding energy around ~ 857.5 ± 0.4 can indicate the presence of Ni^{2+} species present in the $NiAl_2O_4$ phase [55–57]. On the other hand, binding energies around 856.3 ± 1 eV have been associated with Ni^{2+} species in $NiSO_4$ [10,58]. Das et al. attributed this peak to surface nickel sulfide (or sulfur chemisorbed on Ni surface) that has been converted to sulfates when exposed to air. These results would be consistent with those shown by the S 2p XPS spectra.

Fig. 11 shows the Co 2p XPS spectra of the spent catalyst after five SESR cycles for all biogas H_2S concentrations. We can see two peaks corresponding to Co $2p_{3/2}$ and Co $2p_{1/2}$ around 778.7 and 791.9 eV, respectively. In addition, two other peaks corresponding to Co $2p_{3/2}$ and Co $2p_{1/2}$ are around 781.4 and 797.1 eV, respectively. Moreover, two shake-up satellite peaks (circa. 786.2 and 802.7 eV) are detected. A peak at low values of binding energy is detected due to the use of non-monochromatic radiation. Peaks around 779.5 eV and 781.4 eV are due to surface Co^{3+} and Co^{2+} species, respectively [59]. Co $2p_{3/2}$ binding energy around 778.0 eV has been assigned to metallic cobalt [60], Co 2p binding energy around 782.8 eV to Co^{2+} species in $CoSO_4$ [58], while Co 2p binding energy around 783.5 can be associated with the Co^{2+} species in the $CoAl_2O_4$ phase. Therefore, the presence of some Co^{2+} species is confirmed, although XPS analysis does not clarify the presence of $CoSO_4$.

As explained above, in the present work, the spent catalyst and sorbent were subjected to calcination and reduction steps during the last SESR cycle. Therefore, sulfur compounds formed from H_2S during reforming could have been later converted under calcination and reduction conditions. Thus, by increasing the reaction temperature or feeding oxygen, Ni–S species on the catalyst can be cracked. The presence of oxygen can oxidize sulfur on the catalyst surface and convert Ni to NiO or $NiSO_4$ by Eqs. (15) and (16), respectively [61]. Indeed, oxidation at high temperatures is often applied to remove the adsorbed sulfur and regain the active Ni sites [26].

$$Ni–S + 3/2O_2 \leftrightarrow NiO + SO_2 \quad (15)$$

$$Ni–S + 2O_2 \leftrightarrow NiSO_4 \quad (16)$$

In chemical looping reforming (CLR) of biogas, Zheng et al. mainly detected SO_2 in the gas phase from the oxidation of the sulfur compounds attached to the oxygen carrier during the reduction/reforming step (mainly NiS_2) [48]. In chemical looping combustion (CLC) of

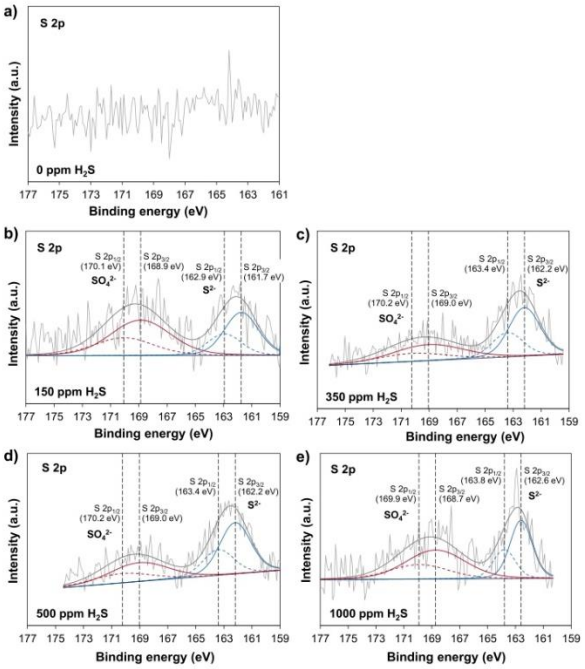

Fig 9. XPS surface spectra for S 2p of the fresh (a) and spent Pd/Ni-Co HT catalyst after five cycles of the SESR process for biogas H_2S concentrations of 150 (b), 350 (c), 500 (d), and 1000 ppm (e). Operating conditions: Biogas = 60/40 CH_4/CO_2 vol.%; T = 600 °C; S/CH_4 = 6 mol/mol; GHSV = 1969 $mL_{CH4}\ g_{cat}^{-1}\ h^{-1}$; sorbent/catalyst ratio = 20 g/g; Pd/Ni-Co HT catalyst and dolomite sorbent.

biogas, Dueso et al. reported that nickel sulfide was found in the oxygen carrier after the reduction step. These authors found that part of the sulfur retained in the solid as nickel sulfide during reforming was later released as SO_2 during oxidation due to nickel sulfide oxidation to form nickel sulphate was favored at high oxygen concentrations (21 vol.%) [54].

In the present study, after calcination, a reduction step under a mixture of hydrogen and nitrogen was carried. Under this atmosphere, nickel compounds, such as Ni_3S_2 and $NiSO_4$ can be reduced by Eqs. (17) and (18), respectively [62].

$$Ni_3S_2 + 2H_2 \rightarrow 3Ni + 2H_2S \quad (17)$$

$$3NiSO_4 + 13H_2 \rightarrow Ni_3S_2 + 12H_2O + 2H_2S \quad (18)$$

Fig. 10 shows that the peak around 854 eV decreases as the H_2S concentration in biogas increases. Conversely, the peak at 864 eV increases with biogas H_2S content. It could indicate that the formation of $NiSO_4$ is higher during the regeneration step, and it is not converted again into sulfide species during reduction. It could contribute to decreasing the catalyst activity as detected for high sulfur concentrations.

3.4. Characterization of spent sorbent after cyclic SESR operation

3.4.1. N_2 Adsorption analysis of the sorbent

Table 2 shows the results of the surface area analysis by N_2 adsorption at − 196 °C after five cycles of the SESR process for different biogas H_2S concentrations. The BET surface area of the fresh sorbent was 23.9 m^2/g and reduced to ~ 11 m^2/g after five cycles of biogas SESR. Likewise, the total pore volume decreased from 0.27 $cm^3\ g^{-1}$ to ~ 0.10 $cm^3\ g^{-1}$ after cycling. A reduction of the surface area and pore volume has been previously reported in cyclic experiments of bio-oil SESR [16] and sorption enhanced water gas shift (SEWGS) [63]. The surface area and pore volume of CaO-based materials decrease with the number of CO_2 capture cycles due to sintering during the regeneration at high temperatures [64]. However, the BET surface area and total pore volume remained unaltered for the different biogas H_2S concentrations.

The decrease in the CO_2 capture capacity of the sorbent shown in Fig. 4 can be explained by deactivation due to the reduction in surface area and pore volume by CaO sintering. The oxidation reactions are highly exothermic, while reduction is endothermic. A high O_2 concentration in oxidation has been shown to cause the sintering of sorbent due to the strong exothermic reaction, which can explain the loss of CO_2 capture capacity in cyclic operation. However, the reduction should not cause the sintering of the sorbent, as previously reported [65].

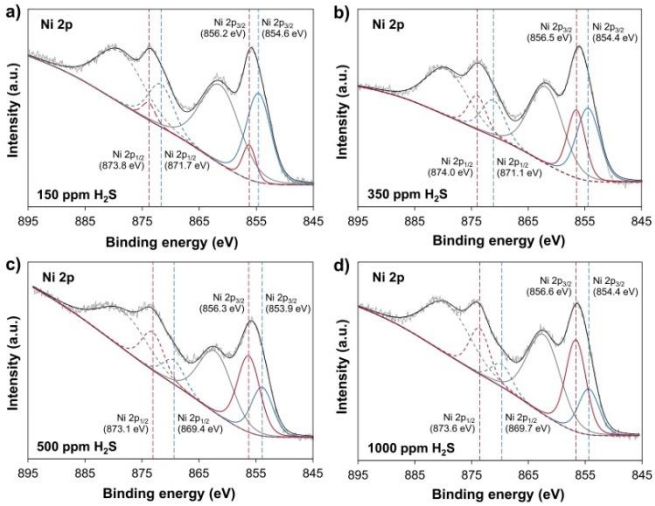

Fig 10. XPS surface spectra for Ni 2p of the spent Pd/Ni-Co HT catalyst after five cycles of the SESR process for biogas H_2S concentrations of 150 (a), 350 (b), 500 (c), and 1000 ppm (d). Operating conditions: Biogas = 60/40 CH_4/CO_2 vol.%; T = 600 °C; S/CH_4 = 6 mol/mol; GHSV = 1969 $mL_{CH4}\ g_{cat}^{-1}\ h^{-1}$; sorbent/catalyst ratio = 20 g/g; Pd/Ni-Co HT catalyst and dolomite sorbent.

3.4.2. Sorbent SEM analysis

SEM analysis of the spent sorbent after five cycles of SESR was carried out for all biogas H_2S concentrations. For comparison purposes, the spent sorbent was analyzed after the first SESR cycle for the experiment with 350 ppm of H_2S. Mapping of S in the spent sorbent by EDX did not detect sulfur under any operating conditions because its concentration was below the detection limit of the SEM analyzer. Fig. 12 shows the SEM images of the fresh sorbent (Fig. 12a), spent sorbent after cycle #1 (Fig. 12b), and spent sorbent after five cycles (Fig. 12c-f) of the SESR process for different biogas H_2S concentrations. If we compare the images of the fresh sorbent with those of the spent sorbent, a growth of the CaO grains in the sorbent is observed after five cycles, as has also been reported in the literature [64]. This effect is less apparent in the spent sorbent after cycle #1. However, no appreciable differences can be seen in the spent sorbent after five cycles for the different initial biogas H_2S concentrations. On the other hand, certain agglomerating and fusion of CaO grains due to sintering can be detected in the spent sorbent after five cycles.

3.4.3. Sorbent XRD analysis

Fig. 13 shows the XRD spectra of the fresh and spent sorbent after five SESR cycles for different biogas H_2S concentrations. The XRD spectra indicate the presence of mainly CaO and MgO phases in the fresh and the spent sorbent samples, although the presence of $Ca(OH)_2$ is also present. CaO can absorb moisture and transform into $Ca(OH)_2$ when the regenerated sorbent contacts an air atmosphere [65]. However, the XRD spectra show no presence of S-containing phases, which may be due to these compounds in the sorbent samples being amorphous or with very low crystallinity or their amounts being too low to reach the detection limit of the XRD analyzer. It is probable that, given the low content of sulfur in the sorbent, neither CaS nor $CaSO_4$ are detectable by XRD analysis.

The average crystal sizes have been estimated from the XRD peaks using the Scherrer equation, and their values are shown in Table 2. There is a slight increase in the CaO crystal sizes after SESR cyclic operation compared to fresh sorbent. As suggested by the decrease in the surface area and pore volume after cycling, the growth in the CaO crystal size can be explained by sorbent sintering. It also agrees with the CaO grains growth observed in the SEM analysis after five SESR cycles.

In addition, the average crystal size of CaO increases (from 36.4 for 150 ppm to 39.6 nm for 1000 ppm) with the biogas H_2S concentration. The H_2S concentration does not influence the MgO crystal size. It has been reported in the literature that MgO is not reactive with sulfur compounds [66], and MgS is an unstable compound [67]. As mentioned, the CaO crystal size growth can be explained by sorbent sintering. As with CaO [68], it has been reported in the literature that sintering of CaS can occur and play a role in reducing the effectiveness of limestone as a high-temperature sorbent for H_2S [69]. According to the XRD results, this effect would be higher as biogas H_2S concentration increases, which could explain the decrease in the CO_2 capture capacity with the H_2S content in biogas.

3.4.4. Sorbent XPS analysis

XPS analysis determined the chemical states of the surface S species present in the spent sorbent after five cycles of the SESR process. Fig. 14 shows the S 2p XPS spectra of the fresh (Fig. 14a) and the spent (Fig. 14b) sorbent after five cycles of SESR of biogas containing 1000 ppm H_2S. Sulfur was not found in the XPS spectra of the fresh sorbent and the spent sorbent for lower concentrations of H_2S (not shown). Fig. 14a shows a small peak at the highest binding energies, which could be associated with a beta satellite peak generated by the excitation of the Al and Mg signals. A similar XPS spectrum to that shown in Fig. 14a is observed for all the sorbent samples after SESR with biogas H_2S contents of 150–500 ppm (data not shown). However, in the case of 1000 ppm

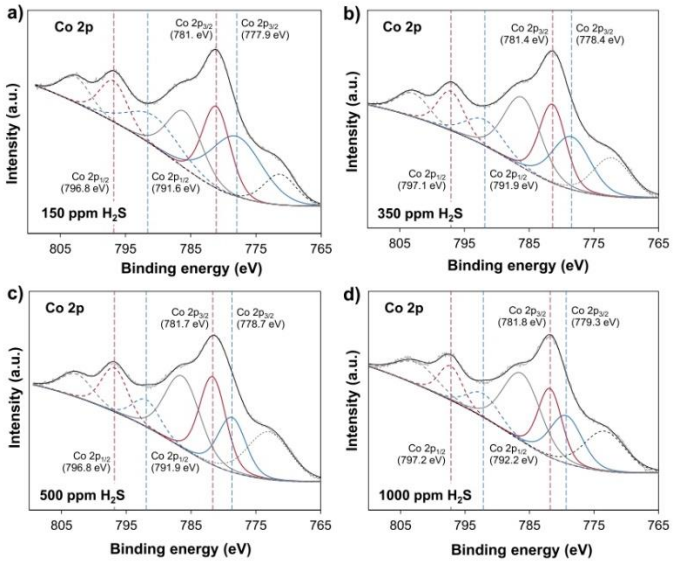

Fig 11. XPS surface spectra for Co 2p of the spent Pd/Ni-Co HT catalyst after five cycles of the SESR process for biogas H_2S concentrations of 150 (a), 350 (b), 500 (c), and 1000 ppm (d). Operating conditions: Biogas = 60/40 CH_4/CO_2 vol.%; T = 600 °C; S/CH_4 = 6 mol/mol; GHSV = 1969 mL_{CH4} g_{cat}^{-1} h^{-1}; sorbent/catalyst ratio = 20 g/g; Pd/Ni-Co HT catalyst and dolomite sorbent.

Table 2
Physical properties of the fresh and spent dolomite sorbent after five cycles of SESR of biogas containing different concentrations of H_2S.

	Dolomite sorbent sample				
	fresh	150 ppm H_2S	350 ppm H_2S	500 ppm H_2S	1000 ppm H_2S
N_2 adsorption at −196 °C					
BET surface area, S_{BET} (m^2 g^{-1})	22.9	10.8	10.7	10.9	11.2
Total pore volume, V_p (cm^3 g^{-1})	0.27	0.12	0.10	0.09	0.10
XRD					
Crystallite size CaO (nm)	35.2	36.4	37.9	38.1	39.6
Crystallite size MgO (nm)	26.7	28.3	28.9	28.5	29.1

Operating conditions: Biogas = 60/40 CH_4/CO_2 vol.%; T = 600 °C; S/CH_4 = 6 mol/mol; GHSV = 1803 mL_{CH_4} $g_{cat}^{-1}h^{-1}$; sorbent/catalyst ratio = 20 g/g; Pd/Ni-Co HT catalyst and dolomite sorbent.

H_2S, the XPS spectrum shows a peak at lower binding energy, as shown in Fig. 14b. This peak was not detected for lower H_2S concentrations probably because the sulfur concentration in these samples was below the detection limit of the XPS analyzer.

The S 2p XPS spectrum for the 1000 ppm sample shows a peak corresponding to S $2p_{3/2}$ and S $2p_{1/2}$ at 160.7 and 161.9 eV, respectively, which suggests the presence of sulfur as the S^{2-} ion [48,52]. These results indicate that H_2S could have reacted with the Ca on the sorbent surface during the reforming step of the SESR process and could have contributed to the decrease of the sorbent CO_2 capture capacity. Since the ratio between the CaO introduced with the calcined dolomite into the reactor and the sulfur introduced with the biogas was very high, H_2S conversion to CaS (Eq. (7)) could occur until equilibrium was reached, as previously reported for sorption enhanced gasification experiments [50].

On the other hand, CaS is a relatively unstable product that can react with O_2 under the oxidant atmosphere of the regeneration step to form stable $CaSO_4$ by Eq. (19) as a tight layer on the surface of the sorbent that reduces the extent of the calcination reaction [70]. This could explain the decrease in the CO_2 capture capacity during cyclic SESR of biogas containing H_2S. If $CaSO_4$ is produced during the SESR cycles, it could contribute to plugging the pores and hinder the mass transfer of CO_2 into the sorbent particles, reducing the CO_2 removal capacity.

$$CaS + 2O_2 \leftrightarrow CaSO_4 \quad (19)$$

Sulfur peaks associated with sulfates formation during the calcination step of the SESR process under an air atmosphere could be found at higher binding energy (around 168–170 eV) [52]. However, these peaks would overlap with the satellite peak shown in Fig. 14b. Besides, as already mentioned, the sulfur concentration in this sample is probably below the detection limit.

3.5. Discussion from the comparison of catalyst deactivation during SESR and conventional SR

It has been widely shown in the literature that Ni catalysts are

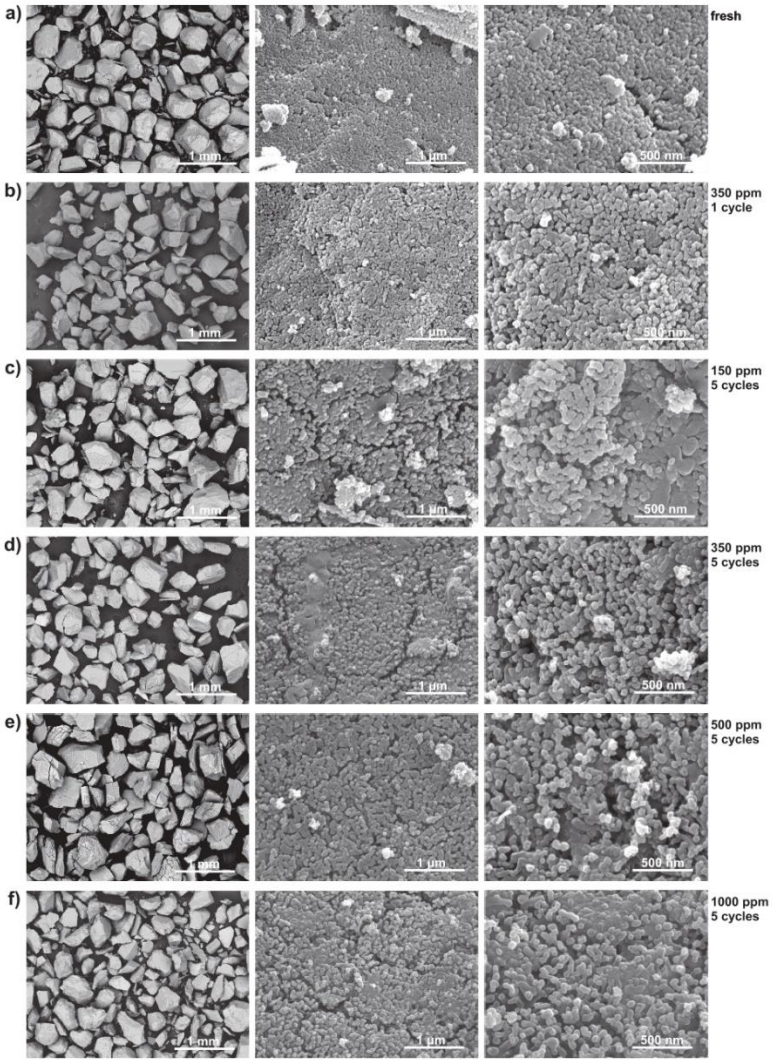

Fig 12. SEM images of the fresh and spent dolomite sorbent after one and five cycles of the SESR process for different biogas H_2S concentrations: (a) fresh sorbent; (b) 350 ppm H_2S, 1 cycle; (c) 150 ppm H_2S, 5 cycles; (d) 350 ppm H_2S, 5 cycles; (e) 500 ppm H_2S, 5 cycles; and (f) 1000 ppm H_2S, 5 cycles. Operating conditions: Biogas = 60/40 CH_4/CO_2 vol.%; T = 600 °C; S/CH_4 = 6 mol/mol; GHSV = 1803 $mL_{CH4}\ g_{cat}^{-1}\ h^{-1}$; sorbent/catalyst ratio = 20 g/g; Pd/Ni-Co HT catalyst and dolomite sorbent.

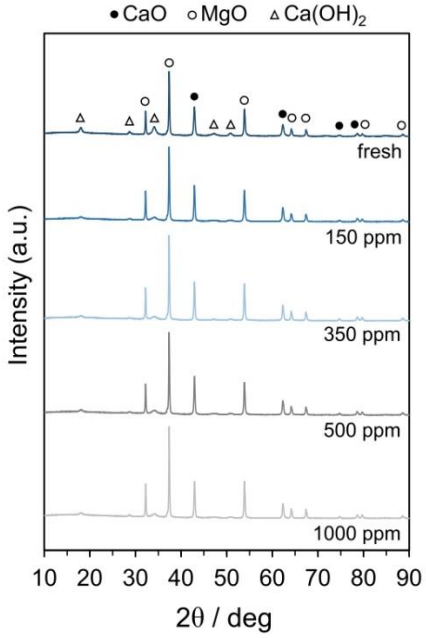

Fig 13. XRD patterns of the fresh and spent dolomite sorbent after five cycles of the SESR process for biogas H_2S concentrations of 150, 350, 500, and 1000 ppm. Operating conditions: Biogas = 60/40 CH_4/CO_2 vol.%; T = 600 °C; S/CH_4 = 6 mol/mol; GHSV = 1803 $mL_{CH4}\ g_{cat}^{-1}\ h^{-1}$; sorbent/catalyst ratio = 20 g/g; Pd/Ni-Co HT catalyst and dolomite sorbent.

deactivated by the presence of H_2S during conventional reforming processes, even at very low H_2S concentrations. Under SR operation, H_2S poisoning resulted in an exponential decrease in the catalyst activity, and even at an H_2S concentration of 30 ppm, the reforming catalyst showed a drop in activity of 86% after 12 h at 700 °C, being the decay much faster at higher sulfur levels [26]. This study also remarked that the poisoned Ni catalyst only kept an acceptable residual activity when working at 900 °C (86% of the original methane conversion with 108 ppm H_2S).

Appari et al. [25] showed that the H_2S presence (20–100 ppm) led to the deactivation of a Ni/Al_2O_3 catalyst in SR experiments of biogas, and higher H_2S concentrations showed faster deactivation. All H_2S concentrations led to almost complete deactivation (98%) of the catalyst at 700 °C. However, at 800 °C, the residual activity remained at 34% of CH_4 conversion for 100 ppm H_2S concentration in the feed gas, 43% for 50 ppm, and 48% for 20 ppm. H_2S poisoning was also detected by Ashrafi et al. [26] during conventional SR for H_2S concentrations of 15–145 ppm and temperatures of 700–800 °C. Almost complete deactivation of a Ni/Al_2O_3 catalyst was also shown by Pawar et al. [34] for the dry reforming of biogas in experiments at 700 and 800 °C with 5 and 10 ppm of H_2S in the feed gas. Das et al. [10] reported that a Ni-MgAl catalyst started to deactivate almost instantaneously and lost approximately 80% of the initial CH_4 conversion activity within 1.5 h in the presence of H_2S during dry methane reforming.

In the present study, the decrease in the activity of the Pd/Ni-Co HT catalyst used for the SESR process of biogas is much lower compared to conventional steam reforming studies, showing a higher H_2S tolerance. Furthermore, steady-state catalytic activity was observed during the sorption enhanced reforming stage. In these SESR experiments, a CaO breakthrough occurs before the catalyst is completely deactivated. In conventional steam reforming processes, the H_2S poisoning effect varies exponentially with time on stream and the final activity of the catalyst depends on the uncovered active surface available [45]. Then, we can infer that active catalytic sites are still active after cyclic SESR.

Yeo et al. [40] reviewed the recent developments in sulfur-resilient catalysts, pointing out that bimetallic formulations involving nickel and another complementary metal such as cobalt, iron or copper seem to impart variable degrees of resistance to sulfur to the catalyst. It has been shown that co-impregnation of cobalt with nickel to obtain a bimetallic catalyst led to increased stability against sulfur poisoning during dry methane reforming (100 ppm of H_2S), suggesting that cobalt played a sacrificial role by intercepting some of the sulfur content in the feed and preventing it from deactivating the nickel sites [30]. Other works in the

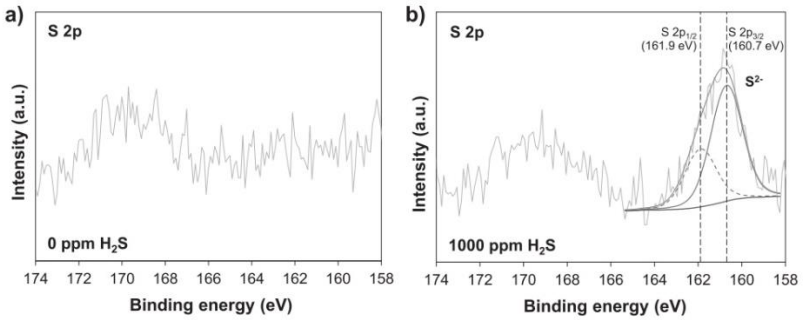

Fig 14. XPS surface spectra for S 2p of the fresh (a) and the spent dolomite sorbent after five cycles of the SESR process for a biogas H_2S concentration of 1000 ppm (b). Operating conditions: Biogas = 60/40 CH_4/CO_2 vol.%; T = 600 °C; S/CH_4 = 6 mol/mol; GHSV = 1803 $mL_{CH4}\ g_{cat}^{-1}\ h^{-1}$; sorbent/catalyst ratio = 20 g/g; Pd/Ni-Co HT catalyst and dolomite sorbent.

literature have reported that adding cobalt delays the deactivation by H_2S compared to a single Ni catalyst. Thus, Jiang et al. [71] showed that catalysts containing both Ni and Co are stable over long periods under dry methane reforming conditions (775 °C; 20–30 ppm of H_2S), while a Ni-only catalyst completely deactivated after contact with sulfur. This was attributed to Ni-Co interaction since the electronic modifications of the Ni in the smaller metal clusters caused by interaction with Co hinder the adsorption of H_2S. Das et al. [10] reported that compared to Ni-MgAl, a NiCo-MgAl catalyst showed much better resistance to the deactivation in H_2S during dry reforming of methane (800 °C; 20 ppm of H_2S), and negligible deactivation was observed for 4 h after the introduction of H_2S, with the CH_4 conversion remaining > 90%, which rapidly decreased after that time. The promoting role of Co on sulfur tolerance is ascribed to an electronic interaction exerted by Co on Ni that alters sulfur chemisorption kinetics. Likewise, Ashok et al. [59] found that deactivation by sulfur poisoning of a Ce-doped Co perovskite catalyst was temporary and reversible during the reforming reaction. All these results indicate that adding Co can decrease the overall rate of sulfur adsorption on the catalyst surface.

In the present work, we prevented the Ni poisoning, not only by using a bi-metallic catalyst that includes Co, but also a CO_2 sorbent that contributed to lower the poisoning of the catalyst, retaining a significant amount of sulfur in the dolomite.

4. Conclusions

Hydrogen production by sorption enhanced steam reforming (SESR) of biogas (60/40 CH_4/CO_2 vol.%) containing H_2S was studied using a Pd/Ni-Co hydrotalcite-like material (HT) catalyst and dolomite as a sorbent material. No relevant catalyst deactivation due to H_2S poisoning was detected during cyclic SESR of biogas for H_2S concentrations of 150 and 350 ppm at 600 °C. However, H_2S concentrations of 500–1000 ppm slightly reduced H_2 yield (between 4.5% and 10.8% points) and H_2 purity (between 2% and 3% points). These results suggest that cleaning the biogas to reduce the levels of H_2S below 350 ppm could enable the use of biogas for hydrogen production by the SESR process. Sulfur was detected in both the spent catalyst and sorbent materials. For 1000 ppm of H_2S in the inlet biogas, most of the sulfur was retained in the spent sorbent particles after cyclic SESR. The XPS characterization of the catalyst revealed that not only S^{2-} species are formed, but also SO_4^{2-} species are present due to the different oxidation/reduction steps involved in the cyclic continuous operation. On the other hand, S^{2-} species were detected in the sorbent, but the presence of SO_4^{2-} could not be confirmed. Future works could be directed towards evaluating higher biogas H_2S concentrations alongside a longer continuous operation (i.e., a higher number of SESR cycles). Besides, kinetics studies could also provide insights on sulfur-catalyst interactions.

Catalyst deactivation during cyclic SESR was notably lower than that usually detected in conventional steam reforming processes, which suggests that, together with the use of a bimetallic catalyst containing Co, the presence of a sorbent that can react with sulfur compounds could make the SESR process more resistant to H_2S. Since the chemisorption of sulfur on nickel is a reversible process, the activity of sulfur-poisoned catalysts could be partly recovered at high temperatures under different atmospheres by the gradual desorption of sulfur. The effect of sorbent calcination conditions (such as temperature, oxygen concentration or gas flow), as well as catalyst reduction operating parameters, on the possible regeneration of the sulfur-poisoned catalyst will be evaluated in future studies.

Declaration of Competing Interest

The authors declare that they have no known competing financial interests or personal relationships that could have appeared to influence the work reported in this paper.

Data availability

Data will be made available on request.

Acknowledgements

The authors thank Franzefoss Minerals AS (Norway) for supplying Arctic dolomite. This work was carried out through Grant PID2020-119539RB-I00, funded by MCIN/AEI /10.13039/501100011033, and Grant IDI/2021/000060 (PCTI) from the Gobierno del Principado de Asturias A. Capa acknowledges a fellowship awarded by the FPI program through Grant PRE2018-083634, funded by MCIN/AEI/ 10.13039/501100011033 and by "ESF Investing in your future". M.V. Gil acknowledges support from the Ramón y Cajal Grant RYC-2017-21937 funded by MCIN/AEI/ 10.13039/501100011033 and by "ESF Investing in your future".

References

[1] D.G. Avraam, T.I. Halkides, D.K. Liguras, O.A. Bereketidou, M.A. Goula, An experimental and theoretical approach for the biogas steam reforming reaction, Int. J. Hydrogen Energy 35 (2010) 9818–9827, https://doi.org/10.1016/j.ijhydene.2010.05.106.

[2] O.W. Awe, Y. Zhao, A. Nzihou, D.P. Minh, N. Lyczko, A Review of Biogas Utilisation, Purification and Upgrading Technologies, Waste and Biomass Valorization. 8 (2017) 267–283, https://doi.org/10.1007/s12649-016-9826-4.

[3] S. Rasi, A. Veijanen, J. Rintala, Trace compounds of biogas from different biogas production plants, Energy 32 (2007) 1375–1380, https://doi.org/10.1016/j.energy.2006.10.018.

[4] Y. Gao, J. Jiang, Y. Meng, F. Yan, A. Aihemaiti, A review of recent developments in hydrogen production via biogas dry reforming, Energy Convers. Manag. 171 (2018) 133–155, https://doi.org/10.1016/j.enconman.2018.05.083.

[5] O. Jönsson, E. Polman, J.K. Jensen, R. Eklund, H. Schyl, S. Ivarsson, Sustainable gas enters the European gas distribution system, Danish Gas Technology Center, 2003.

[6] J.R. Rostrup-Nielsen, J. Sehested, J.K.B.T.-A. in C. Nørskov, Hydrogen and synthesis gas by steam and CO_2 reforming, in: Academic Press, 2002: pp. 65–139. https://doi.org/https://doi.org/10.1016/S0360-0564(02)47006-X.

[7] J.R. Rostrup-Nielsen, Chemisorption of hydrogen sulfide on a supported nickel catalyst, J. Catal. 11 (1968) 220–227, https://doi.org/10.1016/0021-9517(68)90035-3.

[8] C.H. Bartholomew, P.K. Agrawal, J.R. Katzer, Sulfur Poisoning of Metals, in: D.D. Eley, H. Pines, P.B.B.T.-A. in C. Weisz (Eds.), Academic Press, 1982: pp. 135–242. https://doi.org/https://doi.org/10.1016/S0360-0564(08)60454-X.

[9] K.P. Kepp, A Quantitative Scale of Oxophilicity and Thiophilicity, Inorg. Chem. 55 (2016) 9461–9470, https://doi.org/10.1021/acs.inorgchem.6b01702.

[10] S. Das, K.H. Lim, T.Z.H. Gani, S. Aksari, S. Kawi, Bi-functional CeO_2 coated NiCo-MgAl core-shell catalyst with high activity and resistance to coke and H_2S poisoning in methane dry reforming, Appl. Catal. B Environ. 323 (2023), 122141, https://doi.org/10.1016/j.apcatb.2022.122141.

[11] O. Iyoha, R. Enick, R. Killmeyer, B. Morreale, The influence of hydrogen sulfide-to-hydrogen partial pressure ratio on the sulfidization of Pd and 70 mol% Pd-Cu membranes, J. Memb. Sci. 305 (2007) 77–92, https://doi.org/10.1016/j.memsci.2007.07.032.

[12] K.D. Dewoolkar, P.D. Vaidya, Tailored hydrotalcite-based hybrid materials for hydrogen production via sorption-enhanced steam reforming of ethanol, Int. J. Hydrogen Energy 41 (2016) 6094–6106, https://doi.org/10.1016/j.ijhydene.2015.10.034.

[13] C. Dang, H. Yu, H. Wang, F. Peng, Y. Yang, A bi-functional Co-CaO-$Ca_{12}Al_{14}O_{33}$ catalyst for sorption-enhanced steam reforming of glycerol to high-purity hydrogen, Chem. Eng. J. 286 (2016) 329–338, https://doi.org/10.1016/j.cej.2015.10.073.

[14] J. Fermoso, L. He, D. Chen, Production of high purity hydrogen by sorption enhanced steam reforming of crude glycerol, Int. J. Hydrogen Energy 37 (2012) 14047–14054, https://doi.org/10.1016/j.ijhydene.2012.07.084.

[15] G. Esteban-Díez, M.V. Gil, C. Pevida, D. Chen, F. Rubiera, Effect of operating conditions on the sorption enhanced steam reforming of blends of acetic acid and acetone as bio-oil model compounds, Appl. Energy 177 (2016) 579–590, https://doi.org/10.1016/j.apenergy.2016.05.149.

[16] J. Fermoso, M.V. Gil, F. Rubiera, D. Chen, Multifunctional Pd/Ni-Co catalyst for hydrogen production by chemical looping coupled with steam reforming of acetic acid, ChemSusChem 7 (2014) 3063–3077, https://doi.org/10.1002/cssc.201402675.

[17] M.V. Gil, K.R. Rout, D. Chen, Production of high pressure pure H_2 by pressure swing sorption enhanced steam reforming (PS-SESR) of byproducts in biorefinery, Appl. Energy 222 (2018) 595–607, https://doi.org/10.1016/j.apenergy.2018.03.181.

[18] M.V. Gil, J. Fermoso, F. Rubiera, D. Chen, H_2 production by sorption enhanced steam reforming of biomass-derived bio-oil in a fluidized bed reactor: an

assessment of the effect of operation variables using response surface methodology, Catal. Today 242 (2015) 19–34, https://doi.org/10.1016/j.cattod.2014.04.018.
[19] M.V. Gil, J. Fermoso, C. Pevida, D. Chen, F. Rubiera, Production of fuel-cell grade H_2 by sorption enhanced steam reforming of acetic acid as a model compound of biomass-derived bio-oil, Appl. Catal. B Environ. 184 (2016) 64–76, https://doi.org/10.1016/j.apcatb.2015.11.028.
[20] J. Phromprasit, J. Powell, A. Arpornwichanop, A.E. Rodrigues, S. Assabumrungrat, Hydrogen production from sorption enhanced biogas steam reforming using nickel-based catalysts, Eng. J. 17 (2013) 19–34, https://doi.org/10.4186/ej.2013.17.4.19.
[21] J. Phrompprasit, J. Powell, S. Wongsakulphasatch, W. Kiatkittipong, P. Bumroongsakulsawat, S. Assabumrungrat, Activity and stability performance of multifunctional catalyst (Ni/CaO and Ni/$Ca_{12}Al_{14}O_{33}$CaO) for bio-hydrogen production from sorption enhanced biogas steam reforming, Int. J. Hydrogen Energy 41 (2016) 7318–7331, https://doi.org/10.1016/j.ijhydene.2016.03.125.
[22] J. Phrompprasit, J. Powell, S. Wongsakulphasatch, W. Kiatkittipong, P. Bumroongsakulsawat, S. Assabumrungrat, H_2 production from sorption enhanced steam reforming of biogas using multifunctional catalysts of Ni over Zr-, Ce- and La-modified CaO sorbents, Chem. Eng. J. 313 (2017) 1415–1425, https://doi.org/10.1016/j.cej.2016.11.051.
[23] R. García, M.V. Gil, F. Rubiera, D. Chen, C. Pevida, Renewable hydrogen production from biogas by sorption enhanced steam reforming (SESR): a parametric study, Energy 218 (2021), 119491, https://doi.org/10.1016/j.energy.2020.119491.
[24] A. Capa, R. García, D. Chen, F. Rubiera, C. Pevida, M.V. Gil, On the effect of biogas composition on the H_2 production by sorption enhanced steam reforming (SESR), Renew. Energy 160 (2020) 575–583, https://doi.org/10.1016/j.renene.2020.06.122.
[25] S. Appari, V.M. Janardhanan, R. Bauri, S. Jayanti, Deactivation and regeneration of Ni catalyst during steam reforming of model biogas: an experimental investigation, Int. J. Hydrogen Energy 39 (2014) 297–304, https://doi.org/10.1016/j.ijhydene.2013.10.056.
[26] M. Ashrafi, C. Pfeifer, T. Pröll, H. Hofbauer, Experimental study of model biogas catalytic steam reforming: 2. Impact of sulfur on the deactivation and regeneration of Ni-based catalysts, Energy & Fuels. 22 (2008) 4190–4195, https://doi.org/10.1021/ef8000828.
[27] V. Chiodo, S. Maisano, G. Zafarana, F. Urbani, Effect of pollutants on biogas steam reforming, Int. J. Hydrogen Energy 42 (2017) 1622–1628, https://doi.org/10.1016/j.ijhydene.2016.07.251.
[28] S.A. Chattanathan, S. Adhikari, M. McVey, O. Fasina, Hydrogen production from biogas reforming and the effect of H_2S on CH_4 conversion, Int. J. Hydrogen Energy 39 (2014) 19905–19911, https://doi.org/10.1016/j.ijhydene.2014.09.162.
[29] X. Chen, J. Jiang, F. Yan, K. Li, S. Tian, Y. Gao, H. Zhou, Dry reforming of model biogas on a Ni/SiO_2 catalyst: overall performance and mechanisms of sulfur poisoning and regeneration, ACS Sustain. Chem. Eng. 5 (2017) 10248–10257, https://doi.org/10.1021/acssuschemeng.7b02251.
[30] B. Saha, A. Khan, H. Ibrahim, R. Idem, Evaluating the performance of non-precious metal based catalysts for sulfur-tolerance during the dry reforming of biogas, Fuel 120 (2014) 202–217, https://doi.org/10.1016/J.FUEL.2013.12.016.
[31] R.Y. Chein, Y.C. Chen, W.H. Chen, Experimental Study on Sulfur Deactivation and Regeneration of Ni-Based Catalyst in Dry Reforming of Biogas, Catal. 2021, Vol. 11, Page 777. 11 (2021) 777. https://doi.org/10.3390/CATAL11070777.
[32] U. Izquierdo, I. García-García, Á.M. Gutierrez, J.R. Arraibi, V.L. Barrio, J.F. Cambra, P.L. Arias, Catalyst Deactivation and Regeneration Processes in Biogas Tri-Reforming Process. The Effect of Hydrogen Sulfide Addition, Catal. 2018, Vol. 8, Page 12. 8 (2018) 12. https://doi.org/10.3390/CATAL8010012.
[33] P. Wachter, C. Gaber, J. Raic, M. Demuth, C. Hochenauer, Experimental investigation on H_2S and SO_2 sulphur poisoning and regeneration of a commercially available Ni-catalyst during methane tri-reforming, Int. J. Hydrogen Energy 46 (2021) 3437–3452, https://doi.org/10.1016/j.ijhydene.2020.10.214.
[34] V. Pawar, S. Appari, D.S. Monder, V.M. Janardhanan, Study of the combined deactivation due to sulfur poisoning and carbon deposition during biogas dry reforming on supported Ni catalyst, Ind. Eng. Chem. Res. 56 (2017) 8448–8455, https://doi.org/10.1021/acs.iecr.7b01662.
[35] J. Abbasian, A. Rehmat, D. Leppin, D.D. Banerjee, Desulfurization of fuels with calcium-based sorbents, Fuel Process. Technol. 25 (1990) 1–15, https://doi.org/10.1016/0378-3820(90)90091-6.
[36] L.A. Fenouil, S. Lynn, Study of calcium-based sorbents for high-temperature H_2S removal. 1. Kinetics of H_2S sorption by uncalcined limestone, Ind. Eng. Chem. Res. 34 (1995) 2324–2333, https://doi.org/10.1021/ie00046a014.
[37] D.L. Keairns, R.A. Newby, E.P. O'Neill, D.H. Archer, High-temperature sulfur removal system development for the Westinghouse fluidized bed coal gasification process, Am. Chem. Soc. Div. Fuel Chem. Prepr. 21 (1976) 91.
[38] J. Weldon, G.B. Haklipur, D.A. Lewandowski, K.J. Smith, Advanced coal gasification and desulfurization with calcium based sorbents, Am. Chem. Div. Fuel Chem. Prepr. 33 (1986).
[39] M. Husmann, C. Zuber, V. Maitz, T. Kienberger, C. Hochenauer, Comparison of dolomite and lime as sorbents for in-situ H_2S removal with respect to gasification parameters in biomass gasification, Fuel 181 (2016) 131–138, https://doi.org/10.1016/j.fuel.2016.04.124.
[40] T.Y. Yeo, J. Ashok, S. Kawi, Recent developments in sulphur-resilient catalytic systems for syngas production, Renew. Sustain. Energy Rev. 100 (2019) 52–70, https://doi.org/10.1016/J.RSER.2018.10.016.
[41] D.K. Binte Mohamed, A. Veksha, Q.L.M. Ha, W.P. Chan, T.T. Lim, G. Lisak, Advanced Ni tar reforming catalysts resistant to syngas impurities: Current knowledge, research gaps and future prospects, Fuel 318 (2022), 123602, https://doi.org/10.1016/J.FUEL.2022.123602.
[42] J. Sehested, Four challenges for nickel steam-reforming catalysts, Catal. Today 111 (2006) 103–110, https://doi.org/10.1016/j.cattod.2005.10.002.
[43] L. He, H. Berntsen, E. Ochoa-Fernández, J. Walmsley, E. Blekkan, D. Chen, Co–Ni catalysts derived from hydrotalcite-like materials for hydrogen production by ethanol steam reforming, Top. Catal. 52 (2009) 206–217, https://doi.org/10.1007/s11244-008-9157-1.
[44] S. Brunauer, P.H. Emmett, E. Teller, Adsorption of gases in multimolecular layers, J. Am. Chem. Soc. 60 (1938) 309–319, https://doi.org/10.1021/ja01269a023.
[45] S. Appari, V.M. Janardhanan, R. Bauri, S. Jayanti, O. Deutschmann, A detailed kinetic model for biogas steam reforming on Ni and catalyst deactivation due to sulfur poisoning, Appl. Catal. A 471 (2014) 118–125, https://doi.org/10.1016/j.apcata.2013.12.002.
[46] W. Yin, N. Guilhaume, Y. Schuurman, Model biogas reforming over Ni-Rh/$MgAl_2O_4$ catalyst. Effect of gas impurities, Chem. Eng. J. 398 (2020), 125534, https://doi.org/10.1016/J.CEJ.2020.125534.
[47] J. Bøgild Hansen, J. Rostrup-Nielsen, Sulfur poisoning on Ni catalyst and anodes, in, Handb. Fuel Cells (2010), https://doi.org/10.1002/9780470974001.f500064.
[48] T. Zheng, M. Li, D. Mei, J. Ma, B. Wang, Z. Xu, Effect of H_2S presence on chemical looping reforming (CLR) of biogas with a firebrick supported NiO oxygen carrier, Fuel Process. Technol. 226 (2022), 107088, https://doi.org/10.1016/j.fuproc.2021.107088.
[49] F. Dashtestani, M. Nusheh, V. Siriwongrungson, J. Hongrapipat, V. Materic, S. Pang, Effect of H_2S and NH_3 in biomass gasification producer gas on CO_2 capture performance of an innovative CaO and Fe_2O_3 based sorbent, Fuel 295 (2021), 120586, https://doi.org/10.1016/j.fuel.2021.120586.
[50] I. Martínez, M.S. Callén, G. Grasa, J.M. López, R. Murillo, Sorption-enhanced gasification (SEG) of agroforestry residues: Influence of feedstock and main operating variables on product gas quality, Fuel Process. Technol. 226 (2022) 378–3820, https://doi.org/10.1016/J.FUPROC.2021.107074.
[51] J.H. Wang, M. Liu, Computational study of sulfur-nickel interactions: a new S-Ni phase diagram, Electrochem. Commun. 9 (2007) 2212–2217, https://doi.org/10.1016/j.elecom.2007.06.022.
[52] B. Guan, Y. Li, B. Yin, K. Liu, D. Wang, H. Zhang, C. Cheng, Synthesis of hierarchical NiS microflowers for high performance asymmetric supercapacitor, Chem. Eng. J. 308 (2017) 1165–1173, https://doi.org/10.1016/j.cej.2016.10.016.
[53] K. Taira, T. Sugiyama, H. Einaga, K. Nakao, K. Suzuki, Promoting effect of 2000 ppm H_2S on the dry reforming reaction of CH_4 over pure CeO_2, and in situ observation of the behavior of sulfur during the reaction, J. Catal. 389 (2020) (2000) 611–622, https://doi.org/10.1016/j.jcat.2020.06.040.
[54] C. Dueso, M.T. Izquierdo, F. García-Labiano, L.F. de Diego, A. Abad, P. Gayán, J. Adánez, Effect of H_2S on the behaviour of an impregnated NiO-based oxygen-carrier for chemical-looping combustion (CLC), Appl. Catal. B Environ. 126 (2012) 186–199, https://doi.org/10.1016/j.apcatb.2012.07.011.
[55] T. Fan, L. Dou, H. Zhang, Nonprecious mixed oxide catalysts Co_3AlO and Co_2NiAlO derived from nanoflowerlike cobalt-based hydrotalcites for highly efficient oxidation of nitric oxide, RSC Adv. 6 (2016) 110274–110287, https://doi.org/10.1039/c6ra23704e.
[56] J. Ashok, S. Das, N. Dewangan, S. Kawi, Steam reforming of surrogate diesel model over hydrotalcite-derived MO-CaO-Al_2O_3 (M = Ni & Co) catalysts for SOFC applications, Fuel 291 (2021), 120194, https://doi.org/10.1016/j.fuel.2021.120194.
[57] J. Ashok, Y. Kathiraser, M.L. Ang, S. Kawi, Bi-functional hydrotalcite-derived NiO-CaO-Al_2O_3 catalysts for steam reforming of biomass and/or tar model compound at low steam-to-carbon conditions, Appl. Catal. B Environ. 172–173 (2015) 116–128, https://doi.org/10.1016/j.apcatb.2015.02.017.
[58] J. Matienzo, L.I. Yin, S.O. Grim, W.E.J. Swartz, X-ray photoelectron spectroscopy of nickel compounds, Inorg. Chem. 12 (1973) 2762–2769, https://doi.org/10.1021/ic50130a005.
[59] J. Ashok, S. Das, N. Dewangan, S. Kawi, H_2S and NO_x tolerance capability of CeO_2 doped $La_{1-x}Ce_xCo_{0.5}Ti_{0.5}O_{3-\delta}$ perovskites for steam reforming of biomass tar model reaction, Energy Convers. Manag. x. 1 (2019), 100003, https://doi.org/10.1016/j.ecmx.2019.100003.
[60] Z. Ferencz, E. Varga, R. Puskás, Z. Kónya, K. Baán, A. Oszkó, A. Erdőhelyi, Reforming of ethanol on Co/Al_2O_3 catalysts reduced at different temperatures, J. Catal. 358 (2018) 118–130, https://doi.org/10.1016/j.jcat.2017.12.003.
[61] L. Li, C. Howard, D.L. King, M. Gerber, R. Dagle, D. Stevens, Regeneration of sulfur deactivated Ni-based biomass syngas cleaning catalysts, Ind. Eng. Chem. Res. 49 (2010) 10144–10148, https://doi.org/10.1021/ie101032x.
[62] F. García-Labiano, L.F. De Diego, P. Gayán, J. Adánez, A. Abad, C. Dueso, Effect of fuel gas composition in chemical-looping combustion with Ni-based oxygen carriers. 1. Fate of sulfur, Ind. Eng. Chem. Res. 48 (2009) 2499–2508, https://doi.org/10.1021/ie801332e.
[63] T. Noor, M.V. Gil, D. Chen, Production of fuel-cell grade hydrogen by sorption enhanced water gas shift reaction using Pd/Ni-Co catalysts, Appl. Catal. B Environ. 150–151 (2014), https://doi.org/10.1016/j.apcatb.2014.01.002.
[64] Y. Hu, S. Wu, Y. Li, J. Zhao, S. Lu, H_2S removal performance of $Ca_3Al_2O_6$-stabilized carbide slag from CO_2 capture cycles using calcium looping, Fuel Process. Technol. 218 (2021), 106845, https://doi.org/10.1016/j.fuproc.2021.106845.
[65] J. Wang, J. Guo, R. Parnas, B. Liang, Calcium-based regenerable sorbents for high temperature H_2S removal, Fuel 154 (2015) 17–23, https://doi.org/10.1016/j.fuel.2015.02.105.
[66] J. Agnew, E. Hampartsoumian, J.M. Jones, W. Nimmo, The effect of sintering on sulphur capture by limestone and dolomite, J. Energy Inst. 78 (2005) 81–89, https://doi.org/10.1179/174602205X39812.

[67] K.P. Yrjas, C.A.P. Zevenhoven, M.M. Hupa, Hydrogen Sulfide Capture by Limestone and Dolomite at Elevated Pressure. 1. Sorbent Performance, 1996.
[68] A.I. Lysikov, A.N. Salanov, A.G. Okunev, Change of CO_2 carrying capacity of CaO in isothermal recarbonation-decomposition cycles, Ind. Eng. Chem. Res. 46 (2007) 4633–4638, https://doi.org/10.1021/ie0702328.
[69] L.A. Fenouil, G.P. Towler, S. Lynn, Removal of H_2S from coal gas using limestone: kinetic considerations, Ind. Eng. Chem. Res. 33 (1994) 265–272, https://doi.org/10.1021/ie00026a014.
[70] X. Meng, W. De Jong, R. Pal, A.H.M. Verkooijen, In bed and downstream hot gas desulphurization during solid fuel gasification: a review, Fuel Process. Technol. 91 (2010) 964–981, https://doi.org/10.1016/j.fuproc.2010.02.005.
[71] C. Jiang, E. Loisel, D.A. Cullen, J.A. Dorman, K.M. Dooley, On the enhanced sulfur and coking tolerance of Ni-Co-rare earth oxide catalysts for the dry reforming of methane, J. Catal. 393 (2021) 215–229, https://doi.org/10.1016/j.jcat.2020.11.028.

Paper IV

Title: Blends of bio-oil/biogas model compounds for high-purity H_2 production by sorption enhanced steam reforming (SESR): Experimental study and energy analysis.

Authors: S. Rodríguez, A. Capa, R. García, D. Chen, F. Rubiera, C. Pevida, M.V. Gil.

Journal: Chemical Engineering Journal, 432, 2021, doi: https://doi.org/10.1016/j.cej.2021.134396

Abstract

H_2 production by sorption enhanced steam reforming (SESR) of bio-oil/biogas blends was demonstrated in a fluidised bed reactor. It combines steam reforming (SR) with simultaneous CO_2 capture by a solid sorbent. SESR was performed on a Pd/Ni-Co catalyst derived from a hydrotalcite-like material (HT) using dolomite as CO_2 sorbent. Bio-oil from fast pyrolysis of biomass is a carbon–neutral and renewable energy source with great potential for clean H_2 production by steam reforming processes. Biogas is also a promising renewable bio-based resource for hydrogen generation that can be used to increase the H_2 production of a biomass-based plant. In turn, it could improve the energy efficiency of the process due to the exothermic reaction of the CO_2 contained in biogas with the sorbent. Bio-oil composed of acetic acid and acetone (1/1 mol/mol) and biogas composed of CH_4 and CO_2 (60/40 vol%) were used as fuels. They were blended (50 wt% bio-oil + 50 wt% CH_4) to study the SESR process. Effects of temperature, steam/C molar ratio, and pressure on the process performance were evaluated. SESR results showed an effective reforming of bio-oil/biogas blends and an enhancement in the H_2 production and fuel conversion compared to conventional SR. Higher temperature and steam/C ratio, but lower pressure, favored H_2 yield and purity. High H_2 yield (87.1%) and H_2 purity (98.6 vol%) were obtained at 625 ^{o}C and 2.5 bar (steam/C molar ratio three times higher than the stoichiometric value). The thermodynamic energy analysis of the SESR of bio-oil/biogas blends rendered 1.34% higher cold gas efficiency (CGE) than bio-oil SESR.

Annex III

Communications to scientific congresses

Oral communications to scientific congresses out of the work performed during this thesis:

- Accepted Oral: Techno-economic analysis of a 50 MW H_2 production plant by sorption enhanced steam reforming (SESR): Comparing natural gas and biogas. A. Capa, Y. Yan, F. Rubiera, C. Pevida, M. V. Gil, P.T. Clough. EHEC2024- European Hydrogen Energy Conference, Bilbao.
- Accepted Oral: Bio-dimethyl-ether as hydrogen carrier: How to integrate sorption enhanced steam reforming (SESR) of biogas and sorption enahnced DME synthesis (SEDMES). A. Capa, G.Skorikova, V.Dikic, S.Sluijter, I.Tyraskis, F.Rubiera, C.Pevida, M.V.Gil, J.Boon. EHEC2024- European Hydrogen Energy Conference, Bilbao.
- Awarded Keynote: Effect of H_2S in biogas composition on the production of H_2 by sorption enhanced steam reforming (SESR). A. Capa, M.P. González-Vázquez, D. Chen, F. Rubiera, C. Pevida, M. V. Gil. MultiChem2023, Gijón.
- Oral: El biogás como bio-recurso carbonoso para la producción de hidrógeno renovable mediante reformado catalítico con captura de CO_2. Capa, A., García, R., Chen, D., Rubiera, F., Gil, M. V , Pevida, C. JJGEC2022- I Jornadas de Jóvenes Investigadores del GEC, Baeza.
- Oral: Process simulation of renewable hydrogen production by Sorption Enhanced Steam Reforming (SESR) of Biogas. A. Capa, Y. Yan, F. Rubiera, C. Pevida, M. V. Gil, P.T. Clough. EHEC2022- European Hydrogen Energy Conference, Madrid.
- Oral: Blends of bio-oil and biogas for high-purity H_2 production by Sorption Enhanced Steam reforming (SESR). A. Capa, S. Rodríguez, R. García, D. Chen, F. Rubiera, C. Pevida, M. V. Gil. EUBCE2022- 30th European Biomass Conference and Exhibitions.
- Oral: Simulación de un proceso autotérmico de producción de H_2 renovable a partir de biogás mediante reformado con captura in situ de CO_2. A. Capa, Y. Yan, F. Rubiera, C. Pevida, M. V. Gil, P.T. Clough. XV Reunión del GEC en 2022, Granada.
- Oral: Biogas conversion to green hydrogen by catalytic Sorption Enhanced Steam Reforming (SESR): the feasibility study. R. García, A. Capa, D. Chen, F. Rubiera, C. Pevida, M. V. Gil. EUBCE2021- 29th European Biomass Conference and Exhibitions.

Poster communications to scientific congresses out of the work performed during this thesis:

- Poster: Evaluación de diferentes catalizadores para la producción de H_2 mediante reformado con captura in situ de CO_2 de biogás. A. Capa, R. García, D. Chen, F. Rubiera, C. Pevida, M. V. Gil. XVI Reunión del GEC 2023, Gijón.
- Poster: Effect of H_2S on the sorption enhanced steam reforming (SESR) of biogas. A. Capa, M.P. González-Vázquez, D. Chen, F. Rubiera, C. Pevida, M. V. Gil. EUBCE2031- 31st European Biomass Conference and Exhibitions, Bologna, Italy.
- Poster: Hydrogen production by sorption enhanced steam reforming (SESR) of biogas containing H_2S. A. Capa, R. García, M.P. González-Vázquez, D. Chen, F. Rubiera, M. V. Gil, C. Pevida. EHEC2022- European Hydrogen Energy Conference, Madrid.
- Poster: Energy analysis on the effect of biogas composition in the sorption enhanced steam reforming (SESR) for green hydrogen production. A. Capa, R. García, F. Rubiera, C. Pevida, M. V. Gil. EUBCE2021- 29th European Biomass Conference and Exhibitions.